

University of Louisville

## ThinkIR: The University of Louisville's Institutional Repository

---

Electronic Theses and Dissertations

---

12-2011

### Rational design, synthesis and characterization of amide functionalized pyridine and benzimidazole transition metal complexes.

Samuel S. K. Asem  
*University of Louisville*

Follow this and additional works at: <https://ir.library.louisville.edu/etd>

---

#### Recommended Citation

Asem, Samuel S. K., "Rational design, synthesis and characterization of amide functionalized pyridine and benzimidazole transition metal complexes." (2011). *Electronic Theses and Dissertations*. Paper 52.  
<https://doi.org/10.18297/etd/52>

This Doctoral Dissertation is brought to you for free and open access by ThinkIR: The University of Louisville's Institutional Repository. It has been accepted for inclusion in Electronic Theses and Dissertations by an authorized administrator of ThinkIR: The University of Louisville's Institutional Repository. This title appears here courtesy of the author, who has retained all other copyrights. For more information, please contact [thinkir@louisville.edu](mailto:thinkir@louisville.edu).

RATIONAL DESIGN, SYNTHESIS AND CHARACTERIZATION OF AMIDE  
FUNCTIONALIZED PYRIDINE AND BENZIMIDAZOLE TRANSITION METAL  
COMPLEXES

By

Samuel S. K. Asem  
B.A., Berea College, 2000

A Dissertation  
Submitted to the Faculty of the  
Graduate School of the University of Louisville  
In Partial Fulfillment of the Requirements  
For the Degree of

Doctor of Philosophy

Department of Chemistry  
University of Louisville  
Louisville, Kentucky

December 2011

Copyright 2011 by Samuel S.K. Asem

All rights reserved

RATIONAL DESIGN, SYNTHESIS AND CHARACTERIZATION OF AMIDE  
FUNCTIONALIZED PYRIDINE AND BENZIMIDAZOLE TRANSITION METAL  
COMPLEXES

By

Samuel S. K. Asem  
B.A., Berea College, 2000

A Dissertation Approved on

December 14, 2011

by the following Dissertation Committee:

---

Robert M. Buchanan (Dissertation Director)

---

Mark E. Noble

---

Michael H. Nantz

---

David Schultz

## **DEDICATION**

This work is dedicated to my family, wife and son, Joshua. “It takes a community to raise a child”. To my parents Kafui and Philippine, for their priceless values, sacrifices, unconditional love and support.

## ACKNOWLEDGEMENTS

I would like to thank my mentor Dr. Buchanan, for his guidance and invaluable input over the years. Without his insight, time and resourcefulness, this body of work wouldn't have been possible. I would also like to thank my wife and lifelong friend Abby for the support, love and sacrifices over all these years.

I would like to extend my gratitude and thanks to the faculty committee members Drs. Grapperhaus, Nantz, Noble and Schultz for their understanding, ideas and time to serve as committee members, not forgetting their advice and counsel during our numerous interactions over the years.

Special thanks goes to my parents, siblings and extended family both here and abroad for their emotional support and prayers; “no man is an island”. I would be remiss to forget the invaluable contributions and work by Drs. Neal Stolowich and Mark Mashuta; Dr. Stolowich for his assistance and teachings in NMR and Mark Mashuta for his exceptional work on the X-ray structures presented in this work.

Special thanks go to Marina Malovichko for her translation of the Russian articles cited in this work. Finally, this work would not be complete without the diligent work of Lavona K. Casson on the bioassays and Dr. Paula Bates for her insights and laboratory

## ABSTRACT

Rational design, synthesis and characterization of amide functionalized pyridine and benzimidazole transition metal complexes

Samuel S.K. Asem

December 14, 2011

This study expands our efforts to make a new class of Pt (II) compounds analogous to cisplatin and its derivatives using sterically hindered ligands. Pt compounds in this series have been synthesized using specially designed pyridine and benzimidazole ligands. These heterocycles, amide functionalized at position 2 with aryl and alkyl pendants, rapidly change their mode of coordination depending on the pH of the medium. These ligands, synthesized using condensation chemistry, also coordinate to Co(II), Ni(II), Cu(II), and Zn(II) generally as anionic bis-chelates through the benzimidazole nitrogen and the carbonyl oxygen, creating a four-coordinate complex with the exception of an unusual trigonal bipyramidal Zn(II) complex. <sup>1</sup>H NMR temperature studies reveal that these ligands interconvert between imide and amide isomers and that electron withdrawing pendants favor amide isomers. Crystal structures of Co(II) and Ni(II) complexes of N-(1-methylbenzimidazol-2-yl)cyclohexanecarboxamide, for example, show two ligands bind per metal ion when reacted with acetate and nitrate salts. The bis-chelates of these Ni(II) complexes also show expansions of their coordination spheres

from four to five-coordinate. Furthermore, these Ni(II) bis-chelated complexes possess square planar or distorted 4-coordinate geometries.

The synthesis and properties of several new Pt (II) complexes containing these ligands will be presented. A second generation and novel complex class containing metal-binding, linker and recognition domains is reported. Both classes of Pt complexes were obtained using a synthetic methodology which favors the *cis* isomers. The second generation complex crystallizes in the monoclinic space group  $P2_1/n$  with lattice dimensions  $a = 17.7393(5) \text{ \AA}$ ,  $b = 11.4632(3) \text{ \AA}$ ,  $c = 19.3959(5) \text{ \AA}$  and  $\beta = 99.794(3)^\circ$ . These complexes have been characterized using physical methods that include X-ray crystallography,  $^1\text{H}$  &  $^{13}\text{C}$  NMR, Mass spectrometry, UV and IR spectroscopies. Complexes similar in structure to cisplatin and carboplatin show varying cytotoxic properties toward different cancer cell lines. Additionally, some of these new Pt complexes show comparable and promising cytotoxicity against prostate cancer cell lines.



## TABLE OF CONTENTS

<b>DEDICATION</b> .....	<b>iii</b>
<b>ACKNOWLEDGEMENTS</b> .....	<b>iv</b>
<b>ABSTRACT</b> .....	<b>v</b>
<b>LIST OF TABLES</b> .....	<b>xviii</b>
<b>LIST OF FIGURES</b> .....	<b>xx</b>
<b>CHAPTER I</b> .....	<b>1</b>
<b>INTRODUCTION</b> .....	<b>1</b>
<b>CHAPTER II</b> .....	<b>13</b>
<b>SYNTHESIS, CHARACTERIZATION, AND ANALYTICAL PROCEDURES</b> .....	<b>13</b>
<b>A: Procedures for Physical data collection:</b> .....	<b>13</b>
1. Mass Spectrometry (MALDI-TOF) .....	13
2. X-ray Crystallography .....	13
3. KBr-IR Data Acquisition.....	14
4. NMR Data Acquisition.....	15
5. NMR Experiments.....	15
6. UV-vis Titration .....	15
7. Bioassay	16
<b>B: Materials</b> .....	<b>17</b>
<b>C: List of Compounds and Nomenclature</b> .....	<b>19</b>
<b>D: Synthesis of Compounds</b> .....	<b>24</b>
1. N-(N'-1-methylbenzimidazol-2-yl)hexadecanamide (Hmbhda) .....	24
2. N-(N'-1-methylbenzimidazol-2-yl)decanamide (Hmbda).....	25

3.	N-(benzimidazol-2-yl)cyclohexanecarboxamide (Hbchca).....	26
4.	N-(N'-1-methylbenzimidazol-2-yl)cyclohexanecarboxamide (Hmbchca).....	26
5.	N-(N'-1-methylbenzimidazol-2-yl)benzamide (Hmbba).....	27
6.	N-(benzimidazol-2-yl)benzamide (Hbba).....	27
7.	N-(N'-1-methylbenzimidazol-2-yl)-N''-boc-2-amino-2,2-dimethylacetamide (Hisoba) or L <sup>boc</sup> .....	28
8.	N-(N'-1-methylbenzimidazol-2-yl)-2-N'-phthalimidylacetamide (Hmbpha).....	29
9.	N-(N'-1-methylbenzimidazol-2-yl)-2,2-dimethylpropanamide (Hdmmbp).....	29
10.	N-(N'-1-methylbenzimidazol-2-yl)acetamide (Hmba).....	30
11.	N-(N'-1-methylbenzimidazol-2-yl)-2,2,2-trichloroacetamide (Hmbtca) .....	30
12.	N-(benzimidazol-2-yl)-2,2-dimethylpropanamide (Hdmbp).....	31
13.	N-(N'-1-methylbenzimidazol-2-yl)propanamide (Hmbpa) .....	31
15.	Bis[N-(N'-1-methylbenzimidazol-2-yl)decanamido]copper(II) Cu(mbda) <sub>2</sub> .....	31
16.	Bis[N-(N'-1-methylbenzimidazol-2-yl)cyclohexanecarboxamido]nickel(II) Ni (mbchca) <sub>2</sub> .....	32
17.	Bis[N-(N'-1-methylbenzimidazol-2-yl)cyclohexanecarboxamido]cobalt(II) Co(mbchca) <sub>2</sub> .....	32
18.	<i>Trans</i> -Bis[ N-(benzimidazol-2-yl) benzamido][ N-(benzimidazol-2-yl) benzamide]zinc(II) Zn(bba) <sub>2</sub> (Hbba) .....	33
19.	<i>Trans</i> -Bis[2,2-dimethyl-N-(N'-1-methylbenzimidazol-2-yl)propanamido]vanadium(IV) oxide VO(dmmbp) <sub>2</sub> .....	33
20.	Bis[N-(N'-1-methylbenzimidazol-2-yl)decanamido]nickel(II) Ni(mbda) <sub>2</sub> .....	34

21. Bis[N-(N'-1-methylbenzimidazol-2-yl)hexadecanamido]nickel(II)	
Ni(mbhda) <sub>2</sub> .....	34
22. Bis[N-(N'-1-methylbenzimidazol-2-yl)cyclohexanecarboxamido]zinc(II)	
Zn(mbchca) <sub>2</sub> .....	35
23. Bis[N-(N'-1-methylbenzimidazol-2-yl)acetamido]zinc(II)	Zn(Hmba) <sub>2</sub> .....
	35
24. <i>Trans</i> -Bis[(N-pyridin-2-yl)-2,2-dimethylpropanamide](μ-	
tetrakisacetatocopper)copper(II) [Cu <sub>2</sub> (OAc) <sub>4</sub> (Pap) <sub>2</sub> ].....	36
25. <i>Cis</i> -Bis[(N-pyridin-2-yl)-2,2-dimethylpropanamide]platinum(II) diiodide	
c(Pap) <sub>2</sub> PtI <sub>2</sub> .....	36
26. <i>Trans</i> -Bis[(N-pyridin-2-yl)-2,2-dimethylpropanamide]platinum(II) diiodide	
t(Pap) <sub>2</sub> PtI <sub>2</sub> .....	37
27. <i>Trans</i> -Bis[(N-pyridin-2-yl)-2,2-dimethylpropanamido]platinum(II) t(Pap) <sub>2</sub> Pt..	38
28. <i>Cis</i> -Bis[(N-pyridin-2-yl)-2,2-dimethylpropanamide]platinum(II) dichloride	
c(Pap) <sub>2</sub> PtCl <sub>2</sub> .....	39
29. <i>Trans</i> -Bis[(N-pyridin-2-yl)-2,2-dimethylpropanamide]platinum(II) dichloride	
t(Pap) <sub>2</sub> PtCl <sub>2</sub> .....	39
30. Bis[N-(N'-1-methylbenzimidazol-2-yl)decanamido]platinum(II) Pt(mbda) <sub>2</sub> ....	40
31. Bis[N-(N'-1-methylbenzimidazol-2-yl)cyclohexanecarboxamide]platinum(II)	
diiodide Pt(cyclohexylamb) <sub>2</sub> I <sub>2</sub> .....	41
32. Bis[N-(N'-1-methylbenzimidazol-2-yl)cyclohexanecarboxamido]platinum(II)	
Pt(mbchca) <sub>2</sub> .....	41
33. Bis[N-(N'-1-methylbenzimidazol-2-yl)cyclohexanecarboxamide]platinum(II)	
dichloride Pt(mbchca) <sub>2</sub> Cl <sub>2</sub> .....	42

34. Bis[N-(N'-1-methylbenzimidazol-2-yl)hexadecanamido]platinum(II) Pt(mbhda) <sub>2</sub> .....	43
35. <i>Cis</i> -diiodo-Bis[2,2-dimethyl-N-(N'-1-methylbenzimidazol-2-yl) propanamide]platinum(II) Pt(Hdmmbp) <sub>2</sub> I <sub>2</sub> .....	43
36. Bis[2,2-dimethyl-N-(N'-1-methylbenzimidazol-2- yl)propanamido]platinum(II) Pt(dmmbp) <sub>2</sub> .....	44
37. <i>Cis</i> -Bis[2,2-dimethyl-N-(N'-1-methylbenzimidazol-2- yl)propanamide]platinum(II) dichloride Pt(Hdmmbp) <sub>2</sub> Cl <sub>2</sub> .....	44
38. <i>Cis</i> -Bis[(N-benzimidazol-2-yl)-2,2-dimethylpropanamide]platinum(II) diiodide Pt(Hdmbp) <sub>2</sub> I <sub>2</sub> .....	45
39. <i>Cis</i> -Bis[(N-benzimidazol-2-yl)-2,2-dimethylpropanamide]platinum(II) dichloride (Hdmbp) <sub>2</sub> PtCl <sub>2</sub> .....	45
40. Bis[ N-(benzimidazol-2-yl)cyclohexanecarboxamide]platinum(II) diiodide (Hbchca) <sub>2</sub> PtI <sub>2</sub> .....	46
41. <i>Cis</i> -Bis[N-(N'-1-methylbenzimidazol-2-yl)propanamide]platinum(II) dichloride (Hmbp)PtCl <sub>2</sub> .....	46
42. N-(N'-1-methylbenzimidazol-2-yl) benzamide]platinum(II) and platinum(IV) complexes .....	47
46. <i>Cis</i> - Bis[N'- <i>boc</i> -2-amino-2,2-dimethyl (N-(N'-1- methyl benzimidazol-2-yl) acetamide]platinum(II) dichloride ( <i>isoba</i> ) Pt(L <sup>boc</sup> ) <sub>2</sub> Cl <sub>2</sub> .....	48
<b>CHAPTER III.....</b>	<b>49</b>
<b>TRANSITION METAL COMPLEXES.....</b>	<b>49</b>
<b>A: Background Discussion.....</b>	<b>49</b>

<b>B: Synthesis and Characterization of Metal Complexes .....</b>	<b>65</b>
<b>C: FT-IR Analysis of Metal Complexes .....</b>	<b>66</b>
<b>D: UV-vis Analysis of Complexes.....</b>	<b>71</b>
<b>E: Mass Spectrometric Analysis of Coordination Metal Complexes.....</b>	<b>72</b>
<b>F: <sup>1</sup>H NMR Characterization and Analysis of Complexes .....</b>	<b>79</b>
<b>G: X-ray Crystallographic Analysis of Coordination Metal Complexes .....</b>	<b>87</b>
<b>H: Conclusions.....</b>	<b>107</b>
<b>CHAPTER IV .....</b>	<b>110</b>
<b>ISOMERIC CONFORMERS OF PLATINUM (II) COMPLEXES OF 2-PIVALOYL PYRIDINE AND BENZIMIDAZOLE LIGANDS.....</b>	<b>110</b>
<b>A: Background Discussion.....</b>	<b>110</b>
<b>B: Synthesis and Characterization of Platinum (II) Complexes.....</b>	<b>115</b>
<b>C: FT-IR of Pyridine Complexes .....</b>	<b>123</b>
<b>D: X-ray Crystallography of Pyridine Complexes .....</b>	<b>125</b>
<b>E: UV-vis of Pyridine Complexes.....</b>	<b>134</b>
<b>F: X-ray Crystallographic Analysis of Complexes .....</b>	<b>150</b>
<b>G: UV-vis Studies of Complexes .....</b>	<b>166</b>
<b>H: Bioassay of Complexes.....</b>	<b>169</b>
<b>I: Conclusions .....</b>	<b>174</b>
<b>CHAPTER V.....</b>	<b>176</b>
<b>CONCLUDING REMARKS.....</b>	<b>176</b>
<b>REFERENCES .....</b>	<b>180</b>
<b>APPENDIX .....</b>	<b>185</b>

<b>UV-vis of Selected Compounds</b> .....	185
UV-vis absorption trace of compound 16 in 3 mL CH <sub>2</sub> Cl <sub>2</sub> .....	185
UV-vis absorption trace of compound 17 in 3 mL CH <sub>2</sub> Cl <sub>2</sub> .....	185
UV-vis absorption trace of compound 18 in 3 mL CH <sub>2</sub> Cl <sub>2</sub> .....	186
UV-vis absorption trace of compound 19 in 3 mL CH <sub>2</sub> Cl <sub>2</sub> .....	186
UV-vis absorption trace of Compound 20 in 3 mL CH <sub>2</sub> Cl <sub>2</sub> .....	187
UV-vis absorption trace of compound 21 in 3 mL CH <sub>2</sub> Cl <sub>2</sub> .....	187
UV-vis absorption trace of compound 24 in 3 mL CH <sub>2</sub> Cl <sub>2</sub> .....	188
UV-vis absorption trace of compound 30 in 3 mL CH <sub>2</sub> Cl <sub>2</sub> .....	188
UV-vis absorption trace of compound 31 in 3 mL CH <sub>2</sub> Cl <sub>2</sub> .....	189
UV-vis absorption trace of compound 32 in 3 mL CH <sub>2</sub> Cl <sub>2</sub> .....	189
UV-vis absorption trace of compound 33 in 3 mL CH <sub>2</sub> Cl <sub>2</sub> .....	190
UV-vis absorption trace of compound 34 in 3 mL CH <sub>2</sub> Cl <sub>2</sub> .....	190
UV-vis absorption trace of selected compounds in 3 mL CH <sub>2</sub> Cl <sub>2</sub> .....	191
UV-vis spectrum of GSH and compound 37 in anh. CH <sub>2</sub> Cl <sub>2</sub> .....	191
UV-vis spectrum of GSH and compound 37 water reaction .....	192
<b>Mass Spectrometric Traces :</b> .....	192
<b><sup>1</sup>H NMR and <sup>13</sup>C NMR Spectra</b> .....	202
<sup>1</sup> H NMR of compound 12 in CD <sub>2</sub> Cl <sub>2</sub> .....	202
<sup>1</sup> H NMR of compound 30 in CDCl <sub>3</sub> .....	203
<sup>1</sup> H NMR of compound 31 in CDCl <sub>3</sub> .....	204
<sup>1</sup> H NMR of compound 32 in CDCl <sub>3</sub> .....	205
<sup>1</sup> H NMR of compound 33 in CDCl <sub>3</sub> .....	206

<sup>1</sup> H NMR of compound 39 in CDCl <sub>3</sub> .....	207
<sup>1</sup> H NMR of compound 41 in CDCl <sub>3</sub> .....	208
<sup>1</sup> H NMR of compound 46 in CDCl <sub>3</sub> .....	209
<sup>13</sup> C NMR of compound 31 in CDCl <sub>3</sub> .....	210
<sup>13</sup> C NMR spectrum of compound 40 in acetone .....	211
<b>IR Spectra</b> .....	212
IR spectrum of <b>compound 16</b> .....	212
IR spectrum of <b>compound 17</b> .....	212
IR spectrum of <b>compound 25</b> .....	212
IR spectrum of <b>compound 26</b> .....	213
IR spectrum of <b>compound 27</b> .....	213
IR spectrum of <b>compound 28</b> .....	213
Table A1. Crystal data and structure refinement for Compound 4 .....	216
Table A2. Atomic coordinates and equivalent isotropic displacement parameters of Compound 4 .....	217
Table A3. Anisotropic displacement parameters of Compound 4 . .....	217
Table A4. Hydrogen coordinates and isotropic displacement parameters .....	218
Table A5. Crystal data and structure refinement Compound 15 .....	219
Table A6. Atomic coordinates and equivalent isotropic displacement parameters of Compound 15 .....	220
Table A7. Anisotropic displacement parameters of Compound 15 .....	220
Table A8. Hydrogen coordinates and isotropic displacement parameters .....	221
Table A9. Crystal data and structure refinement for Compound 16. ....	222

Table A10. Atomic coordinates and equivalent isotropic displacement parameters for Compound 16 .....	223
Table A11. Anisotropic displacement parameters for Compound 16 .....	223
Table A12. Hydrogen coordinates and isotropic displacement parameters .....	224
Table A13. Crystal data and structure refinement for Compound 17 .....	225
Table A14. Atomic coordinates and equivalent isotropic displacement parameters for Compound 17 .....	226
Table A15. Anisotropic displacement parameters .....	229
Table A16. Hydrogen coordinates and isotropic displacement parameters .....	231
Table A17. Crystal data and structure refinement for Compound 18. ....	233
Table A18. Atomic coordinates and equivalent isotropic displacement parameters for Compound 18 .....	234
Table A19. Anisotropic displacement parameters .....	235
Table A20. Hydrogen coordinates and isotropic displacement parameters .....	236
Table A21. Crystal data and structure refinement for Compound 19 .....	238
Table A22. Atomic coordinates and equivalent isotropic displacement parameters.for Compound 19.....	239
Table A23. Anisotropic displacement parameters .....	240
Table A24. Hydrogen coordinates and isotropic displacement parameters .....	241
Table A25. Crystal data and structure refinement for compound 23. ....	241
Table A26. Atomic coordinates and equivalent isotropic displacement parameters. ....	243
Table A27. Anisotropic displacement parameters. ....	244
Table A28. Hydrogen coordinates and isotropic displacement parameters .....	244



Table A28. Hydrogen coordinates and isotropic displacement parameters .....	245
Table A29. Crystal data and structure refinement for Compound 24 .....	246
Table A30. Atomic coordinates and equivalent isotropic displacement parameters	247
Table A31. Anisotropic displacement parameters .....	247
Table A32. Hydrogen coordinates and isotropic displacement parameters .....	248
Table A33. Crystal data and structure refinement for compound 25 .....	249
Table A34. Atomic coordinates and equivalent isotropic displacement parameters.for Compound 25.....	250
Table A35. Anisotropic displacement parameters .....	251
Table A36. Hydrogen coordinates and isotropic displacement parameters .....	252
Table A37. Crystal data and structure refinement for compound 26 .....	253
Table A38. Atomic coordinates and equivalent isotropic displacement parameters.	254
Table A39. Anisotropic displacement parameters .....	254
Table A40. Hydrogen coordinates and isotropic displacement .....	255
Table A41. Crystal data and structure refinement for compound 27. ....	256
Table A42. Atomic coordinates and equivalent isotropic displacement parameters.for Compound 27.....	257
Table A43. Anisotropic displacement parameters .....	257
Table A44. Hydrogen coordinates and isotropic displacement parameters .....	258
Table A45. Crystal data and structure refinement for compound 28 .....	259
Table A46. Atomic coordinates and equivalent isotropic displacement parameters.	260
Table A47. Anisotropic displacement parameters .....	261
Table A48. Hydrogen coordinates and isotropic displacement parameters .....	262

Table A49. Crystal data and structure refinement for compound 30 .....	263
Table A50. Atomic coordinates and equivalent isotropic displacement parameters.	264
Table A51. Anisotropic displacement parameters .....	265
Table A52. Hydrogen coordinates and isotropic displacement parameters .....	266
Table A53. Crystal data and structure refinement for compound 41 .....	268
Table A54. Atomic coordinates and equivalent isotropic displacement parameters.	269
Table A55. Anisotropic displacement parameters for Compound 41 .....	270
Table A56. Hydrogen coordinates and isotropic displacement parameters .....	271
Table A57. Crystal data and structure refinement for compounds 42a and b .....	272
Table A58. Atomic coordinates and equivalent isotropic displacement parameters.	273
Table A59. Anisotropic displacement parameters .....	274
Table A60. Hydrogen coordinates and isotropic displacement parameters .....	275
Table A61. Crystal data and structure refinement for compound 42c .....	276
Table A62. Atomic coordinates and equivalent isotropic displacement parameters.	277
Table A63. Anisotropic displacement parameters .....	277
Table A64. Hydrogen coordinates and isotropic displacement parameters .....	278
Table A65. Crystal data and structure refinement for compound 46 .....	279
Table A66. Atomic coordinates and equivalent isotropic displacement parameters.	280
Table A67. Anisotropic displacement parameters .....	281
Table A68. Hydrogen coordinates and isotropic displacement parameters .....	282
Table A69. Hydrogen bonds for Compound 18 [ $\text{\AA}$ and $^{\circ}$ ]. .....	283
Table A70. Hydrogen bonds for Compound 24 [ $\text{\AA}$ and $^{\circ}$ ]. .....	283
Table A71. Hydrogen bonds for compound 26 [ $\text{\AA}$ and $^{\circ}$ ]. .....	283

Table A72. Hydrogen bonds for compound 28 [ $\text{\AA}$ and $^\circ$ ].	284
Table A73. Hydrogen bonds for compound 41 [ $\text{\AA}$ and $^\circ$ ].	284
Table A74. Hydrogen bonds for compound 46 [ $\text{\AA}$ and $^\circ$ ].	284
<b>CURRICULUM VITAE</b>	<b>285</b>

## LIST OF TABLES

Table 3.1: Mass spectrometric data of ligands.....	53
Table 3.2: Selected absorption peaks for compounds <b>15-17</b> and <b>36</b> .....	68
Table 3.3: $\lambda_{\max}$ of selected compounds .....	72
Table 3.4: Selected Mass spectrometric data of metal complexes.....	79
Table 3.5: $^1\text{H}$ NMR Chemical Shifts .....	80
Table 3.6: Selected Crystallographic data for compounds . .....	87
Table 3.7: Selected bond lengths and angles for compounds <b>15, 16</b> and <b>17</b> . .....	94
Table 3.8: Selected bond lengths and angles of compounds <b>18, 19</b> and <b>23</b> .....	100
Table 3.9: Hydrogen bonds for Compound <b>18</b> [ $\text{\AA}$ and $^\circ$ ]. .....	101
Table 3.10: Selected bond lengths and angles of compound <b>24</b> .....	104
Table 3.11: Hydrogen bonds for Compound <b>24</b> [ $\text{\AA}$ and $^\circ$ ]. .....	106
Table 3.12: Average bond lengths of selected first row transition $\text{M}^{2+}$ ions benzimidazole complex derivatives. ....	108
Table 4.1: Selected IR data for compound <b>25-29</b> .....	124
Table 4.2: Selected Crystallographic data of compounds <b>25-28</b> .....	125
Table 4.3: Selected bond lengths and angles of compounds <b>25-28</b> .....	126
Table 4.4: Hydrogen bonds for compound <b>28</b> [ $\text{\AA}$ and $^\circ$ ]. .....	134
Table 4.5: UV-vis absorption data for complexes 25-29.....	135
Table 4.6: Crystallographic data for compounds <b>4, 30, 41, 42a, 41b, 41c</b> and <b>46</b> .....	150
Table 4.7: Bond lengths and angles of compounds <b>4, 30, 41, 42a,42b, 42c</b> and <b>46</b> .....	151
Table 4.8: Hydrogen bonds for compound <b>41</b> [ $\text{\AA}$ and $^\circ$ ]. .....	157
Table 4.9: Hydrogen bonds for compound <b>46</b> [ $\text{\AA}$ and $^\circ$ ]. .....	164

Table 4.10: $\lambda_{\max}$ values of selected Pt(II) complexes.....	166
Table 4.11: $IC_{50}$ values ( $\mu M$ ) of selected Pt(II) complexes .....	173

## LIST OF FIGURES

Figure 1.1: Chemical structures of the most important anticancer metal drugs. ....	4
Figure 1.2: Activation of cisplatin. ....	6
Figure 1.3: Types 1 & 2 of the proposed ligand system .....	9
Figure 1.4: Type 2 of the proposed ligand system; showing the three domains; a platinum binding domain, spacer-linker domain and a recognition domain.....	10
Figure 1.5: Substitution of Pt(II), the trans effect. ....	11
Figure 3.1: <sup>1</sup> H NMR spectrum of compound <b>1</b> in CDCl <sub>3</sub> .....	53
Figure 3.2: <sup>1</sup> H NMR spectrum of compound <b>2</b> in CDCl <sub>3</sub> .....	54
Figure 3.3: <sup>1</sup> H NMR spectrum of compound <b>3</b> in DMSO-d <sub>6</sub> .....	55
Figure 3.4: <sup>1</sup> H NMR spectrum of compound <b>5</b> in CDCl <sub>3</sub> .....	56
Figure 3.5: <sup>1</sup> H NMR spectrum of compound <b>7</b> in CDCl <sub>3</sub> .....	57
Figure 3.6: <sup>1</sup> H NMR spectrum of compound <b>8</b> in DMSO-d <sub>6</sub> .....	58
Figure 3.7: <sup>1</sup> H NMR spectrum of compound <b>9</b> in CDCl <sub>3</sub> .....	59
Figure 3.8: <sup>1</sup> H NMR spectrum of compound <b>11</b> in CDCl <sub>3</sub> .....	59
Figure 3.9: <sup>1</sup> H NMR spectrum of compound <b>12</b> in CD <sub>3</sub> OD .....	60
Figure 3.10: Tautomeric and resonance forms of acetyl and phenyl derivatives .....	61
Figure 3.11: Stack plot of compound <b>3</b> in CD <sub>2</sub> Cl <sub>2</sub> ; broadening of the amide peak .....	62
Figure 3.12: Stack plot of compound <b>4</b> in CD <sub>2</sub> Cl <sub>2</sub> ; broadening of the amide peak .....	62
Figure 3.13: Temperature stack plot of compound <b>11</b> in CD <sub>2</sub> Cl <sub>2</sub> .....	63
Figure 3.14: Drawing of compound <b>9</b> .....	64
Figure 3.15: Metal complexes of compound <b>9</b> .....	65
Figure 3.16: IR spectrum of compound <b>15</b> . ....	67

Figure 3.17: IR spectrum of compound <b>18</b> .	68
Figure 3.18: IR spectrum of compound <b>19</b> .	69
Figure 3.19: IR spectrum of compound <b>24</b> .	70
Figure 3.20: UV-vis absorption trace of compounds <b>16</b> and <b>17</b> in 3 mL CH <sub>2</sub> Cl <sub>2</sub> .	71
Figure 3.21: UV-vis absorption trace of compound <b>4</b> , Hmbchca, in 3 mL CH <sub>2</sub> Cl <sub>2</sub> .	71
Figure 3.22: Mass spectrometric trace of compound <b>15</b> .	73
Figure 3.23: Mass spectrometric trace of compound <b>16</b> .	74
Figure 3.24: Mass spectrometric trace of compound <b>17</b> .	74
Figure 3.25: Mass spectrometric trace of compound <b>18</b> .	75
Figure 3.26: Mass spectrometric trace of compound <b>19</b> .	76
Figure 3.27: Mass spectrometric trace of compound <b>20</b> .	76
Figure 3.28: Mass spectrometric trace of compound <b>21</b> .	77
Figure 3.29: Mass spectrometric trace of compound <b>22</b> .	77
Figure 3.30: Mass spectrometric trace of compound <b>24</b> .	78
Figure 3.31: <sup>1</sup> H NMR spectrum of compound <b>16</b> in CDCl <sub>3</sub> .	81
Figure 3.32: <sup>1</sup> H NMR spectrum of compound <b>20</b> in CDCl <sub>3</sub> .	81
Figure 3.33: <sup>1</sup> H NMR spectrum of compound <b>21</b> .	82
Figure 3.34: <sup>1</sup> H NMR spectrum of Ni(dmmbp) <sub>2</sub> .	82
Figure 3.35: <sup>1</sup> H NMR spectrum of compound <b>30</b> .	83
Figure 3.36: <sup>1</sup> H NMR spectrum of compound <b>23</b> in CDCl <sub>3</sub> .	85
Figure 3.37: <sup>1</sup> H NMR spectrum of compound <b>18</b> in CDCl <sub>3</sub> .	86
Figure 3.38: ORTEP diagram of compound <b>15</b> .	88
Figure 3.39: Crystal lattice of compound <b>15</b> .	89

Figure 3.40: Crystal lattice of compound <b>15</b> ; C-H $\cdots\pi$ stacking interactions .....	90
Figure 3.41: ORTEP diagram of compound <b>16</b> .....	91
Figure 3.42: Crystal lattice of compound <b>16</b> point to face interaction.. .....	92
Figure 3.43: ORTEP diagram of compound <b>17</b> .....	93
Figure 3.44: Crystal lattice of compound <b>17</b> .. .....	95
Figure 3.45: ORTEP diagram of compound <b>23</b> .....	96
Figure 3.46: ORTEP diagram of compound <b>23</b> showing packing in a unit cell.....	96
Figure 3.47: ORTEP diagram of compound <b>19</b> .....	97
Figure 3.48. Crystal lattice of compound <b>19</b> ; orientation of V=O bonds along c-axis.....	98
Figure 3.49: ORTEP diagram of compound <b>18</b> .....	99
Figure 3.50: ORTEP diagram of compound <b>18</b> 's crystal lattice. Sites of H-bonding ....	101
Figure 3.51: A tail – tail Hydrogen – $\pi$ interactions of (amb)Ni(dmmbp) <sub>2</sub> .....	102
Figure 3.52: ORTEP diagram of Compound <b>24</b> .....	103
Figure 3.53: ORTEP diagram of Compound <b>24</b> (intramolecular H- bonding).....	105
Figure 3.54: ORTEP diagram of Compound <b>24</b> (intermolecular H- bonding).....	105
Figure 4.1: Active platinum compounds.....	112
Figure 4.2: ORTEP diagram of compound <b>35</b> and a generic free ligand. ....	114
Figure 4.3: <sup>1</sup> H NMR spectrum of compound <b>25</b> in CDCl <sub>3</sub> .....	117
Figure 4.4: <sup>1</sup> H NMR spectrum of compound <b>26</b> in CDCl <sub>3</sub> .....	118
Figure 4.5: <sup>1</sup> H NMR spectrum of compound <b>27</b> in CDCl <sub>3</sub> .....	119
Figure 4.6: <sup>1</sup> H NMR spectrum of compound <b>28</b> in CDCl <sub>3</sub> .....	120
Figure 4.7: <sup>1</sup> H NMR spectrum of compound <b>29</b> in CDCl <sub>3</sub> .....	121
Figure 4.8 : The aromatic region of the <sup>1</sup> H NMR of compound <b>27</b> and its <b>cis</b> -isomer. .	122



Figure 4.9: Compound <b>25</b> dissolved in 0.5 mL <i>d</i> -acetonitrile / 200 $\mu$ L D <sub>2</sub> O solution ...	123
Figure 4.10: IR spectrum of compound <b>25</b> .....	124
Figure 4.11: ORTEP diagram of compound <b>25</b> .....	127
Figure 4.12: Crystal lattice packing diagram of compound <b>25</b> .....	128
Figure 4.13: ORTEP diagram of compound <b>26</b> .....	129
Figure 4.14: Crystal lattice packing diagram of compound <b>26</b> , view along the b-axis. .	130
Figure 4.15: ORTEP diagram of compound <b>27</b> .....	130
Figure 4.16: Crystal lattice packing diagram of compound <b>27</b> ; C-H $\cdots\pi$ interactions .....	131
Figure 4.17: Cooperative slipped $\pi$ -stacking in compound <b>27</b> , view along the a-axis. ..	132
Figure 4.18: ORTEP diagram of compound <b>28</b> .....	133
Figure 4.19: Crystal lattice packing diagram of compound <b>28</b> , view along the b-axis. .	133
Figure 4.20: UV-vis spectrum of compound <b>25</b> in 3 mL dichloromethane.....	134
Figure 4.21: Mass spectrometric trace of compound <b>30</b> .....	138
Figure 4.22: Mass spectrometric trace of compound <b>31</b> .....	139
Figure 4.23: Mass spectrometric trace of compound <b>32</b> .....	140
Figure 4.24: Mass spectrometric trace of compound <b>33</b> .....	141
Figure 4.25: Mass spectrometric trace of compound <b>34</b> .....	142
Figure 4.26: Infrared trace of compound <b>36</b> .....	143
Figure 4.27: Mass spectrometric trace of compound <b>36</b> .....	143
Figure 4.28: Aromatic region of the <sup>1</sup> H NMR spectrum of compound <b>36</b> . .....	143
Figure 4.29: Mass spectrometric trace of compound <b>37</b> .....	144
Figure 4.30: Infrared trace of compound <b>37</b> .....	144
Figure 4.31: Mass spectrometric trace of compound <b>38</b> .....	145

Figure 4.32: Mass spectrometric trace of compound <b>39</b> .....	146
Figure 4.33: Mass spectrometric trace of compound <b>40</b> .....	147
Figure 4.34: Mass spectrometric trace of compound <b>41</b> .....	148
Figure 4.35: Mass spectrometric trace of compound <b>46</b> .....	149
Figure 4.36: ORTEP diagram of compound <b>4</b> .....	152
Figure 4.37: Interactions and contacts in the crystal lattice of compound <b>4</b> .....	152
Figure 4.38: ORTEP diagram of compound <b>30</b> .....	153
Figure 4.39: Unit cell of compound <b>30</b> .....	154
Figure 4.40: ORTEP diagram of compound <b>30</b> packing and H- bonding. ....	155
Figure 4.41: ORTEP diagram of compound <b>41</b> .....	156
Figure 4.42: “Capped-sticks” ORTEP diagram of compound <b>41</b> ; packing and H- bonding .....	157
Figure 4.43: Packing of compounds <b>42a</b> and <b>42b</b> . ....	158
Figure 4.44: ORTEP diagram of compounds <b>42b</b> with a co-crystal of a trans Pt(IV) complex, <b>42a</b> .....	158
Figure 4.45: ORTEP diagram of compound <b>42a</b> .....	159
Figure 4.46: “Capped-sticks” ORTEP diagram of compound <b>42a</b> C-H··· $\pi$ interactions	159
Figure 4.47: “Capped-sticks” ORTEP diagram of compounds <b>42a</b> and <b>42b</b> ; packing ..	160
Figure 4.48: ORTEP diagram of compound <b>42c</b> ; packing and H- bonding interactions	161
Figure 4.49: “Capped-sticks” ORTEP diagram of compound <b>42c</b> H- bonding between chlorides and amide hydrogens in the crystal lattice. ....	162
Figure 4.50: “Capped-sticks” ORTEP diagram of compounds <b>42c</b> packing and some interactions in the crystal lattice. ....	162

Figure 4.51: ORTEP diagram of compound <b>46</b> .	163
Figure 4.52: “Capped-sticks” ORTEP diagram of compound <b>46</b> ; H-bonding.	164
Figure 4.53: “Capped-sticks” ORTEP diagram of compound <b>46</b> semi- encapsulation of the metal, preventing possible interactions with thiols such as glutathione.	165
Figure 4.54: UV-vis spectrum of GSH and compound <b>37</b> in 100% DCM, 70% MeOH/ 30% water, and 80% DMSO/ 20% water	168
Figure 4.55: UV-vis spectrum of GSH, compound <b>37</b> and DMSO/water reaction solution system.	168
Figure 4.56: MTT Assay of Cell line: <b>DU145</b> ; Cytotoxicity of cisplatin and compound <b>37</b>	169
Figure 4.57: MTT Assay of Cell line: <b>DU145</b> . Cytotoxic profiles of compounds <b>28</b> , <b>42b</b> and <b>36</b> .	170
Figure 4.58: MTT Assay of Cell line: <b>RWPE-1</b> . Cytotoxic profiles of compds <b>28</b> , <b>42b</b> and <b>36</b> .	171
Figure 4.59: MTT Assay of Cell line: <b>PC3</b> . Cytotoxic profiles of compounds <b>28</b> , <b>42b</b> and <b>36</b> .	171
Figure 4.60: MTT Assay of the <b>LNCaP</b> Cell line: Cytotoxic profiles of compounds <b>28</b> , <b>42b</b> and <b>36</b> .	171
Figure 4.61: DU145 Cell line: Cytotoxic profiles of compds <b>27</b> , <b>36</b> , <b>42d</b> and <b>32</b> .	172
Figure 4.62: PC3 Cell line: Cytotoxic profiles of compds <b>27</b> , <b>36</b> , <b>42d</b> and <b>32</b> .	172
Figure 4.63: LNCaP Cell line: Cytotoxic profiles of compds <b>27</b> , <b>36</b> , <b>42d</b> and <b>32</b> .	172

## CHAPTER I

### INTRODUCTION

Metalloenzymes and metalloproteins have been of intense interest partly because of their enormous ability to enhance rates of reactions that are orders of magnitude unparalleled by the best chemical catalysts [1-3]. As a result, they have found utility in biofuel production and pharmaceutical processes such as vaccine production and biocells [4-9]. These enzymes are able to enhance reaction rates by utilizing one or a combination of six mechanisms; proximity and orientation effects, acid-base catalysis, covalent catalysis, electrostatic catalysis, preferential binding to the transition state complex and metal ion catalysis[1-3, 10-14].

The discrimination and preference of  $\beta$ -D-glucopyranose over other pyranoses as a substrate of hexokinase in glycolysis is an example of an enzyme that uses proximity and orientation effects. That is, hexokinase's ability might be because  $\beta$ -D-glucopyranose is the only monosaccharide with all its hydroxyl groups in the equatorial position. As such, it is able to engage in hydrogen bonding with all the hydroxyl groups of the monosaccharide. Thus, the binding of glucose for phosphorylation requires the cooperative interactions of all the hydroxyl groups with specific amino acid residues located in and around the active site of the enzyme. The alignment or orientation of these bulky groups might also be critical for both substrate docking at the active site and stabilization [1, 15].

Another mechanistic approach involves the allosteric binding of co-factors to these enzymes. Through these interactions, co-factors are able to induce activation or deactivation of the enzyme by either causing global or local changes. The binding in allosteric sites causes conformational changes resulting in re-positioning of residues in close proximity to the binding site or within the active site. Consequently, residues that once helped to stabilize a substrate will no longer be there resulting in an alteration of the enzyme's activity. That is, subsequent substrates are prevented from docking. An enzyme that uses this approach is ribonucleotide reductase which converts ribose to deoxyribose. The binding of adenosine triphosphate (ATP) to an allosteric site of a subunit of ribonucleotide reductase brings the phenolic side chain of tyrosine within reach for a radical reaction with the Fe(III)-O-Fe(III) cluster. This initiates a cascade of events that converts ribose to deoxyribose via abstraction of hydrogen. The binding of ATP to a different allosteric site deactivates the enzyme. Through these interactions, up-regulation and down regulation of pathways in biological systems are achieved [1].

Metal ion catalysis usually involves transition and p-block metal centers such as Mn, Fe, Ni, Zn and Cu [1, 16-17]. In Cu, Zn-superoxide dismutase for example, the two metals are bridged and bound by the imidazole of the amino acid residue histidine. Superoxide dismutase catalyzes the conversion of superoxide into hydrogen peroxide and oxygen [14, 18-25]. Without the action of superoxide dismutase and a cascade of enzymes, the build up of superoxide, generated during the production of ATP, leads to oxidative stress. Left unchecked, essential components of the cell like the cell membrane are damaged. A damaged cell membrane impairs cell homeostasis, the cell's ability to

regulate flow of nutrients and waste to maintain optimal conditions necessary for cytoplasmic enzymes.

The general structure of these metalloproteins could be described as having primary and secondary coordination spheres. The first coordination sphere, for discussion in this work, refers to the metal binding site, while the second coordination sphere refers to the portion of the enzyme that can participate in substrate stabilization and functionality[26]. The ability of metalloenzymes to perform their respective tasks is largely due to hydrogen bonding, as evident in hexokinase and other non-covalent interactions among side chains of amino acid residues. Desiraju *et. al.* defines the hydrogen bond ,  $X-H\cdots Y-Z$ , as an attractive interaction in which an electropositive H atom intercedes between two electronegative species X and Y( $X, Y = F, O, N$ ) and brings them closer together [27-28]. The strength of these interactions are not only dependent on the electronegativity of X and Y, but also the directionality or angle of contact [27-28]. These interactions have energies between 0.5 to 40 kcal mol<sup>-1</sup> [27] and play key roles in the eventual structure and function of these metalloenzymes. They also affect the primary, secondary and tertiary folding of these enzymes, and in some cases also help stabilize substrate and transition state intermediates of the reactions they catalyze. Interactions between amino acid residues are also utilized in substrate recognition, selectivity and specificity [29]. Additionally, weaker hydrogen bond interactions involving  $X = C, O, N$  and  $Y = O, N, Cl, M-Cl$  have been reported to play important roles in the stabilization of solid-state structures [27-28, 30]. Models to study these enzymes have involved imidazole-transition metal complexes partly because of the numerous histidine bound metalloenzymes [14, 31]. However, these complexes do not show the

same selectivity or secondary coordination environment. Furthermore, imidazole complexes are relatively difficult to synthesize compared to benzimidazole [32]. Benzimidazoles bind in a similar fashion as imidazoles and also offer steric bulk that can be used to shape the secondary coordination environment. Chapter III will examine the complexation of novel functionalized benzimidazole derivatives to selected first row transition metals under basic condition.

Increasingly, transition metals are being studied not only for their catalytic properties [33-34] but also for their role in therapeutics as cures for diseases and disorders [35-44]. Figure 1.1 shows the structures of the most important anticancer metal drugs.

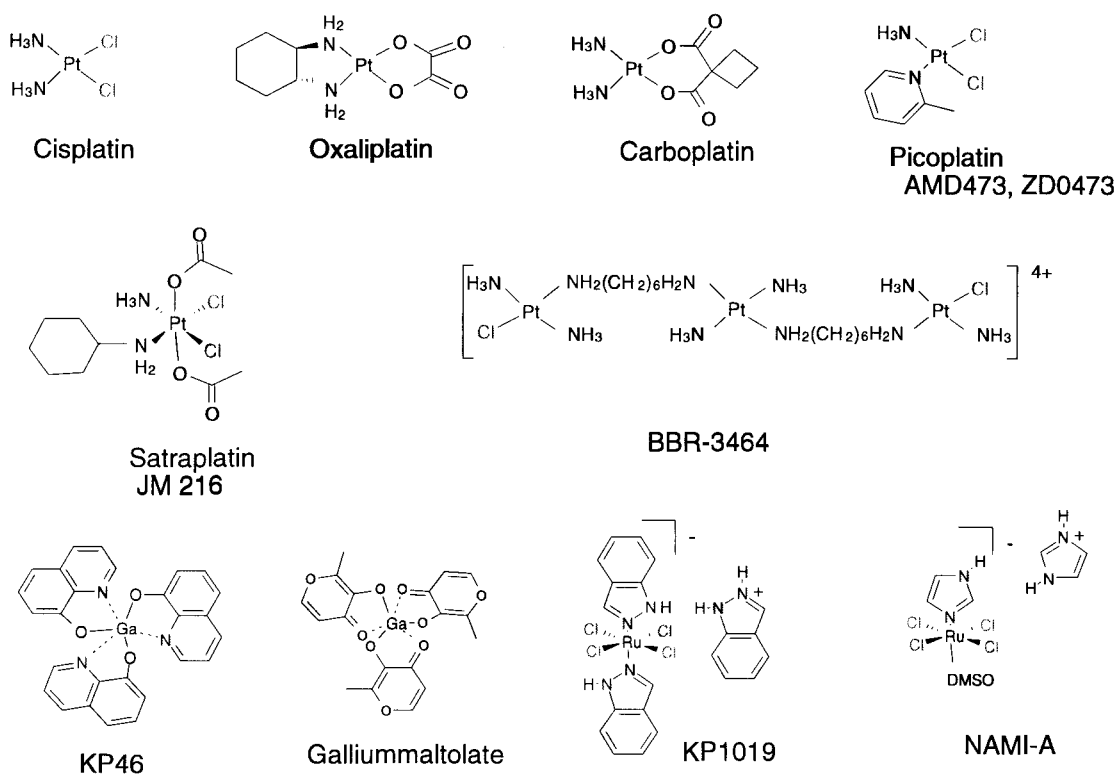


Figure 1.1: Chemical structures of the most important anticancer metal drugs [45].

Vanadium complexes are being investigated for their insulin-like properties as treatments for diabetes [46]. Copper [47-54], ruthenium, rhodium, palladium, osmium and iridium are all under investigation for their anti-tumor properties based on the success of platinum compounds such as cisplatin (diamminedichloroplatinum(II)) [45, 55].

For nearly 40 years, the biological activity of cis-diamminedichloroplatinum(II), known as cisplatin, and its derivatives (e.g. carboplatin) have been the focus of extensive investigation in an attempt to elucidate their mode of action toward a variety of human malignancies [45, 56-58]. Cisplatin is an effective therapeutic toward testicular cancer, and is used to treat ovarian, head and neck, esophageal, cervical, and non-small cell lung cancer, as well as melanoma, bladder carcinoma, and neuroblastoma [44-45, 59-62]. A major drawback associated with the use of cisplatin and other Pt (II) compounds is renal toxicity [45, 59], which can be mitigated by hydration and diuresis therapy. In addition, cisplatin and carboplatin have limited solubility in water and are administered intravenously. Of the thousands of platinum compounds synthesized, only a few have reached clinical trials and still fewer have received approval for clinical use. Newer derivatives have attempted to exploit steric hinderance of associated bulky ligands in retarding thiol coordination; a process believed to play a central role in the deactivation of Pt drugs [45, 63-65]. Other studies have focused on developing orally active Pt compounds containing Pt (IV), which is more inert to ligand substitution compare to Pt (II). The Pt (IV) species are thought to be activated by reduction to Pt (II) by intra- and extra-cellular agents prior to reaction with DNA[66].



Cisplatin is believed to be activated within the cell by the substitution of both chlorides with water. The substitution within the cell is partly predicated on the decrease in chloride concentration. Figure 1.2 shows such an activation. Cisplatin's cytotoxic effects comes from binding to N7 of guanine in nuclear DNA [14, 55-57, 62, 67-80] and an indepth discussion of the mode of action of cisplatin can be found in Chapter IV.

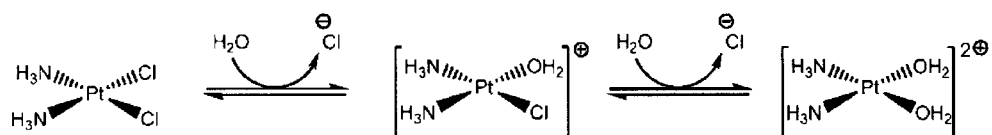


Figure 1.2: Activation of cisplatin.

However, undesirable interactions such as reaction of cisplatin with His19 of Cu,Zn superoxide dismutase [81], ubiquitin [82], albumin [83-85], hemoglobin [86], transferrin [87-89] and other proteins [90-91]; all lead to deactivation and contribute to drug resistance. Furthermore, 65 to 98% of cisplatin administered intravenously after a day is bound to blood plasma proteins with most of the Pt (50-61%) bound to albumin [85]. The binding of cisplatin to these proteins, in many cases, interferes with metabolic pathways and accounts for numerous side-effects including hyperzincuria [85] and hypozincemia [85], associated with cisplatin chemotherapy. Thus, the need for more effective and less toxic drugs. To date only KP1019 (indazolium *trans*-[tetrachlorobis(1Hindazole) ruthenate(III)], FFC14a) [92] and NAMI-A (imidazolium *trans*-[tetrachloro(DMSO) (imidazole) ruthenate(III)] [93] have entered clinical evaluation[45].

A major challenge for most platinated complexes as potential antitumor compounds is reaching their target (nuclear or mitochondrial DNA). This may be due to, in addition to the afore mentioned, the low intracellular concentration attributable to

either low influx or high efflux, and deactivation by thiols. This challenge may be addressed by making the ligands of these platinated compounds more non-polar thereby facilitating diffusion across the cell membrane. Such an approach would also circumvent the reliance on transport proteins that may or may not be present in cell membranes of both small and large cancer cells. Although this approach does not address water solubility, injection of these “compounds” directly into tumors, for instance, makes their water solubility less critical. Additionally, development of new drug delivery systems and the incorporation of these “compounds” into delivery vessels such as liposomes circumvents water solubility. It should be noted that the incorporation of peptide linkages in the second generation of Pt complexes presented in this work and discussed later in this chapter would enhance the water solubility of some of these novel compounds.

Chances for Pt-DNA adduct formation are enhanced during the S-phase of cell division when DNA is unwound and separated from proteins such as histones into double or single strands. The “exposed” DNA strands are now susceptible to reactions with activated platinated di-aqua species, resulting in Pt- DNA adduct formation. The formation of Pt-DNA adducts prevents a cascade of enzymes from “decoding” the DNA and subsequent production of mRNA; a template for the production of amino acids, the building blocks of proteins/enzymes. That is, adduct formation, monofunctional or bifunctional, prevents transcription, translation and replication. As a result, apoptosis is triggered.

Cancerous cells go through the S-phase of cell division more frequently than normal cells, so with more precise targeting, side effects like kidney failure associated with the administration of these platinated species can be minimized. Out of thousands of

platinum compounds synthesized over the years, only a few have been clinically useful (Figure 1.1). Although many compounds have been found to exhibit more potent cytotoxic activity against cancerous cell lines in the lab, none has translated into a comparable or more potent candidate in clinical trials. This is partly because these compounds lack specificity and are unable to differentiate between normal cells and cancerous cells and therefore are not clinically useful.

Reedijk and colleagues have introduced a new class of platinated compounds that are tagged with fluorophores [94]. These compounds are activated *in vivo* through the action of esterases. This approach serves two fundamental purposes. The first of which is to be able to track the platinated compound through the cell. However, this has proven to be more challenging than previously thought because of the limitations of current technology. That is, current technology does not allow the confirmation of the attachment of the platinum component *in vivo* to the activated fluorophore, making it difficult to ascertain the pathway and mechanism of the platinated compound. However, accumulations of fluorophores are in agreement with previous pathways of the action of cisplatin [68]. The second rationale behind this approach is to use the fluorophore as agents of intercalation (between the bases in the DNA helix), thereby facilitating the orientation and binding of the compounds to DNA[68, 95-98].

The framework and design of our platinated compounds shows more flexibility and promise than any other benzimidazole moieties seen in literature [13, 99-107]. The addition of peptidic and in some cases lipophilic features, are all aimed at exploiting the properties of the cell membrane and increasing cellular concentrations of the platinated species. Furthermore, the peptidic sites provide hydrogen bonding sites, similar to

cisplatin, enabling the compounds to bind to DNA. Also, the peptidic sites add water solubility, a property most of these compounds lack. This approach also circumvents the reliance on transport proteins that may or may not be present in both small and large cancer cells. Additionally, the sterics of the ligands minimize interactions and reactions with thiols like glutathione [108-111].

Two types of ligands are presented in this work (Figure 1.3). Ligands of Type 1 are a direct coupling of an acyl chloride moiety to the benzimidazole. As, shown in Figures 1.3 and 1.4, ligands of type 2 have a linker between the metal binding domain and the recognition domain.

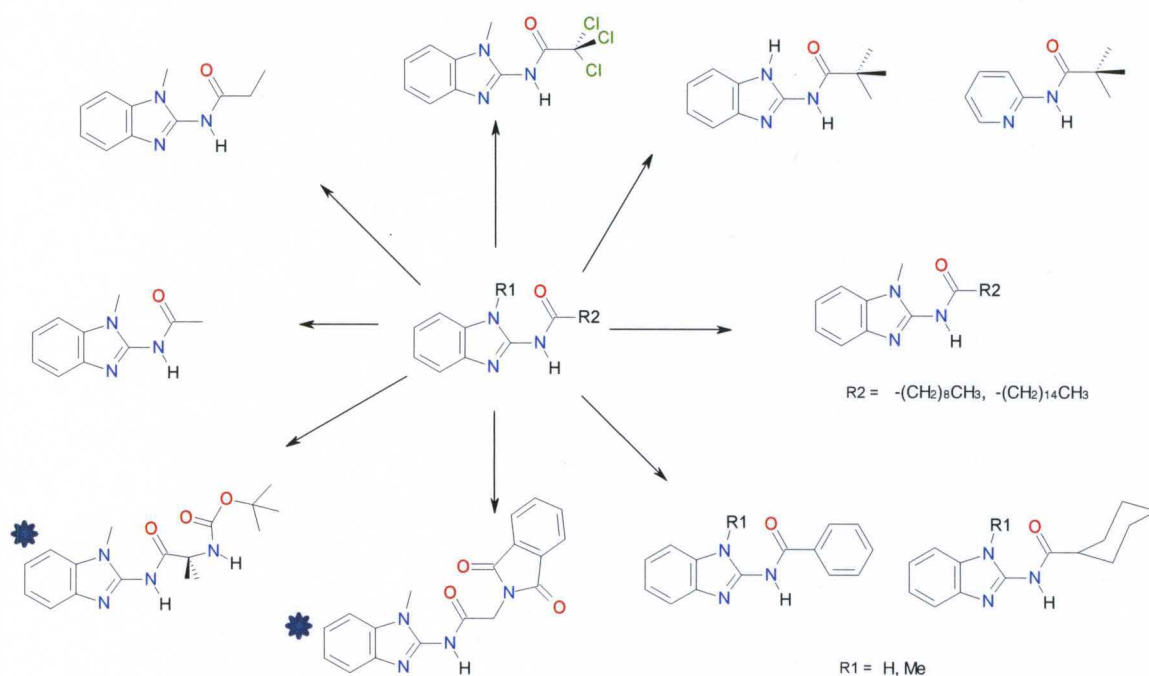


Figure 1.3: Types 1 & 2 of the proposed ligand system

Additionally, the proposed ligand system lends itself to modifications such as substitution of the binding domain with an imidazole or pyridine for example, the

recognition domain with an amino acid, a polypeptide, dye, antibody or a specific sequence of oligonucleotides. These variations will shed light on membrane permeability and mobility of these platinated species through the cell.

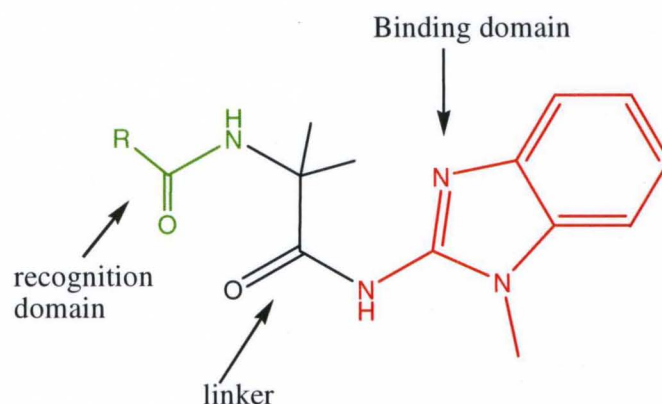


Figure 1.4: Type 2 of the proposed ligand system; showing the three domains; a **platinum binding domain**, spacer-linker domain and a **recognition domain**.

Reactions involving transition metals, to a large extent are governed by the number of electrons in the d-orbital. Platinum(II), a  $d^8$  ion, preferably forms square planar compounds. It is the most studied with regards to substitution chemistry due to its slow reactivity compared to other  $d^8$  ions; Pd(II), Au(III), Rh(I) and Ir(I). These reactions usually proceed with retention of stereochemistry at the metal center and are affected by factors that include *trans* effect, *trans* influence, type of ligand (nucleophilic or electrophilic), *cis* effect or steric effects and solvent type (coordinating or non coordinating) [112].

The most considered and utilized factor in the synthesis of cisplatin analogs is the *trans* effect. This is evident in the choice of tetrachloroplatinate(II) as starting material[54, 59, 63-64, 75, 113-115]. *Trans* effect can be defined as the ability of a bound ligand to weaken the metal-ligand bond *trans* to it. This ability to weaken a bond is also

affected by any pi-back bonding the bound trans ligand may be engaged in with the metal [116]. Consequently, the incoming ligand substitutes at the site of the weakest bond. It should be noted that the extent to which each factor exerts its influence is dependent on the conditions [112, 117-120]. Figure 1.5 shows the *trans* effect.

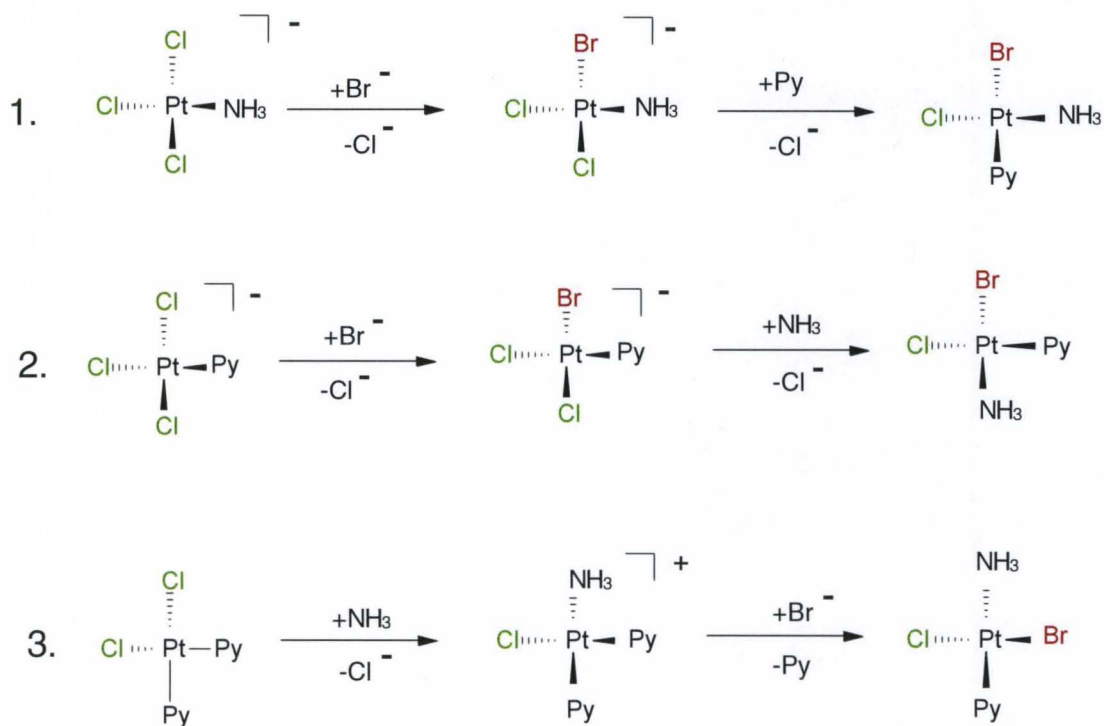


Figure 1.5: Substitution of Pt(II), the *trans* effect.

The first reaction series of Figure 1.5 shows the substitution of a chloride ion by a bromide and pyridine. This illustrates the effect of one of the chloride ions and bromide ion directing the incoming nucleophile to the *trans* position. The second step shows the bromide ligand having a larger *trans* effect than the chloride. Subsequent reactions also show the effects of bromine and pyridine ligands. It is worth noting that in the first two reaction series, both halides are *cis* to each other whereas a *trans* product is obtained in

the latter. Thus, the stereochemistry of a product can be controlled by the order in which ligands/nucleophiles are introduced in the reaction and the starting material. The ranking of the *trans* effect of several species/ligands is shown below.

$\text{CO}, \text{CN}^-, \text{C}_2\text{H}_4 > \text{PR}_3, \text{H}^- > \text{CH}_3^- > \text{C}_6\text{H}_5^-, \text{NO}_2, \text{I}^-, \text{SCN}^- > \text{Br}^-, \text{Cl}^- > \text{Py}, \text{NH}_3, \text{OH}^-, \text{H}_2\text{O}$  [112].

It can be seen from the ranking that iodine possesses a higher *trans* effect than chlorine. As a result, one protocol for the synthesis of cisplatin analogues presented in this dissertation utilizes this property. Thus, the starting material tetrachloroplatinate(II) is converted to tetraiodoplatinate(II) prior to its reaction with desired ligands. The pros and cons of this reaction route is also presented in Chapter IV.

This dissertation evaluates the synthesis of novel amide functionalized 2-amino benzimidazole ligands and their reactivity with selected biologically relevant first row transition metals and platinum. It highlights the successful synthesis of a novel dipeptidic platinum moiety, the first in a series and a framework aimed at facilitating Pt-DNA adduct formation and the minimization of Pt- thiol interactions. The dissertation also examines the packing arrangements of these metal complexes in an attempt to elucidate the types of interactions within their crystal lattice, their second coordination environment, and their potential as biological models. Furthermore, the cytotoxic profiles of selected platinated moieties contained in this series are compared to cisplatin, the leading drug against cancer.

## CHAPTER II

### SYNTHESIS, CHARACTERIZATION, AND ANALYSIS PROCEDURES

This chapter deals with the synthesis, characterization and analysis of the compounds used in this dissertation. Ligands prepared for this work, with the exception of a pyridine analog, have either a 1-methylbenzimidazole or 1-H-benzimidazole repeat motif. Although some compounds were prepared with similar protocols, they have been kept separate because of differences in reaction time and yield.

#### **A: Procedures for Physical data collection:**

##### **1. Mass Spectrometry (MALDI-TOF)**

Data for all the compounds reported in this dissertation, were collected on a PE Biosystems Voyager DE-Pro mass spectrometer with an average laser shot of 70 in the positive mode with 2,5-dihydroxy benzoic acid as the matrix of choice. Laser intensities were varied for each sample to make sure that resultant peaks were not due to laser assisted reactions. The experimental peaks reported in this work are isotopomeric peaks with the highest peak intensity in a given cluster.

##### **2. X-ray Crystallography**

X-ray crystal structures were determined by Dr. Mark Mashuta at the X-ray diffraction laboratory, Department of Chemistry, University of Louisville. A complete listing of data collection, cell parameters, atomic coordinates, bond lengths and angles



are located in the appendix. A single X-ray quality crystal was mounted on a 0.05 mm CryoLoop with Paratone oil. CryoLoop was mounted on a Bruker SMART APEX CCD diffractometer, with the loop under a stream of liquid nitrogen to reduce the temperature to 100 K. A monochromated Mo K $\alpha$  radiation source (0.71073 Å) was used as an X-ray source, and frame  $\omega$ -scan exposures were collected using the SMART software package. Frame data was processed using the SAINT program to determine the final unit cell parameters. The SADABS program was used to correct independent reflections for absorption.

Once data were processed, structures were solved by either direct methods or Patterson Methods, and structures were refined by least-squares methods on F<sup>2</sup>. This was done using SHELXL-97, which is incorporated into the SHELXTL suite of programs. Non-hydrogen atoms were refined anisotropically, unless they were being modeled for disordered. Hydrogen atoms attached to carbon atoms were generally placed in a geometrically ideal position and refined as a riding model. Hydrogen atoms attached to nitrogen or oxygen atoms were allocated difference maps and refined isotropically, unless the heavy atom was modeled for disorder.

### **3. KBr-IR Data Acquisition**

Infrared data were acquired on a Mattson Galaxy series 5000 FTIR using the diffuse reflectance Infrared Fourier transform Spectra mode (32 scan cycles). Pellet samples were prepared by grinding approximately 0.500g KBr (oven dried), with 150mg of the complex.

#### 4. NMR Data Acquisition

The NMR data were acquired on a three-channel Inova 500 MHz spectrometer with pulse-field capability. Sample preparation for  $^1\text{H}$  NMR identification spectra were generally performed by dissolving approximately 5 mg of sample in 0.5 mL of deuterated solvent.  $^1\text{H}$  NMR spectra were typically acquired by combining 8, 16 and 32. Spectra were acquired with a 45 degrees pulse and an average of two seconds delay.  $^{13}\text{C}$  NMR spectra were acquired using standard methods over a 14 hour period. The stars in the spectra in this work represent solvent peaks.

#### 5. NMR Experiments

The general procedure for NMR experiments involves dissolving a measured amount of a purified complex in a solvent system of deuterated acetonitrile and deuterated water (2:1v) in an NMR tube. A  $^1\text{H}$  NMR spectrum is collected before any other reactant was added. Sample tubes were shimmed and data was collected overnight at regular time intervals. For insoluble compounds of this system, deuterated chloroform was used. Temperature based experiments were carried out in deuterated dichloromethane from  $-80\text{ }^\circ\text{C}$  -  $25\text{ }^\circ\text{C}$  at  $10\text{ }^\circ$  intervals.

#### 6. UV-vis Titration

UV-vis spectrophotometric data was obtained using a Varian Cary 50 Bio UV-visible spectrophotometer. Scanning was done at a medium rate from 1100 nm to 200 nm.  $\lambda_{\text{max}}$  were determined from aliquots of samples dissolved in 0.5 mL deuterated chloroform placed in 10 mL quartz cuvette containing 3 mL dichloromethane.

## 7. Bioassay

Bioassays were performed in Dr. Paula Bates laboratory by Lavona K. Casson at the Brown Cancer Center of the University of Louisville. 150  $\mu\text{L}$  of culture media, ~ 1000 cells was pipetted into individual wells of a 96 well plate. The culture contained Dulbecco's Modification of Eagle's Medium supplemented with 10% heat inactivated fetal bovine serum, 100 U/mL penicillin and 100  $\mu\text{g}/\text{mL}$  streptomycin. 95 out of the 96 wells were incubated for 24 hours at 37  $^{\circ}\text{C}$  with 5%  $\text{CO}_2$ . After this incubation period, the culture plates were treated with compounds of varying concentration in a 0.1% DMSO in water (by volume) solvent. Sample plates were treated with similar concentrations of cisplatin in the same solvent, for standard comparison. The sample plates were analyzed for remaining cells after five days of incubation using the MTT method. This method uses a digestible dye, MTT [3-(4,5-dimethylthiazol-2-yl)2,5-diphenyltetrazolium bromide], to quantify the number of living cells present in a given culture medium.

16.7  $\mu\text{L}$  of a 0.5 % solution of MTT in buffer solvent was added to each well, and the plates were allowed to incubate for 4 hours to allow cells time to digest the dye. 83.3  $\mu\text{L}$  of 0.01 M HCl in a 10% sodium lauryl sulfate solution, a lysing agent, was added to each well to halt dye digestion.

The relative concentration of MTT in each well was measured using a multi-path UV-vis spectrophotometer set at 570 nm. The absorbances of prepared blanks (cell cultures with no cytotoxic material) were also measured. Since this method does not directly determine number of cells, relative cell numbers are calculated by using the absorbance of the control wells (cell cultures with no cytotoxic material added) as 0% growth inhibition, and the absorbance of the blank as 100% growth inhibition (complete

cell death). The percent growth inhibition of the cytotoxic compound is given by the ratio of the percentages of the absorbances of treated wells to control wells.

## **B: Materials**

The following is a list of chemicals purchased for the development of this dissertation.

All purchased chemicals were used as received from the manufacturer, unless otherwise specified.

Tetrahydrofuran

Ethanol

Methanol

2-aminobenzimidazole, 97%

2-amino-1-methylbenzimidazole, 95%, purified by recrystallization in hot ethyl acetate

Zinc(II) nitrate hexahydrate,  $\text{Zn}(\text{NO}_3)_2 \cdot 6 \text{H}_2\text{O}$

Zinc(II) acetate dihydrate,  $\text{Zn}(\text{C}_2\text{H}_3\text{O}_2)_2 \cdot 2 \text{H}_2\text{O}$

Nickel(II) nitrate hexahydrate,  $\text{Ni}(\text{NO}_3)_2 \cdot 6 \text{H}_2\text{O}$

Cobalt(II) nitrate hexahydrate,  $\text{Co}(\text{NO}_3)_2 \cdot 6 \text{H}_2\text{O}$

Copper(II) nitrate hexahydrate,  $\text{Cu}(\text{NO}_3)_2 \cdot 6\text{H}_2\text{O}$

Copper(II) chloride dihydrate,  $\text{CuCl}_2 \cdot 2\text{H}_2\text{O}$

Copper(II) acetate monohydrate,  $\text{Cu}(\text{CH}_3\text{COO})_2 \cdot \text{H}_2\text{O}$

Trimethylacetyl chloride

Palmitoyl chloride

Decanoyl chloride

Cyclohexyl carbonyl chloride

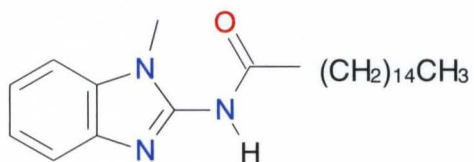
Benzoyl chloride

Diethyl ether  
N,N'-dicyclohexyl carbodiimide (DCC), 99%  
N-boc-2-aminoisobutyric acid, 99%  
Triethylamine  
Dichloromethane  
Dichloromethane, anhydrous  
Silica gel  
Potassium bromide  
Potassium chloroplatinite  
Potassium iodide  
Potassium hydroxide  
Concentrated sulfuric acid  
Sodium chloride  
Dimethyl sulfoxide  
Chloroform  
Deuterated chloroform  
Deuterated methanol  
Deuterated acetonitrile  
Deuterium oxide  
Deuterated dichloromethane  
Deuterated dimethyl sulfoxide  
Acetyl anhydride

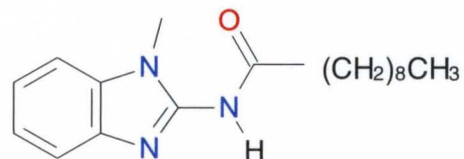
## C: List of Compounds and Nomenclature

### Compound

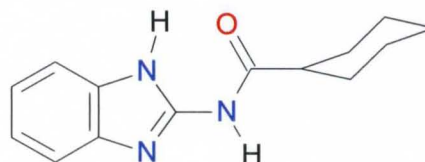
1. N-(N'-1-methylbenzimidazol-2-yl)hexadecanamide (Hmbhda)



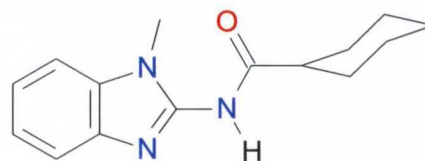
2. N-(N'-1-methylbenzimidazol-2-yl)decanamide (Hmbda)



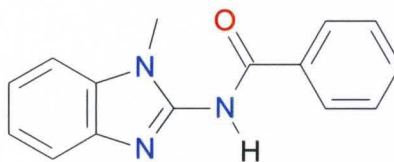
3. N-(benzimidazol-2-yl)cyclohexanecarboxamide (Hbchca)



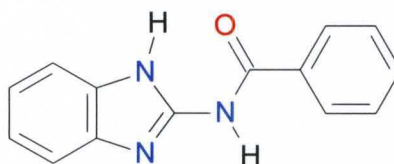
4. N-(N'-1-methylbenzimidazol-2-yl)cyclohexanecarboxamide (Hmbchca)



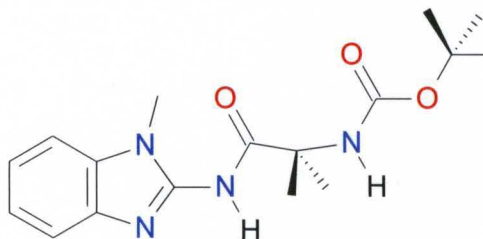
5. N-(N'-1-methylbenzimidazol-2-yl)benzamide (Hmbba)



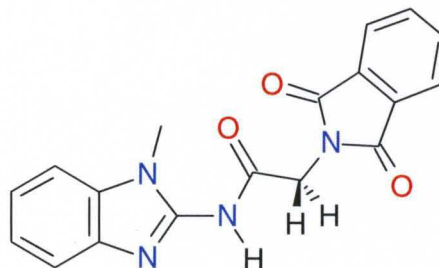
6. N-(benzimidazol-2-yl)benzamide (Hbba)



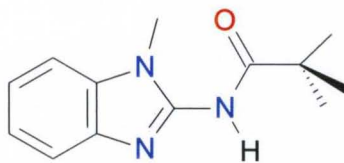
7. N-(N'-1-methylbenzimidazol-2-yl)N''-boc-2-amino-2,2-dimethylacetamide (Hisoba)  $\equiv$  L<sup>boc</sup>



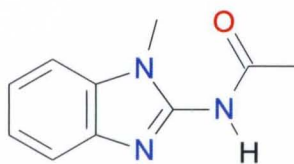
8. N-(N'-1-methylbenzimidazol-2-yl)-2-N'-phthalimidylacetamide (Hmbpha)



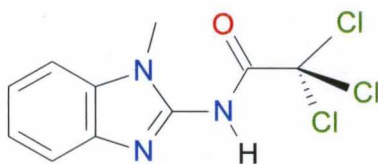
9. N-(N'-1-methylbenzimidazol-2-yl)-2,2-dimethylpropanamide (Hdmmbp)



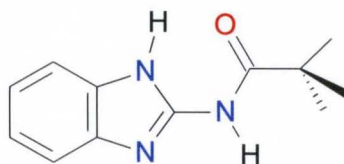
10. N-(N'-1-methylbenzimidazol-2-yl)acetamide (Hmba)



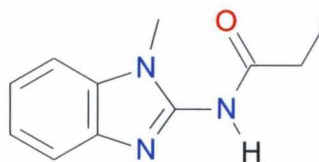
11. N-(N'-1-methylbenzimidazol-2-yl)-2,2,2-trichloroacetamide (Hmbtca)



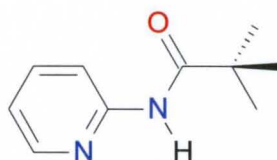
12. N-(benzimidazol-2-yl)-2,2-dimethylpropanamide (Hdmbp)



13. N-(N'-1-methylbenzimidazol-2-yl)propanamide (Hmbpa)

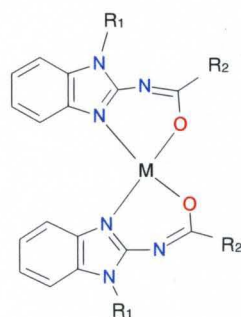


14. 2-(Pivaloylamino)pyridine (Pap)



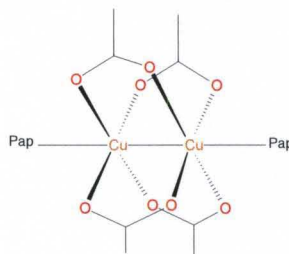


### Compounds 14- 23

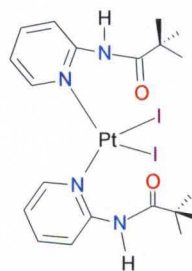


Compound	Ligand(L)	R1	R2	M	Formula
<b>15</b>	<b>2</b>	Me	(CH <sub>2</sub> ) <sub>8</sub> CH <sub>3</sub>	Cu	ML <sub>2</sub>
<b>16</b>	<b>4</b>	Me	C <sub>6</sub> H <sub>11</sub>	Ni	ML <sub>2</sub>
<b>17</b>	<b>4</b>	Me	C <sub>6</sub> H <sub>11</sub>	Co	ML <sub>2</sub>
<b>18</b>	<b>6</b>	H	C <sub>6</sub> H <sub>5</sub>	Zn	ML <sub>3</sub>
<b>19</b>	<b>9</b>	Me	C(CH <sub>3</sub> ) <sub>3</sub>	VO	ML <sub>2</sub>
<b>20</b>	<b>2</b>	Me	(CH <sub>2</sub> ) <sub>8</sub> CH <sub>3</sub>	Ni	ML <sub>2</sub>
<b>21</b>	<b>1</b>	Me	(CH <sub>2</sub> ) <sub>14</sub> CH <sub>3</sub>	Ni	ML <sub>2</sub>
<b>22</b>	<b>4</b>	Me	C <sub>6</sub> H <sub>11</sub>	Zn	ML <sub>2</sub>
<b>23</b>	<b>10</b>	Me	CH <sub>3</sub>	Zn	ML <sub>2</sub>

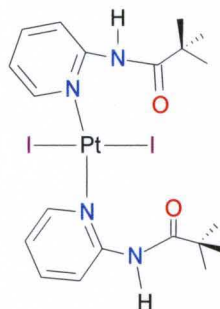
**24. Cu<sub>2</sub>(OAc)<sub>4</sub>(Pap)<sub>2</sub> [Pap = N-2-pivaloylamino pyridine]**



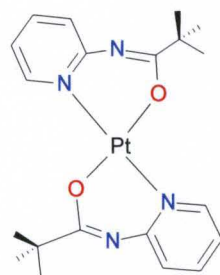
**25. cis-Bis[(N-pyridin-2-yl)-2,2-dimethylpropanamide] Pt(II) diiodide  
c(Pap)<sub>2</sub>PtI<sub>2</sub>**



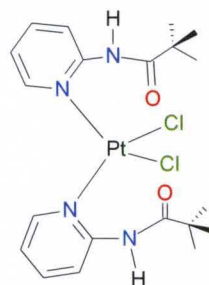
26. **trans-Bis[(N-pyridin-2-yl)-2,2-dimethylpropanamide]Pt(II) diiodide**  
**t(Pap)<sub>2</sub>PtI<sub>2</sub>**



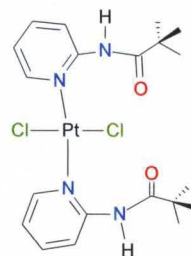
27. **trans-Bis[(N-pyridin-2-yl)-2,2-dimethylpropanamido]Pt(II)**  
**t(Pap)<sub>2</sub>Pt**



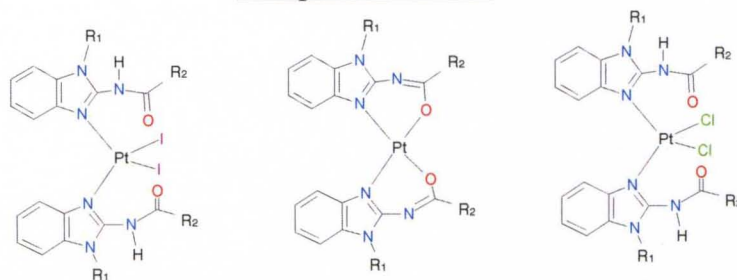
28. **cis-Bis[(N-pyridin-2-yl)-2,2-dimethylpropanamide]Pt(II) dichloride**  
**c(Pap)<sub>2</sub>PtCl<sub>2</sub>**



29. **trans-Bis[(N-pyridin-2-yl)-2,2-dimethylpropanamide]Pt(II)**  
**dichloride t(Pap)<sub>2</sub>PtCl<sub>2</sub>**



### Compounds 30 – 45



Compound	Ligand	R1	R2	Formula
30	2	Me	(CH <sub>2</sub> ) <sub>8</sub> CH <sub>3</sub>	PtL <sub>2</sub>
31	4	Me	C <sub>6</sub> H <sub>11</sub>	PtL <sub>2</sub> I <sub>2</sub>
32	4	Me	C <sub>6</sub> H <sub>11</sub>	PtL <sub>2</sub>
33	4	Me	C <sub>6</sub> H <sub>11</sub>	PtL <sub>2</sub> Cl <sub>2</sub>
34	1	Me	(CH <sub>2</sub> ) <sub>14</sub> CH <sub>3</sub>	PtL <sub>2</sub>
35	9	Me	C(CH <sub>3</sub> ) <sub>3</sub>	PtL <sub>2</sub> I <sub>2</sub>
36	9	Me	C(CH <sub>3</sub> ) <sub>3</sub>	PtL <sub>2</sub>
37	9	Me	C(CH <sub>3</sub> ) <sub>3</sub>	PtL <sub>2</sub> Cl <sub>2</sub>
38	12	H	C(CH <sub>3</sub> ) <sub>3</sub>	PtL <sub>2</sub> I <sub>2</sub>
39	12	H	C(CH <sub>3</sub> ) <sub>3</sub>	PtL <sub>2</sub> Cl <sub>2</sub>
40	3	H	C <sub>6</sub> H <sub>11</sub>	PtL <sub>2</sub> I <sub>2</sub>
41	13	Me	CH <sub>2</sub> CH <sub>3</sub>	PtL <sub>2</sub> Cl <sub>2</sub>
42a	5	Me	C <sub>6</sub> H <sub>5</sub>	PtL <sub>2</sub> Cl <sub>2</sub>
42b	5	Me	C <sub>6</sub> H <sub>5</sub>	PtL <sub>2</sub> Cl <sub>2</sub>
42c	5	Me	C <sub>6</sub> H <sub>5</sub>	PtL <sub>2</sub> Cl <sub>2</sub>
42d	5	Me	C <sub>6</sub> H <sub>5</sub>	PtL <sub>2</sub>
46	7	Me	L <sup>boc</sup>	PtL <sub>2</sub> Cl <sub>2</sub>

## D: Synthesis of Compounds

### 1. N-(N'-1-methylbenzimidazol-2-yl)hexadecanamide (Hmbhda)

Triethylamine (1.60 mL, 11.5 mmol) and (3.00 mL, 9.89 mmol) palmitoyl chloride were added to (1.46 g, 9.92 mmol) 2-amino-1-methylbenzimidazole (amb) dissolved in 100 mL anhydrous tetrahydrofuran. The reaction was left stirring under a blanket of nitrogen in a capped round-bottom flask for 5 days. The solvent was stripped using a rotary vacuum evaporator. The product (1.44 g) was extracted with 60 mL ether. Isolation of the product was achieved via evaporation of the solvent using a rotary vacuum evaporator.

Yield: 3.74 mmol, 37.5 %; Calcd mass: 385.31 g/mol, exptl mass: *m/z* (%) [M]<sup>+</sup>: 386.64

(100) [(Hmbhda)H]<sup>+</sup>, 408.58 (55) [(Hmbhda-H)Na]<sup>+</sup>; <sup>1</sup>H NMR (CDCl<sub>3</sub>): δ: 7.23 (4H, m, benzimidazole), 3.79 (3H, s, N-CH<sub>3</sub>), 2.50 (4H, t, -CH<sub>2</sub>-, *J* = 7.5 Hz), 2.38 (2H, t, -CH<sub>2</sub>-, *J* = 7.5 Hz), 1.76 (4H, t, -CH<sub>2</sub>-, *J* = 7.0 Hz), 1.68 (2H, broad-t, -CH<sub>2</sub>-), 1.26 (16H, broad-m, -CH<sub>2</sub>-), 0.887 (3H, t, -CH<sub>3</sub>, *J* = 7.0 Hz).

## 2. N-(N<sup>1</sup>-1-methylbenzimidazol-2-yl)decanamide (Hmbda)

**Method A:** (0.789 g, 5.36 mmol) amb was dissolved in 70 mL anhydrous CH<sub>2</sub>Cl<sub>2</sub>. After 45 minutes, (1.40 mL, 10.0 mmol) Et<sub>3</sub>N and (1.20 mL, 5.78 mmol) decanoyl chloride was added to the reaction flask. The reaction was left stirring under a blanket of nitrogen in a capped round-bottom flask for 7 days. The solvent was stripped via rotary vacuum evaporation and the product (1.40 g) was obtained after extraction with 60 mL diethyl ether and evaporation of the diethyl ether. (Yield: 4.66 mmol, 86.9 %)

**Method B:** (0.904 g, 6.14 mmol) amb was dissolved in 42 mL anhydrous dichloromethane. Decanoyl chloride (1.30 mL, 6.26 mmol) was added together with (1.20 mL, 8.61 mmol) Et<sub>3</sub>N to the round-bottom reaction flask. The reaction was allowed to stir at room temperature for 24 hours after blowing nitrogen gas for one minute to create a blanket. The reaction was rotavaped and reconstituted with 20 mL dichloromethane. The solution was treated with a saturated sodium chloride solution. 5 mL diethyl ether was added after a second rotary vacuum evaporation. 1.05 g of product was isolated. (Yield: 3.49 mmol, 56.8 %); Calcd mass: 301.22 g/mol, exptl mass: *m/z* (%) [M]<sup>+</sup>: 301.04 (48) [Hmbda]<sup>+</sup>, 322.92 (20) [(Hmbda-H)Na]<sup>+</sup>; <sup>1</sup>H NMR (CDCl<sub>3</sub>): δ: 7.28 (4H, m, benzimidazole), 3.66 (3H, s, N-CH<sub>3</sub>), 2.51 (2H, t, -CH<sub>2</sub>-, *J* = 7.5 Hz), 1.75 (2H, q, -CH<sub>2</sub>-, *J* = 7.5 Hz, *J* = 15.0 Hz), 1.30, 1.38 (12H, broad-m, -CH<sub>2</sub>-), 0.893 (3H, t, -CH<sub>3</sub>, *J* = 7.0 Hz)

### 3. N-(benzimidazol-2-yl)cyclohexanecarboxamide (Hbchca)

A solution of cyclohexyl carbonyl chloride (2.72 mL, 20.0 mmol) in 10 mL dry dimethyl formamide) was added dropwise to a stirring solution of (1.33 g, 10.0 mmol) 2-aminobenzimidazole (ab) and triethylamine (5.58 mL, 40.0 mmol) in dry DMF (10 mL). The solution was stirred at room temperature for 2 hours and refluxed for 6 hours. It was then allowed to cool to room temperature and added dropwise to 350 mL distilled water. The resulting precipitate was filtered and washed with 10 mL water. The solid was insoluble in methanol and chloroform and was recrystallized in acetone after 5 minutes of heating. 1.38 g of product was recovered.

Yield: 5.68 mmol, 56.8 %, Calcd mass: 243.13 g/mol, exptl mass:  $m/z$  (%)  $[M]^+$ : 243.26 (100)  $[Hbchca]^+$ ;  $^1H$  NMR (DMSO- $d_6$ ):  $\delta$ : 12.02 (1H, s, N-H), 11.38 (1H, s, N-H), 7.42 (2H, s, benzimidazole), 7.06 (2H, dd,  $J = 4.0$  Hz,  $J = 2.5$  Hz, benzimidazole), 1.83 (2H, d,  $J = 12.0$  Hz, cyclohexyl), 1.75 (2H, d,  $J = 13.0$  Hz, cyclohexyl), 1.64 (2H, d,  $J = 11.0$  Hz, cyclohexyl), 1.43 (2H, m, cyclohexyl), 1.24 (2H, m, cyclohexyl)

### 4. N-(N'-1-methylbenzimidazol-2-yl)cyclohexanecarboxamide (Hmbchca)

Cyclohexyl carbonyl chloride (1.00 mL, 7.36 mmol) was added to a 70 mL solution of anhydrous dichloromethane containing (1.20 mL, 8.61 mmol) triethylamine and (1.08 g, 7.35 mmol) amb. The reaction was stirred under a blanket of nitrogen for 3 days. The reaction solvent was stripped under vacuum (rotavap). 1.50 g of desired product was isolated after extraction with diethyl ether followed by rotary vacuum evaporation. Yield: 5.83 mmol, 79.3 %; Calcd mass: 257.15 g/mol, exptl mass:  $m/z$  (%)  $[M]^+$ : 258.48 (68)  $[(Hmbchca) H]^+$ , 280.45 (56)  $[(Hmbchca-H) Na]^+$ , 296.36 (76)  $[(Hmbchca) K]^+$ ;  $^1H$  NMR (CDCl $_3$ ):  $\delta$ : 12.22 (1H, s, N-H), 7.23 (4H, m, benzimidazole), 3.65 (3H, s, N-CH $_3$ ),

2.42 (1H, t,  $J = 11.0$  Hz, cyclohexyl), 2.02 (2H, d,  $J = 12.0$  Hz, cyclohexyl), 1.80 (2H, d,  $J = 11.0$  Hz, cyclohexyl), 1.68 (2H, d,  $J = 10.5$  Hz, cyclohexyl), 1.53 (2H, dd,  $J = 12.5$  Hz,  $J = 11.5$  Hz cyclohexyl), 1.34 (2H, m, cyclohexyl)

#### 5. N-(N'-1-methylbenzimidazol-2-yl)benzamide (Hmbba)

Benzoyl chloride (0.356 mL, 2.53 mmol) was added to a stirring solution of (0.451 g, 3.06 mmol) amb in 15 mL tetrahydrofuran. Triethylamine (491  $\mu$ L, 3.52 mmol) was added to the mixture. The solution was stirred at room temperature for four days. 0.557 g of product was isolated after extraction with diethyl ether followed by rotary vacuum evaporation. Yield: 2.22 mmol, 87.7 %; Calcd mass: 251.11 g/mol, exptl mass:  $m/z$  (%)  $[M]^+$ : 251.20 (100)  $[Hmbba]^+$ , 273.04 (22)  $[(Hmbba-H) Na]^+$  289.02 (19)  $[(Hmbba-H) K]^+$ ;  $^1H$  NMR ( $CDCl_3$ ):  $\delta$ : 12.40 (1H, s, amide proton), 8.38 (2H, d,  $J = 7.0$  Hz, ortho-benzoyl), 7.48 (3H, m,  $J = 7.0$  Hz, para, meta-benzoyl), 7.30 (4H, m, benzimidazole), 3.78 (3H, s, N- $CH_3$ )

#### 6. N-(benzimidazol-2-yl)benzamide (Hbba)

A solution of benzoyl chloride (2.32 mL, 20.0 mmol) in 10 mL dry dimethylformamide was added dropwise to a stirring solution of (1.33 g, 10.0 mmol) ab and triethylamine (5.58 mL, 40.0 mmol) in dry DMF (10 mL). The solution was stirred at room temperature for 2 hours and refluxed for 6 hours. It was then allowed to cool to room temperature and added dropwise to 350 mL distilled water. The resulting precipitate was recrystallized in chloroform. 1.05 g of product was recovered.

Yield: 4.43 mmol, 44.45 % Calcd mass: 237.09 g/mol, exptl mass:  $m/z$  (%)  $[M]^+$ : 238.39 (69)  $[(Hbba) H]^+$ ;  $^1H$  NMR ( $DMSO-d_6$ ):  $\delta$ : 12.23 (1H, s, amide proton), 8.11 (2H, d,  $J =$

7.0 Hz, ortho-benzoyl), 7.58 (1H, t,  $J = 7.0$  Hz, para-benzoyl), 7.51 (2H, t,  $J = 7.0$  Hz, meta-benzoyl), 7.44 (2H, s, benzimidazole), 7.12 (2H, s, benzimidazole)

**7. N-(N'-1-methylbenzimidazol-2-yl)-N''-boc-2-amino-2,2-dimethyl acetamide  
(Hisoba) or L<sup>boc</sup>**

**Method A:** N-boc-2-aminoisobutyric acid (NBAB) (0.481 g, 2.37 mmol) and (0.288 g, 1.40 mmol) N,N'-dicyclohexylcarbodiimide (DCC) was poured into a round bottom flask . 25 mL anhydrous CH<sub>2</sub>Cl<sub>2</sub> was added to the reaction flask and the reaction was left to run overnight. Amb (0.348 g, 2.36 mmol) was added to the reaction mixture. After 7 days, the mixture was filtered and the precipitate was washed with methanol and acetone. The subsequent solvent of the filtrate was removed under reduced pressure and the product (0.339 g) was extracted from the precipitate using 40 mL ether. (Yield: 1.02 mmol, 43.2%)

**Method B:** (0.832 g, 4.09 mmol) NBAB and (0.414g, 2.01 mmol) N,N'-dicyclohexyl carbodiimide (DCC) were poured into a round bottom flask . Anhydrous CH<sub>2</sub>Cl<sub>2</sub> (40 mL) was added to the reaction flask and the reaction was left to run overnight. A white precipitate was observed. Amb (0.301 g, 2.05 mmol) was added to the reaction mixture. The mixture was filtered after 3 more days and the precipitate was washed with 15 mL methanol and 15 mL acetone. The solvent of the filtrate was then removed under reduced pressure and the desired product (0.0635 g) was extracted from the precipitate with ether. Yield: 0.191 mmol, 9.3 %; Calcd mass: 332.18 g/mol, exptl mass:  $m/z$  (%) [M]<sup>+</sup>: 333.56 (100) [(Hisoba)H]<sup>+</sup>, 355.50 (78) [(Hisoba-H)Na]<sup>+</sup>; <sup>1</sup>H NMR (CDCl<sub>3</sub>):  $\delta$ : 7.254 (4H, m, benzimidazole), 6.20 (1H, s, N-H), 3.68 (3H, s, N-CH<sub>3</sub>, benzimidazole), 1.65 (6H, s, CH<sub>3</sub>), 1.48 (9H, s, tert-butyl)

### 8. N-(N'-1-methylbenzimidazol-2-yl)-2-N'-phthalimidyl acetamide (Hmbpha)

Anhydrous dichloromethane (10 mL) was added to amb (0.196 g, 1.33 mmol).  $\text{CHCl}_3$  (1.0 mL) and  $\text{Et}_3\text{N}$  (0.200 mL, 1.43 mmol) were added to the mixture. The resulting solution was combined with phthalylglycyl chloride (0.355 g, 1.59 mmol) dissolved in 3.0 mL anhydrous dichloromethane. Nitrogen gas was blown over the reaction flask for approximately 2 minutes. The solution turned yellow and a precipitate started forming after 5 minutes of stirring. 0.245 g of product was isolated via filtration. Yield: 0.733 mmol, 55.1 %; Calcd mass: 334.11 g/mol, exptl mass:  $m/z$  (%)  $[\text{M}]^+$ : 334.93 (100)  $[\text{Hmbpha}]^+$ , 357.93 (11.73)  $[(\text{Hmbpha})\text{Na}]^+$ ;  $^1\text{H NMR}$  ( $\text{DMSO-d}_6$ ):  $\delta$ : 12.46 (1H, s, N-H), 7.91 (4H, d, aromatic), 7.42 (2H, s, aromatic), 7.21 (2H, m, aromatic), 4.40 (2H, s,  $-\text{CH}_2$ ), 3.44 (3H, s, N- $\text{CH}_3$ )

### 9. N-(N'-1-methylbenzimidazol-2-yl)-2,2-dimethylpropanamide (Hdmmbp)

Amb (0.751 g, 5.10 mmol) was dissolved in 40 mL anhydrous  $\text{CH}_2\text{Cl}_2$ .  $\text{Et}_3\text{N}$  (1.00 mL, 7.17 mmol) was added to the solution. Pivaloyl chloride (0.700 mL, 5.53 mmol) was added after 15 minutes and the reaction was left for 5 days.

Purification: A slurry of NaCl, 9.03 g NaCl in 20 mL  $\text{H}_2\text{O}$ , was added to a separating funnel that had 30 mL of the product solution. The mixture was shaken vigorously and allowed to equilibrate. The aqueous layer was drained off and 70 mL  $\text{CH}_2\text{Cl}_2$  was added to the organic layer. 20 mL  $\text{H}_2\text{O}$  was added to the undissolved NaCl and added to the 100 mL  $\text{CH}_2\text{Cl}_2$ , shaken for a few minutes and drained. The organic layer was transferred into a round bottom flask and the solvent stripped via rotary vacuum evaporation.



Yield: 1.15 g, 4.99 mmol, 97.8%; Calcd mass: 231.14 g/mol, exptl mass:  $m/z$  (%)  $[M]^+$ : 232.43 (100)  $[(Hdmmbp)H]^+$ ;  $^1H$  NMR ( $CDCl_3$ ):  $\delta$ : 7.26 (4H, m, benzimidazole), 3.64 (3H, s, N- $CH_3$ ), 1.30 (9H, s, t-butyl)

#### 10. N-(N'-1-methylbenzimidaz-2-yl)acetamide (Hmba)

Amb (0.733 g, 4.98 mmol) was dissolved in 2 mL chloroform. Acetyl anhydride (1.0 mL, 10.6 mmol) was added to the reaction flask. 0.449 g of product was isolated after rotary evaporation and ether extraction. Yield: 2.37 mmol, 47.7 % ; Calcd mass: 189.09 g/mol, exptl mass:  $m/z$  (%)  $[M]^+$ : 190.62 (100)  $[(Hmba)H]^+$ , 212.44 (81)  $[(Hmba-H) Na]^+$ , 228.39 (64)  $[(Hmba-H)K]^+$ ;  $^1H$  NMR ( $CDCl_3$ ):  $\delta$ : 12.24 (1H, s, N-H ), 7.28 (4H, m, benzimidazole), 3.66 (3H, s, N- $CH_3$ ), 2.28 (3H, s, - $CH_3$ ).

#### 11. N-(N'-1-methylbenzimidaz-2-yl)-2,2,2-trichloroacetamide (Hmbtca)

Amb (1.05 g, 7.12 mmol) was dissolved in 50 mL anhydrous THF. 2,2,2-trichloroacetyl chloride (1.20 mL, 10.8 mmol) and  $Et_3N$  (1.20 mL, 8.61 mmol) was added to the reaction flask. The reaction was stirred under a blanket of nitrogen for 6 days. A white precipitate that weighed 1.05 g was obtained after filtration. The solid was dissolved in 25 mL EtOH. The solution was heated for 5 minutes to reduce the volume of the solvent. The solvent was allowed to evaporate and 0.825 g of white crystals were obtained.

Yield: 2.84 mmol, 39.8 %; Calcd mass: 290.97 g/mol, exptl mass:  $m/z$  (%)  $[M]^+$ : 289.51 (95)  $[(Hmbtca-H)]^+$ , 290.48 (60)  $[Hmbtca]^+$ ;  $^1H$  NMR ( $CDCl_3$ ):  $\delta$ : 11.67 (1H, s, N-H ), 7.28 (4H, m, benzimidazole), 3.78 (3H, s, N- $CH_3$ ).

### 12. N-(benzimidazol-2-yl)-2,2-dimethylpropanamide (Hdmbp)

Ab (0.549 g, 4.12 mmol) was dissolved in 40 mL anhydrous DMF. Pivaloyl chloride (0.659 mL, 5.08 mmol) and Et<sub>3</sub>N (3.0 mL, 21.5 mmol) was added to the reaction flask. An additional 20 mL DMF was added after 30 minutes and the reaction was left for 9 days. 0.215 g of product was isolated after precipitation in water followed by recrystallization using ethanol. Yield: 0.990 mmol, 24.0%, Calcd mass: 217.12 g/mol, exptl mass: *m/z* (%) [M]<sup>+</sup>: 217.34 (100) [Hdmbp]<sup>+</sup>, 239.24(38) [(Hdmbp)Na]<sup>+</sup>, 255.13(18) [(Hdmbp)K]<sup>+</sup>; <sup>1</sup>H NMR (CD<sub>3</sub>OD): δ: 7.37 (2H, d, benzimidazole, *J*= 8.5Hz), 7.07 (2H, d, benzimidazole, *J*= 9.5Hz), 1.25 (9H, s, t-butyl)

### 13. N-(N'-1-methylbenzimidaz-2-yl)propanamide (Hmbpa)

Amb (0.706 g, 4.80 mmol) was dissolved in 10 mL chloroform. Propionic anhydride (1.0 mL, 7.80 mmol) was added to the reaction flask and the reaction was stirred at room temperature for four days. The reaction solvent was removed under reduced pressure. 0.170 g of product was isolated following extraction with diethyl ether and rotary vacuum evaporation. Yield: 0.837 mmol, 17.4 %; Calcd mass: 203.11 g/mol, exptl mass: *m/z* (%) [M]<sup>+</sup>: 203.99 (100) [Hmbpa]<sup>+</sup>

### 15. Bis[N-(N'-1-methylbenzimidazol-2-yl) decanamido]copper(II) Cu(mbda)<sub>2</sub>

Copper(II) nitrate hexahydrate (0.237 g, 1.26 mmol) was dissolved in 2 mL methanol. A solution containing N-(N'-1-methylbenzimidazol-2-yl)decanamide (0.482 g, 1.60 mmol) in 5 mL methanol was added dropwise to the stirring copper nitrate solution. The copper nitrate solution turned green upon addition of ligand. A green precipitate formed immediately upon addition of triethylamine (0.029 mL, 0.208 mmol). The precipitate was

isolated by vacuum filtration. X-ray quality crystals (green needles/rods) were obtained by dissolving the precipitate in 1 mL dichloromethane, layered with 5 mL methanol.

Yield: 0.263 g, 0.396 mmol, 31.4 %; Calcd mass: 663.34 g/mol, exptl mass:  $m/z$  (%)  $[M]^+$ : 663.20 (40)  $[Cu(m\text{bda})_2]^+$ , 302.42 (70)  $[(H\text{mbda})H]^+$ ; KBr-IR ( $\text{cm}^{-1}$ ):  $\nu_{\text{C-H}} = 3129$ , 3058, 2957, 2920, 2853  $\nu_{\text{C=C}} = 1621$

#### 16. Bis[N-(N'-1-methylbenzimidazol-2-yl)cyclohexanecarboxamido]nickel(II)

##### Ni (mbchca)<sub>2</sub>

Nickel(II) nitrate hexahydrate (0.0502 g, 0.173 mmol) was added to a 5 mL MeOH/10 mL  $\text{CH}_2\text{Cl}_2$  solution containing N-(N'-1-methylbenzimidazol-2-yl)cyclohexanamide (0.119 g, 0.463 mmol). A pale blue color was observed after 1 minute of addition of the Nickel(II) nitrate hexahydrate. Triethylamine (0.0500 mL, 0.359 mmol) was added to the blue solution resulting in a pale blue precipitate after 1 minute. 5 mL  $\text{H}_2\text{O}$  was added to the mixture. The product was recovered after vacuum filtration. Crystals were obtained from via layering using a  $\text{CH}_2\text{Cl}_2$  / ether combination. Yield: 0.0747 g, 0.131 mmol, 75.7%; Calcd mass: 570.22 g/mol, exptl mass:  $m/z$  (%)  $[M]^+$ : 576.87 (100)  $[(\text{mbchca})_2\text{Ni}]^+$ , 892.30 (50)  $[(\text{mbchca})_3\text{Ni}_2]^+$ ;  $^1\text{H}$  NMR ( $\text{CDCl}_3$ ):  $\delta$ : 9.24, 5.01, 2.23, 1.72, 1.54, 1.33; KBr-IR ( $\text{cm}^{-1}$ ):  $\nu_{\text{N-H}} = 3435$ ,  $\nu_{\text{C-H}} = 3120$ , 3053, 2930, 2859  $\nu_{\text{C=C}} = 1617$

#### 17. Bis[N-(N'-1-methylbenzimidazol-2-yl)cyclohexanecarboxamido]cobalt(II)

##### Co(mbchca)<sub>2</sub>

N-(N'-1-methylbenzimidazol-2-yl)cyclohexanamide (0.119 g, 0.463 mmol) was dissolved in 10 mL  $\text{CH}_2\text{Cl}_2$  and added dropwise to a stirring solution of cobalt(II) nitrate hexahydrate (0.0671 g, 0.231 mmol) dissolved in 5 mL methanol. Triethylamine (0.05

mL, 0.359 mmol) was added to the reaction vessel. The resulting precipitate was recrystallized in 2 mL acetone / 2 mL ether. Yield: 0.0412 g, 0.0721 mmol, 15.6 %; Calcd mass: 571.22 g/mol, exptl mass:  $m/z$  (%)  $[M]^+$ : 573.89 (95)  $[((\text{mbchca})_2\text{Co})\text{H}_2]^+$ ; 258.45 (100)  $[(\text{Hmbchca})\text{H}]^+$ , 281.43 (20)  $[((\text{Hmbchca})\text{H})\text{Na}]^+$ , 471.21 (62)  $[(\text{Hmbchca})(\text{DBA-matrix})\text{Co}]^+$ ; KBr-IR ( $\text{cm}^{-1}$ ):  $\nu_{\text{C-H}} = 3063, 2930, 2813$   $\nu_{\text{C=C}} = 1622$

**18. *Trans*-Bis[ N-(benzimidazol-2-yl)benzamido][N-(benzimidazol-2-yl)benzamide]zinc(II)      Zn(bba)<sub>2</sub>(Hbba)**

Zinc(II) nitrate hexahydrate (0.132 g, 0.444 mmol) was dissolved in 5 mL methanol. A solution containing N-(benzimidazol-2-yl)benzamide (0.211 g, 0.888 mmol) in 5 mL methanol was added dropwise to the zinc nitrate solution with stirring. Triethylamine (0.140 mL, 1.38 mmol) was added to the solution. The resulting mixture was filtered and the solvent of the filtrate was allowed to slowly evaporate yielding x-ray quality crystals. Yield: 0.0466 g, 0.0603 mmol, 13.6 %; Calcd mass: 773.18 g/mol, exptl mass:  $m/z$  (%)  $[M]^+$ : 539.26 (35)  $[\text{Zn}(\text{bba})_2]^+$ ;  $^1\text{H NMR}$  ( $\text{CDCl}_3$ ):  $\delta$ : 7.98 (6H, ortho-benzoyl) 7.16 (9H, meta, para-benzoyl), 7.55, 7.38, 7.20 (12H, benzimidazole); KBr-IR ( $\text{cm}^{-1}$ ):  $\nu_{\text{N-H}} = 3322$   $\nu_{\text{C-H}} = 3062, 2974, 2755$   $\nu_{\text{C-O, C=C}} = 1764, 1662$

**19. *trans*- Bis[2,2-dimethyl-N-(N'-1-methylbenzimidazol-2-yl)propanamido]vanadium(IV) oxide      VO(dmmbp)<sub>2</sub>**

Vanadyl acetyl acetonate (0.0560 g, 0.211 mmol) was dissolved in 1.0 mL methanol. Excess N-(N'-1-methylbenzimidazol-2-yl)-2,2-dimethylpropanamide dissolved in methanol was added. An instant color change, blue-green solution to purple solution was

observed. A purple precipitate followed and was filtered via vacuum filtration. The precipitate was allowed to dry, weighed and recrystallized from methylene chloride and methanol. Yield: 0.0659 g, 0.125 mmol, 59.2 %; Calcd mass: 527.20 g/mol, exptl mass:  $m/z$  (%)  $[M]^+$ : 528.27(100)  $[(VO(dmmbp)_2)H]^+$ ; KBr-IR ( $cm^{-1}$ ):  $\nu_{C-H}$  = 3057, 2960  $\nu_{C=C}$  = 1618

**20. Bis[N-(N'-1-methylbenzimidazol-2-yl)decanamido]nickel(II) Ni(mbda)<sub>2</sub>**

N-(N'-1-methylbenzimidazol-2-yl)decanamide (0.482 g, 1.60 mmol) was dissolved in 10 mL methanol. Nickel(II) nitrate hexahydrate (0.224 g, 0.770 mmol) dissolved in 5 mL was added to the ligand. The solution became cloudy after the addition of triethylamine (0.200 mL, 1.40 mmol). A pale green precipitate was isolated via vacuum filtration (0.670 g, 1.02 mmol). Purple needle crystals were obtained by dissolving the pale green powder in 3 mL diethyl ether. The crystals dissolved upon exposure to air.

Yield: 1.02 mmol, 63.45 %; Calcd mass: 658.35 g/mol, exptl mass:  $m/z$  (%)  $[M]^+$ : 302.42 (30)  $[(Hmbda)H]^+$ ; 659.24 (100)  $[(mbda)_2Ni]H]^+$ ;  $^1H$  NMR ( $CDCl_3$ ):  $\delta$ : 8.58, 5.76, 3.48, 2.77, 2.15, 1.56, 1.30, 1.21; KBr-IR ( $cm^{-1}$ ):  $\nu_{C-H}$  = 3153, 3057, 2904, 2857  $\nu_{C=C}$  = 1618

**21. Bis[N-(N'-1-methylbenzimidazol-2-yl)hexadecanamido]nickel(II)**

**Ni(mbnda)<sub>2</sub>**

Nickel(II) nitrate hexahydrate (0.0457 g, 0.157 mmol) was added to a 5 mL MeOH/ 5 mL  $CH_2Cl_2$  solution containing N-(N'-1-methylbenzimidazol-2-yl)hexadecanamide (0.122 g, 0.317 mmol). A pale blue color was observed after 1 minute of addition of the Nickel(II) nitrate hexahydrate. Triethylamine (0.0438 mL, 0.314 mmol) was added to the blue solution resulting in a pale blue precipitate. 5 mL  $H_2O$  was added to the mixture. The

product was recovered after vacuum filtration. Yield: 0.0418 g, 0.505 mmol, 32.2 %; Calcd mass: 826.53 g/mol, exptl mass:  $m/z$  (%)  $[M]^+$ : 827.40 (100)  $[(Ni(mbhd_a)_2)H]^+$ , 386.57 (28)  $[(Hmbhd_a)H]^+$ ;  $^1H$  NMR ( $CDCl_3$ ):  $\delta$ : 8.658 (8H, s, benzimidazole), 5.722 (6H, s, N- $CH_3$ ), 2.876, 2.202, 1.547, 1.285 ( 28H,s, - $CH_2$ -), 0.886 (6H,s, - $CH_3$ ) ; KBr-IR ( $cm^{-1}$ ):  $\nu_{C-H}$  = 3145, 3056, 2917 (broad)  $\nu_{C=C}$  = 1618

## 22. Bis (N-(N'-1-methylbenzimidazol-2-yl)cyclohexanecarboxamido)zinc(II)

### Zn(mbchca)<sub>2</sub>

Zn(NO<sub>3</sub>)<sub>2</sub>·6H<sub>2</sub>O (0.0469 g, 0.158 mmol) was dissolved in a 5 mL methanol / 5 mL dichloromethane. N-(N'-1-methylbenzimidazol-2-yl)cyclohexanamide (0.104 g, 0.153 mmol) was added to the flask. After 30 minutes, Et<sub>3</sub>N (0.044 mL, 0.316 mmol) was added. 2 mL CH<sub>2</sub>Cl<sub>2</sub> and 4 mL ethanol was added to the reaction mixture. It was then heated for 10 minutes and filtered. The precipitate was weighed 0.0126 g. Yield: 0.0219 mmol, 13.8%; Calcd mass: 576.22 g/mol, exptl mass:  $m/z$  (%)  $[M]^+$  ; 150.44 (64)  $[(amb)H]^+$  ; 257.74 (66)  $[(Hmbchca)H]^+$ ; 578.21 (100)  $[(Zn(mbchca)_2)H_2]^+$ : 726.24 (14) $[Zn(mbchca)_2(C_6H_{11})CO]^+$

## 23. Bis[N-(N'-1-methylbenzimidazol-2-yl)acetamido]zinc(II) Zn(Hmba)<sub>2</sub>

N-(N'-1-methylbenzimidazol-2-yl) acetamide (0.0290 g, 0.153 mmol) was dissolved in 5mL methanol. Zn(NO<sub>3</sub>)<sub>2</sub>· 6H<sub>2</sub>O (0.0217 g, 0.729 mmol) was added to the stirring solution. Et<sub>3</sub>N (0.021mL, 0.151 mmol) was added to the solution after 30 minutes. An instant white precipitate was observed. The reaction was allowed to continue for 20 minutes after which the precipitate was filtered and washed with 10 mL water. The

precipitate was recrystallized in chloroform. Yield: 24.3  $\mu$ mol, 33.4%;  $^1\text{H NMR}$  ( $\text{CDCl}_3$ ):  $\delta$ : 7.26, 7.25, 7.15 (8H, benzimidazole), 3.79(6H, s, N-CH<sub>3</sub>), 2.30 (6H, s, -CH<sub>3</sub>)

**24. *Trans*-Bis[(N-pyridin-2-yl)-2,2-dimethylpropanamide]( $\mu$ -tetrakisacetatocopper) copper(II) [Cu<sub>2</sub>(OAc)<sub>4</sub>(Pap)<sub>2</sub>]**

A stirring solution of N-2-pivaloylamino pyridine (0.415 g, 2.33 mmol) in acetone (10 mL) was combined with a solution of Cu(CH<sub>3</sub>COO)<sub>2</sub> · H<sub>2</sub>O (0.232 g, 1.16 mmol) in methanol (20 mL). The reaction was refluxed for an hour and stirring was continued for 24 hours at room temperature. The reaction mixture was filtered and the solvent of the filtrate was removed via rotary evaporation. The resulting solid weighed 0.194 g and the desired product was extracted and reconstituted in diethyl ether for recrystallization.

Dark green crystals weighing 0.113 g were obtained.

Yield: 0.157 mmol, 13.5 %; Calcd mass: 718.13 g/mol, exptl mass:  $m/z$  (%) [M]<sup>+</sup>: 583.73 (15) [Cu<sub>2</sub>(OAc)(Pap)<sub>2</sub>O]<sup>+</sup>; 242.76 (100) [CuPap]<sup>+</sup>; KBr-IR (cm<sup>-1</sup>):  $\nu_{\text{O-H}}$  = 3394  $\nu_{\text{N-H}}$  = 3213, 3201  $\nu_{\text{C-H}}$  = 3139, 3086, 2981, 2873  $\nu_{\text{C-O}}$  = 2550, 2359, 2011, 1866

**25. *Cis*-Bis[(N-pyridin-2-yl)-2,2-dimethylpropanamide]platinum(II) diiodide c(Pap)<sub>2</sub>PtI<sub>2</sub>**

KI (1.34 g, 8.09 mmol) was added to K<sub>2</sub>PtCl<sub>4</sub> (0.419 g, 1.01 mmol) dissolved in 5 mL H<sub>2</sub>O. The solution was stirred for 40 minutes and added dropwise to N-2-(pivaloylamino)pyridine (0.360 g, 2.02 mmol) dissolved in 5 mL methanol in a 25 mL Erlenmeyer flask. Upon addition of 3 mL methanol and 3 mL water to the reaction flask, an instant yellow precipitate was observed. The reaction was maintained at 50°C and allowed to run for 1 hour 18 minutes. The yellow precipitate was filtered and washed

with 10 mL H<sub>2</sub>O. The product was recovered after vacuum filtration. Yield: 0.532 g, 0.661 mmol, 65.4 %; Calcd mass: 804.99 g/mol, exptl mass:  $m/z$  (%) 680.77 (70) [M-I]<sup>+</sup>. <sup>1</sup>H NMR (CDCl<sub>3</sub>): δ 10.64 (2H, s, N-H), 8.41 (2H, d,  $J = 4.25$  Hz, pyridine), 8.16 (2H, dd,  $J = 2.5$  Hz,  $J = 1.00$  Hz, pyridine), 7.74 (2H, t,  $J = 7.5$  Hz,  $J = 1.5$  Hz, pyridine), 6.95 (2H, t,  $J = 6.0$  Hz,  $J = 1.5$  Hz, pyridine), 1.62 (18H, s, tert-butyl); KBr-IR (cm<sup>-1</sup>):  $\nu_{\text{N-H}} = 3306$ ,  $\nu_{\text{C-H}} = 2969$ , 2871  $\nu_{\text{C-O}} = 1713$

**26. *Trans*-Bis[(N-pyridin-2-yl)-2,2-dimethylpropanamide]platinum(II) diiodide**  
**t(Pap)<sub>2</sub>PtI<sub>2</sub>**

N-2-(pivaloylamino)pyridine (0.435 g, 2.44 mmol) was dissolved in 6 mL acetonitrile. K<sub>2</sub>PtCl<sub>4</sub> (0.506 g, 1.22 mmol) was dissolved in 5 mL H<sub>2</sub>O. KI (1.62 g, 9.75 mmol) was added to the flask containing potassium tetrachloroplatinate(II). The resulting solution was added dropwise to the 6 mL solution of ligand and allowed to stir for 30 minutes. 8 x 68 μL 3.93 M KOH was added to the yellow solution after 53 minutes. The resulting pale yellow precipitate was vacuum filtered after an hour. The yellow precipitate weighed 0.249 g and was later identified as the bis chelated amido form. The filtrate was transferred into a vial and layered with CH<sub>2</sub>Cl<sub>2</sub> and ethanol (1:1v). Golden crystals were obtained after a few days. Yield: 0.364 g, 0.452 mmol, 37.1%; Calcd mass: 804.99 g/mol, exptl mass:  $m/z$  (%) [M]<sup>+</sup> : 678.33 (65) [M-I]<sup>+</sup>. <sup>1</sup>H NMR (CDCl<sub>3</sub>): δ 10.19 (2H, s, N-H), 8.54 (2H, dd,  $J = 24.0$  Hz,  $J_a, J_b = 5.0, 8.5$  Hz, pyridine), 7.75 (2H, t,  $J = 7.5$  Hz pyridine), 7.03 (2H, t,  $J = 6.0$  Hz, pyridine), 1.60 (18H, s, tert-butyl); KBr-IR (cm<sup>-1</sup>):  $\nu_{\text{N-H}} = 3300$ ,  $\nu_{\text{C-H}} = 2963$ , 2871  $\nu_{\text{C-O}} = 1713$



**27. *Trans*-Bis[(*N*-pyridin-2-yl)-2,2-dimethylpropanamido]platinum(II) t(Pap)<sub>2</sub>Pt**

**Method A:** KI (2.31 g, 13.9 mmol) was added to a 25 mL Erlenmeyer flask containing K<sub>2</sub>PtCl<sub>4</sub> (0.721 g, 1.74 mmol) dissolved in 6 mL H<sub>2</sub>O. An additional 5 mL H<sub>2</sub>O was added to the flask. *N*-2-(pivaloylamino)pyridine (0.619 g, 3.47 mmol) dissolved in 12 mL acetonitrile was added dropwise to the reaction flask after 26 minutes of stirring. 4 x 572 μL 3.93M KOH was added after 46 minutes. The resulting pale yellow precipitate was vacuum filtered and washed with 25 mL H<sub>2</sub>O after an hour and 41 minutes. 0.444 g of product was obtained. The sample was purified by recrystallization using chloroform as solvent. (Yield: 0.808 mmol, 46.5 %).

**Method B:** (0.103 g, 0.128 mmol) PapPtI<sub>2</sub> was added to 12 mL acetonitrile / water solution (3:1v). The resulting slurry was put on a hot plate at 85°C. 80 μL 3.93M KOH was added in increments of 0.010 mL. The mixture became clear after the addition of 0.030 mL of the potassium hydroxide. The solvent was stripped *in vacuo* after an hour. The yellow solid was reconstituted in a mixture of 2 mL CH<sub>2</sub>Cl<sub>2</sub> / 6 mL MeOH. (Yield: 20.0 %)

**Method C:** (Pap)<sub>2</sub>PtCl<sub>2</sub> (0.198 g, 0.317 mmol) was added to 10 mL acetonitrile / 5 mL water solution. The resulting slurry was put on a hot plate at 85°C. 0.105 mL of 3.93M KOH was added to the mixture. A light green / yellow solution was observed after 15 minutes of addition of base. After 1 h 30 min, the reaction was allowed to cool to room temperature (10 minutes). A yellow solid (0.0274 g) was recovered after filtration. Yield: 0.0499 mmol, 15.8 %; Calcd mass: 549.17 g/mol, exptl mass: *m/z* (%) 551.49 (100) [MH<sub>2</sub>]<sup>+</sup>. <sup>1</sup>H NMR (CDCl<sub>3</sub>): δ: 8.82 (2H, d, *J* = 5.5 Hz, pyridine), 7.67 (2H, t, *J* = 7.5

Hz, pyridine), 7.11 (2H, d,  $J = 9.0$  Hz, pyridine), 6.87 (2H, t,  $J = 6.0$  Hz, pyridine), 1.26 (18H, s, tert-butyl); KBr-IR ( $\text{cm}^{-1}$ ):  $\nu_{\text{C-H}} = 3121, 3093$   $\nu_{\text{C-O}} = 1616$

**28. *Cis*-Bis[(*N*-pyridin-2-yl)-2,2-dimethylpropanamide]platinum(II) dichloride**

***c*(Pap)<sub>2</sub>PtCl<sub>2</sub>**

(2-pivaloylamino)pyridine (0.185 g, 1.04 mmol) dissolved in 10 mL methanol, was added dropwise to an orange K<sub>2</sub>PtCl<sub>4</sub> solution (0.213 g, 0.514 mmol) K<sub>2</sub>PtCl<sub>4</sub> dissolved in 6 mL H<sub>2</sub>O. The reaction was maintained at 50°C. The solution became cloudy after 30 minutes and intensified through the course of the reaction. Stirring of the reaction was discontinued after two hours. The pale yellow precipitate was filtered, washed with 8.4 mL water, dried and weighed (0.107 g, 0.172 mmol). The filtrate was returned onto the hot plate after 10 minutes and stirred at 50°C for an additional 6 hours 35 minutes. The solvent of the filtrate was stripped via rotor vacuum and 0.152 g of product was recovered. Both samples were combined and recrystallized in chloroform. Yield: 0.245 mmol, 81.31 %; Calcd mass: 621.12 g/mol, exptl mass:  $m/z$  (%) 588.8 (95) [M-Cl]<sup>+</sup>. <sup>1</sup>H NMR (CDCl<sub>3</sub>):  $\delta$ 10.66 (2H, s, N-H), 8.33 (2H, d,  $J = 4.0$  Hz, pyridine), 8.09 (2H, s, pyridine), 7.76 (2H, t,  $J = 7.0$  Hz, pyridine), 6.89 (2H, t,  $J = 6.0$ , Hz pyridine), 1.57 (18H, s, tert-butyl) KBr-IR ( $\text{cm}^{-1}$ ):  $\nu_{\text{N-H}} = 3294$ ,  $\nu_{\text{C-H}} = 3106, 2951$   $\nu_{\text{C-O}} = 1700$

**29. *Trans*-Bis[(*N*-pyridin-2-yl)-2,2-dimethylpropanamide]platinum(II) dichloride**

***t*(Pap)<sub>2</sub>PtCl<sub>2</sub>**

*Trans*-Bis[(*N*-pyridin-2-yl)-2,2-dimethylpropanamido]platinum(II) (0.403 g, 0.733 mmol) was dissolved in 33 mL anhydrous dichloromethane. HCl gas, from a sulfuric acid – sodium chloride generator, was bubbled through the solution for 18 minutes. The

reaction was stirred for 14 hours 12 minutes. A pale yellow precipitate was observed at the end of the reaction. The precipitate was filtered and weighed. A weight of 0.0211 g of mixed product was obtained. The solvent of the filtrate was stripped (*in vacuo*) and 0.130 g of desired product was recovered. Yield: 28.6%; Calcd mass: 621.12 g/mol, exptl mass:  $m/z$  (%) 587.83 (58)  $[M-Cl]^+$ .  $^1H$  NMR ( $CDCl_3$ ):  $\delta$  10.43 (2H, s, N-H), 8.60 (2H, s, pyridine), 8.43 (2H, d,  $J = 4.0$  Hz, pyridine), 7.82 (2H, t,  $J = 8.0$  Hz pyridine), 7.08 (2H, t,  $J = 6.0$  Hz pyridine), 1.56 (18H, s, tert-butyl); KBr-IR ( $cm^{-1}$ ):  $\nu_{N-H} = 3336$ ,  $\nu_{C-H} = 3140, 2969$   $\nu_{C-O} = 1700$

### 30. Bis[N-(N'-1-methylbenzimidazol-2-yl)decanamido]platinum(II) Pt(mbda)<sub>2</sub>

A dark purple solution containing KI (1.02 g, 0.766 mmol) and potassium tetrachloroplatinite(II) (0.318 g, 0.766 mmol) dissolved in 5 mL H<sub>2</sub>O, was added dropwise to a 10 mL acetonitrile solution of N-(N'-1-methylbenzimidazol-2-yl)decanamide (0.461 g, 1.53 mmol). A pale yellow precipitate (0.591 g) was isolated via filtration after the addition of two equivalence of 3.93 M KOH. Yield: 0.741 mmol, 96.7%; Calcd mass: 797.40 g/mol, exptl mass:  $m/z$  (%)  $[M]^+$ : 795.55 (20)  $[((mbda)_2Pt)-H_2]^+$ , 302.57 (20)  $[(Hmbda)H]^+$ ; 340.46 (10)  $[(Hmbda)K]^+$ ;  $^1H$  NMR ( $CDCl_3$ ):  $\delta$ : 7.15 (2H, d,  $J = 7.5$  Hz, benzimidazole), 7.03 (2H, t,  $J = 7.5$  Hz, benzimidazole), 6.67 (2H, t,  $J = 7.5$  Hz, benzimidazole), 6.37 (2H, t,  $J = 8.5$  Hz, pyridine), 3.77 (6H, s, N-CH<sub>3</sub>), 2.53 (4H, t,  $J = 7.5$  Hz, -CH<sub>2</sub>-), 1.82 (4H, dd,  $J_1 = 14.5$  Hz,  $J_2 = 8.0$  Hz, -CH<sub>2</sub>-), 1.61 (8H, s, -CH<sub>2</sub>-), 1.44 (4H, m, -CH<sub>2</sub>-), 1.36, 1.29 (12H, broad, -CH<sub>2</sub>-), 0.881 (6H, t, -CH<sub>3</sub>); KBr-IR ( $cm^{-1}$ ):  $\nu_{C-H} = 2952, 2880$   $\nu_{C=C} = 1615$

### 31. Bis[N-(N'-1-methylbenzimidazol-2-yl)cyclohexanecarboxamide]platinum(II)

#### Pt(cyclohexylamb)<sub>2</sub>I<sub>2</sub>

KI (0.513 g, 3.09 mmol) was added to potassium tetrachloroplatinite(II) (0.152 g, 0.365 mmol) dissolved in 5 mL H<sub>2</sub>O. The dark purple solution was combined with a 10 mL solution of acetonitrile containing N-(N'-1-methylbenzimidazol-2-yl)cyclohexanamide (0.243 g, 0.946 mmol). A yellow precipitate was observed. 0.275 g of product was isolated after suction filtration. Yield: 286 μmol, 78.4 %; Calcd mass: 963.08 g/mol, exptl mass: *m/z* (%) [M]<sup>+</sup>: 965 (13) [((mbchca)<sub>2</sub>PtI<sub>2</sub>)H<sub>2</sub>]<sup>+</sup>, 258.46 (100) [(mbchca)H]<sup>+</sup>; <sup>1</sup>H NMR (CDCl<sub>3</sub>): δ: 9.73 (2H, s, N-H), 7.55 (2H, d, *J* = 8.0 Hz, benzimidazole), 7.15 (6H, m, benzimidazole), 3.67 (6H, s, N-CH<sub>3</sub>), 2.80 (2H, t, *J* = 3.25 Hz, cyclohexyl), 2.45 (4H, d, *J* = 12.5 Hz, cyclohexyl), 2.29 (4H, d, *J* = 12.5 Hz, cyclohexyl), 1.96 (4H, t, *J* = 3.5 Hz, cyclohexyl), 1.500 (4H, m, cyclohexyl), 1.395 (4H, t, cyclohexyl); <sup>13</sup>C NMR (CDCl<sub>3</sub>): δ: 174.84(C=O), 144.82, 136.83, 132.76, 124.06, 123.74, 122.79, 117.00, 111.38, 110.02, 108.87(C=C), 48.42, 45.70, 32.27, 29.22, 28.28, 25.97(C<sub>sp3</sub>-)

### 32. Bis[N-(N'-1-methylbenzimidazol-2-yl)cyclohexanecarboxamido]platinum(II)

#### Pt(mbchca)<sub>2</sub>

KI (0.513 g, 3.09 mmol) was added to potassium tetrachloroplatinite(II) (0.152 g, 0.365 mmol) dissolved in 5 mL H<sub>2</sub>O. The dark purple solution was combined with a 10 mL solution of acetonitrile containing N-(N'-1-methylbenzimidazol-2-yl)cyclohexanamide (0.243 g, 0.944 mmol). A yellow precipitate (0.275 g), identified later as the cis-diiodo product, was observed. The mixture was filtered and (4 x 71 μL) 3.93 M KOH was added to the filtrate. 0.0139 g of product was isolated after filtration.

Yield: 0.0197 mmol, 5.40 %; Calcd mass: 707.25 g/mol, exptl mass:  $m/z$  (%)  $[M]^+$ : 708.13 (100)  $[((mbchca)_2Pt)H]^+$ , 258.35 (46)  $[(Hmbchca)H]^+$ ;  $^1H$  NMR ( $CDCl_3$ ):  $\delta$ : 7.14 (2H, d,  $J = 4$  Hz, benzimidazole), 7.02 (2H, t,  $J = 7.0$  Hz, benzimidazole), 6.66 (2H, d,  $J = 8.0$  Hz, benzimidazole), 6.38 (2H, d,  $J = 4.25$  Hz, benzimidazole), 3.65 (3H, s, N- $CH_3$ ), 2.54 (2H, tt, cyclohexane), 2.11 (4H, t,  $J = 16.5$  Hz, cyclohexane), 1.83 (4H, t, cyclohexane), 1.70 (2H, t, cyclohexane), 1.63 (2H, t, cyclohexane), 1.57 (2H, s, cyclohexane), 1.36 (2H, m, cyclohexane); KBr-IR ( $cm^{-1}$ ):  $\nu_{C-H} = 3059, 2925, 2852$   $\nu_{C=C} = 1615$

**33. Bis[N-(N'-1-methylbenzimidazol-2-yl) cyclohexanecarboxamide]platinum(II) dichloride  $Pt(mbchca)_2Cl_2$**

$K_2PtCl_4$  (0.161 g, 0.388 mmol) dissolved in 5 mL  $H_2O$  was added dropwise to a slurry of 5 mL MeOH / 5 mL MeCN / 6 mL  $CHCl_3$  / 10 mL  $CH_2Cl_2$  and N-(N'-1-methylbenzimidazol-2-yl)cyclohexanecarboxamide (0.200 g, 0.777 mmol) on a hot plate. The temperature of the mixture was adjusted from 95°C to 60°C after 5 minutes. The temperature was raised to 75 °C, 30 minutes into the reaction. 5 mL MeOH was added after 2.25 hours. A yellow homogenous solution was observed. The solvent of the solution was removed by rotary evaporation after 30 minutes. The resulting solid, 0.208 g, was washed with 40 mL  $H_2O$  and recrystallized in 5 mL  $CHCl_3$ . Yield: 0.267 mmol, 68.7 %; Calcd mass: 779.21 g/mol, exptl mass:  $m/z$  (%)  $[M]^+$ : 745.37 (35)  $[((mbchca)_2PtCl)H]^+$ , 258.48(100)  $[(Hmbchca)H]^+$ , 280.46 (10)  $[HmbchcaNa]^+$ ;  $^1H$  NMR ( $CDCl_3$ ):  $\delta$ : 10.05 (2H, s, N-H), 7.19 (8H, m, benzimidazole), 3.62 (6H, s, benzimidazole), 2.68 (2H, s,  $-CH_2-$ ), 2.31 (2H, s,  $-CH_2-$ ), 2.15 (2H, s,  $-CH_2-$ ), 1.55 (22H, m,  $-CH_2-$ )

### 34. Bis [N-(N'-1-methylbenzimidazol-2-yl) hexadecanamido]platinum(II)

#### **Pt(mbhda)<sub>2</sub>**

K<sub>2</sub>PtCl<sub>4</sub> (0.156 g, 0.377 mmol) was added to a 15 mL (2:1v) acetonitrile/ water solution. The mixture was stirred for 30 minutes after which potassium iodide (0.500 g, 0.301 mmol) was added. After 30 minutes, N-(N'-1-methylbenzimidazol-2-yl) hexadecanamide (0.290 g, 0.754 mmol), dissolved in 5 mL acetonitrile, was added to the solution. A yellow precipitate was observed after the addition of two equivalents of 3.93 M KOH. The product was isolated via suction filtration. Yield: 152 μmol, 40.4% Calcd mass: 965.58 g/mol, exptl mass: *m/z* (%) [M]<sup>+</sup>: 964.18 (30)[Pt(mbhda)<sub>2</sub>-H]<sup>+</sup>, 386.45(100) [(Hmbhda)H]<sup>+</sup>, 735.43(88) [Pt(mbhda)(matrix-DBA)]<sup>+</sup> .

### 35. *Cis*-diiodo-Bis[2,2-dimethyl-N-(N'-1-methylbenzimidazol-2-

#### **yl)propanamide]platinum(II) Pt(Hdmmbp)<sub>2</sub>I<sub>2</sub>**

K<sub>2</sub>PtCl<sub>4</sub> (0.146 g, 0.351 mmol) was added to a 5 mL (2:1v) acetonitrile/ water solution. The mixture was stirred for 30 minutes after which potassium iodide (0.486 g, 2.93 mmol) was added. After 30 minutes, two equivalents of 2,2-dimethyl-N-(N'-1-methylbenzimidazol-2-yl)propanamide. An instant yellow precipitate was observed. A weight of 0.300 g of product was isolated from filtration and drying (*in vacuo*). Yield: 0.329 mmol, 93.8 %. <sup>1</sup>H NMR (CDCl<sub>3</sub>): δ: 9.91 (2H, s, N-H), 7.47 (2H, d, *J* = 8.0 Hz, benzimidazole), 7.17 (4H, s, benzimidazole), 7.13 (2H, s, benzimidazole), 3.68 (6H, s, N-CH<sub>3</sub>), 1.67 (18H, s, tert-butyl).

### 36. Bis[2,2-dimethyl-N-(N'-1-methylbenzimidazol-2-yl)propanamido]platinum(II)

#### Pt(dmmbp)<sub>2</sub>

10 mL acetonitrile / water solution (2:1v) was added to (0.300 g, 0.329 mmol) Pt(dmmbp)<sub>2</sub>I<sub>2</sub> in a 25 mL Erlenmeyer flask. Four aliquots of 71 μL of 3.93 M KOH was added to the mixture under stirring. A color change (yellow to pale yellow) of the solute was observed. The pale yellow precipitate was filtered and dried after 2 hours. 0.180 g of product was recovered. Yield: 0.274 mmol, 83.2 % <sup>1</sup>H NMR (CDCl<sub>3</sub>): 7.14 (2H, d, *J* = 8.0 Hz, benzimidazole), 7.02 (2H, t, *J* = 7.5 Hz, benzimidazole), 6.68 (2H, d, *J* = 7.5 Hz, benzimidazole), 6.40 (2H, d, *J* = 8.0 Hz, benzimidazole), 3.75 (3H, s, N-CH<sub>3</sub>), 1.36 (18H, s, tert-butyl); KBr-IR (cm<sup>-1</sup>): ν<sub>C-H</sub> = 3061, 3047, 2964, 2871 ν<sub>C-O</sub> = 1708

### 37. *Cis* - Bis[2,2-dimethyl-N-(N'-1-methylbenzimidazol-2-

#### yl)propanamide]platinum(II) dichloride Pt(Hdmmbp)<sub>2</sub>Cl<sub>2</sub>

**Method A:** Pt(dmmbp)<sub>2</sub> (0.180 mg, 0.274 mmol) was dissolved in 25 mL of dichloromethane. HCl gas (from a conc. H<sub>2</sub>SO<sub>4</sub>/NaCl generator) was bubbled through the stirring solution for 15 minutes. The light yellow solution became more intensely yellow over the 15 minutes. The solvent was evaporated (*in vacuo*) after 6 hours of stirring. The residue was recrystallized in 2 mL CH<sub>2</sub>Cl<sub>2</sub>/ 2 mL ether. Yellow crystals weighing 0.193 g were obtained. (yield: 0.265 mmol, 96.9 %)

**Method B:** K<sub>2</sub>PtCl<sub>4</sub> (0.925 g, 0.223 mmol) dissolved in 5 mL H<sub>2</sub>O was added dropwise to a stirring solution of N-(N'-1-methylbenzimidazol-2-yl)-2,2-dimethylpropanamide (0.103 g, 0.446 mmol) in 5 mL ethanol. The reaction was maintained at 50°C. A yellow precipitate started forming after 4 hours. The reaction was stopped after 8 hours 35 minutes. 0.106 g of product was isolated after recrystallization in 2 mL CH<sub>2</sub>Cl<sub>2</sub>/ 2 mL

diethyl ether. Yield: 0.146 mmol, 65.4 %. Calcd mass: 727.18 g/mol, exptl mass:  $m/z$  (%)  
[M]<sup>+</sup>: 731.80 (8) [(Pt(Hdmmbp)<sub>2</sub>Cl<sub>2</sub>)H<sub>4</sub>]<sup>+</sup>, 232.59 (100) [(Hdmmbp)H]<sup>+</sup>; <sup>1</sup>H NMR  
(CDCl<sub>3</sub>): δ: 10.39 (2H, s, N-H), 7.19 (6H, m, benzimidazole), 7.11 (2H, d,  
benzimidazole), 3.72 (6H, s, N-CH<sub>3</sub>), 1.64 (18H, s, tert-butyl) ; KBr-IR (cm<sup>-1</sup>): ν<sub>N-H</sub> =  
3267, 3218 ν<sub>C-H</sub> = 3063, 3047, 2964, 2871 ν<sub>C-O</sub> = 1708

**38. *Cis* -Bis[(N-benzimidazol-2-yl)-2,2-dimethylpropanamide]platinum(II) diiodide  
Pt(Hdmbp)<sub>2</sub>I<sub>2</sub>**

K<sub>2</sub>PtCl<sub>4</sub> (0.258 g, 0.622 mmol) and potassium iodide (0.798 g, 4.81 mmol) dissolved in 5  
mL water, was added dropwise to (N-benzimidazol-2-yl) 2,2-dimethyl propanamide  
(0.261 g, 1.20 mmol) in 14 mL acetonitrile / 10 mL methanol. A yellow precipitate was  
observed and suction filtered after 7 hours. Yield: 0.172 g, 0.195 mmol, 31.3%. Calcd  
mass: 883.02 g/mol, exptl mass:  $m/z$  (%) [M]<sup>+</sup>: 888.49 (26.92) [(Pt(Hdmbp)<sub>2</sub>I<sub>2</sub>)H<sub>5</sub>]<sup>+</sup>,  
218.86 (100) [(Hdmbp)H]<sup>+</sup>; KBr-IR (cm<sup>-1</sup>): ν<sub>N-H</sub> = 3325 (broad), ν<sub>C-H</sub> = 2965, 2870 ν<sub>C-O</sub>  
= 1708

**39. *Cis* - Bis[(N-benzimidazol-2-yl)-2,2-dimethylpropanamide]platinum(II)  
dichloride (Hdmbp)<sub>2</sub>PtCl<sub>2</sub>**

K<sub>2</sub>PtCl<sub>4</sub> (0.416 g, 1.00 mmol) dissolved in 10 mL water was added dropwise to a 10 mL  
tetrahydrofuran solution of (N-benzimidazol-2-yl)-2,2-dimethylpropanamide. An instant  
precipitate was observed upon the dropwise addition, disappearing after a minute. The  
orange solution was maintained at 50°C overnight. The yellow precipitate was filtered  
and dried. A weight of 0.0324 g of desired product was obtained.



Yield: 0.463 mmol, 46.3%; Calcd mass: 699.14 g/mol, exptl mass:  $m/z$  (%)  $[M]^+$ : 665.58 (40)  $[(Pt(Hdmbp)_2Cl)H]^+$ , 219.04 (100)  $[(Hdmbp)H_2]^+$ ;  $^1H$  NMR ( $CDCl_3$ ):  $\delta$ : 11.33 (2H, s, amide protons), 10.44 (2H, s, benzimidazole), 8.20 (2H, s, benzimidazole), 7.39 (2H, d,  $J = 4.5$  Hz, benzimidazole), 7.32 (4H, t,  $J = 7.5$  Hz, benzimidazole), 1.48 (18H, tert-butyl)

**40. Bis[ N-(benzimidazol-2-yl) cyclohexane carboxamide] platinum(II) diiodide**  
**(Hbchca)<sub>2</sub>PtI<sub>2</sub>**

Potassium iodide (1.16 g, 6.98 mmol) was added to  $K_2PtCl_4$  (0.383 g, 0.923 mmol) dissolved in 5 mL water under stirring. The resulting purple solution was added dropwise to a slurry of N-benzimidazol-2-yl cyclohexanecarboxamide (0.442 g, 1.74 mmol) in 10 mL methanol. 10 mL acetonitrile and 5 mL water was added to the mixture. A yellow precipitate was observed after 1 h 45 minutes. A weight of 0.724 g of product was recovered and recrystallized using dimethylformamide and ethanol. Yield: 0.774 mmol, 83.9 %; Calcd mass: 935.05 g/mol, exptl mass:  $m/z$  (%)  $[M]^+$ : 808.12(43.98)  $[(Hbchca)_2PtI-H]^+$ , 244.88 (100)  $[(Hbchca)H]^+$ , 266.96 (24)  $[Hbchca Na]^+$ , 282.73 (8)  $[HbchcaK]^+$ ;  $^{13}C$  NMR ( $(CD_3)_2CO$ ):  $\delta(m)$ : 123.15, 122.45 (d), 118.86 (s), 111.94 (2H), 44.77 (s), 35.23 (s), 26.53 (s), 26.53 (s), 25.44(s), 25.19(s); KBr-IR ( $cm^{-1}$ ):  $\nu_{N-H} = 3312$ ,  $\nu_{C-H} = 3058, 2929, 2853$   $\nu_{C-O} = 1708$

**41. Cis - Bis[N-(N'-1-methylbenzimidazol-2-yl)propanamide]platinum(II) dichloride**  
**(Hmbp)PtCl<sub>2</sub>**

$K_2PtCl_4$  (0.0879 g, 0.212 mmol) was dissolved in 5 mL water and added to a stirring solution of N-(N'-1-methylbenzimidazol-2-yl)propanamide (0.0866 g, 0.424 mmol) in

5 mL methanol. The reaction was allowed to continue for 17 hours. The yellow precipitate was filtered, washed with 5 mL H<sub>2</sub>O and recrystallized in chloroform. Yield: 0.101 g, 0.150 mmol, 70.9%, Calcd mass: 671.11 g/mol, exptl mass:  $m/z$  (%) [M]<sup>+</sup>: 637.23 (17.91) [(Pt(Hmbp)<sub>2</sub>Cl)H<sub>2</sub>]<sup>+</sup>, 204.82 (100) [(Hmbp)H]<sup>+</sup>, 600.33 (30) [Pt(Hmbp)<sub>2</sub>]<sup>+</sup>; <sup>1</sup>H NMR (CDCl<sub>3</sub>): δ: 10.20 (2H, s, amide), 7.17, 7.08 (8H, m, benzimidazole), 3.74 (6H, s, N-CH<sub>3</sub>), 1.21 (4H, -CH<sub>2</sub>-), 0.815 (6H, t, -CH<sub>3</sub>); KBr- IR (cm<sup>-1</sup>): ν<sub>N-H</sub> = 3251, 3145 ν<sub>C-H</sub> = 2978, 2941 ν<sub>C-O</sub> = 1732, 1699

#### **42. N-(N'-1-methylbenzimidazol-2-yl) benzamide] platinum(II) and platinum(IV) complexes**

K<sub>2</sub>PtCl<sub>4</sub> (0.146 g, 0.351 mmol) was added to a 5 mL (2:1v) acetonitrile/ water solution. The mixture was stirred for 30 minutes after which (0.486 g, 2.93 mmol) potassium iodide was added. After 30 minutes, two equivalents of N-(N'-1-methylbenzimidazol-2-yl)benzamide, Hmbba, were added. A yellow precipitate was observed. A weight of 0.300 g of product was isolated from filtration and drying (*in vacuo*). A 10 mL acetonitrile-water solution (2:1v) was added to (0.300 g, 0.330 mmol) Pt(Hmbba)<sub>2</sub>I<sub>2</sub> in a 25 mL Erlenmeyer flask. Four aliquots of 71 μL of 3.93M KOH were added to the mixture under stirring. A color change (yellow to pale yellow) of the solute was observed. The pale yellow precipitate, 0.180 g, was filtered and dried after 2 hours. (0.180 g, 0.274 mmol) Pt(mbba)<sub>2</sub> was dissolved in 25 mL of dichloromethane. HCl gas (from a conc. H<sub>2</sub>SO<sub>4</sub>/NaCl generator) was bubbled through the stirring solution for 15 minutes. The light yellow solution became more intensely yellow over the 15 minutes. The solvent was evaporated (*in vacuo*) after 2 hours of stirring.

**46. *Cis* - Bis[N'-boc-2-amino-2,2-dimethyl (N-(N''-1- methylbenzimidazol-2-yl)acetamide)]platinum(II) dichloride (*isoba*) Pt(L<sup>boc</sup>)<sub>2</sub>Cl<sub>2</sub>**

K<sub>2</sub>PtCl<sub>4</sub> (0.0403 g, 0.971 mmol) was dissolved in 5 mL water and added to a stirring solution of N'-boc-2-amino-2,2-dimethyl(N-(1- methyl benzimidazol-2-yl)acetamide (0.0645 g, 0.194 mmol) in 10 mL methanol. The reaction was stirred at 80°C for 24 hrs and allowed to stir at room temperature for nine days. The yellow precipitate was filtered and washed with 5 mL H<sub>2</sub>O. 0.0631 g of desired product was obtained.

Yield: 67.86 μmol, 69.9 %; Calcd mass: 929.27 g/mol, exptl mass: *m/z* (%) [M]<sup>+</sup>: 933.02 (23) [(Pt(Hisoba)<sub>2</sub>Cl<sub>2</sub>)H<sub>4</sub>]<sup>+</sup>; <sup>1</sup>H NMR (CDCl<sub>3</sub>): δ: 10.59 (4H, s, amide ), 7.17 (8H, m, benzimidazole), 3.90 (6H, s, N-CH<sub>3</sub>), 2.00 (6H, s, -CH<sub>3</sub>), 1.76 (6H, s, -CH<sub>3</sub>), 1.45 (18H, s, t-butyl).

## CHAPTER III

### TRANSITION METAL COMPLEXES

#### **A: Background Discussion**

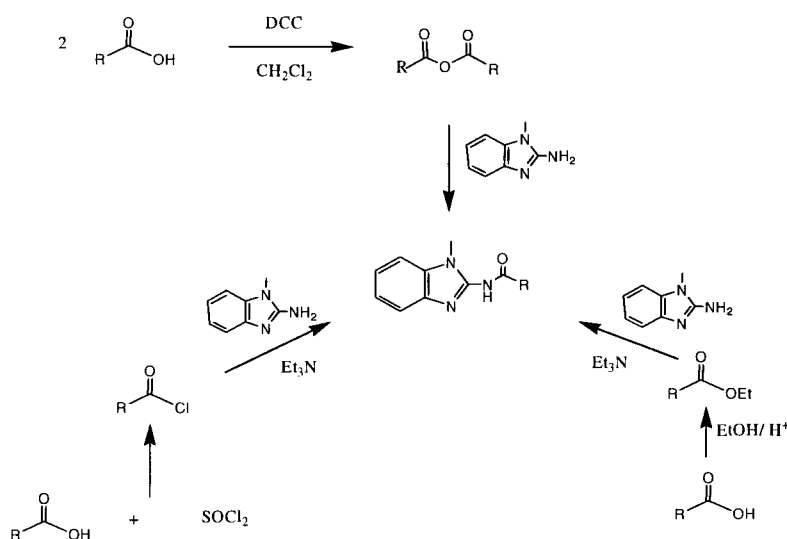
The interest in first row transition metals is partly due to an effort to understand their vital biological roles in metalloproteins and their potential in medicinal chemistry. Ions such as  $\text{Co}^{2+/3+}$  [17],  $\text{Fe}^{2+/3+}$  [1, 17],  $\text{Cu}^{2+}$  and  $\text{Zn}^{2+}$  [18, 25] can be found in the active sites of such enzymes as glutamase mutase and methionine synthase for cobalt, hemoglobin and cytochromes for iron, superoxide mutase and tyrosinase for copper, and carbonic anhydrase for zinc, just to name a few. Vanadium(IV) compounds for example are being investigated for their insulin-like and anti-tumor activities [17, 46].

Unlike the s-block metals, transition metals have varying oxidative states. In addition to the varying oxidative states, transition metals, because of partially filled d-orbitals and comparatively low energy barriers between their d-orbitals, are able to promote electrons resulting in low or high spin states. Additionally, different coordination numbers result for the same oxidative state depending on the ligand field. For example, Fe(II) ion in hemoglobin, transitions between a five coordinate (deoxyhemoglobin) and a six coordinate complex when bound to  $\text{O}_2$  without the oxidation of the iron center, allowing the transfer of oxygen from the lungs to inner tissues in the human body [121]. In cytochrome c however, the iron is used in the transfer of electrons in the synthesis of ATP in the mitochondria and cycles between +2

and +3 oxidation states [122-125]. Carboxypeptidase has at its core a Zn(II) ion, a p-block metal with filled d-orbitals, has a N<sub>2</sub>O<sub>2</sub> donor set with a water molecule coordinated in the fifth position. The nitrogens are from histidine residues, while the oxygen atoms are from a glutamate residue [17]. This enzyme hydrolyzes peptidic bonds without a change in the oxidative state of the metal. Other biological roles of these metals include involvement in catalytic pathways, electrochemical processes and radical chemistry as evident in methylation during methionine synthesis, proton gradient formation during ATP synthesis, or the synthesis of RNA by RNA polymerase.

In an effort to gain more insight into transition metal behavior, ligands containing 2-aminobenzimidazole and 2-amino-1-methylbenzimidazole were functionalized into amides and complexed to selected biologically relevant metals. This chapter examines the coordination modes, coordination numbers and crystal lattice packing arrangements of these complexes, synthesized using a 1:2 metal-ligand ratio.

## B: Synthesis and Characterization of Ligands



Scheme 1: Reaction protocol of 2-amino-1-methylbenzimidazole ligands.

Scheme 1 shows some standard reactions that can be used to functionalize an amine into an amide. Some of the reaction routes that lead to amide formation involve a Fischer acid esterification of a carboxylic acid, followed by reaction with a primary amine. Another involves the reaction of an anhydride with a primary amine. A third method usually employed is the reaction of an acyl chloride with the primary amine under basic conditions. The acyl chloride could be generated by reacting a carboxylic acid and thionyl chloride or could be commercially obtained. Generally, acyl chlorides gave comparatively higher amide product yields than either anhydrides or esters. Therefore reaction routes involving anhydrides or esters were employed only when their respective acyl chlorides were not commercially available. Compounds **1-6** and **8-12** were synthesized by reacting either 2-amino-1-methylbenzimidazole or 2-amino benzimidazole with the respective acyl chloride. Compounds **3** and **6** were synthesized using published procedures of Rastogi *et al.* [126]. Compound **7** was synthesized by the generation of the anhydride (*in situ*) via DCC coupling, followed by reaction with 2-amino-1-methylbenzimidazole. Compound **9** was synthesized based on established procedures by Philip Bauer [32].

The initial solubility of 2-amino-1-methylbenzimidazole crystals is low in methylene chloride (~10 mg in 10 mL). However, its solubility is enhanced with the addition of triethylamine (usually 1.5 molar equivalence). The use of a solvent such as methylene chloride in the synthetic route provides the advantage of the separation of triethylammonium chloride from the product solution by simple filtration. The excess triethylamine is removed by treatment of the product solution with brine solution in a separating funnel. The methylene chloride is then stripped via rotary evaporation. The

product is extracted using diethyl ether followed by stripping of the solvent via rotary evaporation. Thus, chromatography is avoided.

Unlike its 1- methyl derivative, 2-aminobenzimidazole has two sites for amidation (N1 and 2-amino). Consequently reactions done at room temperature are likely to produce mixed products. Additionally, 2-aminobenzimidazole is not soluble in methylene chloride. As a result, reactions involving 2-aminobenzimidazole were carried out in dimethylformamide according to published protocols by Rastogi *et al.* with four equivalence of triethylamine and six hours of reflux [126]. The product solution is poured into a beaker of water (~350-500 mL) upon cooling to room temperature, and the desired product is recovered using filtration. The change in solvent and subsequent work-up introduces two potential problems, the first of which is the possible protonation of the N3, the site necessary for metal-ligand complexation. This is only problematic when dealing with platinum complexation discussed in the next chapter. The second potential problem involves pi-stacking of these ligands due to hydrophobicity.

#### **A. <sup>1</sup>H NMR and Mass Spec. Analysis of Ligands**

Table 3.1 below displays the mass spectrometric data for ligands used in this work.

Reported below are the exact masses of the most intense isotopomers in selected peak clusters. The spectra of these compounds can be located in the appendix. Examination of the data reveals agreement of the calculated masses and the experimental masses.

Table 3.1: Mass spectrometric data of ligands

Compd	Calcd. Mass (Rel. ab'dance %)	Expt'l mass m/z (peak intensity%) peak characterization
1	385.31 (75)	386.64 (100) [(Hmbhda)H] <sup>+</sup> , 408.58 (60) [(Hmbhda)Na] <sup>+</sup>
2	301.22 (81)	301.04 (46) [Hmbda] <sup>+</sup> , 322.92 (20) [(Hmbda)Na] <sup>+</sup> , 340 (10) [(Hmbda)K] <sup>+</sup>
3	243.14 (84)	243.26 (100) [Hbchca] <sup>+</sup>
4	257.15 (83)	258.48 (68) [(Hmbchca)H] <sup>+</sup> , 280.45(56) [(Hmbchca) Na] <sup>+</sup> , 296.36 (76) [(Hmbchca)K] <sup>+</sup>
5	251.11 (83)	251.20 (100) [Hmbba] <sup>+</sup> , 273.04 (22) [(Hmbba-H) Na] <sup>+</sup> , 289.02 (19) [(Hmbba-H)K] <sup>+</sup>
6	237.09 (84)	238.39 (69) [(Hbba)H] <sup>+</sup>
7	332.18 (81)	333.56 (100) [(Hisoba)H] <sup>+</sup> , 355.50 (75) [(Hisoba-H) Na] <sup>+</sup> , 372.36 (46) [(Hisoba) K] <sup>+</sup>
8	334.11 (80)	334.93 (100) [Hmbpa] <sup>+</sup> , 357.93 (10) [(Hmbpa)Na] <sup>+</sup>
9	231.14 (85)	232.43 (100) [(Hdmbmp)H] <sup>+</sup>
10	189.09 (88)	190.62 (100) [(Hmba)H] <sup>+</sup> , 212.44 (82) [(Hmba) Na] <sup>+</sup> , 228.39 (64) [(Hmba)K] <sup>+</sup>
11	290.97 (38)	289.51 (95) [(Hmbtca)-H] <sup>+</sup> , 290.48 (60) [Hmbtca] <sup>+</sup> , 174.41 (55) [(methylbenzimidazole)C=O] <sup>+</sup>
12	217.12 (86)	217.34 (100) [Hdmbp] <sup>+</sup> , 239.24 (38) [(Hdmbp-H)Na] <sup>+</sup> , 255.13 (18) [(Hdmbp-H)K] <sup>+</sup>
13	203.11 (87)	203.99 (100) [Hmbpa] <sup>+</sup>

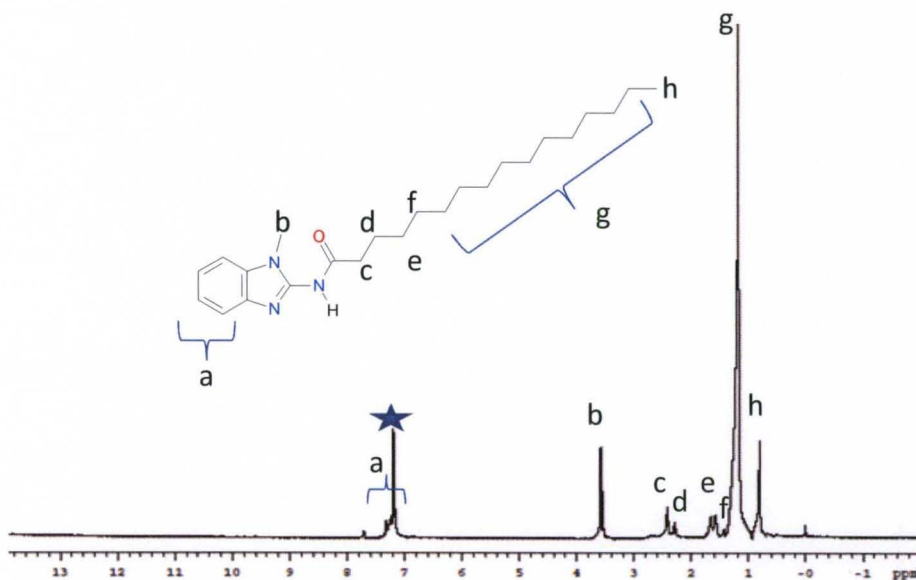


Figure 3.1: <sup>1</sup>H NMR spectrum of compound **1** in CDCl<sub>3</sub>

The <sup>1</sup>H NMR spectrum of compound **1**, Figure 3.1, reveals a multiplet centered at 7.23 ppm and corresponds to the four aromatic protons of the benzimidazole. The peak at 3.79 ppm corresponds to the methyl protons attached to the nitrogen (N1) of the



benzimidazole. Peaks appear as triplets at 2.50 ppm, 2.38 ppm, 1.76 ppm, 1.68 ppm and 0.886 ppm, corresponding to protons of the aliphatic palmitoyl pendant and are in the ratio 4H:2H:4H:2H:3H respectively. The broad peak at 1.26 ppm integrates to 16H (-CH<sub>2</sub>- protons).

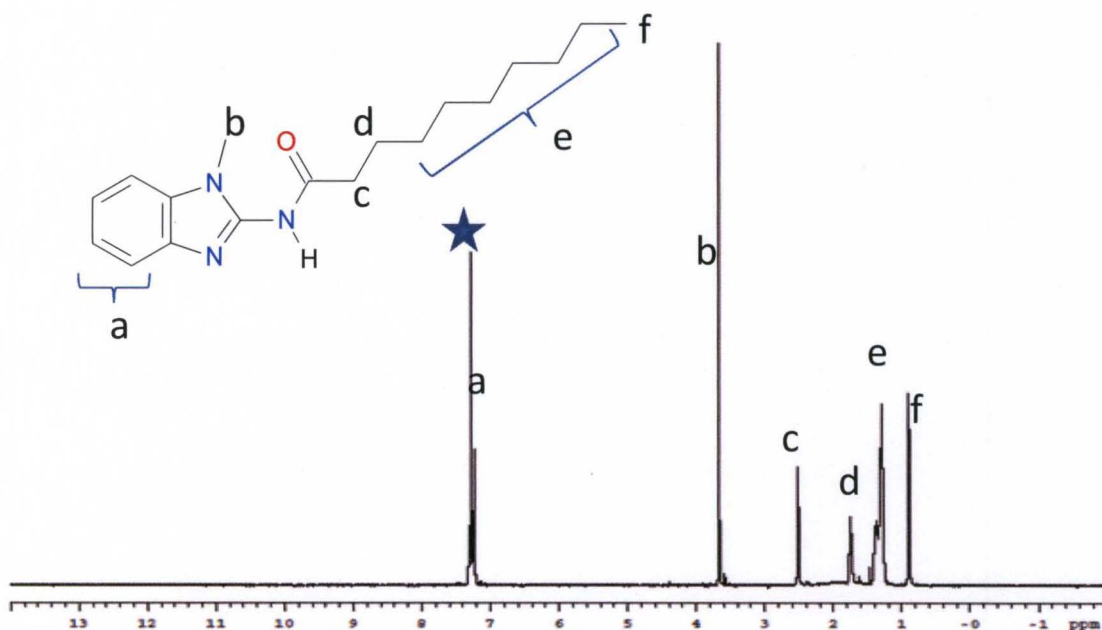


Figure 3.2: <sup>1</sup>H NMR spectrum of compound **2** in CDCl<sub>3</sub>

The <sup>1</sup>H NMR spectrum of compound **2** in CDCl<sub>3</sub>, Figure 3.2, displays a multiplet around 7.28 ppm that represents the aromatic protons of the benzimidazole moiety. The peak at 3.66 ppm corresponds to the methyl protons of N1 of the benzimidazole. The peak at 2.51 ppm, a triplet, corresponds to the two protons of the carbon, (C<sub>α</sub>), alpha to the carbonyl carbon. The peaks at 1.75 ppm and 0.893 ppm appear as a quartet and triplet respectively. They represent C<sub>β</sub>- protons and the terminal methyl protons. The broad peak at 1.38 ppm integrates to twelve -CH<sub>2</sub>- protons.

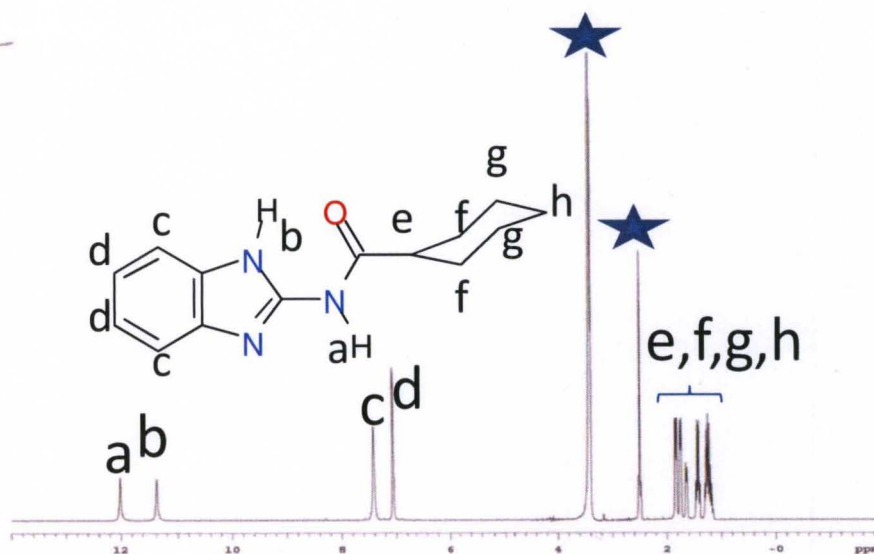


Figure 3.3:  $^1\text{H}$  NMR spectrum of compound **3** in  $\text{DMSO-d}_6$

The  $^1\text{H}$  NMR of compound **3** in deuterated dimethyl sulfoxide ( $\text{DMSO-d}_6$ ), shows two single peaks at 12.02 ppm and 11.38 ppm. These peaks correspond to the amide and benzimidazole protons respectively. The aromatic peaks of the benzimidazole appear at 7.42 ppm and 7.06 ppm. The peaks at 1.834 ppm, 1.75 ppm, 1.64 ppm and 1.43 ppm appear as doublets and multiplets and correspond to the ortho and meta protons. The para protons appear as a multiplet at 1.24 ppm. The ipso proton peak is masked by the water peak, a common impurity in  $\text{DMSO-d}_6$ , at 2.50 ppm. Its 1-methylbenzimidazole derivative, compound **4**, has a similar  $^1\text{H}$  NMR spectrum with the aromatic region having a multiplet at 7.23 ppm corresponding to the four aromatic protons of the benzimidazole. An amide peak appears at 12.22 ppm. A singlet with a chemical shift of 3.65 ppm corresponds to the methyl substituent of the benzimidazole moiety. Cyclohexyl protons of compound **4** appear at 2.42 ppm (t), 2.02 ppm (d), 1.80 ppm (d), 1.68 ppm (d), 1.53 ppm (dd) and 1.34 ppm (m) in  $\text{CDCl}_3$ .

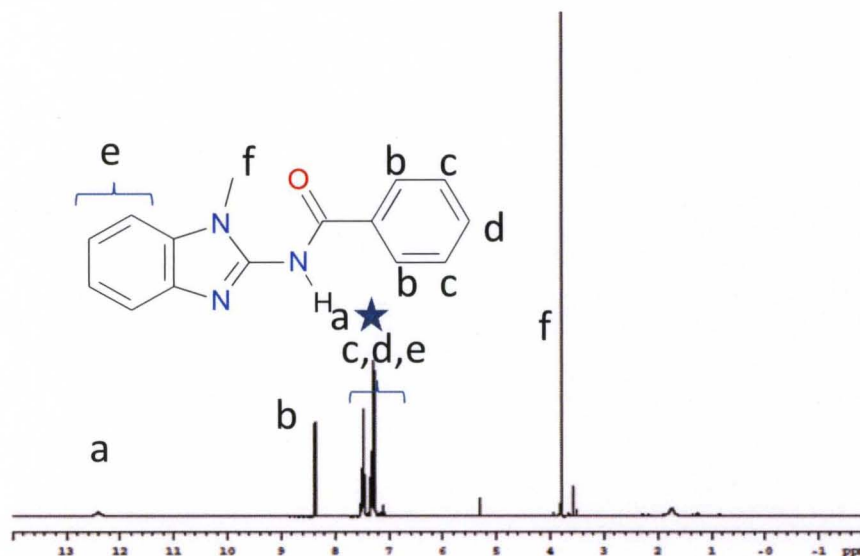


Figure 3.4:  $^1\text{H}$  NMR spectrum of compound **5** in  $\text{CDCl}_3$

Figure 3.4 shows the  $^1\text{H}$  NMR spectrum of compound **5** in  $\text{CDCl}_3$ . The singlet displayed at 12.40 ppm represents the amide proton. The doublet centered at 8.38 ppm ( $J = 7.0$  Hz), represents the two ortho protons of the phenyl, whilst the multiplet at 7.48 ppm corresponds to the three protons at the para and meta positions of the phenyl group. A multiplet at 7.28 ppm, corresponds to the four aromatic protons of the benzimidazole. The singlet with a chemical shift of 3.80 ppm represents the methyl substituent of the benzimidazole moiety. The 2-aminobenzimidazole derivative, compound **6**, has a similar proton spectrum with chemical shifts, in  $\text{DMSO-d}_6$ , at 12.23 ppm (s), 8.11 ppm (d), 7.12 ppm (d), 7.58 ppm (m), 7.51 ppm (m) and 7.44 ppm (m). The multiplets at 7.58 ppm, 7.51 ppm and 7.44 ppm represent ortho, meta and para protons of the phenyl group.

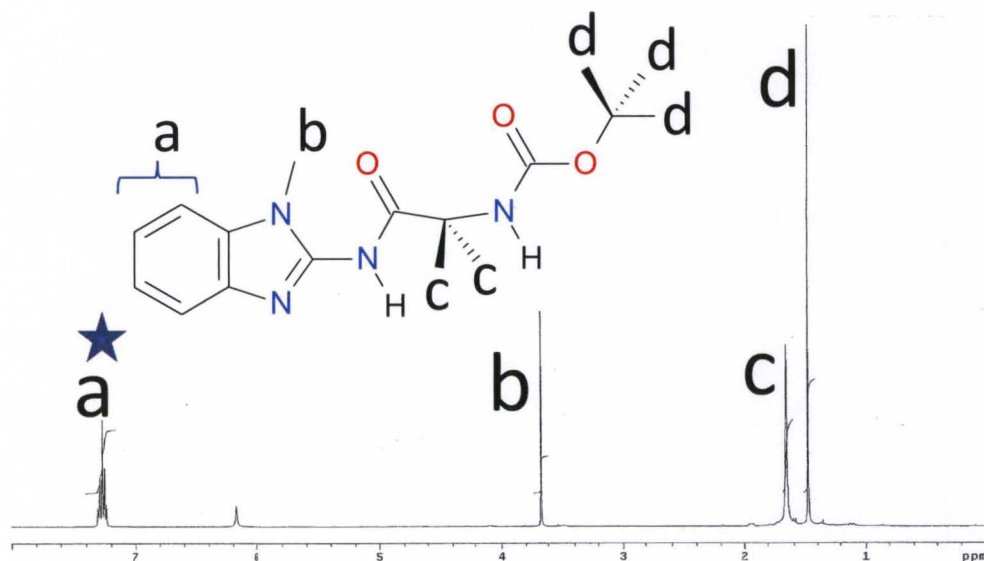


Figure 3.5:  $^1\text{H}$  NMR spectrum of compound **7** in  $\text{CDCl}_3$

Figure 3.5 displays the  $^1\text{H}$  NMR spectrum of compound **7**, N-(N'-1-methylbenzimidazol-2-yl)-N''-boc-2-amino-2,2-dimethylacetamide (Hisoba), in  $\text{CDCl}_3$ . A multiplet at 7.25 ppm represents the four aromatic protons of the benzimidazole. The peak at 6.20 ppm represents the amide proton (boc). Peaks at 3.68 ppm, 1.65 ppm and 1.48 ppm represent the methyl group of the 1-methylbenzimidazole, dimethyl of the acetyl group and the tert-butyl of the boc protecting group respectively.

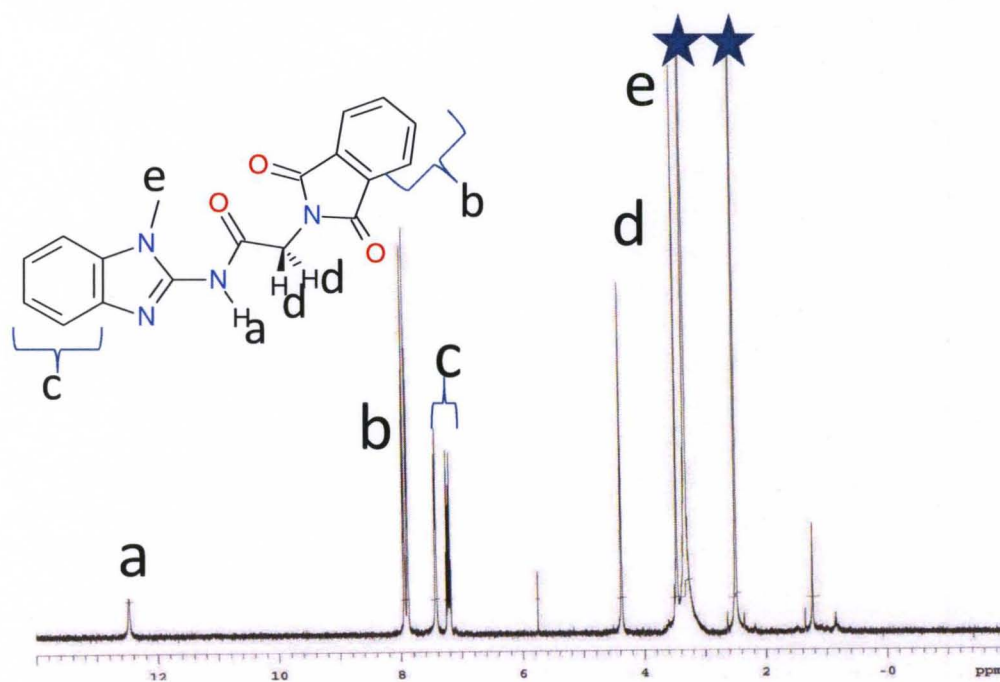


Figure 3.6:  $^1\text{H}$  NMR spectrum of compound **8** in  $\text{DMSO-d}_6$

The  $^1\text{H}$  NMR of compound **8** in  $\text{DMSO-d}_6$  is displayed in Figure 3.6. The spectrum shows an amide peak at 12.46 ppm. The aromatic region displays a doublet, singlet and multiplet at 7.91 ppm, 7.42 ppm and 7.21 ppm with an integration ratio of 4H: 2H: 2H respectively. The peaks at 4.40 ppm and 3.44 ppm correspond to the two protons of the acetyl group and the methyl group of the benzimidazole respectively. Figure 3.7 shows the  $^1\text{H}$  NMR spectrum of compound **9**, abbreviated Hdmmmbp elsewhere in the text, in  $\text{CDCl}_3$ .

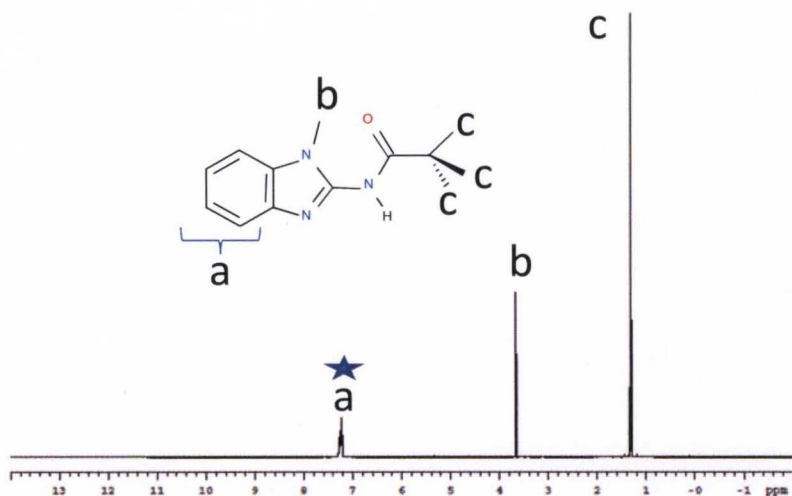


Figure 3.7:  $^1\text{H}$  NMR spectrum of compound **9** in  $\text{CDCl}_3$

The multiplet at 7.26 ppm corresponds to the four aromatic protons of the 2-amino-1-methylbenzimidazole. The singlet at 3.64 ppm represents the methyl protons of the N1 atom (benzimidazole). The nine tert-butyl protons appear as a singlet with a chemical shift at 1.30 ppm. Similarly, compound **10** has a multiplet around 7.28 ppm corresponding to the benzimidazole protons. Additional peaks at 12.24 ppm, 3.66 ppm and 2.28 ppm represents an amide, N-methyl and acetyl protons respectively. The  $^1\text{H}$  NMR of compound **11** in  $\text{CDCl}_3$ , Figure 3.8, shows an amide peak at 11.67 ppm.

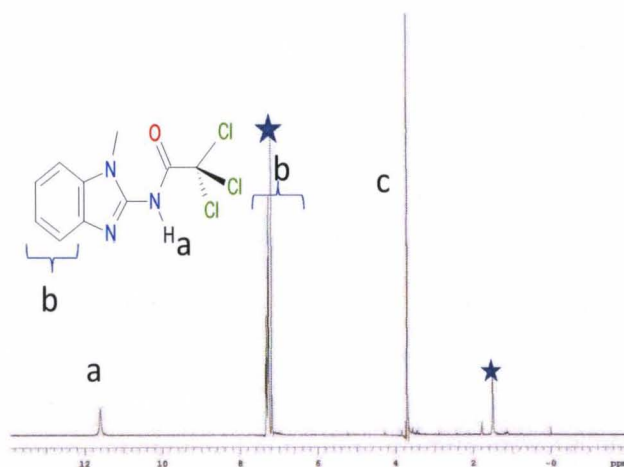


Figure 3.8:  $^1\text{H}$  NMR spectrum of compound **11** in  $\text{CDCl}_3$

The four aromatic protons of the benzimidazole appear as a multiplet at 7.28 ppm. The methyl substituent of the benzimidazole appears as a singlet at 3.78 ppm. The peak at 1.50 ppm is a water peak impurity commonly found in  $\text{CDCl}_3$  [127].

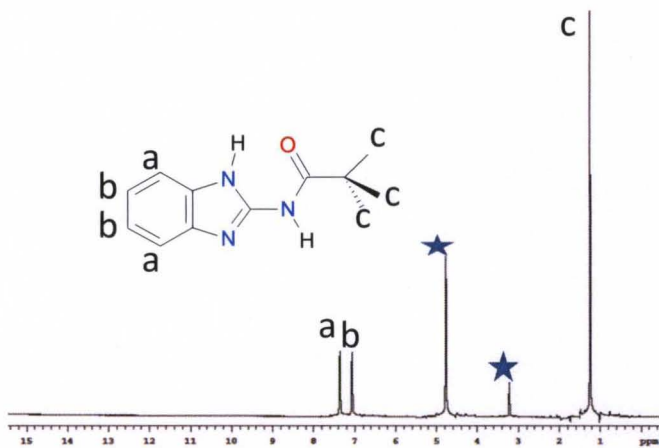


Figure 3.9:  $^1\text{H}$  NMR spectrum of compound **12** in  $\text{CD}_3\text{OD}$

The  $^1\text{H}$  NMR spectrum of compound **12** in  $\text{CD}_3\text{OD}$ , Figure 3.9, shows two doublets centered at 7.37 ppm and 7.07 ppm with coupling constants of 8.50 Hz and 9.50 Hz respectively. Both doublets integrate to four protons and represent the aromatic protons of the 1H-benzimidazole. The peak at 1.25 ppm represents the tert-butyl group. Both the amide peak and the hydrogen attached to the nitrogen of the benzimidazole are absent and might be due to rapid proton exchange with the solvent or tautomerization. However, they do show up in  $\text{CD}_2\text{Cl}_2$  at  $-80^\circ\text{C}$  at 12.15 ppm and 11.51 ppm respectively (spectrum in appendix). Additionally, the aromatic protons appear as singlets in the ratio 1:1:2 with chemical shifts of 7.57 ppm, 7.35 ppm and 7.21 ppm. The tert-butyl peak appears at 1.26 ppm.

The  $^1\text{H}$  NMR of the ligands performed in  $\text{CDCl}_3$ , 2-amino-1-methylbenzimidazole derivatives, compounds **1**, **2**, **4**, **5**, **7**, **9** and **10**, show broad amide

proton peaks with little or no peak intensity. In some cases, amide peaks are not visible. From a  $^1\text{H}$  NMR data interpretation view point, the absence of an amide peak is problematic. However, the aromatic proton signals of the 2-amino-1-methylbenzimidazole aggregate into a single multiplet peak when the primary amine is coupled to the carbonyl carbon of the acyl chloride. This can be used as a diagnostic tool for this system. The variation in amide peak intensity might be due to rapid proton exchange with the solvent or conversion between tautomeric conformers in solution. The tautomeric and resonance forms (1, 2 and 3) for the acetyl and benzamide derivatives in both solid and solution are shown in Figure 3.10 [128-135].

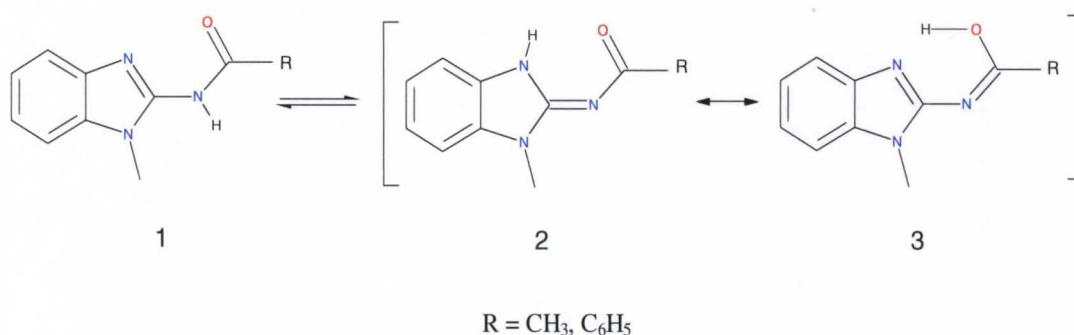


Figure 3.10: Tautomeric and resonance forms of acetyl and phenyl derivatives adapted and modified [32] Furthermore, the tendency of these ligands to exist as imides, ((2) in Figure 3.10), is directly proportional to the electron withdrawing strength of the attached amide coupling group [32]. The dominance of the imide form over the amide, may be due to resonance assisted hydrogen bonding [134-135]. Out of the seven  $^1\text{H}$  NMR spectra obtained in  $\text{CDCl}_3$ , only compound **11**, the most electron withdrawing of the series, shows a sharp amide peak. What this suggests is that compound **11** has either a comparatively slower proton exchange with solvent at room temperature or a preference of one tautomer over the other in solution, unlike the acetyl derivative or the tert-butyl derivative (compound



9). To investigate this phenomenon,  $^1\text{H}$  NMR temperature experiments from  $-80^\circ\text{C}$  to  $25^\circ\text{C}$  were carried out in  $\text{CD}_2\text{Cl}_2$  using compounds **3**, **4**, **9** and **11**. Figures 3.11- 3.13 display the stacked plots for these experiments.

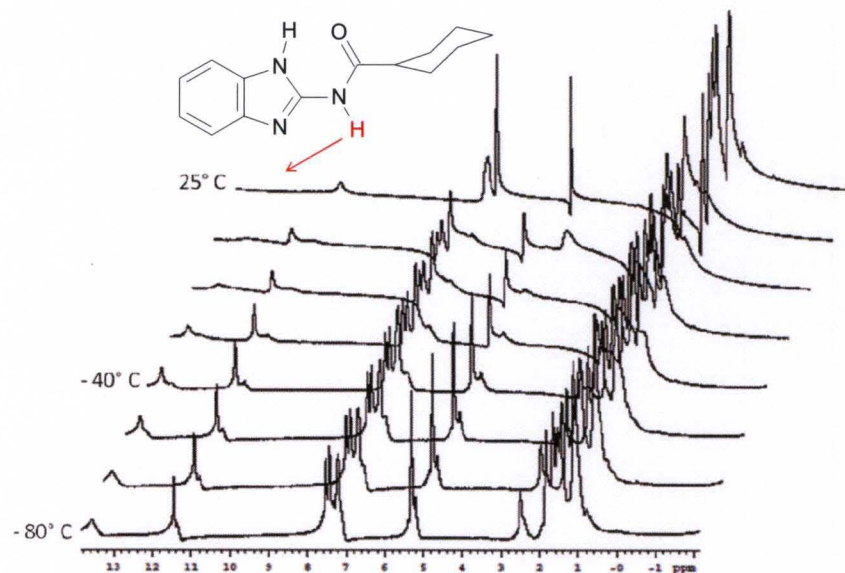


Figure 3.11: Stack plot of compound **3** in  $\text{CD}_2\text{Cl}_2$ ; showing the broadening of the amide peak with rise in temperature. **H** is tautomerized proton.

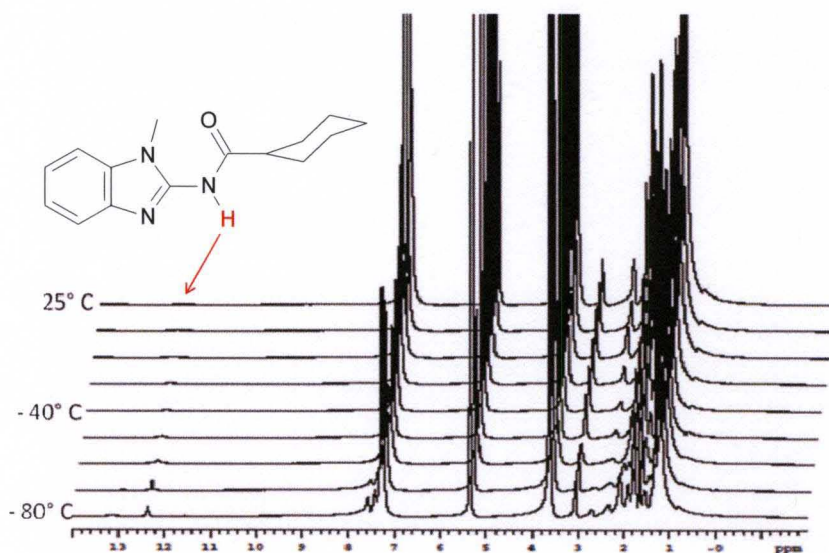


Figure 3.12: Stack plot of compound **4** in  $\text{CD}_2\text{Cl}_2$ ; showing the broadening of the amide peak with rise in temperature.

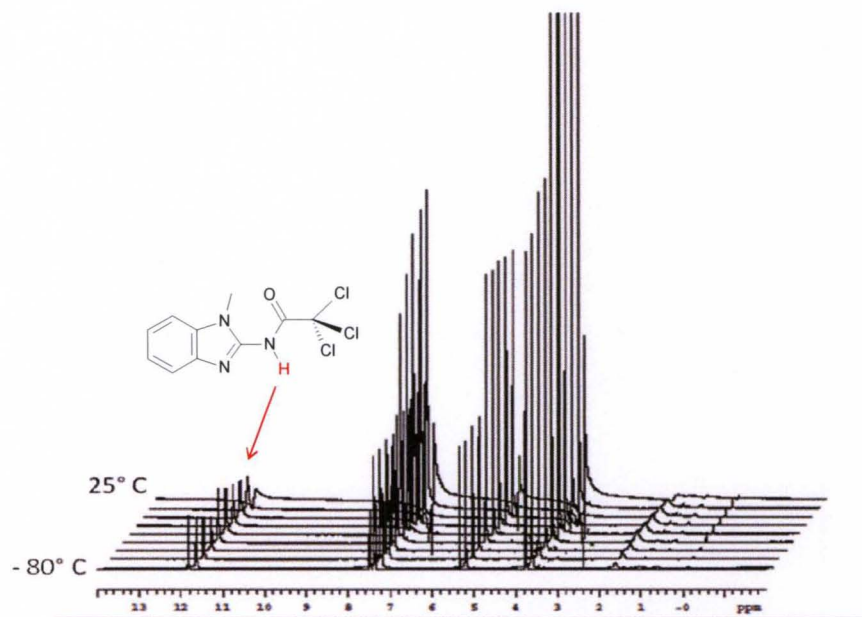


Figure 3.13: Temperature stack plot of compound **11** in  $\text{CD}_2\text{Cl}_2$

At  $-80\text{ }^\circ\text{C}$ , the tautomeric process is slow to a point where the amide peaks of all three compounds (**3**, **4** and **11**) can be seen. As the temperature is increased, the amide peaks of compounds **3** and **4** begin to broaden as a result of an increase in the rate of interconversion between imide and amide isomeric forms. The amide peak of compound **11**, however, remains sharp at all the temperatures ( $-80\text{ }^\circ\text{C}$  to  $25\text{ }^\circ\text{C}$ ), indicating a lack of interconversion between isomeric forms. The implication and significance of this in terms of property and tendency towards metal chelation will be explored in the next chapter. Additionally, proton exchange with the solvent can be ruled out since dichloromethane is a non-coordinating solvent and therefore cannot engage in the traditional (Bronsted) acid/base proton exchange with molecules in this series. It should be noted that compound **9** displays a temperature profile similar to that of compounds **3** and **4**. Compound **9** has been extensively investigated in our laboratory.

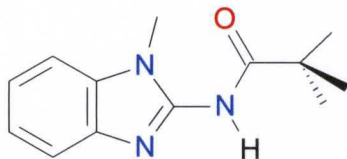


Figure 3.14: Drawing of compound **9**

Work done by Philip Bauer shows a preference for the imide isomer in the solid state [32]. Furthermore, theoretical calculations for the isomeric form 3 of compound **9**, (Figure 3.10), show that the energy barrier is too high, making this form not easily accessible. This however does not preclude this state as a possible intermediate step in its binding to metals. Furthermore, additional stability is gained through resonance in some 2-acylamido forms of similar heterocyclic moieties [132-133]. The pKa and coordination of compound **9** to  $\text{Co}^{2+}$ ,  $\text{Ni}^{2+}$ ,  $\text{Cu}^{2+}$  and  $\text{Zn}^{2+}$  ions, having acetate or nitrate as counterions, has also been investigated [32]. In his study, the pKa of compound **9**, Hdmmbp, was determined as 4.25, lower than acetic acid (4.74). Thus, the conjugate base of acetic acid should be able to deprotonate Hdmmbp, transforming it into a bis chelate anion, consequently promoting metal complex formation using metal acetate salt as starting material. Based on the experimental data, it was shown that the binding properties of Hdmmbp was pH dependant. Thus, the ligand has a propensity of forming predominantly neutral four coordinate complexes with the aforementioned first row transition metals (Figure 3.15) [32].

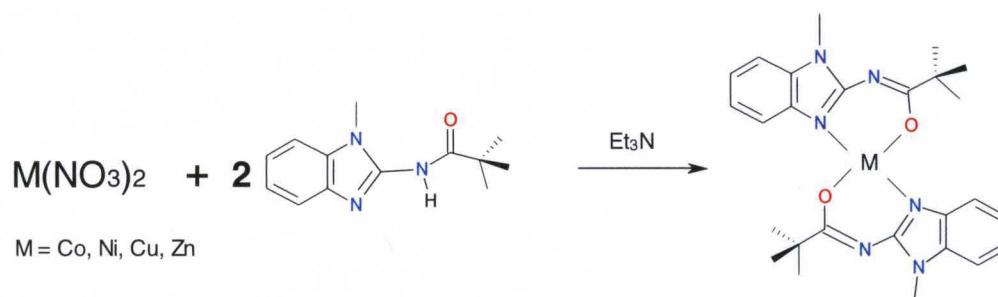


Figure 3.15: Metal complexes of compound **9**

The above study has been extended to include vanadium and is discussed later in the chapter. Additionally, a similar study involving the pyridine analog of compound **9**, 2- pivaloyl amino pyridine, purchased from Sigma-Aldrich is discussed in more detail in the next chapter.

## B: Synthesis and Characterization of Metal Complexes

Based on findings from previous studies, benzimidazole metal-complex derivatives were synthesized using metal nitrate salts and base. The preference of nitrate salts over acetate salts was primarily driven by an effort to increase yield. Except for the vanadyl complex, all metal complexes were obtained with a metal to ligand ratio of 1 : 2. Excess ligand was used in the case of vanadium to drive the reaction towards the formation of the bis chelated complex (diamido form).

Color changes were observed upon the combination of the dissolved metal salt and ligand methanol solutions of  $Cu^{2+}$ ,  $Co^{2+}$  and  $Ni^{2+}$ . These findings are consistent with similar 2-aminobenzimidazole complexes [32]. The color change occurs with the formation of the monodentate intermediate of the respective ligand, occurring through the coordination of the nitrogen of the benzimidazole, designated as N3, to the metal [32].

An attempt to generate similar four coordinate complexes of the pyridine analog of compound **9** for comparison, failed using the same synthetic method. This is consistent with the findings of Nonoyama *et al.* using an acetyl pyridine analog, N-(2-pyridyl) acetamide [136]. Nonoyama *et al.* concluded that the deprotonation of this ligand under alkaline conditions was facilitated only by Pd(II), hence the successful synthesis of the bis chelated square planar Pd(II) complex. However, copper, nickel and cobalt precipitated their respective hydroxides regardless of the starting metal salts used ( $\text{Cl}^-$ ,  $\text{Br}^-$ ,  $\text{NO}_3^-$ ,  $\text{NCS}^-$ ) [136].

Scheller-Krattiger *et al.* have reported two bis-chelated forms of the ligand with Ni(II) and Zn(II) using nitrate salts of the metal as starting material. Unlike the Pd(II) complex, the axial positions are occupied by water, making the complex octahedral [137]. In an effort to obtain the bis-chelated copper (II) complex in our lab, a second approach involving the reflux of the ligand in a copper acetate solution for one hour followed by stirring at room temperature for 24 hr was employed, resulting in compound **24**.

### **C: FT-IR Analysis of Metal Complexes**

Infrared spectroscopy helps elucidate functional groups in a complex. Amide complexes have characteristic absorption peaks around  $\sim 3200 \text{ cm}^{-1}$  and  $\sim 1700 \text{ cm}^{-1}$  indicative of amide proton and carbonyl stretching frequencies respectively. Figure 3.16 displays the KBr-IR absorption spectrum of compound **15**. The spectrum displays a broad stretching frequency peak in a region usually associated with the O-H stretch of water or an alcohol moiety.

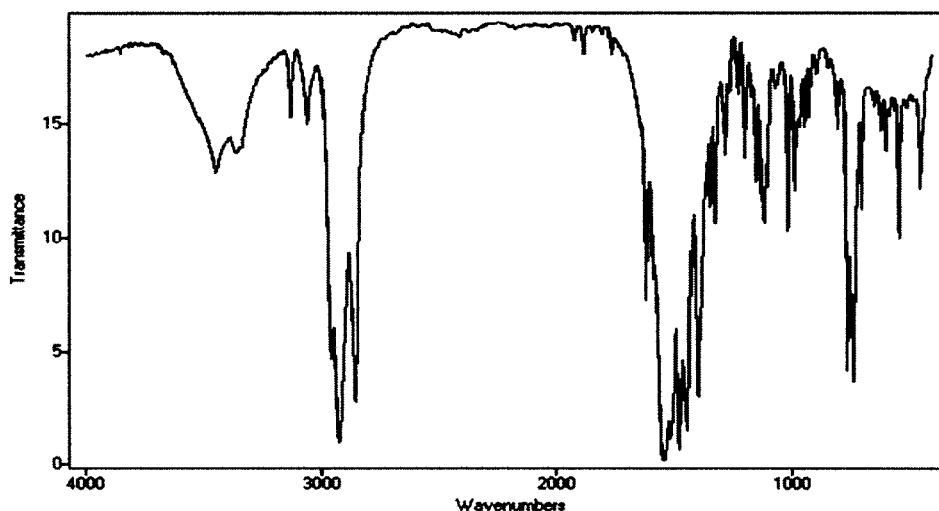


Figure 3.16: IR spectrum of compound **15**.

However, this is absent from the IR spectrum of compounds **16**, **17** and **36**, all bis-chelates. This suggests that this peak is due to an impurity, possibly water.

Furthermore, the peaks at  $3129\text{ cm}^{-1}$  and  $3058\text{ cm}^{-1}$  are similar to those seen in the spectra of compounds **16** and **17**, and are indicative of  $\text{C}_{\text{sp}2}\text{-H}$  stretching frequencies. These peaks correspond to the aromatic proton stretches of the benzimidazole.  $\text{C}_{\text{sp}3}\text{-H}$  stretching frequencies for compound **15** appear at  $2957\text{ cm}^{-1}$ ,  $2920\text{ cm}^{-1}$  and  $2853\text{ cm}^{-1}$ . The  $\text{C}=\text{C}$  stretching frequency of compound **15** appears at  $1621\text{ cm}^{-1}$ . The absence of an intense stretching peak at  $1700\text{ cm}^{-1}$  confirms an absence of a carbonyl. The absence of both the carbonyl and amide stretching frequency peaks suggest that the ligand, *N*-(*N*'-1-methylbenzimidazol-2-yl)decanamide, is chelated to the metal and is in its anionic form. Table 3.2 contains selected IR data for compounds **15-17** and **36** with their respective metal ions. It should be noted that compounds **16** and **17** have the same ligand, *N*-(*N*'-1-methylbenzimidazol-2-yl)cyclohexanecarboxamide .

Table 3.2: Selected absorption peaks for compounds **15-17** and **36**

Compound	Metal	C <sub>sp2</sub> -H	C <sub>sp3</sub> -H	C = C
<b>15</b>	Cu	3129 cm <sup>-1</sup> , 3058 cm <sup>-1</sup>	2957 cm <sup>-1</sup> , 2920 cm <sup>-1</sup> , 2853 cm <sup>-1</sup>	1621 cm <sup>-1</sup>
<b>16</b>	Ni	3120 cm <sup>-1</sup> , 3053 cm <sup>-1</sup>	2930 cm <sup>-1</sup> , 2859 cm <sup>-1</sup>	1617 cm <sup>-1</sup>
<b>17</b>	Co	3063 cm <sup>-1</sup>	2930 cm <sup>-1</sup> , 2813 cm <sup>-1</sup>	1622 cm <sup>-1</sup>
<b>36</b>	Pt	3061 cm <sup>-1</sup>	2960 cm <sup>-1</sup> , 2936cm <sup>-1</sup> , 2863 cm <sup>-1</sup>	1618 cm <sup>-1</sup>

The KBr-IR absorption spectrum of compound **17** is similar to compounds **16** and **36** (table 3.2). However, unlike compound **16**, only one C<sub>sp2</sub>-H stretch with doubled intensity is seen for compound **17**. Taken together, both the intensity and type of stretching frequencies present for the same ligand in compounds **16** and **17** suggests a slightly different coordination environment and hence geometry. This is confirmed by the X-ray crystallographical data discussed later in this chapter. C<sub>sp3</sub>-H stretches, for compound **17** appear at 2930cm<sup>-1</sup> and 2813 cm<sup>-1</sup>. The absence of a carbonyl and N-H stretching frequencies confirms an anionic form of the chelating ligand, N-(N'-1-methylbenzimidazol-2-yl)cyclohexanecarboxamide for both complexes.

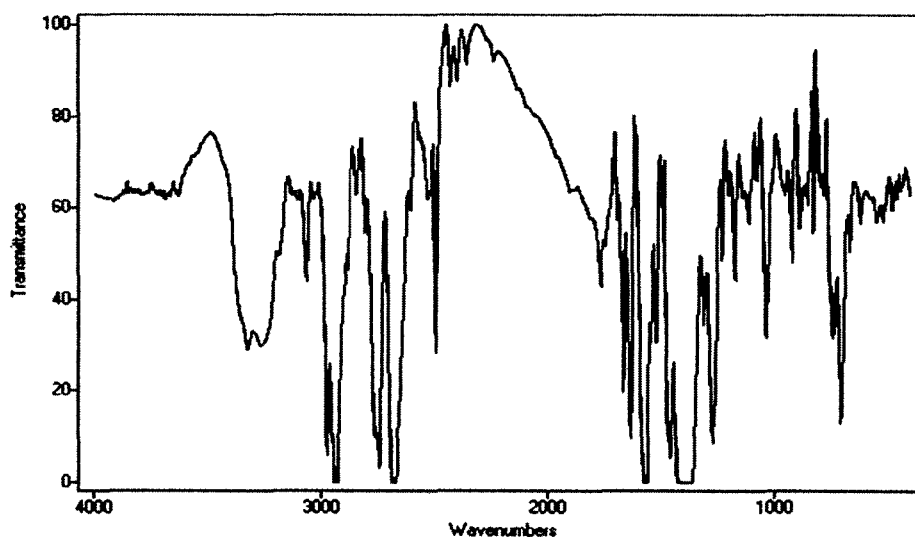


Figure 3.17: IR spectrum of compound **18**.

The KBr-IR absorption spectrum of compound **18**, Figure 3.17, displays a spectrum different from the other bis-chelated complexes of this series. This suggests more variations in the coordination mode of the ligand to the metal. The crystallographic data, discussed later in this chapter, shows a five coordinate complex with ligands in both anionic and neutral modes. This is confirmed by the additional stretching frequencies seen in the infra-red spectrum. The N-H stretch appears at  $3322\text{ cm}^{-1}$  and is similar to values reported by Garnovskii *et al.* [138].  $\text{C}_{\text{sp}^3}\text{-H}$  and  $\text{C}_{\text{sp}^2}\text{-H}$  stretches appear at  $3062\text{ cm}^{-1}$ ,  $2974\text{ cm}^{-1}$  and  $2755\text{ cm}^{-1}$ . The carbonyl stretch appears at  $1764\text{ cm}^{-1}$  and has a lower stretching frequency usually seen for this series. A  $\text{C}=\text{C}$  stretch appears at  $1662$  and is a lower stretching frequency compared to the previous bis-chelated complexes. The carbonyl and additional stretches in the  $1000\text{ cm}^{-1} - 2000\text{ cm}^{-1}$  region also suggest the presence of both protonated and anionic forms of the ligand. This is confirmed by the N-H stretch at  $3322\text{ cm}^{-1}$ .

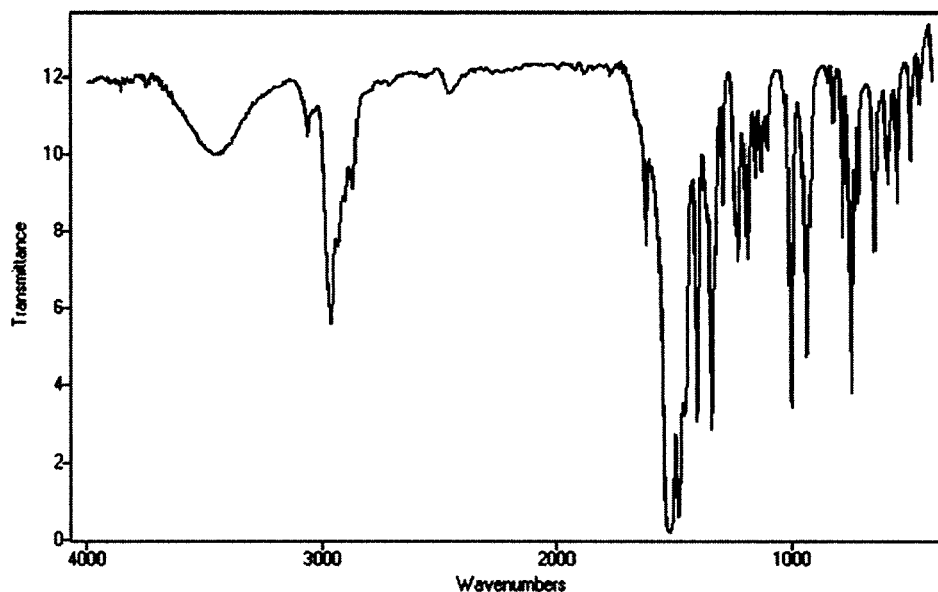


Figure 3.18: IR spectrum of compound **19**.



Figure 3.18 displays the IR absorption spectrum of compound **19**. This trace is also similar to compound **36**. The absence of a N-H stretch and carbonyl stretch suggests an anionic form of the ligand, 2,2-dimethyl-N-(N'-1-methylbenzimidazol-2-yl)propanamide. Absorption stretches at  $3057\text{ cm}^{-1}$  and  $2960\text{ cm}^{-1}$  confirm  $\text{C}_{\text{sp}2}\text{-H}$  and  $\text{C}_{\text{sp}3}\text{-H}$  stretches. Also, a stretching peak at  $1618\text{ cm}^{-1}$  is indicative of an unsaturated carbon stretch, typically a  $\text{C}=\text{C}$  stretch. The crystallographic data discussed later in the chapter, agrees with the infrared data, all showing the ligand is in its anionic form.

The KBr-IR absorption spectrum of compound **24**, Figure 3.19, shows a N-H stretch at  $3379\text{ cm}^{-1}$ . Stretching frequency peaks at  $2972\text{ cm}^{-1}$ ,  $2936\text{ cm}^{-1}$  and  $2880\text{ cm}^{-1}$  correspond to the  $\text{C}_{\text{sp}2}\text{-H}$  and  $\text{C}_{\text{sp}3}\text{-H}$  stretching frequencies.

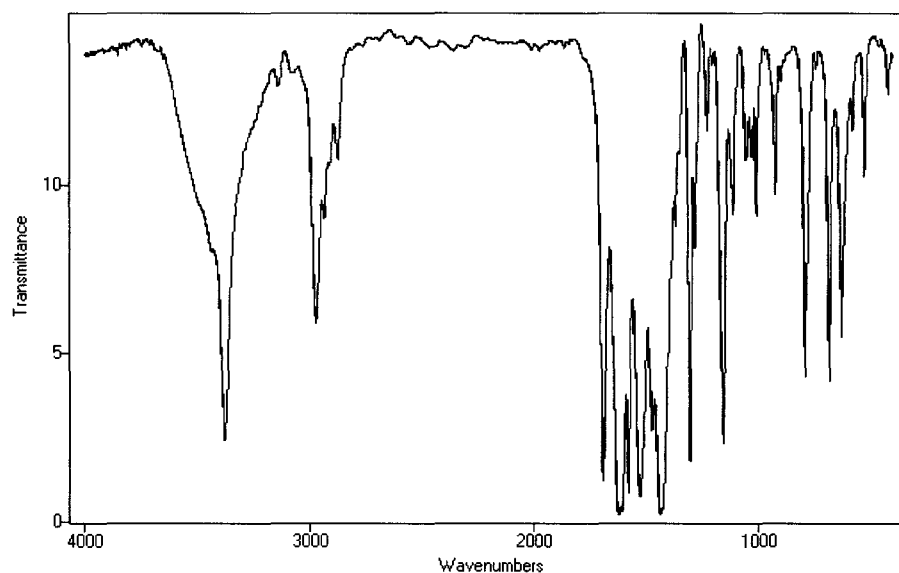


Figure 3.19: IR spectrum of compound **24**.

The absence of an absorption at  $2200\text{ cm}^{-1}$  suggests the absence of  $\text{C}_{\text{sp}}\text{-H}$  functional group. The carbonyl peak appears at  $1704\text{ cm}^{-1}$ . The presence of both the carbonyl and amine stretching frequencies are indicative of a monodentately bound ligand, (N-pyridin-

2-yl)-2,2-dimethylpropanamide. This is also supported by the X-ray crystal structure data.

#### D: UV-vis Analysis of Complexes

Figure 3.21 show the UV-vis spectra typical for these complexes. Figure 3.20 displays weak d-d transitions for compounds **16** and **17**. The spectrum of the free ligand for both compounds **16** and **17**, compound **4**, is displayed in Figure 3.21.

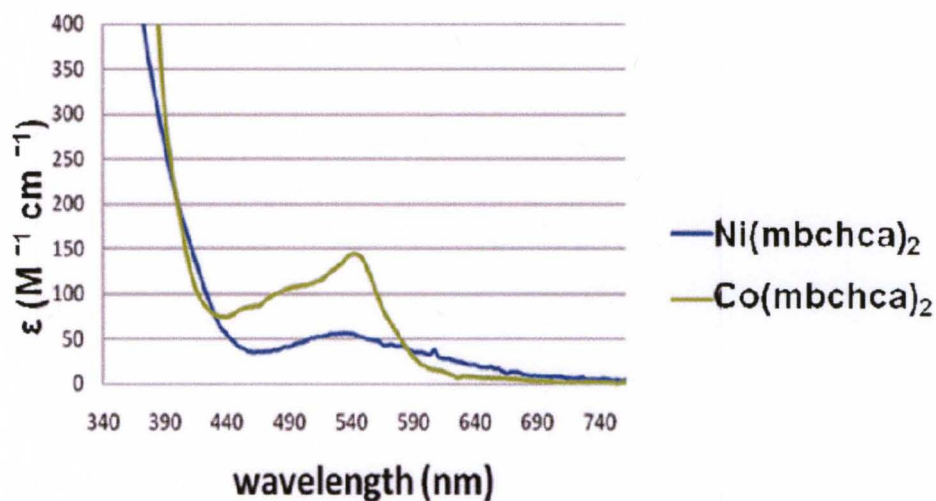


Figure 3.20: UV-vis absorption trace of compounds **16** and **17** in 3 mL  $\text{CH}_2\text{Cl}_2$ .

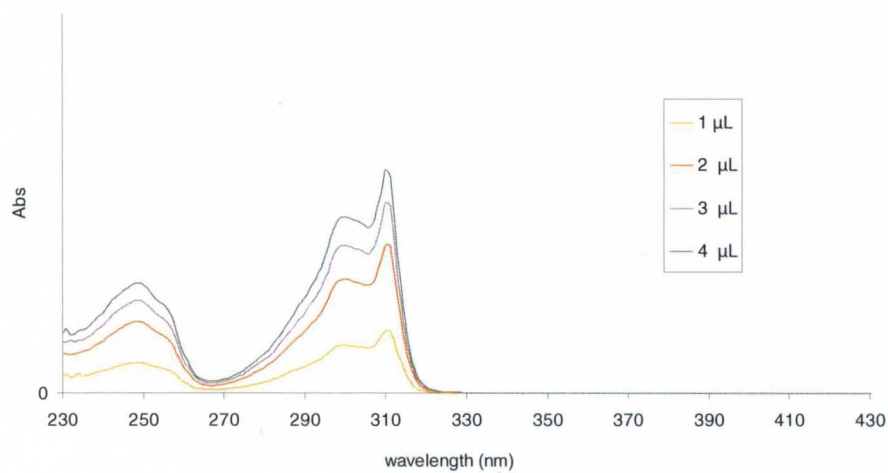


Figure 3.21: UV-vis absorption trace of compound **4**, Hmbchca, in 3 mL  $\text{CH}_2\text{Cl}_2$ .

Figure 3.21 shows the ultraviolet spectrum of compound **4**, N-(N'-1-methyl benzimidazol-2-yl)cyclohexanecarboxamide, with concentrations in the  $\mu\text{M}$  range. These complexes obey Beer's law. At  $\mu\text{M}$  concentrations, the spectra for these complexes are predominantly ligand absorptions. The weak d-d transitions for compounds **16** and **17** appear at mM concentrations with  $\lambda_{\text{max}}$  at 533 nm and 542 nm respectively. This is consistent with previous complexes synthesized in our lab [32] and results of similar Ni(II) complexes with trans  $\text{N}_2\text{O}_2$  donor set reported by Knoch and colleagues [139]. Additionally, a square planar Ni(II) complex with a  $\text{N}_2\text{O}_2$  donor set reported by Nejo and co-workers had  $\lambda_{\text{max}}$  at 482 nm and 387 nm with molar absorptivities 173 and 402 respectively [140]. Table 3.3 shows the  $\lambda_{\text{max}}$  of selected compounds with their respective molar absorptivity.

Table 3.3:  $\lambda_{\text{max}}$  of selected compounds

Compound	Complex	$\lambda_{\text{max}}(\text{nm}), [\epsilon (\text{M}^{-1} \text{cm}^{-1})]$
<b>4</b>	Hmbchca	249[17]; 300[26]; 310[34]
<b>16</b>	Ni(mbchca) <sub>2</sub>	310[82]; 533[56]
<b>17</b>	Co(mbchca) <sub>2</sub>	305[15]; 542[145]
<b>18</b>	Zn(bba) <sub>2</sub> (Hbba)	302[63]
<b>19</b>	VO(dmmbp) <sub>2</sub>	309[31]
<b>20</b>	Ni(mbda) <sub>2</sub>	300[293]; 310[313]
<b>21</b>	Ni(mbhda) <sub>2</sub>	309[76]
<b>24</b>	Cu <sub>2</sub> (OAc) <sub>4</sub> (Pap) <sub>2</sub>	235[18]; 277[8]

It is worth noting that all three nickel complexes show a ligand  $\lambda_{\text{max}}$  around 310 nm.

### E: Mass Spectrometric Analysis of Coordination Metal Complexes

Mass spectrometry provides enormous information about the molecular mass and structure of a given sample. This information stems from the fragmentation pattern of the spectrum. However, a minor draw back of this technique is the appearance of additional peaks in the spectra that are due to sample ionization reactions,  $\text{K}^+$  and  $\text{Na}^+$  salts. The  $\text{K}^+$

and  $\text{Na}^+$  ions are common contaminants introduced into the sample by matrix. It is worth noting that the number of additional peaks is proportional to the laser intensity.

Consequently, samples contained in this work were collected at various laser intensities to eliminate these additional peaks.

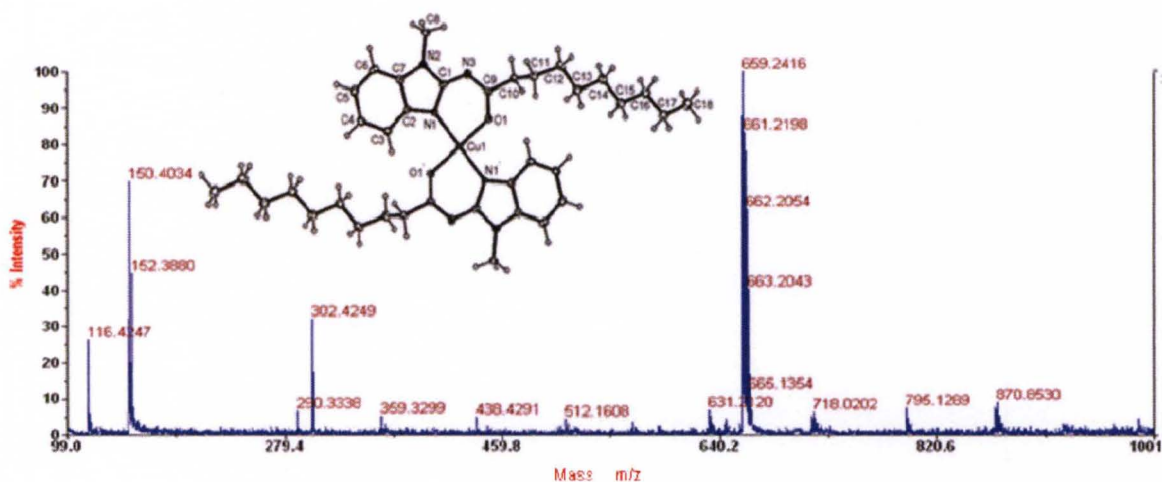


Figure 3.22: Mass spectrometric trace of compound **15**

The mass spectrometric trace of compound **15** (Figure 3.22) shows a molecular peak at 663.20 m/z with an intensity of 40%. This peak is due to the molecular ion fragment  $[\text{Cu}(\text{mbda})_2]^+$ . Two daughter peaks appear at 150.40 m/z and 302.42 m/z. The peak at 150.40 m/z represents the protonated fragment of 1-methylbenzimidazole with a relative intensity of 70% whilst the base peak at 302.42 m/z corresponds to the protonated free ligand,  $[(\text{Hmbda})\text{H}]^+$ .

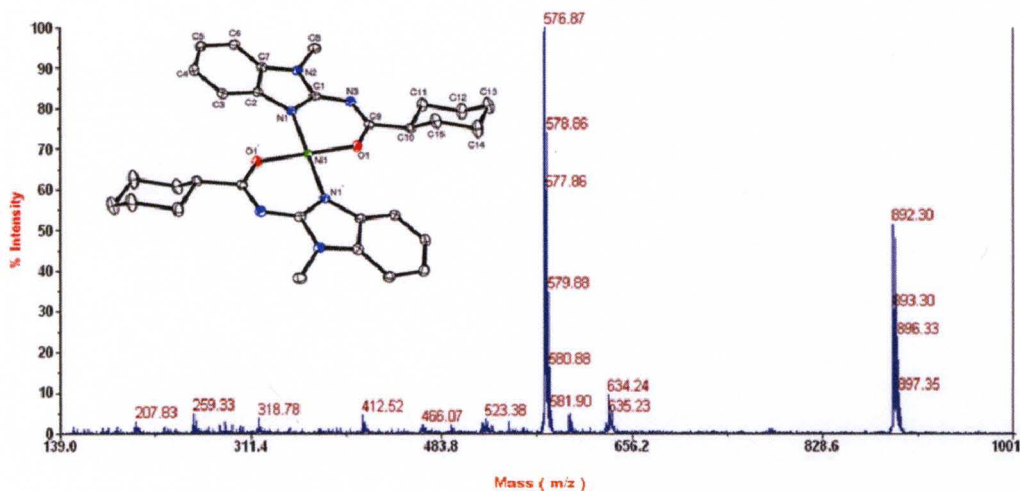


Figure 3.23: Mass spectrometric trace of compound **16**

Figure 3.23 displays the mass spectrometric trace of compound **16** showing an ion peak at 576.87 m/z with an intensity of 100 %. This peak is due to the molecular fragment  $[(mbchca)_2Ni]^+$ . The molecular ion peak at 892.30 m/z has a relative intensity of 50 % and corresponds to the fragment  $[(mbchca)_3Ni_2]^+$ .

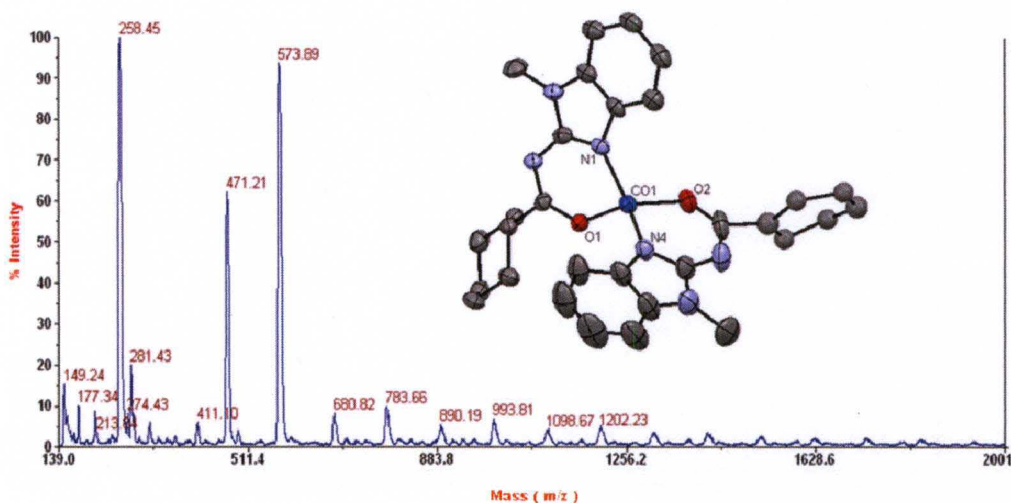


Figure 3.24: Mass spectrometric trace of compound **17**

The mass spectrometric spectrum of compound **17** (Figure 3.24) shows an ion peak at 258.45 m/z with an intensity of 100% and represents the ligand,  $[Hmbchca]^+$ . The peak at

281.43 m/z with an intensity of 20% is due to the molecular fragment [(Hmbchca)Na]<sup>+</sup>, a sodium ion peak. Molecular ion peaks at 471.21 m/z and 573.89 m/z have relative intensities of 62 % and 95%. These peaks correspond to the fragments [(mbchca)(DBA-matrix)Co]<sup>+</sup>, and [(mbchca)<sub>2</sub>Co]<sup>+</sup> respectively.

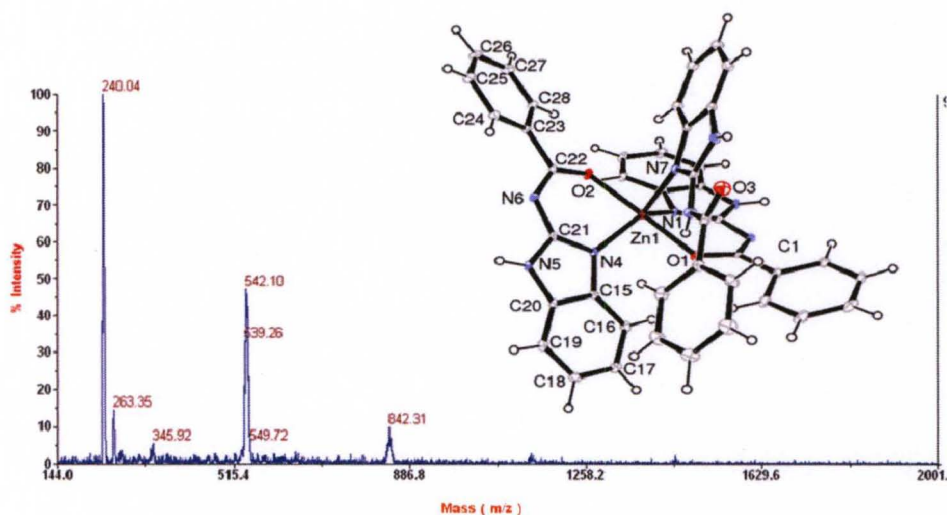


Figure 3.25: Mass spectrometric trace of compound **18**

Figure 3.25 displays the mass spectrometric trace of compound **18**. The ion peak at 240.04 m/z has an intensity of 100%. This peak is due to the molecular fragment [Hbba]<sup>+</sup>, a protonated ligand ion. Molecular ion peaks at 263.35 m/z, 542.10 m/z and 842.31 m/z have relative intensities of 14 %, 47 % and 9.75 %; corresponding to the fragments [HbbaNa]<sup>+</sup>, [Zn(bba)<sub>2</sub>]<sup>+</sup> and [Zn<sub>2</sub>(bba)<sub>2</sub>(Hbba)]<sup>+</sup> respectively.

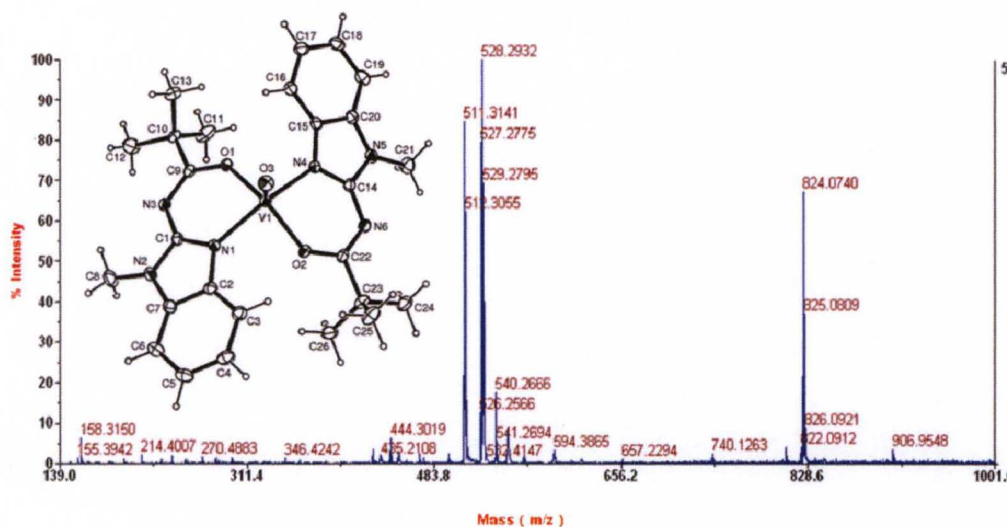


Figure 3.26 : Mass spectrometric trace of compound **19**

The mass spectrometric trace of compound **19** (Figure 3.26) shows an ion peak at 511.31 m/z with an intensity of 85%. This peak is due to the molecular fragment  $[(VO(Hdmmbp)_2-CH_4)]^+$ . Molecular ion peaks at 528.27 m/z and 824.02 m/z have relative intensities of 100 % and 70 %. These peaks correspond to the fragments  $[(VO(dmmbp)_2)H]^+$  and  $[(VO)_2(dmmbp)_3]^+$  respectively.

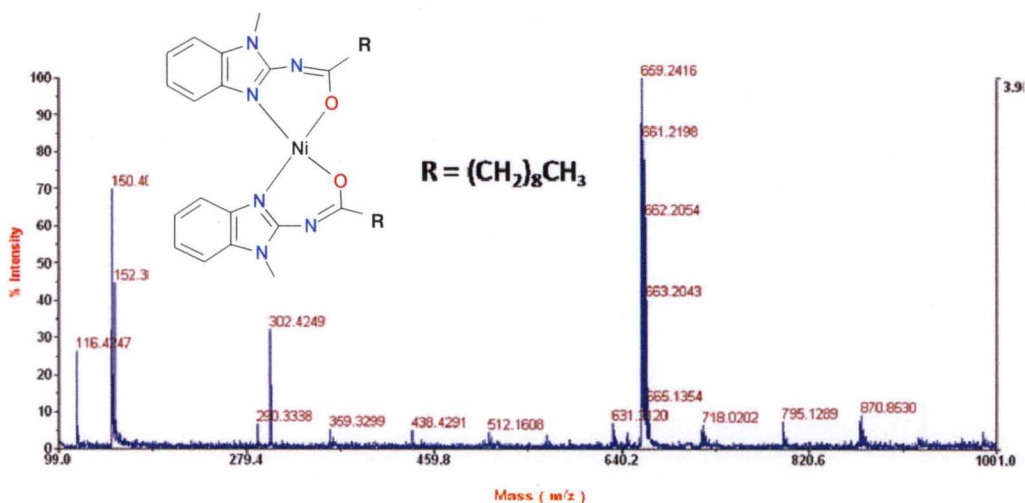


Figure 3.27: Mass spectrometric trace of compound **20**

The mass spectrometric trace of compound **20** (Figure 3.27) shows a base peak at 659.24 m/z that corresponds to the fragment  $[(mbda)_2Ni]^+$ . Daughter peaks appear at 116.4 m/z,

150.4 m/z and 302.42 m/z. The peak at 302.42 m/z represents the ligand fragment [Hmbda]<sup>+</sup> and has intensity of 30%.

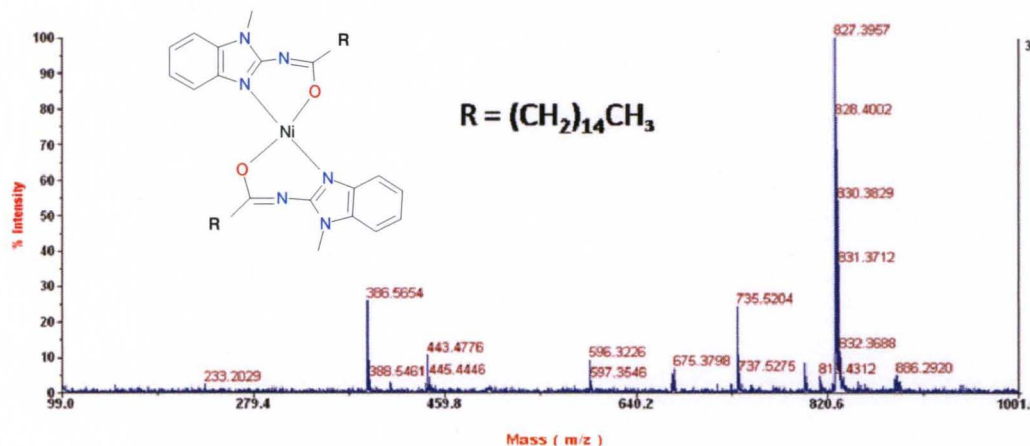


Figure 3.28: Mass spectrometric trace of compound **21**

The mass spectrometric trace of compound **21** (Figure 3.28) shows an ion peak at 386.57 m/z with an intensity of 28%. This peak is due to the molecular fragment, [Hmbhda]<sup>+</sup>. The ion peak at 827.40 m/z has a relative intensity of 100 % and corresponds to the molecular ion fragment [Ni(mbhda)<sub>2</sub>]<sup>+</sup>.

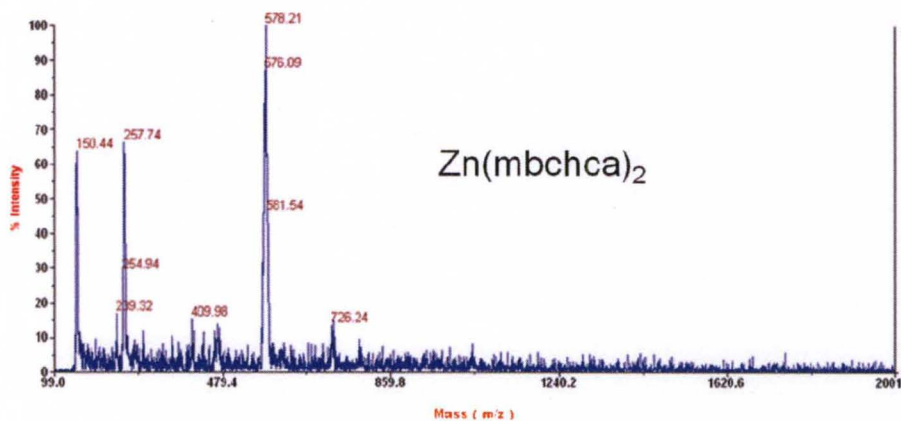


Figure 3.29: Mass spectrometric trace of compound **22**



The mass spectrometric spectrum of compound **22**, Figure 3.29, shows an ion peak at 150.44 m/z with an intensity of 64%. This peak is due to the molecular fragment of a protonated benzimidazole ion [Hamb]<sup>+</sup>. Molecular ion peaks at 257.74 m/z, 578.21 m/z and 726.24 m/z have relative intensities of 66 %, 100 % and 14 %. These peaks correspond to the fragments [mbchca]<sup>+</sup>, [Zn(mbchca)<sub>2</sub>]<sup>+</sup> and [Zn(mbchca)<sub>2</sub>(C<sub>6</sub>H<sub>11</sub>)CO]<sup>+</sup> respectively.

The mass spectrometric trace of compound **24** (Figure 3.30) shows an ion peak at 583.73 m/z with an intensity of 15 %. This peak is due to the molecular fragment [Cu<sub>2</sub>OAc(Pap)<sub>2</sub> K]<sup>+</sup> and is inconsistent with the crystal structure, discussed later in the chapter. Daughter peaks appear at 242.76 m/z and 179.47 m/z with relative intensities of 100 % and 16 %.

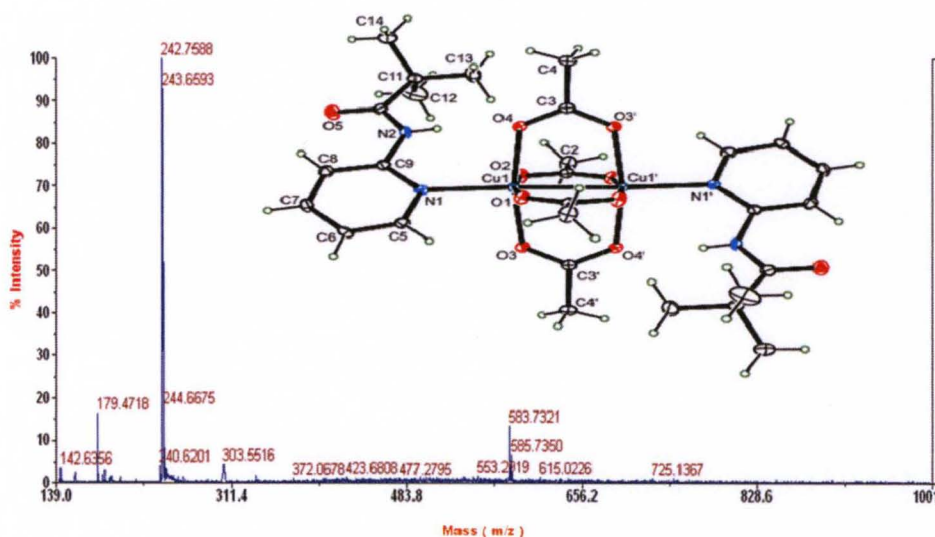


Figure 3.30: Mass spectrometric trace of compound **24**

These peaks correspond to the fragments [CuPap]<sup>+</sup> and the protonated ligand 2-pivaloylamino pyridine ion [HPap]<sup>+</sup> respectively. Table 3.4 shows a compilation of the theoretical and experimental masses of metal complexes.

Table 3.4: Selected Mass spectrometric data of metal complexes

Compound	Metal complex	Theoretical mass(Rel. Ab'dance %)	Experimental mass
<b>15</b>	Cu(mbda) <sub>2</sub>	663.34 (45)	659.24, 663.20
<b>16</b>	Ni(mbchca) <sub>2</sub>	570.23 (48)	576.87, 892.30
<b>17</b>	Co(mbchca) <sub>2</sub>	571.22 (70)	573.89
<b>18</b>	Zn(bba) <sub>2</sub> (Hbba)	773.18 (29)	542.10, 842.31
<b>19</b>	VO(dmmbp) <sub>2</sub>	527.20 (72)	528.27
<b>20</b>	Ni(mbda) <sub>2</sub>	658.35 (44)	659.24
<b>21</b>	Ni(mbchca) <sub>2</sub>	826.54 (39)	827.40
<b>22</b>	Zn(mbchca) <sub>2</sub>	576.22 (34)	578.21
<b>24</b>	Cu <sub>2</sub> (OAc) <sub>4</sub> (Pap) <sub>2</sub>	718.13 (34)	583.73

With the exception of compounds **18** and **24**, theoretical and experimental masses for the metal complexes are in agreement. The molecular ion peak, M<sup>+</sup>, of compound **18** is [Zn<sub>2</sub>(bba)<sub>2</sub>(Hbba)]<sup>+</sup>. This ion fragment varies from the x-ray crystal structure by a Zn<sup>2+</sup> ion and is attributable to ionization reactions. The molecular ion fragment for compound **24** however shows a fragment [Cu<sub>2</sub>(OAc)(Pap)<sub>2</sub>O]<sup>+</sup> less in mass compared to the structure elucidated by x-ray. Additionally, the ion peak (892.30 m/z) for compound **16**, [(mbchca)<sub>3</sub>Ni<sub>2</sub>]<sup>+</sup>, also results from ionization-complexation reactions.

### F: <sup>1</sup>H NMR Characterization and Analysis of Complexes

Four coordinate Nickel (II) compounds form either square planar or tetrahedral complexes. It is diamagnetic when planar and paramagnetic in the later. Similar chemical shifts result in the <sup>1</sup>H NMR spectrum of the chelate and free ligand, when the structure of the complex in solution is planar. In contrast, peak broadening and very different chemical shifts for the chelate are observed in the case of tetrahedral. Figures 3.31-3.34,

show  $^1\text{H}$  NMR of bis- chelated nickel (II) complexes. The  $^1\text{H}$  NMR of the bis-chelate of compound **9**,  $\text{Ni}(\text{dmmbp})_2$ , displayed in Figure 3.34 has been included for comparison. This compound is planar and *trans* in the solid state. With the exception of compound **20**, the color of the solid powder is purple for all the Ni (II) complexes under discussion for this series. This purple color is maintained in  $\text{CDCl}_3$  suggesting that all four compounds stay four coordinate in solution. Table 3.5 shows the  $^1\text{H}$  NMR chemical shifts for these compounds. Another  $d^8$  ion and Pt- analog of compound **20**, compound **30** discussed later in Chapter IV, has also been added for comparison. The aromatic region of compound **30** appears as four peaks with the splitting pattern doublet, triplet, triplet and doublet. X-ray crystal structure data show that this splitting pattern is associated with square planar *cis*-bischelates of this series.

Table 3.5:  $^1\text{H}$  NMR Chemical Shifts

Compd	Metal complex	Chemical Shifts, $\delta$ (ppm) in $\text{CDCl}_3$
<b>16</b>	$\text{Ni}(\text{mbchca})_2$	13.6, 10.8, 9.24, 5.01, 2.23, 1.72, 1.54, 1.33
<b>20</b>	$\text{Ni}(\text{mbda})_2$	8.58, 5.76, 3.48, 2.77, 2.15, 1.56, 1.30, 1.21, 0.839
<b>21</b>	$\text{Ni}(\text{mbhchca})_2$	8.66, 5.72, 2.88, 2.20, 1.55, 1.29, 0.886
	$\text{Ni}(\text{dmmbp})_2$	12.79, 10.13, 7.28, 4.17, 3.66, 2.51, 1.73, 1.58, 1.319, 0.855
<b>30</b>	$\text{Pt}(\text{mbda})_2$	7.15, 7.03, 6.67, 6.37, 3.77, 2.53, 1.82, 1.61, 1.44, 1.36, 1.29, 0.881

The lack of similar splitting patterns in the  $^1\text{H}$  NMR spectra (Figure 3.31-3.34) of these Ni(II) complexes suggests that they are paramagnetic.

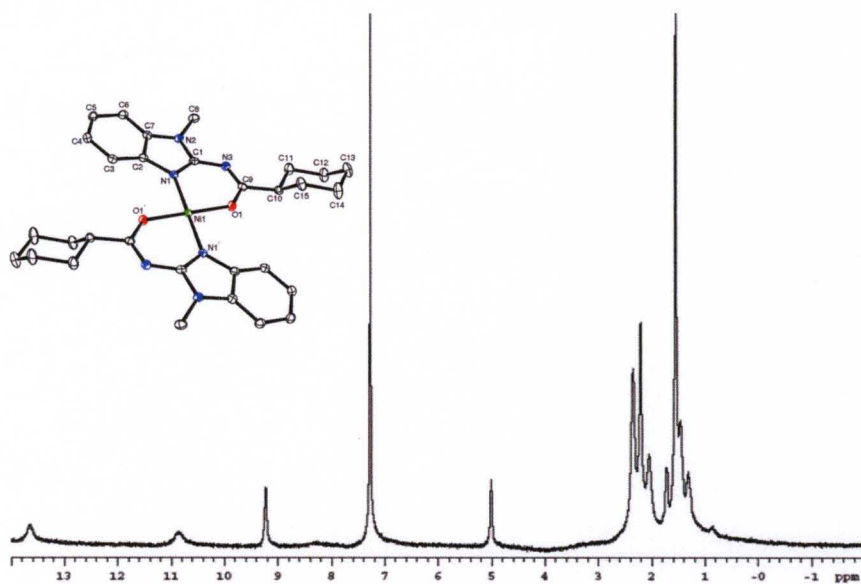


Figure 3.31:  $^1\text{H}$  NMR spectrum of compound **16** in  $\text{CDCl}_3$

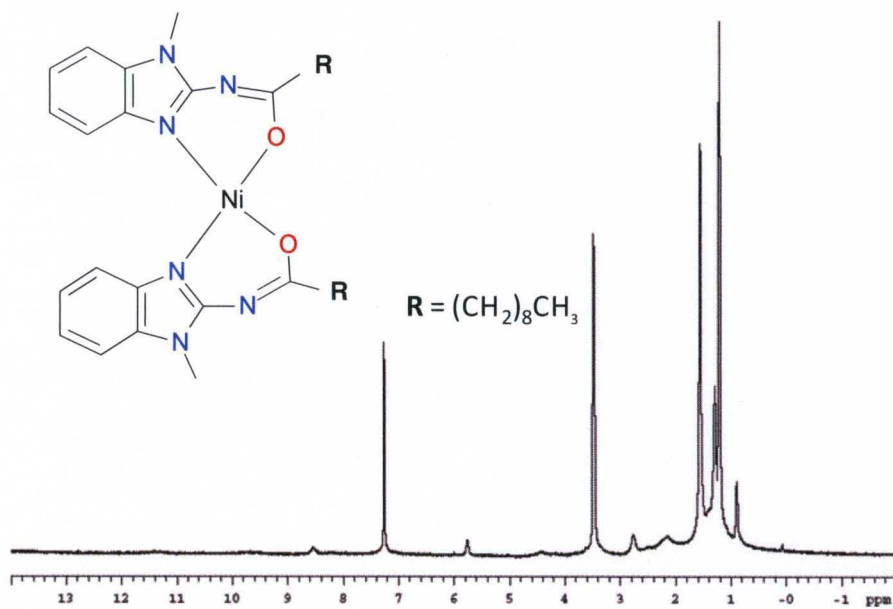


Figure 3.32:  $^1\text{H}$  NMR spectrum of compound **20** in  $\text{CDCl}_3$

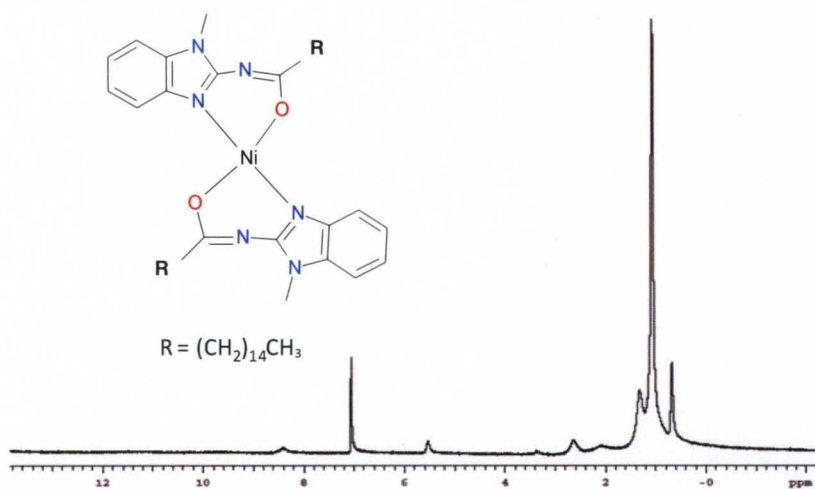


Figure 3.33:  $^1\text{H}$  NMR spectrum of compound **21**

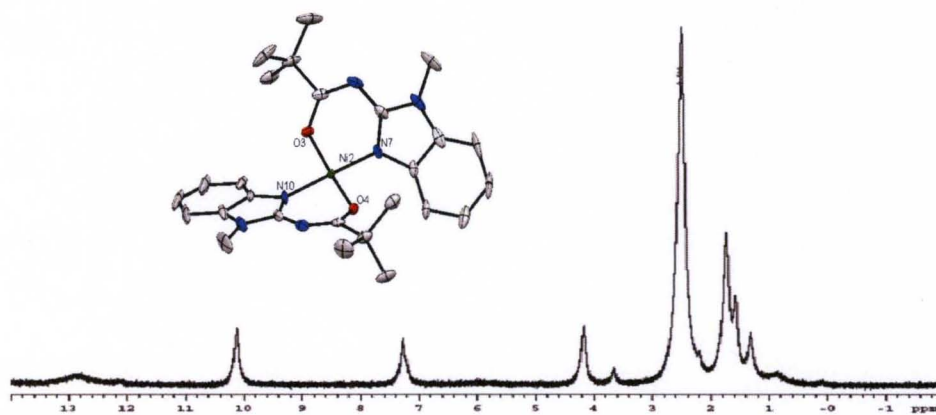


Figure 3.34:  $^1\text{H}$  NMR spectrum of  $\text{Ni}(\text{dmmbp})_2$ . Hydrogen atoms of the ortep have been omitted for clarity.

The peak at 7.28 ppm is the solvent peak ( $\text{CDCl}_3$ ).

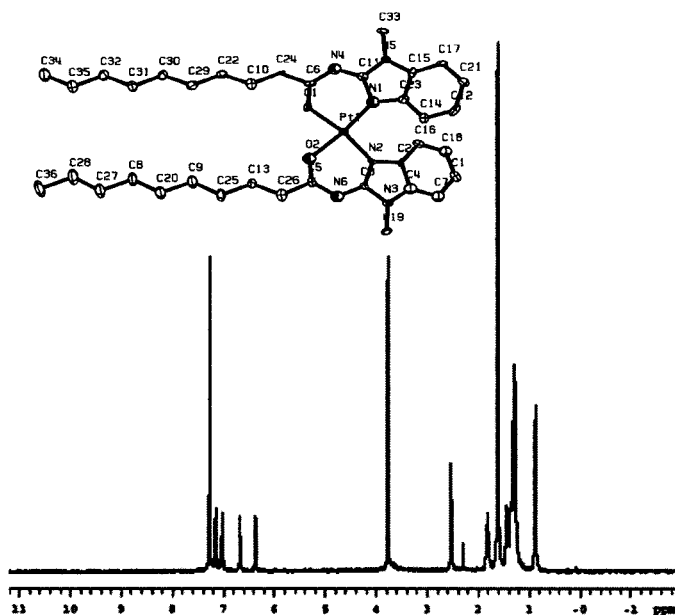


Figure 3.35:  $^1\text{H}$  NMR spectrum of compound **30**

Roquette and co-workers have assigned paramagnetic chemical shifts of bisguanidine Ni (II) complexes by using paramagnetic shifts with the aid of diamagnetic NMR spectra of analogous Zn complexes and DFT calculations[34]. However, the goal here is to use the spectra to predict structure and isomerism. The spectra for compounds **20** and **21** are identical and differ from Ni(dmmbp)<sub>2</sub> and compound **16**. Furthermore, they both show no peaks beyond 9.00 ppm for the given spectral window. This is not surprising since these two compounds have aliphatic hydrocarbons “tails” that differ only by a few hydrocarbons (C<sub>6</sub>H<sub>12</sub>). However, the peak at 3.48 ppm for compound **20** does not appear prominently in any of the other Ni (II) complexes. This is significant because this is usually the chemical shift of the methyl substituents (N-CH<sub>3</sub>) of the benzimidazole, seen in both the spectra of the free ligands and that of their diamagnetic Pt(II) analogues (Figure 3.35 discussed in the next chapter). This suggests distortion for compounds **20** and **21** are different and might be due to the difference in “tail” length. Another

possibility will be a combination of a chelate and monodentate ligation of the ligand with a nitrate ion attached at the fourth coordination point. In this mode, the shielding effect of the metal will be different for the respective monodentate and chelate ligands since their chemical environments are different. However, both the IR and mass spectrometric data support a bis-chelated four coordinate Ni (II) complex. It is therefore likely that compounds **20** and **21** have different geometries / configurations in the solid phase. Consequently, the geometry in solution might be limited by sterics in two different ways. Thus, the difference in spectra.

Crystal structures of both compound **16** and Ni(dmmbp)<sub>2</sub> reveal that both complexes are square planar and *trans*. Crystals of compound **20** were obtained only in diethyl ether. However, the crystalline property was lost upon exposure to air, possibly due to solvent evaporation. Thus, its geometry in the solid phase could not be elucidated.

Nevertheless, the UV-vis spectrum of compound **16** is consistent with similar tetrahedral Ni (II) complexes with *trans* N<sub>2</sub>O<sub>2</sub> donor sets [139]. In solution Ni (II) complexes of type NiN<sub>2</sub>O<sub>2</sub> are in equilibria between either a planar and tetrahedral geometry [139] on one hand and an octahedral, planar and tetrahedral interconversion [141] on the other. The configurational isomerism observed in these complexes is very rapid and the dominant geometry is determined by the nature of ligand and the type of solvent. For instance, steric bulk of the ligands and some organic solvents favor tetrahedral geometry. Conversely, lewis bases such as pyridine and methanol favor octahedral geometry and coordinate to the metal center at the axial positions [142]. It can therefore be concluded, based on the <sup>1</sup>H NMR chemical shifts of the peaks, UV data, and the steric bulk of ligands that all the Ni (II) complexes of this series assume tetrahedral

geometry in solution and are consistent with trans NiN<sub>2</sub>O<sub>2</sub> complexes found in literature [139-144]. Furthermore, this does not preclude factors such as additional shielding or deshielding effects felt by these protons brought about by ring currents as a result of their proximity to the center of a neighboring ring. This phenomenon is common to ring systems of this nature largely due to their chelation mode. Based on the <sup>1</sup>H NMR spectra, it can be concluded that compounds **20** and **21** are in the *syn/cis* and *antitrans* coordination modes respectively.

Unlike nickel (II) complexes, Zinc (II) complexes, with N<sub>2</sub>O<sub>2</sub> 1-methylbenzimidazole donor sets, show little or no change in chemical shifts of their <sup>1</sup>H NMR spectra. Figure 3.36 shows the <sup>1</sup>H NMR spectrum for compound **23**. The spectrum is similar to Zn(dmmbp)<sub>2</sub> [32]. The aromatic region shows three peaks with chemical shifts at 7.26 ppm, 7.25 ppm and 7.15 ppm corresponding to the eight protons of the benzimidazole.

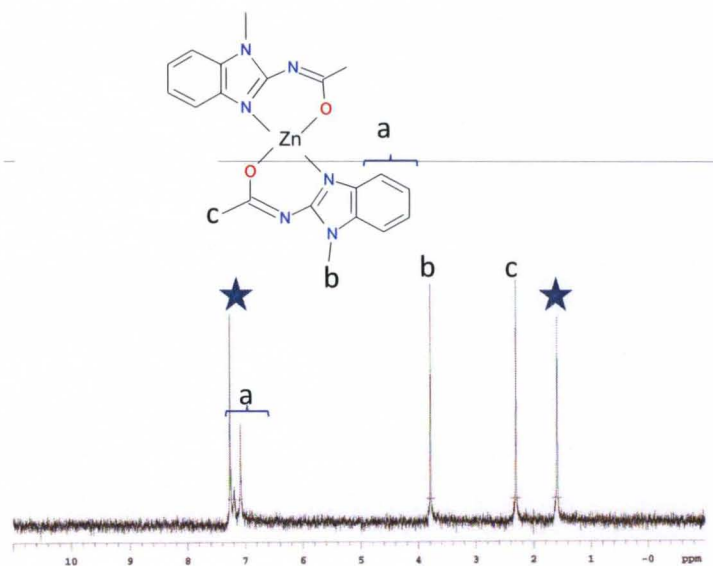


Figure 3.36: <sup>1</sup>H NMR spectrum of compound **23** in CDCl<sub>3</sub>



The peak at 3.79 ppm corresponds to the methyl substituents of the nitrogen at position one of the benzimidazole and integrates to six protons. The peak at 2.30 ppm represents six protons corresponding to the two sets of methyl protons of the acetyl pendant. The peak at 1.59 ppm is a water peak, an impurity often found in deuterated chloroform. It is worth noting that the aromatic protons peaks are no longer aggregated compared to the free ligand. This suggests the ligands are bound to the metal, but not as monodentates.

Figure 3.37 shows the  $^1\text{H}$  NMR of compound **18**.

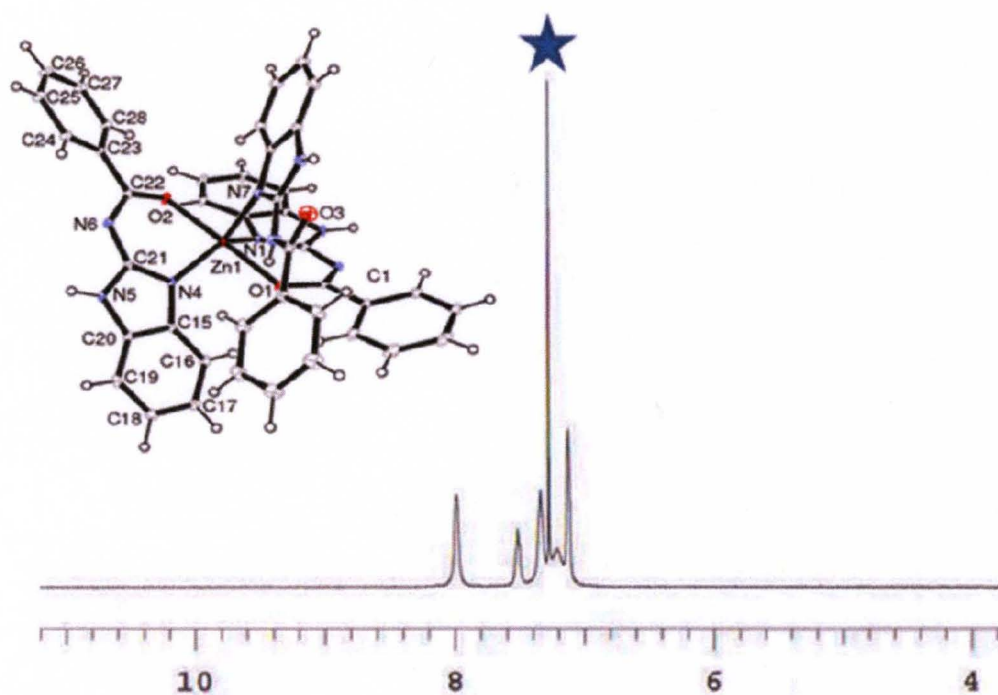


Figure 3.37:  $^1\text{H}$  NMR spectrum of compound **18** in  $\text{CDCl}_3$

The peaks at 7.98 ppm and 7.16 ppm correspond to the phenyl protons whilst the peaks at 7.55 ppm, 7.38 ppm and 7.20 ppm represent the aromatic protons of the benzimidazole. The amide and N1 protons do not show up in the spectrum and might be due to rapid solvent exchange. Again, the aromatic protons of the benzimidazole do not aggregate like in the free ligand.

## G: X-ray Crystallographic Analysis of Coordination Metal Complexes

Previous studies of X-ray crystal structure analysis of compound **9** bis-chelated complexes of  $\text{Co}^{2+}$ ,  $\text{Ni}^{2+}$ ,  $\text{Cu}^{2+}$  and  $\text{Zn}^{2+}$  performed in our laboratory, revealed that these complexes formed neutral four coordinated species ranging from tetrahedral to square planar from 2:1 ligand to metal ratio reactions. The interactions in the lattices of these complexes are predominantly pi-stacking. Six new crystal structures of these complexes together with a dinuclear  $\text{Cu}^{2+}$  compound have been elucidated. This section examines the interactions within these new complexes and compares them to previous works. Table 3.6 contains selected crystallographic data of the metal complexes in this series. With the exception of compounds **18** and **19**, complexes crystallize as monoclinics.

Table 3.6: Selected Crystallographic data for compounds .

	Compd 15	Compd 16	Compd 17	Compd 18	Compd 19	Compd 23	Compd 24
Crystal System	Monoclinic	Monoclinic	Monoclinic	Triclinic	Orthorhombic	Monoclinic	Monoclinic
Space Group	$P2_1/c$	$P2_1/c$	$P2_1/c$	$P\bar{1}$	$Pbca$	$P2_1/c$	$P2_1/c$
a	18.505(3) Å	14.1057(8) Å	13.0866(4) Å	9.7627(5) Å	12.9214(13) Å	8.2544(14) Å	13.8508(8) Å
b	5.1189(7) Å	15.1769(8) Å	23.0690(5) Å	10.0352(5) Å	17.1388(17) Å	22.984(4) Å	11.0612(5) Å
c	17.344(3) Å	6.4460(4) Å	19.5697(5) Å	19.3560(11) Å	23.445(2) Å	10.3376(18) Å	11.0301(6) Å
$\alpha$	90°	90°	90°	98.663(4)°	90°	90°	90°
$\beta$	93.823 °	102.9570 °	106.002 °	95.786(4) °	90°	100.364(3)°	104.508(6)°
$\gamma$	90°	90°	90°	100.010°	90°	90°	90°
Volume	1639.3 Å <sup>3</sup>	1344.83 Å <sup>3</sup>	5679.0 Å <sup>3</sup>	1830.38 Å <sup>3</sup>	5192.1 Å <sup>3</sup>	1929.2 Å <sup>3</sup>	1635.98 Å <sup>3</sup>
Z	2	4	4	2	8	4	4
Density	1.346 Mg/m <sup>3</sup>	1.411 Mg/m <sup>3</sup>	1.310 Mg/m <sup>3</sup>	1.406 Mg/m <sup>3</sup>	1.350 Mg/m <sup>3</sup>	1.521 Mg/m <sup>3</sup>	1.461 Mg/m <sup>3</sup>
GOF	1.061	1.086	1.089	1.027	1.061	1.087	1.058
R1	0.0556	0.0450	0.0741	0.0353	0.0537	0.0753	0.0335
wR2	0.0952	0.1063	0.1706	0.0539	0.1088	0.1508	0.0951

The crystal structure of compound **15**, shown below, forms monoclinic crystals in the space group  $P2_1/c$ . The coordination sphere around the Cu (II) ion, a  $d^9$  ion, can be described as square planar (Figure 3.38).

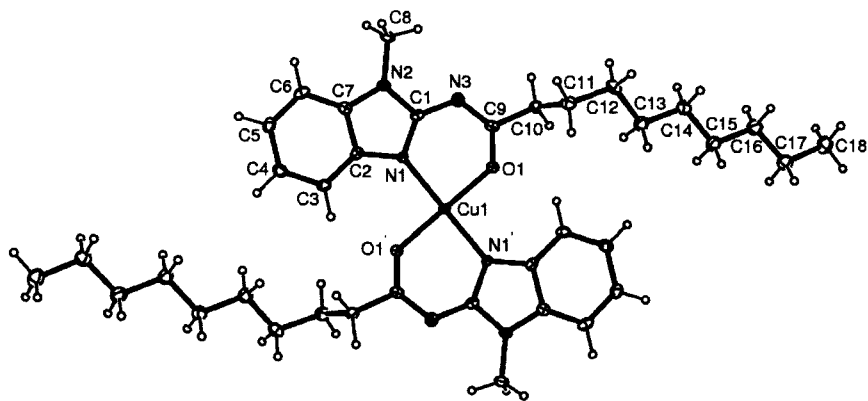


Figure 3.38: ORTEP diagram of compound **15**. Ellipsoids are shown at 30% probability.

The ligand, N-(1-methylbenzimidazol-2-yl)decanamide, is in its anionic form and chelates to the Cu (II) ion through the nitrogen of the benzimidazole and the oxygen of the carbonyl. The chelated ligand assumes a *trans* configuration around the central atom with an average Cu-N bond length of 1.994(3) Å. The average Cu-O and C-O bond lengths are 1.916(2) Å and 1.280(4) Å respectively. Compound **15** has bond angles of 180.00(17) Å, 88.92(10) Å, 91.08(10) Å and 180.00(15) Å corresponding to N(1) – Cu – N(1'), N(1) – Cu – O(1), N(1) – Cu – O(1') and O(1) – Cu – O(1') respectively (Table 3.4).

The crystal lattice can be described as alternating parallel cylindrical sheets of molecules engaged in cooperative H- $\pi$  stacking interactions, along the b axis of the unit cell. These sheets are intercalated obliquely by similar parallel sheets (Figure 3.39). This

results in an occasional edge to face hydrogen-  $\pi$  interactions between adjacent sheets, helping to further stabilize the long aliphatic chains of the ligand.

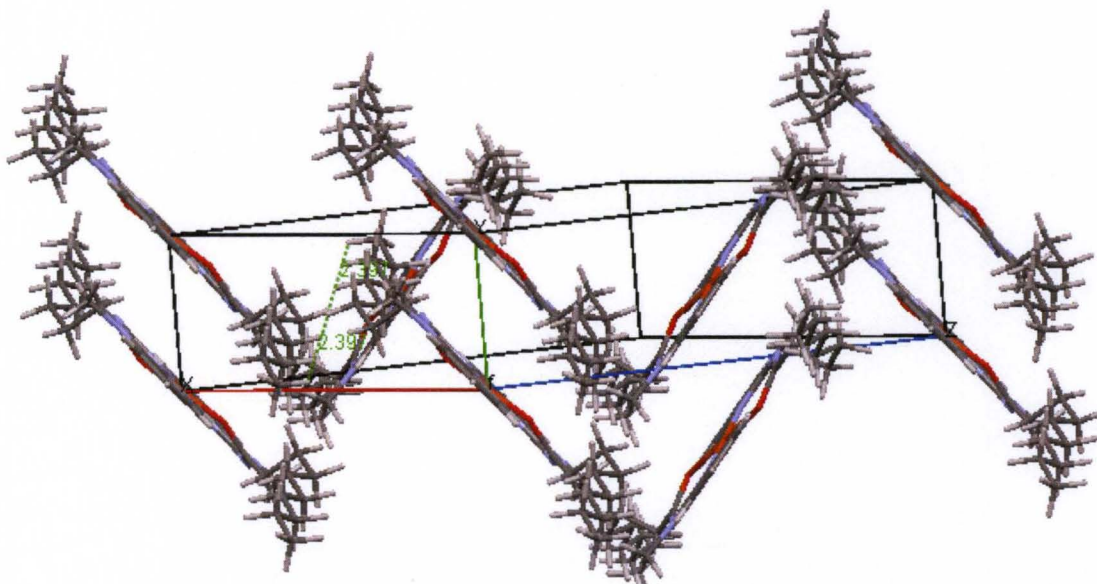


Figure 3.39: Crystal lattice of compound **15**. Alternating parallel sheets and Intercalating molecules displaying a point to face interaction.

The hydrogens of  $C_{\alpha}$  are engaged in weak  $C-H\cdots\pi$  interactions (Figure 3.40). H10B is engaged in an interaction with the  $\pi$ -bond of C2-N1 of the adjacent molecule whilst H10A is engaged in an interaction with the amido oxygen (H10A-O distance = 2.83(4)Å). These interactions help stabilize the aliphatic “tails” of adjacent molecules and places H10B 2.62(7) Å and 2.74(8)Å from C2 and N1 respectively making a C2-H10B-N1 angle of 30.05°. The cooperative  $C-H\cdots\pi$  stacking, places adjacent Cu centers an average distance of 5.11(4) Å apart. It is worth noting that the Cu-Cu distance is greater than the typical 3.3-3.8 Å separation typically seen for perfect alignment of aromatic rings of these types of heterocyclic systems and confirms a slipped, parallel displaced  $\pi$ -stacking arrangement [145]. As a result, aliphatic hydrogens of the stacked molecules become separated by an average distance of 3.27 Å.

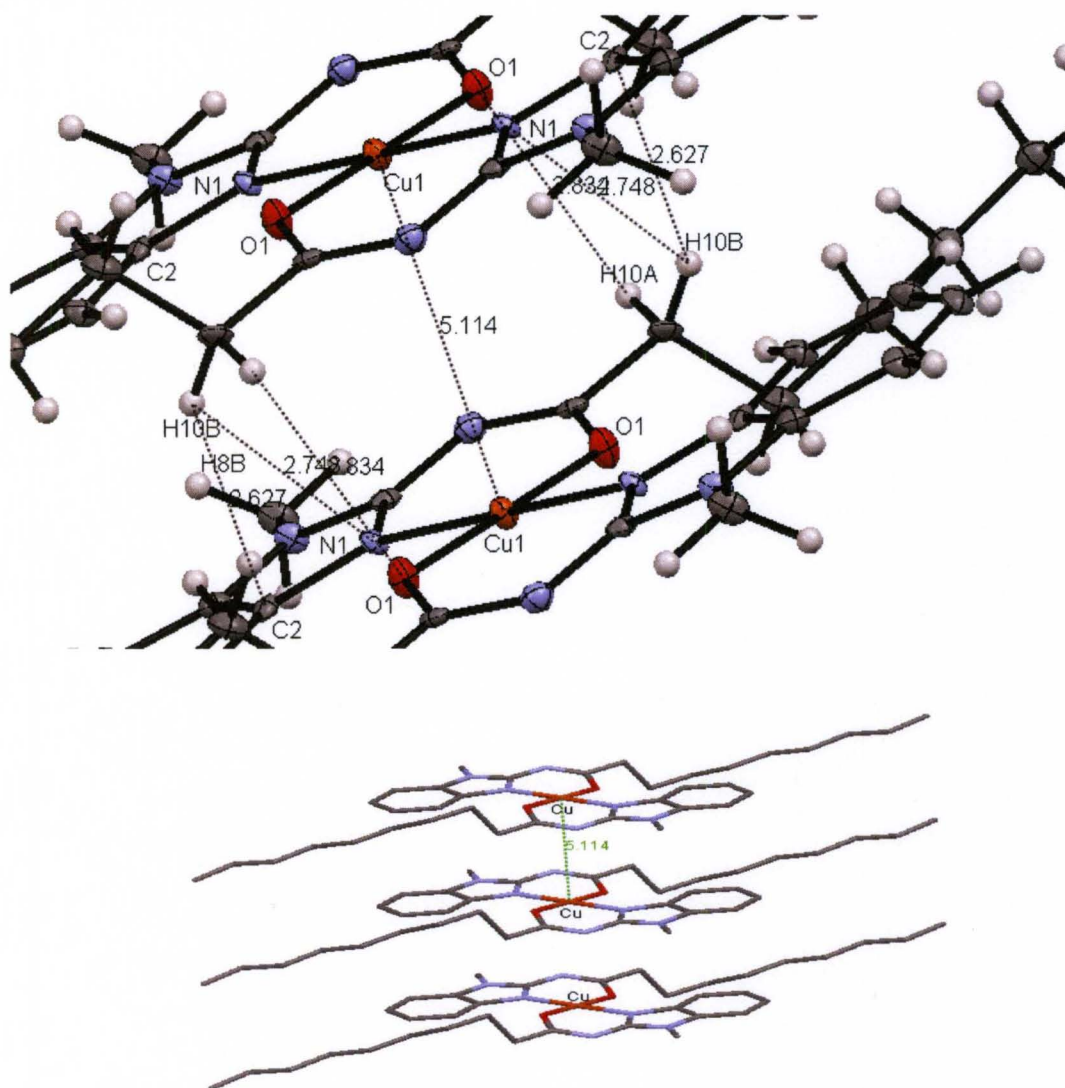


Figure 3.40: Crystal lattice of compound **15** displaying (a) C-H... $\pi$  stacking interactions (top diagram).

(b) Hydrogens have been omitted for the bottom figure for clarity.

The stacking arrangement differs from that of *trans* bis-chelate Cu (II) and Ni (II) amido complexes of compound **9**. In the Cu (II) amido complex, the twist of one chelate with respect to the other results in a torsional angle of  $103.08^\circ$  along the c-axis of the unit cell, whereas a torsional angle of  $128.32^\circ$  is seen in the lattice of the Ni (II) complex.

Additionally, the pi-stacking between adjacent benzimidazoles, in both cases, are almost

orthogonal to each other. That is, compound **15** does not show the distortion from square planar geometry as seen in the previous copper(II) and nickel(II) amido complexes in this series of ligands. This might be due to the need to stabilize the long aliphatic hydrocarbon chain in order to attain optimal overall packing.

Figure 3.41 shows the crystal structure of compound **16** which crystallizes as a monoclinic in the space group  $P2_1/c$ . The molecular geometry is square planar.

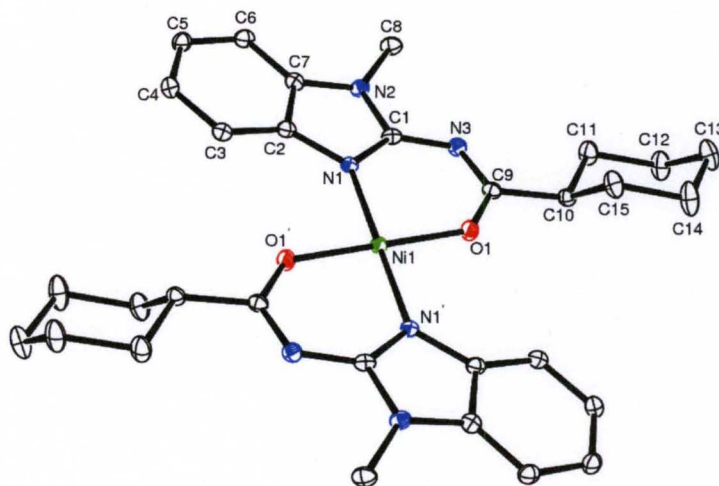


Figure 3.41: ORTEP diagram of compound **16**. Ellipsoids are shown at 30% probability. Hydrogen atoms on the complex were removed for clarity.

Examination of the coordination sphere shows that the nickel (II) ion is coordinated to two ligands in a *trans* configuration with a  $N_2O_2$  donor set (the nitrogen of the benzimidazole and the oxygen of the carbonyl). Compound **16** has bond angles of  $180.0^\circ$ ,  $91.12(7)^\circ$ ,  $88.88(7)^\circ$  and  $179.998(1)^\circ$  corresponding to  $N(1) - Ni - N(1')$ ,  $N(1) - Ni - O(1)$ ,  $N(1) - Ni - O(1')$  and  $O(1) - Ni - O(1')$  respectively. The average Ni-N, Ni-O and C-O bond distances are  $1.9174(18) \text{ \AA}$ ,  $1.8386(16) \text{ \AA}$  and  $1.291(3) \text{ \AA}$  respectively.

The crystal lattice of compound **16** is similar to that of compound **4**, its free ligand. In both lattices, the cyclohexyl group is in the chair configuration and is at an oblique angle to the benzimidazole plane. The average Ni...Ni distance is 6.45Å. Unlike Ni(dmmbp)<sub>2</sub>, there are no visible pi-stacking in the crystal lattice. Instead, a

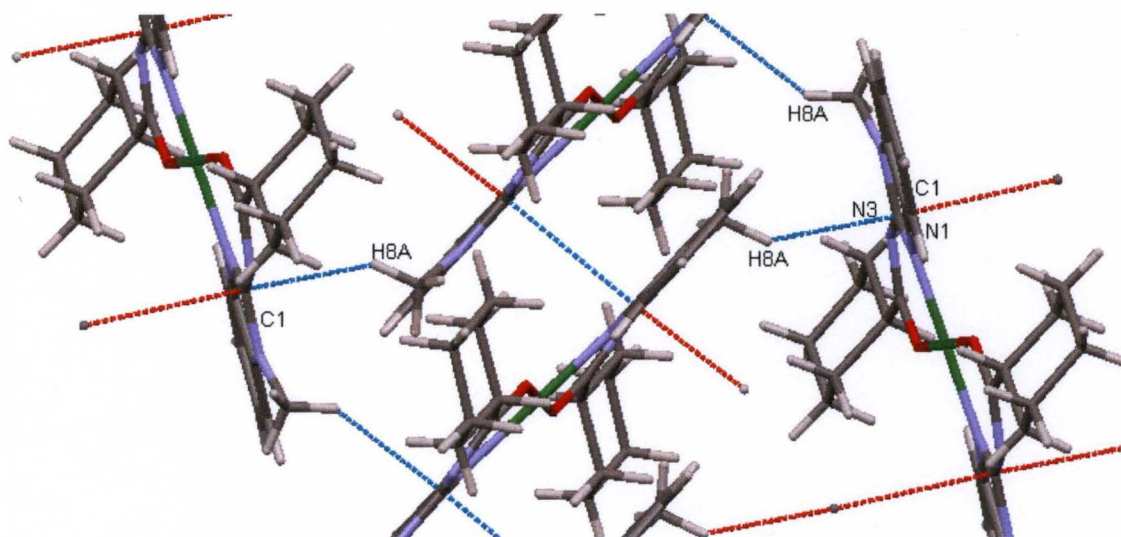


Figure 3.42: Crystal lattice of compound **16**. Intercalating molecules displaying an point to face interaction.

All adjacent pi-stacking molecules have been omitted for clarity.

network of edge to face C-H... $\pi$  interactions, (H8...C1, Figure 3.42), hold the lattice together. These interactions have distances ranging from 2.72(6) Å to 3.33(5)Å. As a result, adjacent Ni (II) metal centers are diagonal to each other and each cyclohexyl group interacts with a benzimidazole of the adjacent molecule.

Compound **17** (Figure 3.43), forms a monoclinic crystal in the space group P2<sub>1</sub>/c. Compound **17** can be described as having a slightly distorted tetrahedral geometry. Examination of the coordination sphere shows that the cobalt (II) ion, a d<sup>7</sup> ion, is coordinated to two anionic bidentate ligands with a N<sub>2</sub>O<sub>2</sub> donor set.

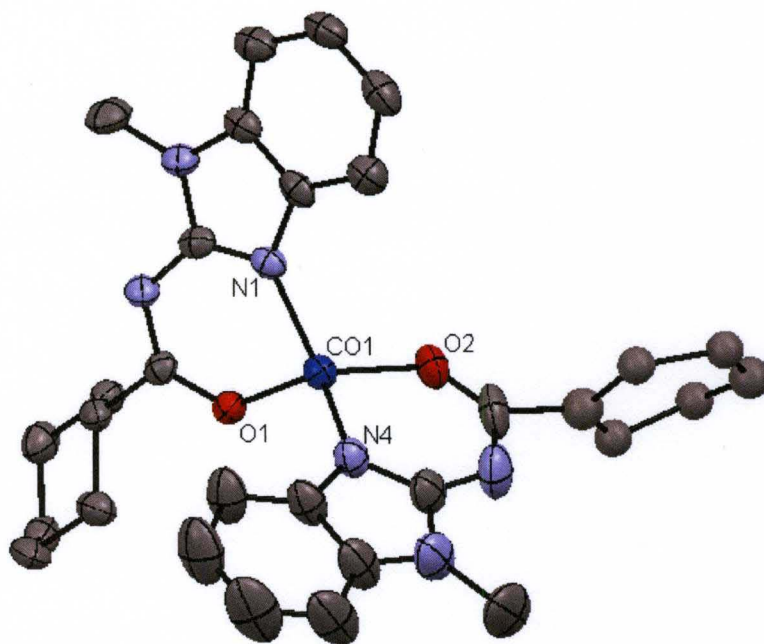


Figure 3.43: ORTEP diagram of compound **17**. Ellipsoids are shown at 50% probability. Hydrogen atoms on the complex were removed for clarity. Additionally, one of the cyclohexyl pendant is positionally disordered and has been modeled.

The ligand, (N-1-methyl benzimidazol-2-yl)cyclohexylcarboxamido, chelates in a *trans* configuration around the central cobalt(II) atom. The Co-N bond length is 1.96Å which is shorter than an amb monodentate reported by Antsyshkina which measured 2.108(9)Å [146]. Compound **17** has angles of 130.05(16)°, 91.58(14)°, 113.71(15)°, 112.55(15)°, 92.22(16)°, and 119.40(14)° corresponding to N1–Co–N4, N1–Co–O1, N1–Co–O2, N4–Co–O1, N4–Co–O2 and O1–Co–O2 respectively. One cyclohexyl group is positionally disordered and has been refined accordingly. Also, a co-crystal of compound **17** shows slightly different bond angles but similar bond lengths and is labeled **17b** in Table 3.7. Table 3.7 summarizes the bond lengths and angles of compounds **15-17**.



Table 3.7: Selected bond lengths and angles for compounds 15, 16 and 17.

<b>Bond Lengths (Å)</b>				
	<b>Compd 15</b>	<b>Compd 16</b>	<b>Compd 17</b>	<b>Compd 17b</b>
M-N1	1.994(3)	1.9175(18)	1.953(4)	1.956(4)
M-N4	1.994(3)	1.9174(18)	1.957(4)	1.964(4)
M-O1	1.916(2)	1.8387(16)	1.942(3)	1.938(3)
M-O2	1.916(2)	1.8386(16)	1.949(3)	1.956(3)
C-O1	1.280(4)	1.291(3)	1.291(5)	1.293(6)
C-O2			1.287(7)	1.286(5)
<b>Bond Angles (°)</b>				
	<b>Compd 15</b>	<b>Compd 16</b>	<b>Compd 17</b>	<b>Compd 17b</b>
N1-M-N4	180.00(17)	180.0	130.05(16)	123.48(17)
N1-M-O1	88.92(10)	91.12(7)	91.58(14)	91.65(15)
N1-M-O2	91.08(10)	88.88(7)	113.71(15)	120.94(15)
N4-M-O1	91.08(10)	88.88(7)	112.55(15)	114.94(15)
N4-M-O2*	88.92(10)	91.12(7)	92.22(16)	92.01(16)
O1-M-O2	180.00(15)	179.998(1)	119.40(14)	115.99(15)

\* N4 = NO1' and O2 = O1'

Both N1-Co-O2 and N1-Co-N4 angles of the co-crystals differ by seven degrees. The crystal lattice of compound **17** reveals an alternating  $\pi$ -stacking of benzimidazole and cyclohexyl pendants. Similarly, the cyclohexyl pendant is in the chair configuration with its hydrogen atoms engaged in hydrogen-  $\pi$  interactions.

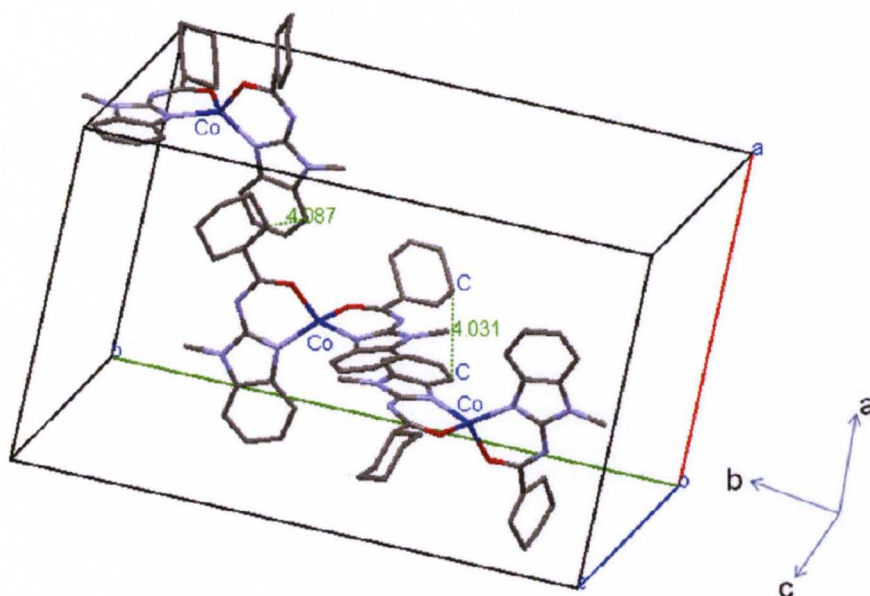


Figure 3.44: Crystal lattice of compound **17**. Hydrogens have been omitted for clarity.

As a result of these interactions, the benzimidazole and cyclohexyl carbons are separated by an average distance of 4.04 Å. Consequently, the cobalt centers become separated an average of 8.32 Å from each other.

Compound **23** (Figure 3.45), crystallizes as a monoclinic in the space group  $P2_1/c$ . Examination of the coordination sphere shows that the  $Zn^{2+}$  ion, a  $d^{10}$  ion, is coordinated to two anionic bidentate ligands with a  $N_2O_2$  donor set. The ligands, N-(benzimidazol-2-yl)acetamido, bond to the central zinc (II) ion such that both ligands are orthogonal to one another.

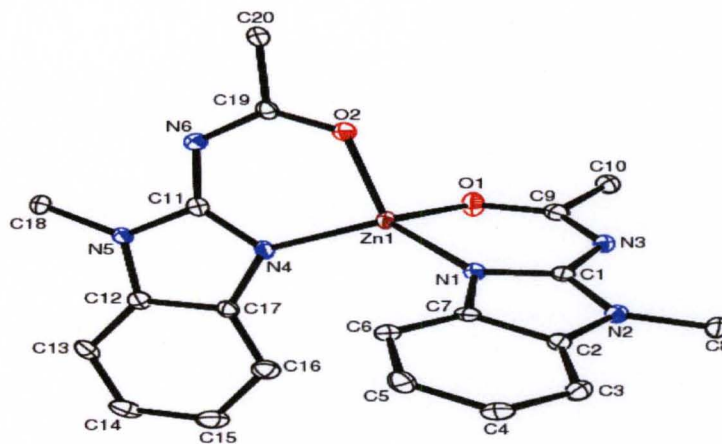


Figure 3.45: ORTEP diagram of compound **23**. Ellipsoids are shown at 30% probability. Hydrogen atoms have been omitted for clarity.

Compound **23** can therefore be described as having a slightly distorted tetrahedral geometry. The compound has angles of  $122.45(16)^\circ$ ,  $92.04(15)^\circ$ ,  $124.72(15)^\circ$ ,  $123.94(16)^\circ$ ,  $92.40(15)^\circ$ , and  $102.48(15)^\circ$  corresponding to N1–Zn–N4, N1–Zn–O1, N1–Zn–O2, N4–Zn–O1, N4–Zn–O2 and O1–Zn–O2 respectively (table 3.8). The average Zn–O, Zn–N and C–O bond lengths are  $1.963(3)\text{Å}$ ,  $1.943(9)\text{Å}$  and  $1.277(6)\text{Å}$ . The unit cell is displayed below (Figure 3.46).

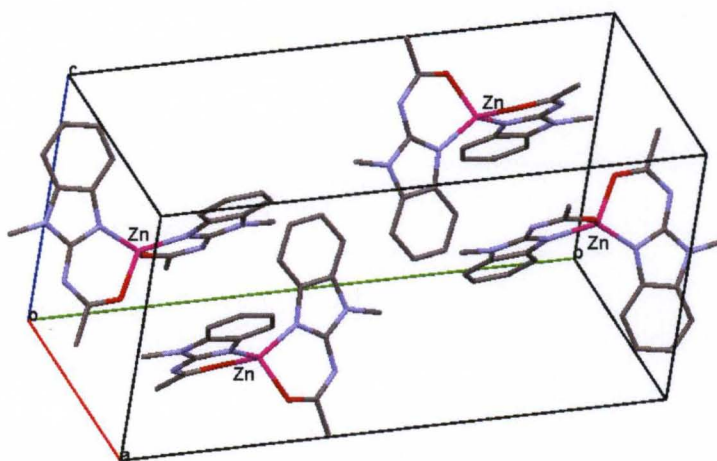


Figure 3.46: ORTEP diagram of compound **23** showing packing in a unit cell. Ellipsoids are shown at 30% probability and hydrogens have been omitted for clarity.

The lattice of compound **23** can be described as having alternating parallel cooperative  $\pi$ -stacking interactions intercalated by orthogonal  $\pi$ -stacking between ligands of adjacent molecules. As a result of these packing arrangements, channels are created in the lattice.

Figure 3.47 shows the ortep diagram of compound **19**. Compound **19** crystallizes as orthorhombic and belongs to the space group *Pbca*. Its geometry can be described as distorted square pyramidal. The central vanadium atom, a  $d^1$  ion, is coordinated to two bidentate chelates in a *trans* configuration through a  $N_2O_2$  donor set and an oxygen atom.

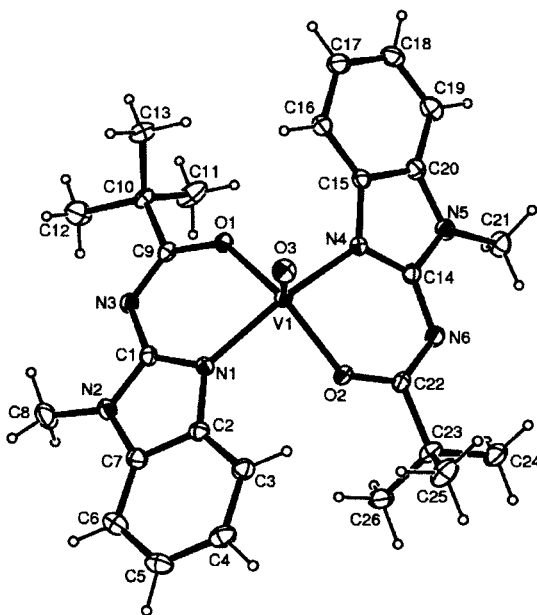


Figure 3.47: ORTEP diagram of compound **19**. Ellipsoids are shown at 30% probability

The oxygen atom located at the apex of the molecule is double bonded to the central vanadium atom. The other bonds to the central vanadium atom are the nitrogen of the benzimidazole and the oxygen of the carbonyl. The distortion seen in the crystal lattice can be attributed to the repulsion between the V-O double bond and the other V-O and V-N single bonds. Average C - O and V-N bond lengths are 1.294(8) Å and 2.060(2) Å. The

V-O bond lengths 1.9703(17) Å, 1.9560(17) Å, and 1.5850(19) Å correspond to the single and double bonds respectively. The following bond angles 92.04(15)°, 124.72(15)°, 123.94(16)°, 92.40(15)° and 102.48(15)° represent N1-V-O1, N1-V-O2, N4-V-O1, N4-V-O2 and O1-V-O2. The separation between adjacent heterocyclic rings is 3.49(4)Å (Figure 3.48).

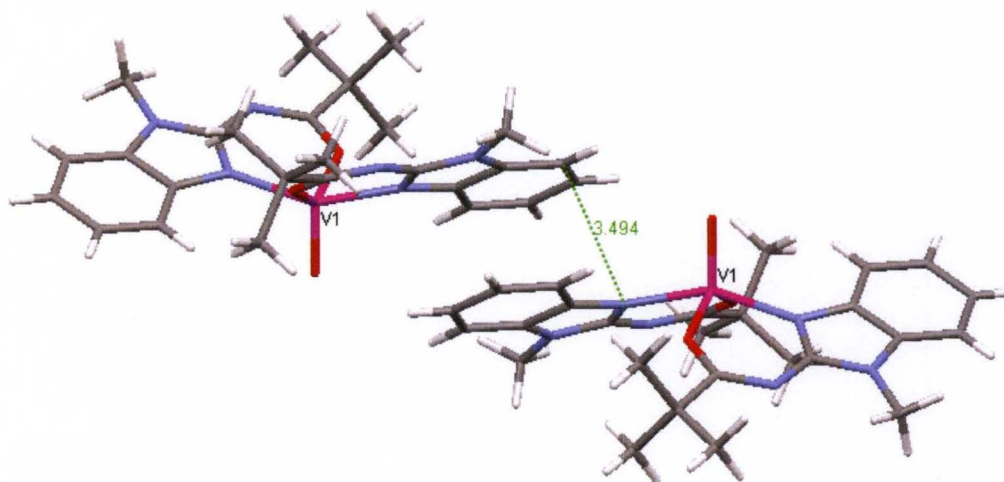


Figure 3.48: Crystal lattice of compound **19** showing the orientation of V=O bonds along c-axis.

Additionally, the V=O bonds are oriented diagonally in pairs in an antiparallel manner. This allows for  $\pi$ -stacking interactions between the benzimidazoles of some adjacent molecular pairs, a feature common amongst its  $\text{Cu}^{2+}$ ,  $\text{Ni}^{2+}$ ,  $\text{Co}^{2+}$  and  $\text{Zn}^{2+}$  analogs.

Structures considered thus far, are consistent with the neutral bis-chelates of  $\text{Cu}^{2+}$ ,  $\text{Ni}^{2+}$ ,  $\text{Co}^{2+}$  and  $\text{Zn}^{2+}$  derivatives of compound **9**, previously synthesized. However, with the exception of compounds **17** and **19**, they differ in the types of interactions found in their respective lattices. That is, they do not display  $\pi$ -stacking interactions, but rather engage in C-H $\cdots$  $\pi$  interactions; suggesting a correlation between the types of interactions in a lattice and the size and nature of the pendants.

We report a new five coordinated complex from these 1:2 metal-ligand reactions, compound **18** (Figure 3.49). It crystallizes into the space group  $P\bar{1}$  and can be described as having a distorted trigonal bipyramidal geometry with the oxygens occupying the axial positions and  $\tau$  index of 30% ( $\beta=135.8^\circ$ ,  $\alpha=117.6^\circ$ ) or 50% ( $\beta=135.8^\circ$ ,  $\alpha=105.9^\circ$ ) [147]. Examination of the coordination sphere shows that the zinc atom, a  $d^{10}$  ion, is coordinated to three ligands; two of which are bidentate chelates ( $N_2O_2$  donor set) and the third bonded through the nitrogen of the benzimidazole as a monodentate ligand.

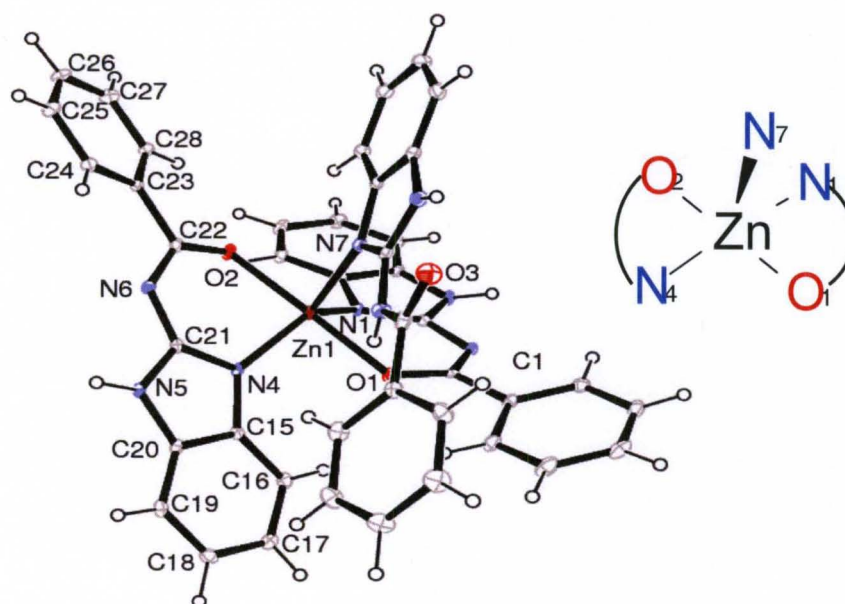


Figure 3.49: ORTEP diagram of compound **18**. Ellipsoids are shown at 30% probability.

The chelates adopt a *trans* configuration around the zinc (II) ion and are located in different planes. The resulting tilt of the individual ligands could be due to space maximization and most importantly, the minimization of electron repulsion of the aromatic rings. Consequently, the electron cloud of the rings are almost orthogonal to each other resulting in a point to face  $C-H\cdots\pi$  interaction. The average Zn – O bond length is 2.0871(63) Å, whilst the average Zn- N bond length of the chelates is

2.0026(66) Å. Similarly, the C = O is 1.2257 Å whilst that for C-O measures 1.27Å. The Zn- N bond length of the monodentate is slightly elongated and is 0.0867Å longer than the bis – chelate. Table 3.8 summarizes the bond lengths and angle for compounds **18**, **19** and **23**.

Table 3.8: Selected bond lengths and angles of compounds **18**, **19** and **23**

	<b>Compound 18</b>	<b>Compound 19</b>	<b>Compound 23</b>
M-N1	1.9885(15)	2.067(2)	1.945(4)
M-N4	2.0168(16)	2.053(2)	1.942(4)
M-O1	2.1103(13)	1.9703(17)	1.966(3)
M-O2	2.0640(13)	1.9560(17)	1.960(3)
M-O3		1.5850(19)	
M-N7	2.1038(16)		
C-O(1)	1.278(2)	1.291(3)	1.280(6)
C-O(2)	1.268(2)	1.298(3)	1.274(6)
C-O(3)	1.226(2)		
	<b>Compound 18</b>	<b>Compound 19</b>	<b>Compound 23</b>
N1-M-N4	135.80(6)	152.08(8)	122.45(16)
N1-M-O1	86.66(6)	83.98(8)	92.04(15)
N1-M-O2	101.76(6)	86.83(8)	124.72(15)
N1-M-O3		103.92(9)	
N1-M-N7	105.91(6)		
N4-M-O1	88.31(6)	85.70(8)	123.94(16)
N4-M-O2	86.90(6)	83.96(8)	92.40(15)
N4-M-O3		103.99(9)	
N4-M-N7	117.61(6)		
O1-M-O2	171.38(5)	138.68(8)	102.48(15)
O1-M-O3		110.46(9)	
O2-M-O3		110.86(9)	
O1-M-N7	86.90(5)		
O2-M-N7	88.99(6)		

Bond angles of 171.38(5)°, 86.66(6)°, 88.31(6)°, 86.90(5)°, 101.76(6)°, 86.90(6)°, 88.99(6)°, 135.80(6)°, 105.91(6)° and 117.61(6)° correspond to O1 – Zn –O2, O1 – Zn – N1, O1 – Zn –N4, O1 – Zn – N7, O2 – Zn –N1, O2 – Zn –N4, O2 – Zn – N7, N1 – Zn – N4, N1 – Zn –N7 and N4 – Zn –N7 respectively.

The interactions observed in compound **18** include side to side intermolecular hydrogen bonding between the imide nitrogen (N6) and the hydrogen of the

benzimidazole of adjacent chelating ligands along the a-c plane of the unit cell (Figure 3.50).

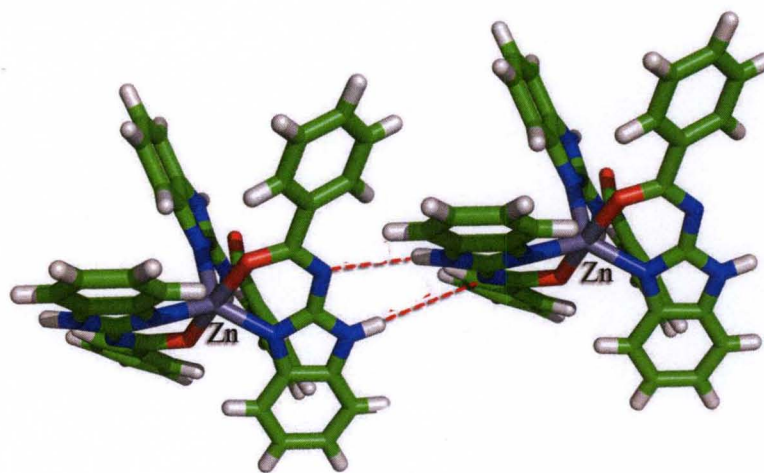


Figure 3.50: ORTEP diagram of compound **18**'s crystal lattice. Sites of hydrogen bonding between molecules are shown in red dotted lines.

Orthogonal to this (b-c plane), are point to face intramolecular interaction of the phenyl groups, coupled with an intermolecular  $\pi$ -stacking interaction between phenyl and adjacent benzimidazole. This orientation not only minimizes the electron cloud repulsion of the  $\pi$ - electrons, but also adds to the overall stability of the lattice. The parameters of the hydrogen bonding interactions observed in the lattice are shown in table 3.9.

Table 3.9: Hydrogen bonds for Compound **18** [ $\text{\AA}$  and  $^\circ$ ].

D-H	d(D-H)	d(H..A)	$\angle$ DHA	d(D..A)	A
N2-H2N	0.911	1.940	172.96	2.846	N6 [ x+1, y, z ]
N5-H5N	0.900	1.987	171.01	2.880	N3 [ x-1, y, z ]
N8-H8N	0.840	2.085	124.99	2.657	O3
N9-H9N	0.823	2.133	145.75	2.852	O1



The expanded five coordination environment of the zinc (II) ion is similar to a bis-chelated amido Ni complex of compound **9**, (amb)Ni(dmmbp)<sub>2</sub>, reported by Philip Bauer [32] and is only the second in this series of functionalized benzimidazole ligands produced in our laboratory (Figure 3.50). Unlike compound **18**, (amb)Ni(dmmbp)<sub>2</sub> was generated from the titration of amb and Ni(dmmbp)<sub>2</sub>.

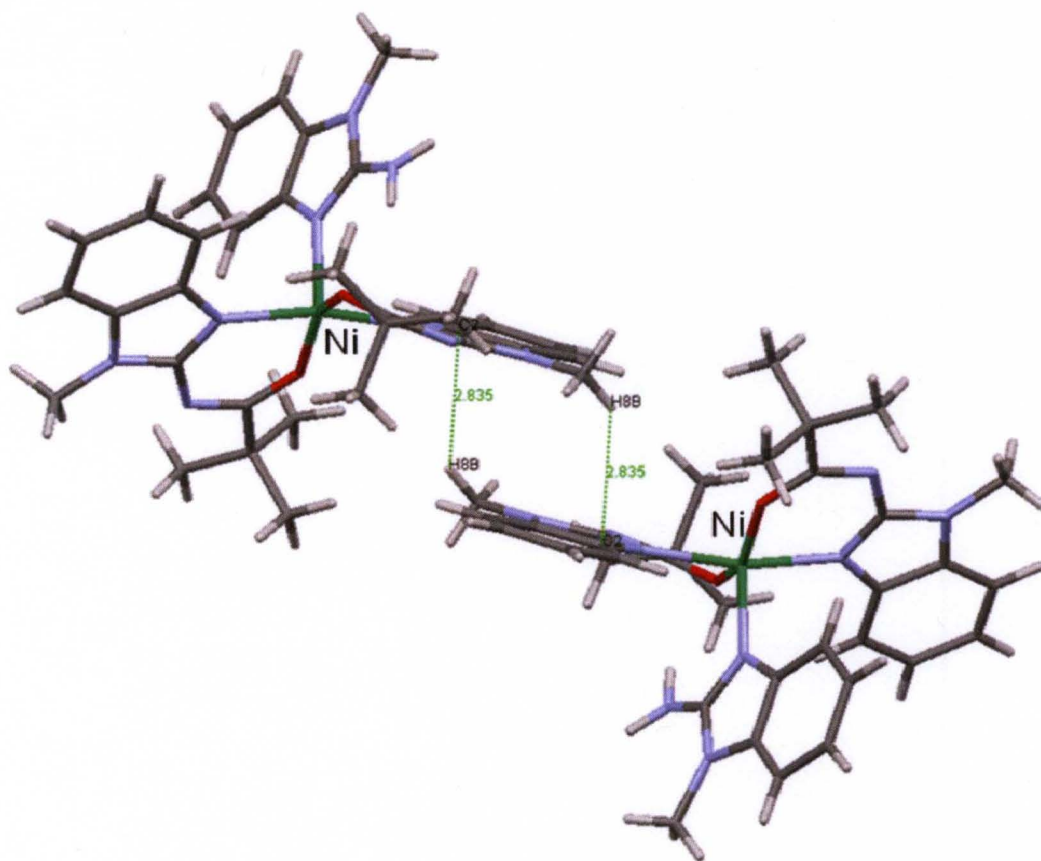


Figure 3.51: A tail – tail Hydrogen –  $\pi$  interactions of (amb)Ni(dmmbp)<sub>2</sub> along the c-axis of the unit cell.

2-amino-1-methylbenzimidazole (amb) pointed in opposite directions of the bis-chelate plane

The bis-chelated ligands in both compounds show a convex bend, allowing for hydrogen- $\pi$  interactions of the apex ligand of the adjacent molecule in the lattice. However, the

Ni(II) complex does not possess the hydrogen bonding between the N1 hydrogen of the benzimidazole and the imido nitrogen of the adjacent chelate. This is because the N1 position of the benzimidazole in the Ni(II) complex is occupied by a methyl group instead of a hydrogen. Consequently, the Ni(II) complex opts for a slipped  $\pi$ -stacking interaction with an adjacent benzimidazole ring (Figure 3.51). This interaction has an average distance of 2.83(5) Å. Also, one of the hydrogens of the 2-amino group is involved in a hydrogen bonding interaction perpendicular to the bis-chelates (b-c plane) with an average distance of 2.09 Å.

A dinuclear copper complex, compound **24** (Figure 3.52), was obtained, in an attempt to generate a metal pyridine analog of compound **9**.

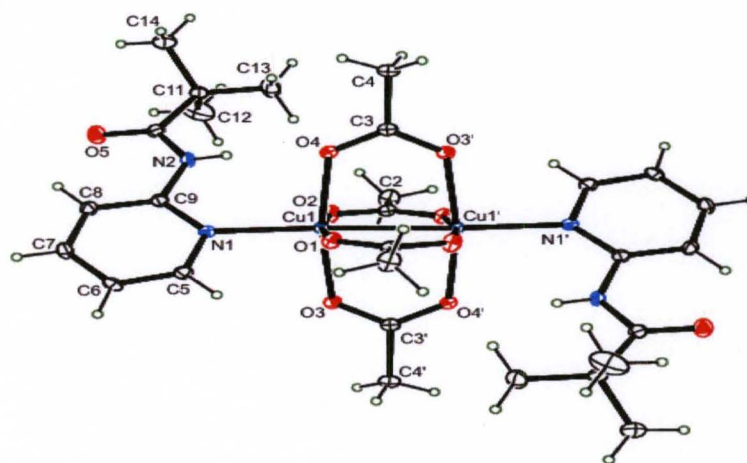


Figure 3.52: ORTEP diagram of Compound **24**. Ellipsoids are shown at 30% probability.

Compound **24** crystallizes into the space group  $P2_1/c$ . Both metal centers could be said to have distorted octahedral geometry. The Cu centers are bridged by four acetate ligands and a Cu-Cu bond. The sixth positions for each Cu center is occupied by the nitrogen of the ligand N(-pyridin-2-yl)-2,2-dimethylpropanamide. The monodentate ligands are *trans*

with respect to each other. Table 3.10 summarizes the various bond lengths and angles of the compound.

**Table 3.10: Selected bond lengths and angles of compound 24**

<b>Bond Lengths (Å)</b>	
<b>Compound 24</b>	
Cu(1)-O(1)	1.9752(19)
Cu(1)-N(1)	2.200(2)
Cu(1)-Cu(1')	2.6162(6)
O(3)-C(3')	1.265(3)
O(5)-C(10)	1.214(3)
<b>Bond Angles (°)</b>	
<b>Compound 24</b>	
O(3)-Cu(1)-O(1)	89.41(8)
O(2)-Cu(1)-O(1)	169.04(8)
O(3)-Cu(1)-N(1)	94.59(8)
O(2)-Cu(1)-N(1)	99.30(8)
O(3)-Cu(1)-Cu(1')	83.90(6)
O(4)-Cu(1)-Cu(1')	85.15(6)
O(2)-Cu(1)-Cu(1')	86.97(6)
O(1)-Cu(1)-Cu(1')	82.15(6)
N(1)-Cu(1)-Cu(1')	173.58(6)
C(1')-O(1)-Cu(1)	125.53(17)
C(3')-O(3)-Cu(1)	123.86(17)
C(1)-O(2)-Cu(1)	119.81(18)

The crystal lattice is stabilized by a network of intra- and intermolecular hydrogen bond interactions. The intramolecular hydrogen bonding, Figure 3.53, is between an amide proton and an oxygen of the acetate with an average bond distance of 2.70 Å.

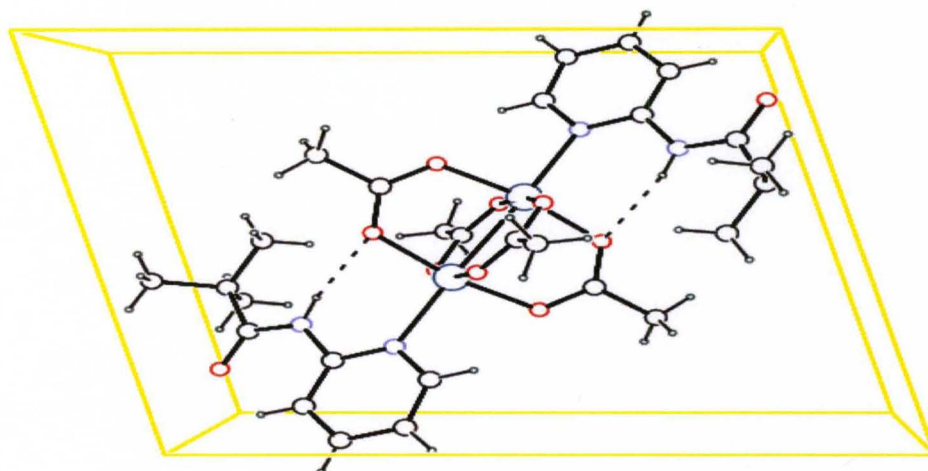


Figure 3.53: ORTEP diagram of Compound **24** showing the intramolecular hydrogen bonding within crystal lattice.

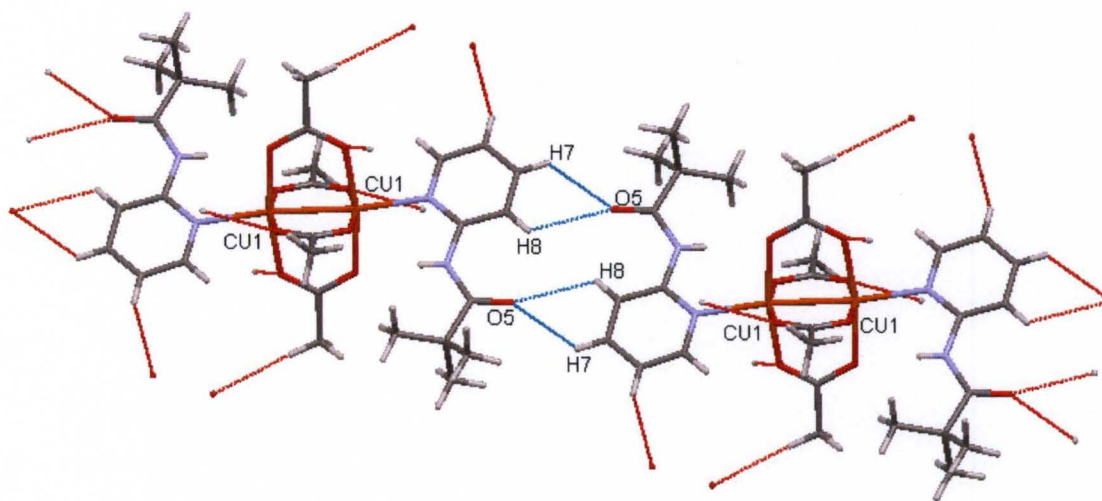


Figure 3.54: ORTEP diagram of Compound **24** showing intermolecular hydrogen bonding within crystal lattice.

Intermolecular hydrogen bonding interactions, Figure 3.54, with average bond distances of 2.67(3) Å, at acute angles to the a-b plane of the unit cell, are observed between a meta pyridinyl proton and the oxygen of the carbonyl of an adjacent molecule's pyridinyl ligand. Other pyridinyl protons interact with either the oxygen of an acetate or carbonyl of an adjacent molecule with average distances of 2.69(5) Å. The methyl protons of the acetyl group are also involved in occasional hydrogen bonding with the oxygen of the acetate of adjacent molecules and have average distances of 2.65(3) Å. Table 3.11 contains the parameters associated with some of these hydrogen bonding interactions.

Table 3.11: Hydrogen bonds for Compound **24** [Å and °].

D-H	d(D-H)	d(H..A)	<DHA	d(D..A)	A
N2-H20	0.768	2.420	152.24	3.121	O4
C8-H8	0.933	2.253	119.20	2.822	O5

These interactions are very identical to the secondary coordination environment of a bis (2-aminopyridine)copper(II) diaceto complex, reported by Garnovskii *et al.* The complex shows hydrogen bonding interactions between the hydrogens of the 2-amino group and the oxygens of the acetyl chelates [148]. Another structure, a bis (2-amino-1-methylbenzimidazole)copper(II) diacetate complex, has been reported by Antsyshkina *et al.*[149]. However, unlike the previous compound, the primary environment of this complex reveals that both acetate ions are bound to a mononuclear copper(II) ion center through both oxygens. The secondary interactions in this complex comes from the protons of the 2-amino group and the oxygen of the acetate carbonyl (2.86Å).

After a study of copper(II) acetate complexes of 2-amino substituted imidazole, thiazole, pyrimidines, benzimidazoles and pyridine derivatives with the general formula  $\text{Cu}(\text{OAc})_2\text{L}_2$ , Garnovskii *et al.* came to the conclusion that the IR spectra for these complexes usually display less intense N-H stretching frequencies. This can be attributable to their hydrogen bonding interactions [138]. However, compound **24** displays a very intense N-H stretching frequency around  $3379\text{cm}^{-1}$  even though it exhibits similar hydrogen bonding interactions.

## **H: Conclusions**

The IR, mass spectrometric data, and in some cases  $^1\text{H}$  NMR and X-ray crystallographic data, all show that the benzimidazole ligands discussed in this series bond to the metal ions as chelates forming mostly four coordinate compounds. The chelation of these ligands is always through the nitrogen of the benzimidazole and the oxygen of the carbonyl.

Only V, Zn and Ni exhibited coordination environments greater than four. In these five coordinate compounds, the benzimidazoles were distorted from the ideal in an effort to minimize electron cloud repulsion. The crystal lattice of these compounds exhibited  $\pi$ -stacking interactions with occasional point to face C-H $\cdots\pi$  interactions that help to stabilize the overall lattice. Both intermolecular and intramolecular interactions worked in tandem in a cooperative sense with  $\pi$ -stacking interactions influenced by the length of the attached pendant of the ligand. These interactions are a result of the distortions and deviations from ideal geometry in an effort to achieve maximum stability.

As a group, the interactions found in the lattices of these complexes to a large extent are governed by the appendants of the benzimidazole ligands. That is, one would expect

pi-stacking to be a predominant interaction given the benzimidazole repeat motif of these complexes. However, interactions arise as a result of steric bulk of appendants, efficiency of packing molecules, and repulsion minimization. Repulsion minimization is evident in the five coordinates, where a tilt of the benzimidazole chelates occur. Pi-stacking dominates only the small pendant tetrahedral complexes in this series and is consistent with our previous findings.

Table 3.12 shows the average bond lengths of metal-nitrogen and metal-oxygen bond distances of selected  $M^{2+}$  ion benzimidazole derivatives synthesized in our laboratory.

Table 3.12: Average bond lengths of selected first row transition  $M^{2+}$  ions benzimidazole complex derivatives.

Bond type	$V^{4+}$	$Co^{2+}$	$Ni^{2+}$	$Cu^{2+}$	$Zn^{2+}$	$Zn^{2+}$
M-N (Å)	2.060(2)	1.955(6)	1.895(9)	1.963(9)	2.060(2)	1.942(4)
M-O (Å)	1.963(1)	1.945(1)	1.848(9)	1.916(9)	1.963(2)	1.966(3)
Shape	Sq.Pyramidal	tetrahedral	Sq. planar	Sq.planar	Trig.bipyramidal	tetrahedral

The Ni- N bond measures 1.895(9) Å and is shorter than the Co – N bond length, a phenomenon consistent with the periodic trend, periodicity of the p-block (i.e effective nuclear charge effect). However, this phenomenon is not seen in similar four - coordinate compounds of Cu or Zn ions for this series. A comparison of the four-coordinate compounds of the Cu and Zn reveals a longer and intermediate bond length respectively. This might be due to several factors among which are the nature of the binding ligand, subsequent alignment (presence or absence of intra/intermolecular interactions), resultant molecular strain, or torque of the moiety attached to the carbonyl. That is, the long chain carbon pendant of compound **15**, for example, results in a longer Cu- N bond compared to the methyl group of compound **23**. Much more stabilization is attained from the  $\pi$ -stacking of the benzimidazole in the case of compound **15** in the planar configuration

than tetrahedral because of the long carbon chain. It is worth noting that for the same ligand, N-(1-methylbenzimidazol-2-yl)cyclohexanecarboxamido, cobalt (II) prefers tetrahedral ( $e^4, t_2^3$ ) geometry whilst nickel (II) prefers square planar.

The next chapter deals with the reactions of these ligands with platinum.



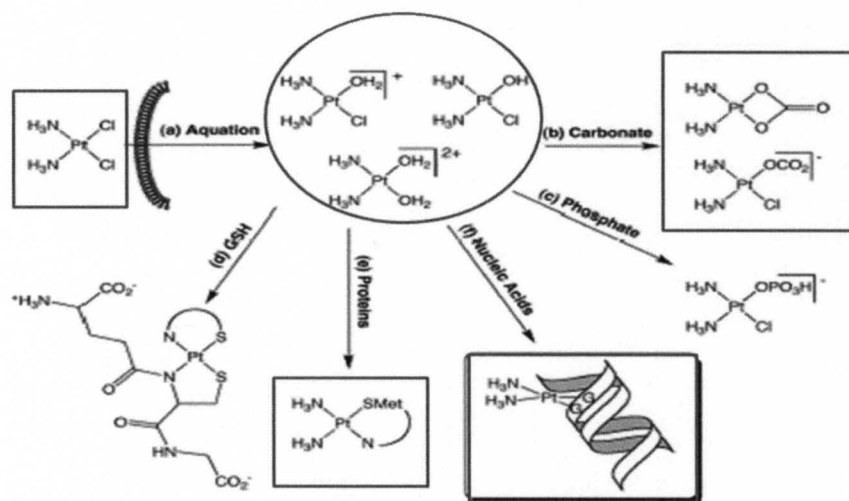
**CHAPTER IV**  
**ISOMERIC CONFORMERS OF PLATINUM (II) COMPLEXES OF 2-  
PIVALOYL PYRIDINE AND BENZIMIDAZOLE LIGANDS**

**A: Background Discussion**

Cisplatin, cis-diamminedichloroplatinum(II) (Figure 4.1), to date is one of the most successful anti-cancer drugs on the market [150]. It is highly effective in the treatment of ovarian and testicular cancers and is also utilized in the treatment of bladder, cervical, head and neck, esophageal and small cell lung cancers [151-152]. However, its' cytotoxicity leaves patients with numerous side effects including organ failure [73, 153]. Also, like most drugs on the market, efficacy diminishes due to the activity of the multidrug resistance protein (MRP) and acquired resistance [79, 150, 154]. It is in this regard that the constant need for new, less toxic and more effective compounds cannot be overemphasized.

The mode of action of cisplatin on DNA has been extensively investigated and documented. Lippard *et al.* in a 1999 review, discussed and compared the efficacy of various platinum (II) and (IV) complexes including cisplatin. Cisplatin is believed to enter the cell through passive diffusion. The dichlorides are substituted by two molecules of water within the cell. This substitution does not happen outside the cell due to the high levels of chlorides within the intercellular space. Once activated, the diaquo platinum complex can bind to several targets among which are genomic DNA (gDNA),

mitochondrial DNA (mtDNA), cytoskeletal microfilaments, thiol containing proteins, and RNA. It should be noted that cisplatin has a high affinity for the N 7 of guanine and adenosine bases. Binding to these bases result in a 1, 2- intrastrand cross-link. It is this bifunctional cross-link that prevents transcription of important proteins, resulting in induced apoptosis. Necrosis or apoptosis is induced by cisplatin via binding to the afore-mentioned targets in the cell, resulting in interference of metabolic pathways thereby compromising energy production and/or immune defense system deactivation. The other targets of cisplatin are phospholipids and phosphotidylserine of the cell membrane. Scheme 4.1 shows the various adducts of cisplatin.



Scheme 4.1[153]: mode of action of cisplatin

However, non small cell lung cancers and colorectal cancers have intrinsic resistance to cisplatin, while ovarian and small cell lung cancers develop resistance. It is believed in most academic circles that acquired resistance to cisplatin is conferred mainly through the deactivating actions of thiol metal-binding proteins such as glutathione (GSH) and metallothionein (MT) [57, 151]. After nearly four decades of intense research only a handful of compounds have showed some promise (Figure 4.1). The latest

compounds are satraplatin and picoplatin. Satraplatin is under consideration for approval by the FDA whilst picoplatin is in phase III of clinical trials [79].

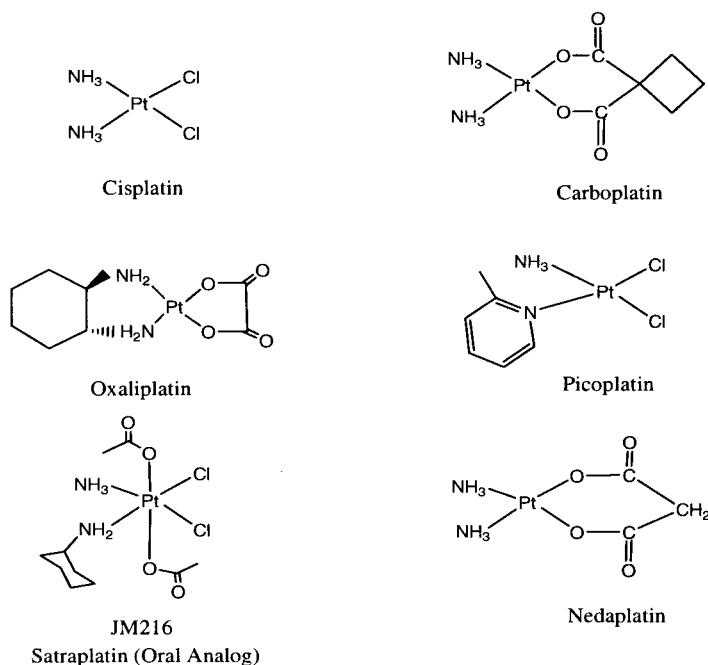


Figure 4.1: Active platinum compounds.

It is still not clear why large tumors are resistant to cisplatin. Membrane transport proteins ATP-binding cassette (ABC) family and solute carrier (SLC) transporters to a large extent control the efflux of drugs in cells [150]. Any modifications to these proteins will greatly determine intracellular drug concentration and efficacy. However, since cisplatin enters the cells through passive diffusion, modifications to these transport proteins do not directly affect cellular intake. A possible explanation for the diminished efficacy could be a combination of cell membrane disruption and increased MRP activity. Evidence of membrane modification in some cancer cells has been reported by Ying Huang [155]. It is not clear whether these modifications disrupt membrane fluidity. What is clear however, is that the intracellular concentration is lowered through the action of copper pumping protein ATPase A and B [45, 150].

Another consideration with regards to a decrease in drug efficacy will be the role of hydrolytic enzymatic action. However, most drugs are designed with the actions of these enzymes in mind and an inspection of the compounds under discussion (Figure 4. 1) reveals no enzymatic actions are required for these small compounds. Therefore enzymatic action can be ruled out.

Platinum (II), a  $d^8$ , typically forms square planar compounds. Due to its geometry, it is susceptible to nucleophilic attack, among others, from the top or bottom face. It is known that only 5-10% of covalently bound cell-associated cisplatin is found in the DNA fraction, whereas 75-85% of the drug binds to proteins [151, 153, 156-158]. A large amount of the cisplatin-protein interactions involves interactions with thiol containing proteins such as glutathione (GSH) and metallothionein (MT) which result in the deactivation of cisplatin and an increase in resistance acquisition. Accordingly, Heffeter *et. al* in a 2008 review cited elevated GSH levels and the thioredoxin system as playing a major role in chemotherapy resistance [45].

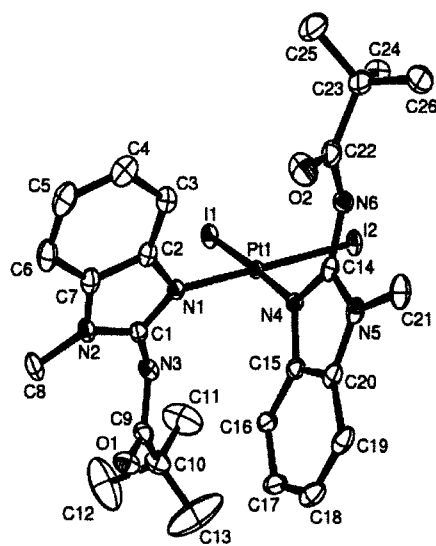
It is currently understood that factors that lead to drug resistance, including cisplatin, can be broadly categorized into four parts;

- (i) reduced intracellular accumulation due to reduced drug uptake and/ or enhanced efflux.*
- (ii) conjugation with intracellular thiols like metallothionein (MT) and / or glutathione (GSH).*
- (iii) enhanced repair of platinum DNA adducts or enhanced tolerance of these adducts.*
- (iv) changes in molecular pathways involved in regulation of cell survival and/ or cell death [45, 151]*

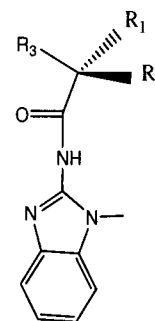
In an effort to overcome or circumvent these factors, combination therapy regimens including non-platinated complexes such as ruthenium, arsenic and gallium, have had to be employed. However, not much progress has been made [159]. Also, a

bifunctional DNA-binding trinuclear platinum complex BBR-3464 was suspended after phase II trials [45].

It is in light of the above four resistance acquisition factors that we propose a new series of platinated species that contain a 2-amino-1-methylbenzimidazole moiety that makes the platinum less accessible to thiol containing proteins as evident in Figure 4.2- i. That is, unlike previous drugs, the benzimidazole ligand, for example, assumes a conformation that makes access to the platinum core more difficult, thereby minimizing deactivation of the complex from reactions with thiols.



(i) Compound **35**



$R_1, R_2, R_3 = \text{H, CH}_3, \text{NH}_2, \text{NHR, NR}_2, \dots$

(ii) free ligand

Figure 4.2: ORTEP diagram of compound **35** and a generic free ligand.

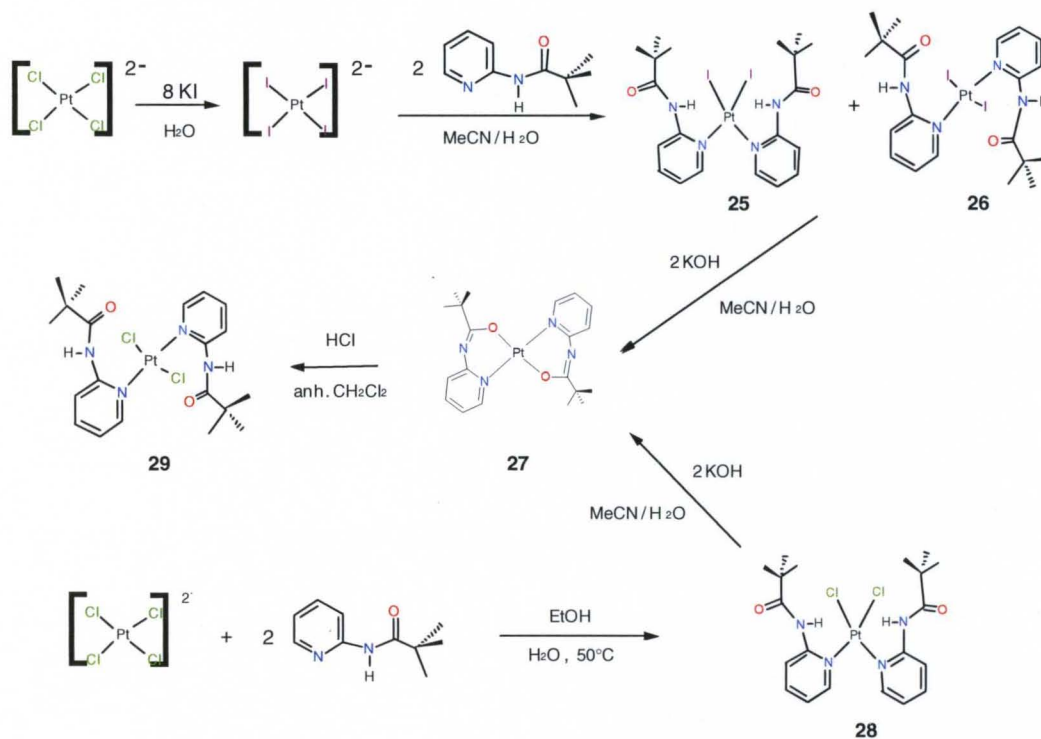
The proposed framework also offers enormous flexibility including variation of attached pendants that can help probe alterations in sterics of the benzimidazole and its effect on reactivity towards targets such as DNA. Preliminary testing of the dichloride analogue of the compound in Figure 4.2-(i) compound **37**, a type 1 complex, done by Dr. Fan using non-small lung cancer cells (A549) shows four-fold toxicity as compared to

cisplatin (i.e.  $LD_{50} < 1\mu M$  compared to cisplatin's  $LD_{50}$  value). Also the antitumor activity is enhanced when used in conjunction with a selenide reagent (MSA). The four-fold toxicity of compound **37** has led to an examination of its pyridine analogue, 2-pivaloylamino pyridine. This ligand was purchased from Sigma-Aldrich and was characterized using  $^1H$  NMR.

## B: Synthesis and Characterization of Platinum (II) Complexes

### (i) 2-Pivaloyl Pyridine complexes;

**Synthesis of complexes:** The platinum complexes were synthesized as shown in Scheme 4.2, a methodology developed for 2-amino-1-methylbenzimidazole platinum(II) derivatives that selectively isolates cis-isomers[32]. Unlike the 2-amino-1-methylbenzimidazole system, the pyridine ligand system gives a mixture of products. Scheme 4.2 shows reactions routes used for these compounds.



Scheme 4.2: Generation of dichloroplatinum(II) compounds

Compound **25** precipitates out of solution as a yellow solid at room temperature with a yield of 21% in a 6 mL acetonitrile / 5 mL methanol / 10 mL water solution upon addition of stoichiometric amount of potassium hydroxide (ligand:base). The yield increases to 65.7% when the reaction is carried out in a methanol / water solution (1:1 v/v) at 50°C for 1.25 h. Compound **26** can be isolated via filtration, from a acetonitrile / water solution (6:5 v/v) and the addition of equimolar amount of potassium hydroxide (yield: 25.4%). Compound **27** precipitates with its *cis* conformer in a 4:1 (Scheme 4.2) ratio over a four- hour period (yield 64.7%), when the reaction is carried out in an acetonitrile / water solution (4:1 v/v) upon addition of stoichiometric amount of potassium hydroxide (ligand:base). However, a 3:1 ratio is obtained when the solution ratio is changed to 12:5. Furthermore, a 1:1 isomeric ratio was obtained for the solvent system 2:1. This phenomenon is different from what is observed in the 2-amino-1-methylbenzimidazole system discussed later in the chapter, which gives exclusively one isomer over the other, most often favoring the *cis* isomer over the *trans*.

### Characterization of Pyridine complexes

The  $^1\text{H}$  NMR spectrum of compound **25** in  $\text{CDCl}_3$ , Figure 4.3, displays a singlet at 10.64 ppm that corresponds to two amide protons. The aromatic protons of both pyridines show up as a doublet ( $J = 4.25$  Hz), doublet of doublets ( $J = 2.50$  Hz, 1.00 Hz) and two triplets ( $J = 7.50$  Hz)

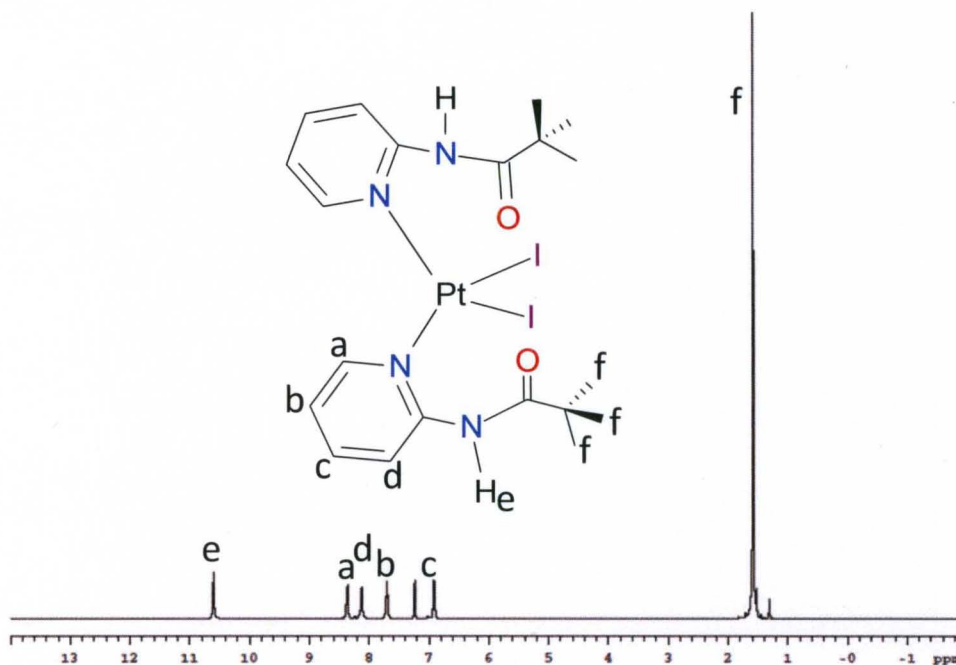


Figure 4.3:  $^1\text{H}$  NMR spectrum of compound **25** in  $\text{CDCl}_3$ .

at 8.41 ppm, 8.16 ppm, 7.74 ppm and 6.95 ppm respectively. However, these peaks appear as singlets in the ratio 2:1:1 in acetone- $d_6$  with chemical shifts of 8.38 ppm, 7.98 ppm and 7.09 ppm. The peak at 1.62 ppm represents the 18 protons of the tert-butyl group. The mass spectrum of compound **25** displays ion peaks at 180.38 m/z, 289.76 m/z, 318.02 m/z, 553.32 m/z, and 680.77 m/z. The molecular ion peak at 680.77 represents the ion  $[\text{H}_2(\text{Pap})_2\text{PtI}]^+$  and has an intensity of 70%. The ion peak at 180.38 m/z is due to the fragment  $[\text{HPap}]^+$  and has a relative intensity of 100%. The peak at 289.76 m/z represents a  $[\text{Pt}(\text{Pap-pivaloyl})]^+$  with a relative intensity of 70%, whilst the peak at 318.02 m/z is due to a  $[\text{Pt}(\text{pivaloyl})\text{K}]^+$  ion with an intensity of 35%. The peak at 553.32 m/z is due to a  $[\text{Pt}(\text{Pap})_2]^+$  with an intensity of 18%.



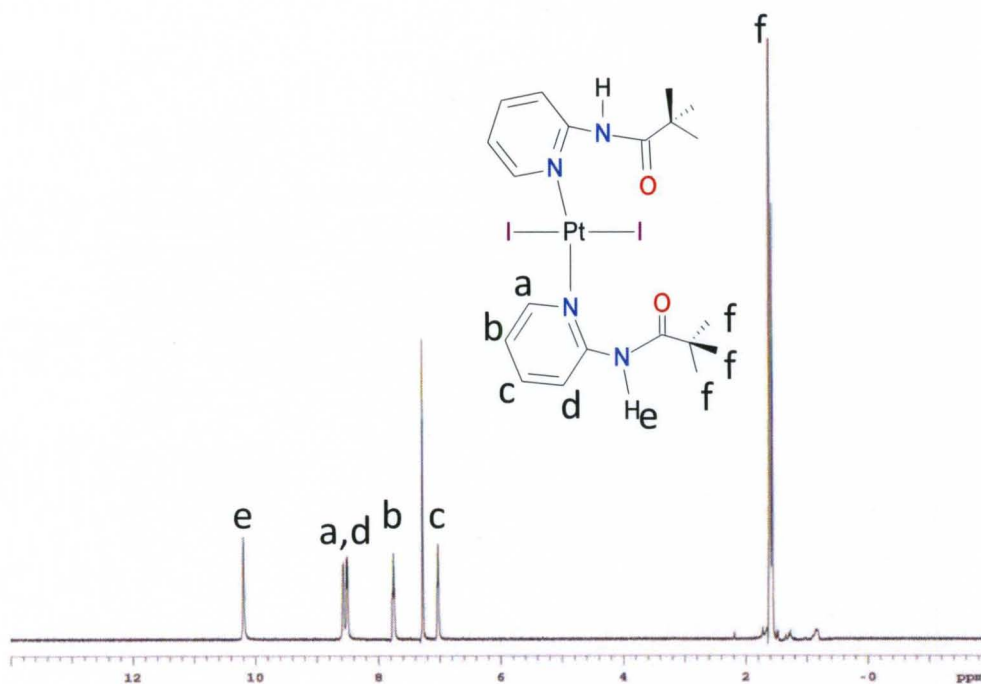


Figure 4.4:  $^1\text{H}$  NMR spectrum of compound **26** in  $\text{CDCl}_3$

Figure 4.4 shows the  $^1\text{H}$  NMR spectrum of compound **26** in  $\text{CDCl}_3$ . The singlet at 10.19 ppm corresponds to the two amide protons. The aromatic protons of the pyridine moiety show up as a doublet of doublets ( $J = 24.0$  Hz;  $J_a, J_b = 5.0, 8.5$  Hz), and two triplets ( $J = 7.5$  Hz) at 8.54 ppm, 7.75 ppm and 7.03 ppm respectively. The peak at 1.60 ppm represents the eighteen methyl protons. Examination of the mass spectrum shows ion peaks at 179.40 m/z, 288.59 m/z, 550.45 m/z and 678.33 m/z with relative intensities of 100 %, 22 %, 15 % and 65 % respectively. These peaks correspond to the ion fragments  $[\text{HPap}]^+$ ,  $[\text{Pt}(\text{Pap-pivaloyl})]^+$ ,  $[(\text{Pap})_2\text{Pt}]^+$  and  $[(\text{Pap})_2\text{Pt I}]^+$ . The spectral traces of the *cis* and *trans* iodo complexes show similar fragmentation pattern and is consistent with Haake *et al.* results [160].

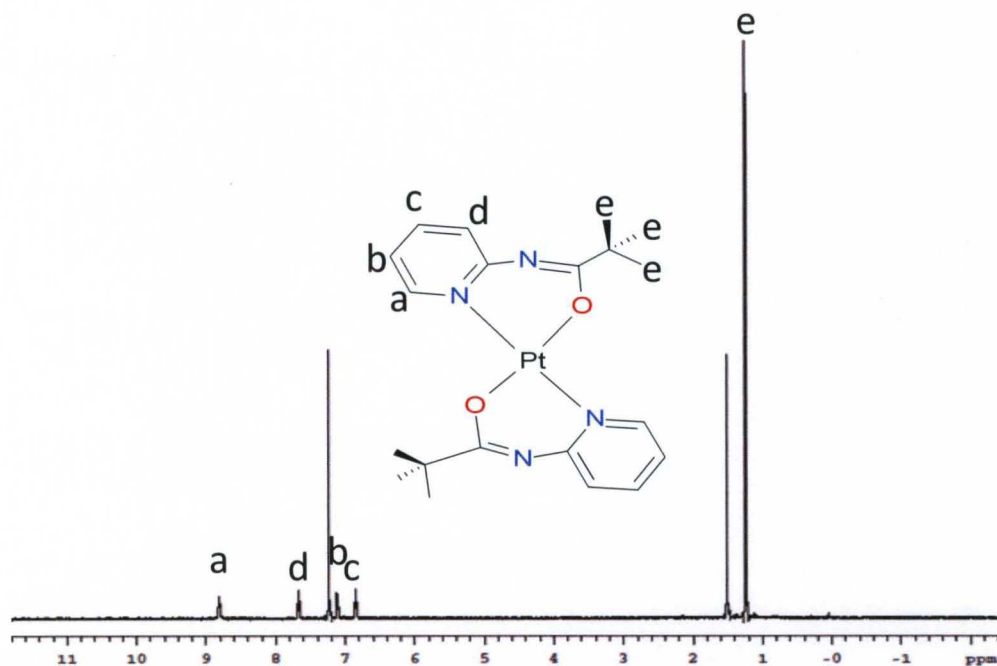


Figure 4.5:  $^1\text{H}$  NMR spectrum of compound **27** in  $\text{CDCl}_3$ .

The  $^1\text{H}$  NMR spectrum of compound **27** in  $\text{CDCl}_3$ , Figure 4.5, shows two doublets and two triplets in the aromatic region. The doublets are centered at 8.82 ppm and 7.11 ppm with coupling constants of 5.50 Hz and 9.00 Hz respectively. Both doublets integrate to four protons. The triplets appear at 7.67 ppm and 6.87 ppm with coupling constants,  $J$ , 7.50 Hz and 6.00 Hz. The peak at 1.26 ppm represents the eighteen protons of the two tert-butyl groups whilst the peak at 1.56 ppm is a water peak, a common solvent contaminant [127]. The mass spectrum of compound **27** shows a molecular peak  $[(\text{Pt}(\text{Pap})_2)\text{H}_2]^+$  at 551.49 m/z.

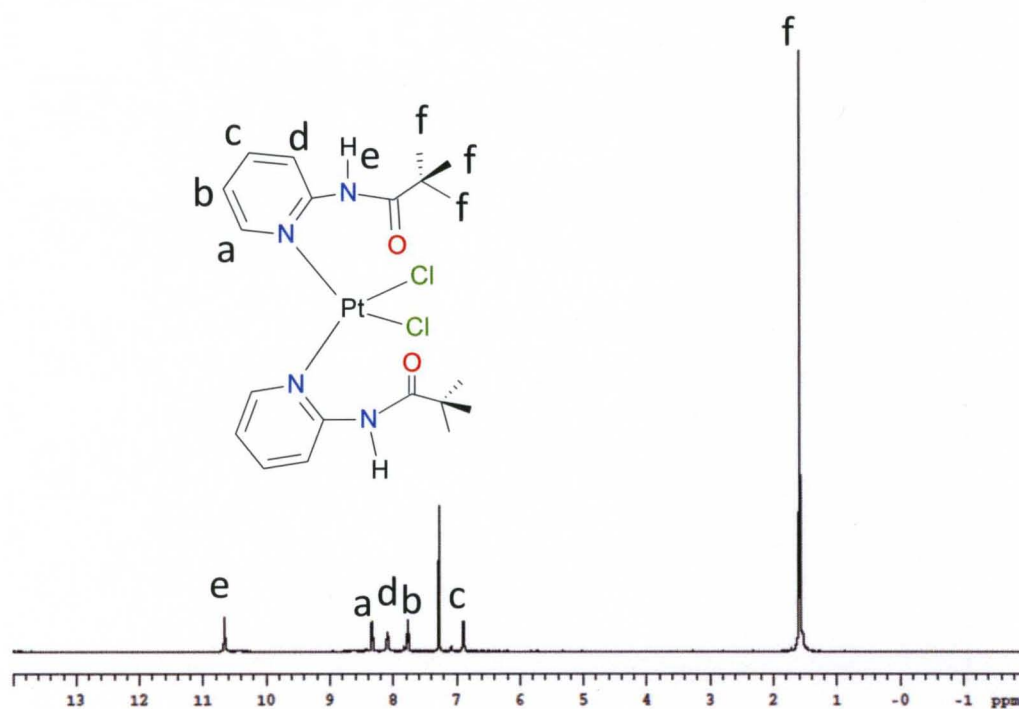


Figure 4.6:  $^1\text{H}$  NMR spectrum of compound **28** in  $\text{CDCl}_3$ .

Figure 4.6 displays the  $^1\text{H}$  NMR of compound **28** in  $\text{CDCl}_3$ . The spectrum shows an amide peak at 10.66 ppm that integrates to two protons. The aromatic region displays a doublet, singlet and two triplets all centered at 8.33 ppm ( $J = 4.00$  Hz), 8.09 ppm, 7.76 ppm ( $J = 7.00$  Hz) and 6.89 ppm ( $J = 6.00$  Hz) respectively. These peaks integrate to a total of eight protons. The mass spectrum of compound **28** displays peaks at 180.24 m/z, 289.87 m/z, 553.44 m/z, and 588.76 m/z with relative intensities of 100 %, 18 %, 20 % and 95 %, respectively. These peaks correspond to the ion fragments  $[\text{H}_2\text{Pap}]^+$ ,  $[\text{Pt}(\text{Pap-pivaloyl})]^+$ ,  $[(\text{Pap})_2\text{Pt}]^+$  and  $[(\text{Pap})_2\text{PtCl}]^+$ .

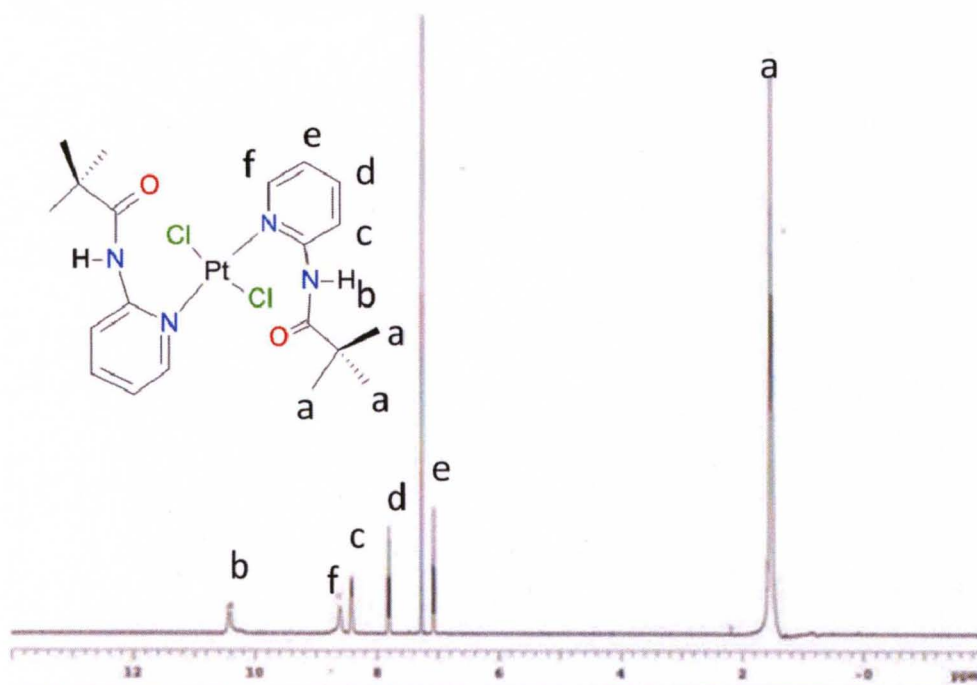
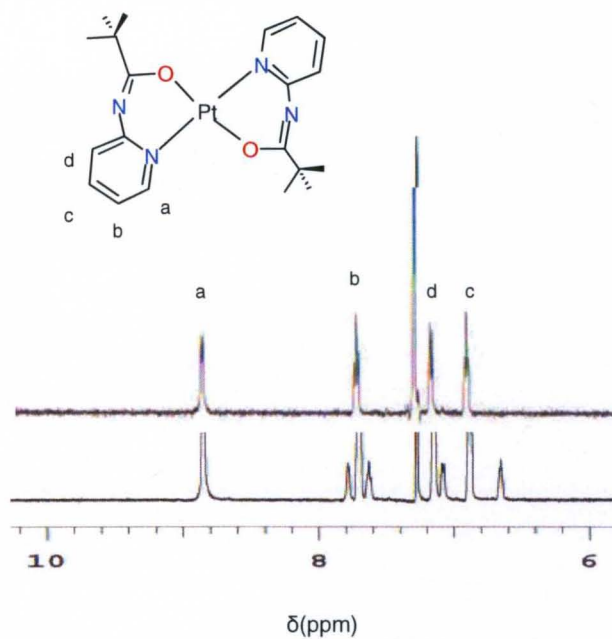


Figure 4.7:  $^1\text{H}$  NMR spectrum of compound **29** in  $\text{CDCl}_3$ .

The  $^1\text{H}$  NMR of compound **29** in  $\text{CDCl}_3$  is displayed in Figure 4.7. The spectrum shows an amide peak at 10.43 ppm. The aromatic region displays a singlet, doublet and two triplets centered at 8.60 ppm, 8.43 ppm, 7.82 ppm and 7.08 ppm respectively. These peaks integrate to eight pyridine protons. The peak for the eighteen protons of the two tert-butyl groups, appear at 1.56 ppm. The mass spectrum of compound **29** displays peaks at 179.53 m/z, 288.80 m/z, 485.61 m/z, 551.84 m/z and 587.83 m/z with relative intensities of 100%, 9.92%, 20%, 15.73% and 60% respectively.

The aromatic region of the  $^1\text{H}$  NMR spectrum of compound **27** shows a similar splitting pattern to its *cis*-conformer (Figure 4.8). However, the aromatic protons are relatively shifted downfield. These proton appear as a doublet ( $J = 3.00$  Hz), triplet ( $J = 7.50$  Hz), doublet ( $J = 4.00$  Hz) and a triplet ( $J = 4.00$  Hz), with chemical shifts in deuterated chloroform of 8.85 ppm, 7.71 ppm, 7.15 ppm and 6.88 ppm respectively.



(ii) <sup>1</sup>H NMR of *trans* and *cis* amido complexes in a ratio of 4:1 in CDCl<sub>3</sub>

Figure 4.8 : The aromatic region of the <sup>1</sup>H NMR of compound **27** and its *cis*-isomer.

In an effort to optimize the yield for the *cis*- isomer, Method C of compound **27** was employed. However even at relatively high temperatures, the *trans*-form seems to be dominant or the preferred state. A <sup>1</sup>H NMR experiment, (Figure 4.9), was performed to understand why this system differed from the system of benzimidazole platinum derivatives, (discussed later in the chapter), which gave *cis*- isomers exclusively.

Figure 4.14 shows the <sup>1</sup>H NMR stacked plot spectrum of the reaction of Compound **25** (0.0023g, 4.1 μM), dissolved in 0.5 mL *d*-acetonitrile / 200μL D<sub>2</sub>O solution with 4μL 3.93M KOH. The reaction was monitored over 10 h.

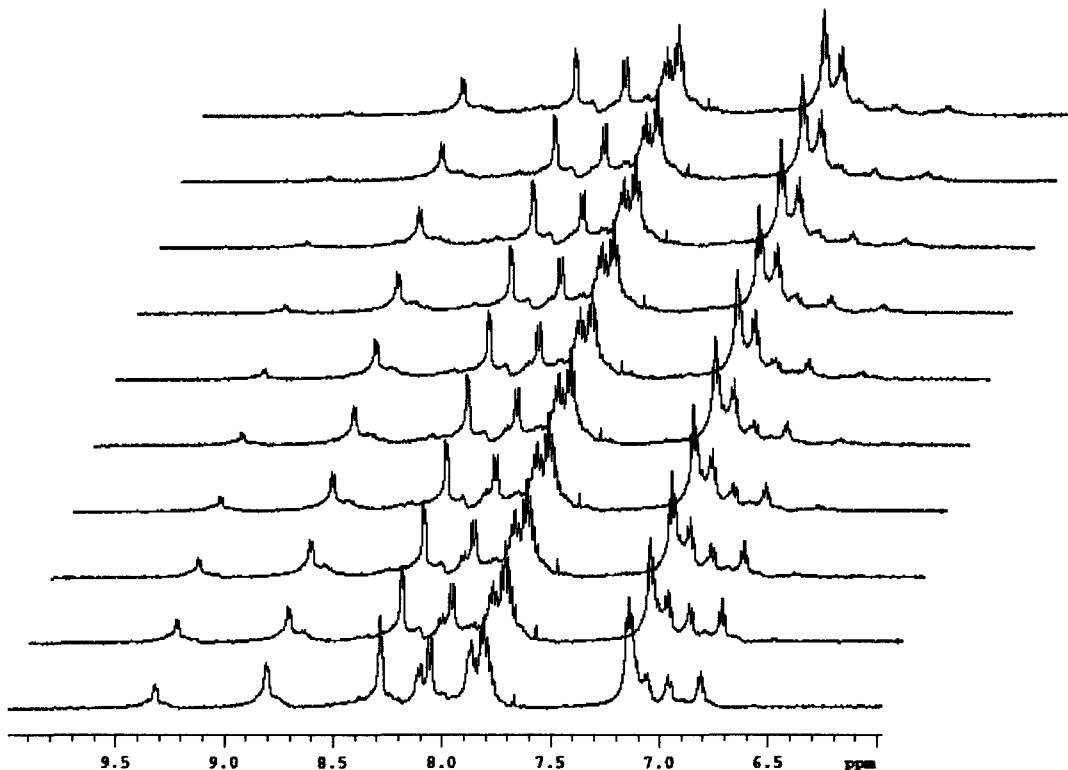


Figure 4.9: Compound **25** dissolved in 0.5 mL *d*-acetonitrile / 200 $\mu$ L D<sub>2</sub>O solution with 4 $\mu$ L 3.93M KOH

The amide peak appears at approximately 9.4 ppm and its intensity diminishes with time due to the conversion of compound **25** to compound **27**. It should be noted that the amount of base used was 2.7 times more than the required amount. A repeat of the above experiment with 1.3 times base yielded similar results. The free rotation of the pyridine ring around the Pt-N bond axis coupled with the less steric bulk and ring strain could be why the *trans* state is preferred.

### C: FT-IR of Pyridine Complexes

Figure 4.10 displays a KBr-IR absorption spectrum of compound **25** that is representative of these platinated pyridine complexes. A N-H stretch appears at 3306 cm<sup>-1</sup>.

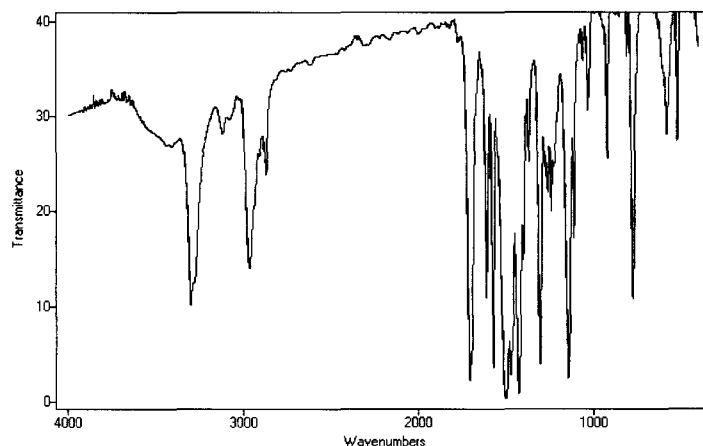


Figure 4.10: IR spectrum of compound **25**

The  $C_{sp^2}$ -H absorption stretch appears at  $3113\text{ cm}^{-1}$ . Peaks at  $2969\text{ cm}^{-1}$  and  $2871\text{ cm}^{-1}$  are indicative of  $C_{sp^3}$ -H stretches. The carbonyl stretch appears at  $1713\text{ cm}^{-1}$ . Selected IR data for compound **25-29** have been compiled in the table below (Table 4.1).

Table 4.1: Selected IR data for compound **25-29**

Compound	$\nu_{\text{N-H}}\text{ (cm}^{-1}\text{)}$	$\nu_{\text{C}_{sp^2}\text{-H}}\text{ (cm}^{-1}\text{)}$	$\nu_{\text{C}_{sp^3}\text{-H}}\text{ (cm}^{-1}\text{)}$	$\nu_{\text{C=O}}\text{ (cm}^{-1}\text{)}$
<b>25</b>	3306	3113 (w)	2969, 2871	1713
<b>26</b>	3300	3113 (w)	2963, 2871	1713
<b>27</b>		3128, 3097	2963, 2871	
<b>28</b>	3294	3106	2951	1700
<b>29</b>	3336	3140	2969	1700

The presence of the N-H and carbonyl stretching frequencies for compounds **25**, **26**, **28** and **29** suggest that the respective ligands are ligated to the metal as monodentates. The  $3000\text{ cm}^{-1}$  to  $4000\text{ cm}^{-1}$  region of compound **27** is identical to compound **36**, its 1-methylbenzimidazole analogue. A stretching frequency at  $1621\text{ cm}^{-1}$ , indicative of a C=C functionality can be seen in the spectrum of compound **27**. The absence of a carbonyl stretch indicates that the ligand is chelated to the platinum metal.

The amide protons of compound **25**, the *cis* isomer, is more deshielded than the *trans* isomer, compound **26**. Accordingly, their IR spectra show that the amide peak for compound **25** has a higher stretching frequency. However, such is not the case for the dichloro- isomers, compounds **28** and **29**. Eventhough their amide peaks follow the same order in terms of deshielding, their IR stretching frequencies are reversed. Since IR to some extent is an indication of bond strength, this finding suggests different reactivity for the various compounds and might be significant in an acid-base reaction. The observed phenomenon might be due to different s-character contributions towards the N-H bond. Additionally, the conversion of compound **25** to compound **27** can be carried out at room temperature, whereas compound **28** requires higher temperatures.

#### D: X-ray Crystallography of Pyridine Complexes

X-ray crystal analysis was performed on four of the six isomers. Tables 4.2 and 4.3 contain selected x-ray crystallographic parameters that include bond angles and lengths for these complexes.

Table 4.2: Selected Crystallographic data of compounds **25-28**

	<b>25</b>	<b>26</b>	<b>27</b>	<b>28</b>
Crystal System	Triclinic	Orthorhombic	Monoclinic	Triclinic
Space Group	P $\bar{1}$	Pbca	P 2 $_1$ /c	P $\bar{1}$
a	9.502(2) Å	12.78166(14) Å	6.0476(2) Å	8.5986(3) Å
b	10.692(3) Å	9.19192(9) Å	13.5698(5) Å	11.1609(4) Å
c	14.141(4) Å	20.5324(2) Å	11.8620(4) Å	13.2153(4) Å
$\alpha$	102.244(4)°	90°	90°	77.623(2)°
$\beta$	98.049(4)°	90°	95.157(3)°	85.944(2)°
$\gamma$	113.604(3)°	90°	90°	72.662(3)°
Volume	1245.3(5) Å <sup>3</sup>	2412.30(4) Å <sup>3</sup>	969.52(6) Å <sup>3</sup>	1182.45(7) Å <sup>3</sup>
Z	2	4	4	2
Density	2.142 Mg/m <sup>3</sup>	2.218 Mg/m <sup>3</sup>	1.882 Mg/m <sup>3</sup>	1.748 Mg/m <sup>3</sup>
GOF	1.050	1.022	1.038	1.086
R1	0.0281	0.0222	0.0193	0.0160
wR2	0.0719	0.0628	0.0477	0.0390



Table 4.3: Selected bond lengths and angles of compounds **25-28**

Bond lengths (Å)				
	<b>25</b>	<b>26</b>	<b>27</b>	<b>28</b>
Pt(1)-N(1)	2.060(4)	2.037(2)	2.024(3)	2.0441(19)
Pt(1)-N(3)	2.071(4)	2.037(2)	2.024(3)	2.0354(18)
Pt(1)-X(2)	2.5846(7)	2.59749(18)		2.2889(5)
Pt(1)-X(1)	2.5890(7)	2.59750(18)		2.2907(6)
Pt(1)-O(avg)			1.986(2)	
C – O(avg)	1.213(1)	1.217(4)	1.292(3)	1.208(3)
Bond angles (°)				
	<b>25</b>	<b>26</b>	<b>27</b>	<b>28</b>
N(3)-Pt(1)-N(1)	88.42(15)	180.0	180.0	88.85(7)
N(3)-Pt(1)-X(1)	175.53(10)	91.17(7)		179.12(5)
N(1)-Pt(1)-X(1)	87.11(10)	88.83(7)		91.09(5)
N(1')-Pt(1)-X(1')		88.83(7)		
N(3)-Pt(1)-X(2)	91.08(10)			89.02(6)
N(1)-Pt(1)-X(2)	179.41(10)			177.06(5)
N(1)-Pt(1)-X(1')		91.17(7)		
X(1)-Pt(1)-X(2)	93.395(13)	180.0		91.07(2)
N(1)-Pt(1)-O(1)			90.74(7)	
N(1)-Pt(1)-O(1_3)			89.26(7)	
N(1_3)-Pt(1)-O(1)			89.26(7)	
N(1_3)-Pt(1)-O(1_3)			90.74(7)	
O(1)-Pt(1) –O(1_3)			180.00(2)	

Compound **25** forms triclinic crystals in the space group  $P\bar{1}$  and has two molecules per unit cell (table 4.2). The coordination sphere around the Pt (II) ion, a  $d^8$  ion, can be described as square planar (Figure 4.11). The ligands bind to the metal as monodentates through the nitrogen of the pyridine derivative. One of the Pt-N bond lengths is elongated and longer than the shorter (2.060(4) Å) by 0.011 Å. The Pt-I bonds measure 2.5846(7) Å and 2.5890(7) Å respectively. The average C-O bond length is 1.213(1) Å. Figure 4.15 shows an ortep diagram of compound **25**.

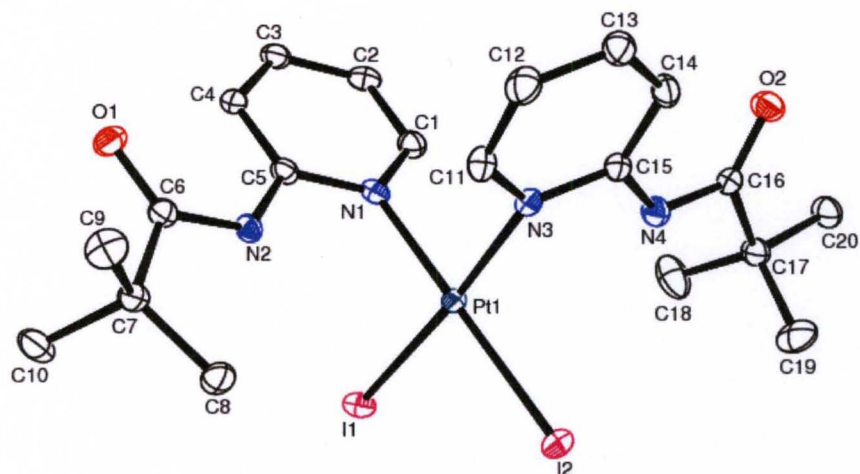


Figure 4.11: ORTEP diagram of compound **25**. Ellipsoids are shown at 30% probability. Hydrogen atoms on the complex were removed for clarity.

Compound **25** has bond angles of  $88.42(15)^\circ$ ,  $175.53(10)^\circ$ ,  $87.11(10)^\circ$ ,  $91.08(10)^\circ$  and  $179.41(10)^\circ$  corresponding to N(3)-Pt(1)-N(1), N(3)-Pt(1)-I(1), N(1)-Pt(1)-I(1), N(3)-Pt(1)-I(2) and N(1)-Pt(1)-I(2) respectively (table 4.3). The crystal lattice of compound **25**, displays a network of slipped  $\pi$ -stacking (C1-C2,  $3.68(7)\text{\AA}$ ) and interactions between pyridine hydrogens (H12) and the oxygen (O1) of the carbonyl with an average distance of  $2.50(5)\text{\AA}$  ( $\ll$  C12-H12-O1 angle of  $133.13^\circ$  and torsional angle of  $98.06^\circ$ ). A third interaction of the pyridine rings is with the tert-butyl hydrogens with an average distance of  $2.75\text{\AA}$ . Figure 4.12 displays some of these interactions of the lattice.

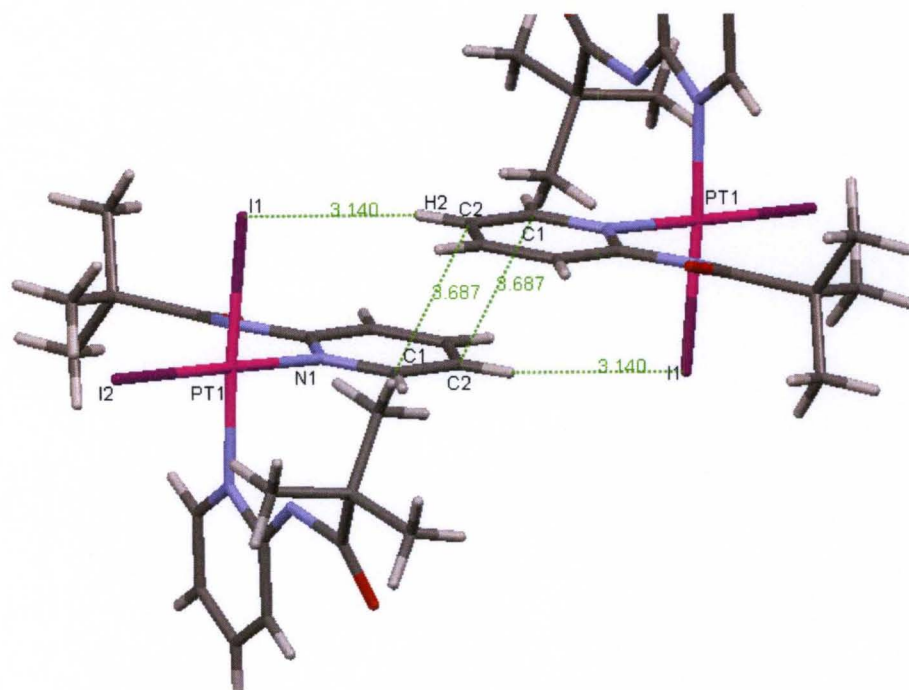


Figure 4.12: Crystal lattice packing diagram of compound **25**.

These interactions are similar to those of its 2-amino-1-methylbenzimidazole analogue, compound **35**. However, unlike its analogue there are no methylene chloride molecules involved in the network of interactions. The iodides are engaged in a C-H... $\pi$  interaction with the tert-butyl group and have an average distance of 3.14 Å (not shown in Figure 4.12). Also visible are interactions with pyridine hydrogens. Compound **26** forms orthorhombic crystals in the space group *Pbca*. The coordination sphere around the Pt (II) ion can be described as square planar (Figure 4.13).

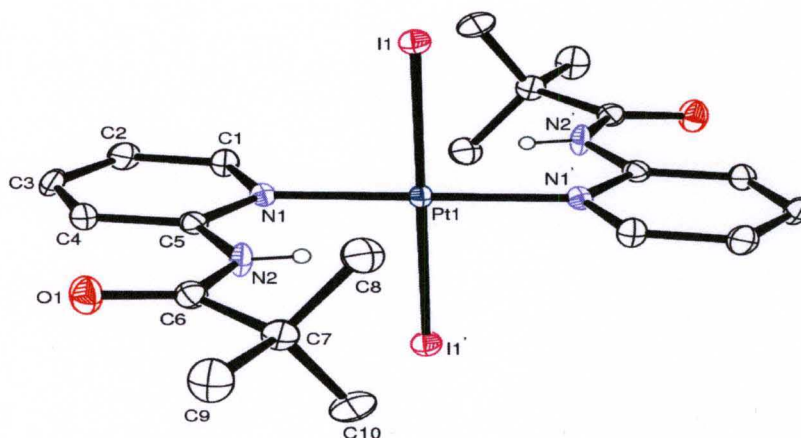


Figure 4.13: ORTEP diagram of compound **26**. Ellipsoids are shown at 50% probability. Except amide protons, hydrogen atoms on the complex were removed for clarity.

The ligands bind to the metal as monodentates through the nitrogen of the pyridine derivative. Both Pt-N bond lengths are equidistant (2.04 Å) and differ from the results of Wimmer *et. al.* by 0.05 Å [161]. However, the Pt-I bond lengths are identical and measure 2.60 Å (table 4.2). The average C-O bond length is 1.22 Å. Compound **26** has bond angles of 180.0°, 91.17(7)°, 88.83(7)°, 88.83(7)°, and 91.17(7)° corresponding to N1'-Pt1-N1, N1'-Pt1-I1, N1-Pt1-I1, N1'-Pt1-I1' and N1-Pt1-I1' respectively (table 4.3). The crystal lattice of compound **26**, displays a network of interactions between pyridine hydrogens and the oxygen of the carbonyl (2.51Å). A second set of interactions involves the tert-butyl hydrogens and the pyridine rings in an edge/point to face  $\pi$ -hydrogen interaction similar to its *cis* isomer, with an average distance of 2.75Å. However, unlike its *cis* isomer, the pyridine rings are oriented parallel to each other and show no sign of cooperative  $\pi$ -stacking. The I-Pt-I bonds have an alternating diagonal orientation along the a-axis of the unit cell. The iodides are engaged in C-H... $\pi$

interactions with the tert-butyl group with average distances of 3.14 Å and 4.09 Å (Figure 4.14).

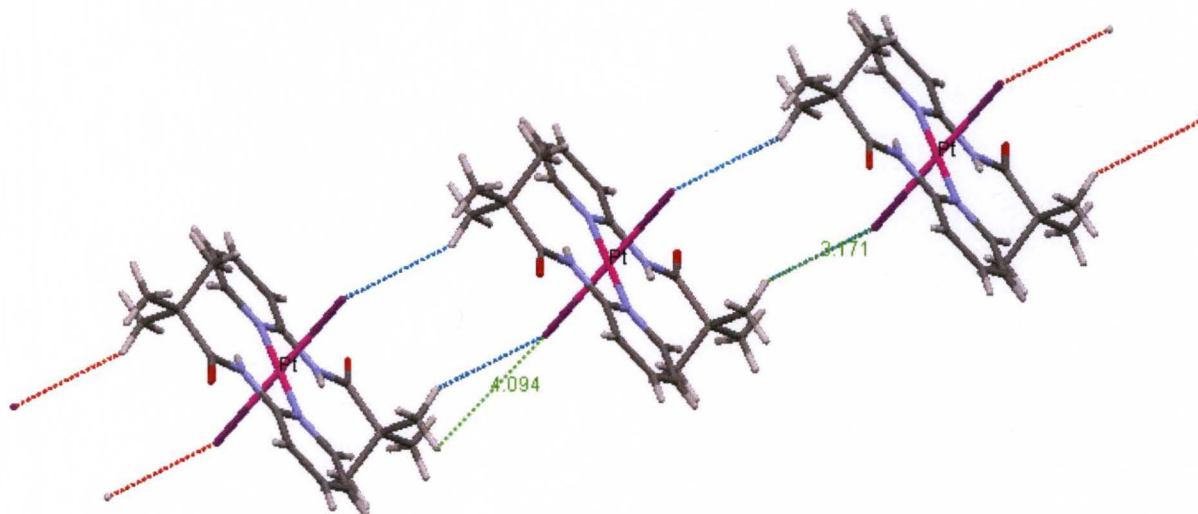


Figure 4.14: Crystal lattice packing diagram of compound **26**, view along the b-axis.

Compound **27** forms monoclinic crystals in the space group  $P 2_1/c$ . The coordination sphere around the Pt (II) ion is square planar with a  $N_2O_2$  donor set (Figure 4.15).

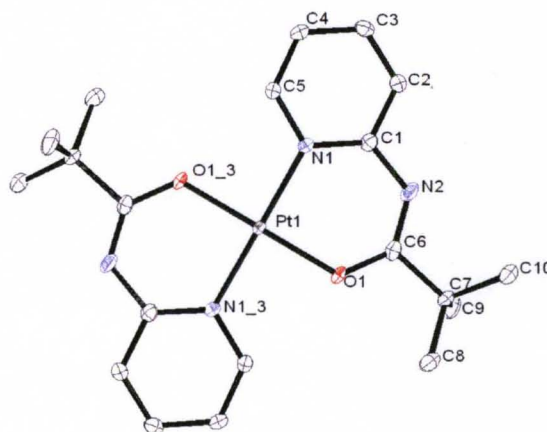


Figure 4.15: ORTEP diagram of compound **27**. Ellipsoids are shown at 50% probability. Hydrogen atoms have been omitted for clarity.

The ligands are in their anionic form and are chelated to the central Pt (II) ion as bidentates in a *trans* configuration. The Pt-N bond lengths are shorter than compounds **25**, **26** and **28**. However, the C-O bond is longer (1.29 Å). Compound **27** has bond angles of 90.74(7)°, 89.26(7)°, 89.26(7)°, 90.74(7)° and 180.00(2)° corresponding to N(1)-Pt(1)-O(1), N(1)-Pt(1)-O(1\_3), N(1\_3)-Pt(1)-O(1), N(1\_3)-Pt(1)-O(1\_3) and O(1)-Pt(1)-O(1\_3) respectively (table 4.3). The average Pt-O bond distance is 1.99 Å and is shorter than the monodentate nitrate reported by Tessier *et al.* [162]. The crystal lattice of compound **26**, Figure 4.16, displays a network of interactions between pyridine rings and the hydrogens of the tert-butyl group of adjacent molecules with an average distance of 3.36 Å.

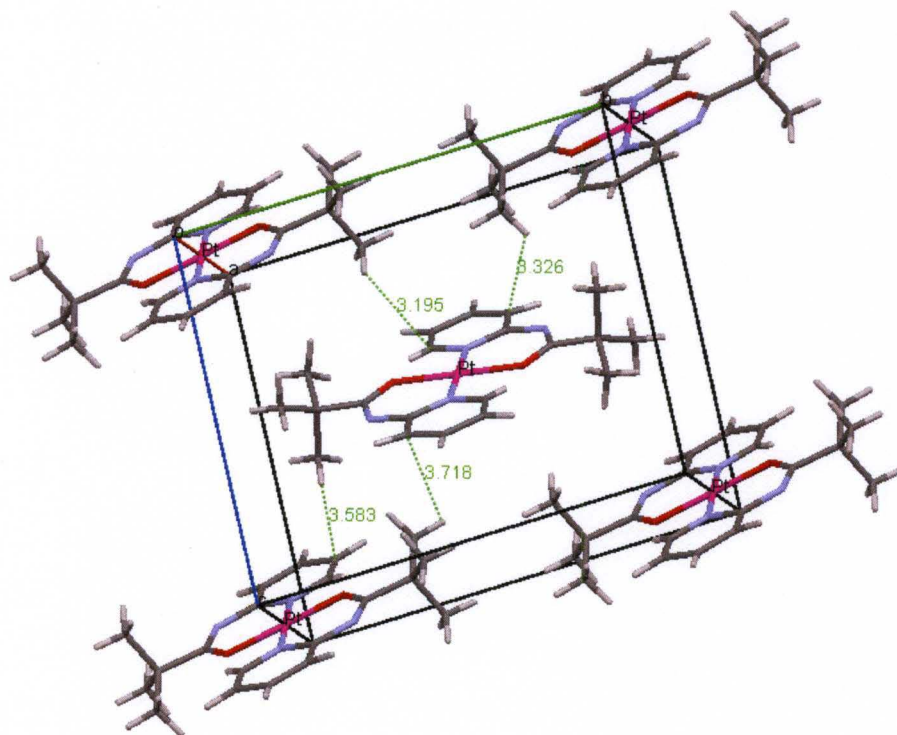


Figure 4.16: Crystal lattice packing diagram of compound **27**, showing C-H... $\pi$  interactions

The lattice also shows cooperative pi- stacking between molecules (Figure 4.17). The average distance between adjacent molecules is 3.36Å. This cooperative interaction is not seen in the 2-amino-1-methylbenzimidazole analogue. Also, unlike the analogue the chelates are in the same plane.

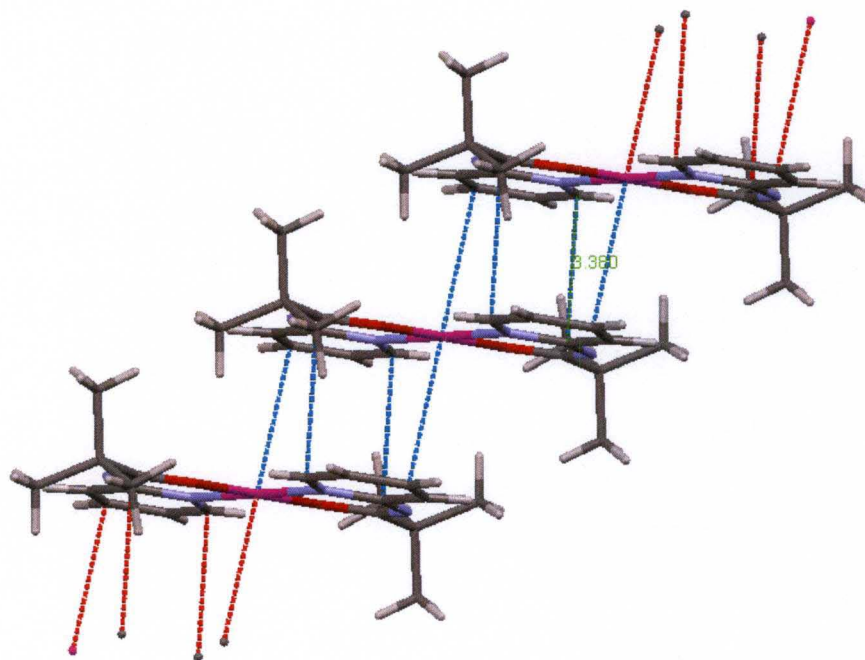


Figure 4.17: Cooperative slipped  $\pi$ -stacking in compound **27**, view along the a-axis.

Compound **28** forms triclinic crystals in the space group  $P\bar{1}$ . The coordination sphere around the Pt (II) ion is also square planar with a  $N_2Cl_2$  donor set (Figure 4.18 ). The ligands binds to the metal as monodentates. One of the Pt-N bond lengths is elongated and therefore longer than the shorter (2.04Å) by 0.0087 Å. The Pt-Cl bonds are equidistance and measure 2.29 Å (comparable to Kato *et al.* [163]). The average C-O bond length is 1.21 Å. Compound **28** has bond angles of 88.85(7)°, 179.12(5)°, 91.09(5)°, 89.02(6)° and 177.06(5)° corresponding to N(3)-Pt(1)-N(1) , N(3)-Pt(1)-Cl(1), N(1)-Pt(1)-Cl(1), N(3)-Pt(1)-Cl(2) and N(1)-Pt(1)-Cl(2) respectively (table 4.3).

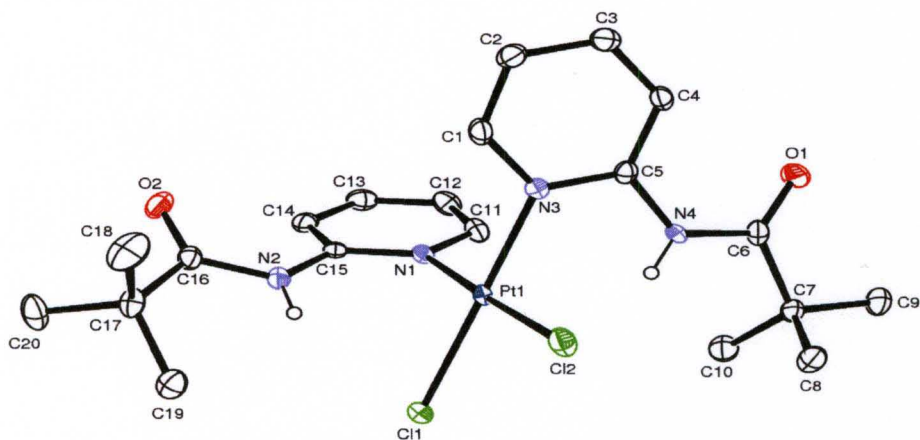


Figure 4.18: ORTEP diagram of compound **28**. Ellipsoids are shown at 40% probability. Hydrogen atoms (except amide protons) have been removed for clarity.

The crystal lattice of compound **28**, displays a network of interactions similar to compound **25** with an average distance of 2.51 Å.

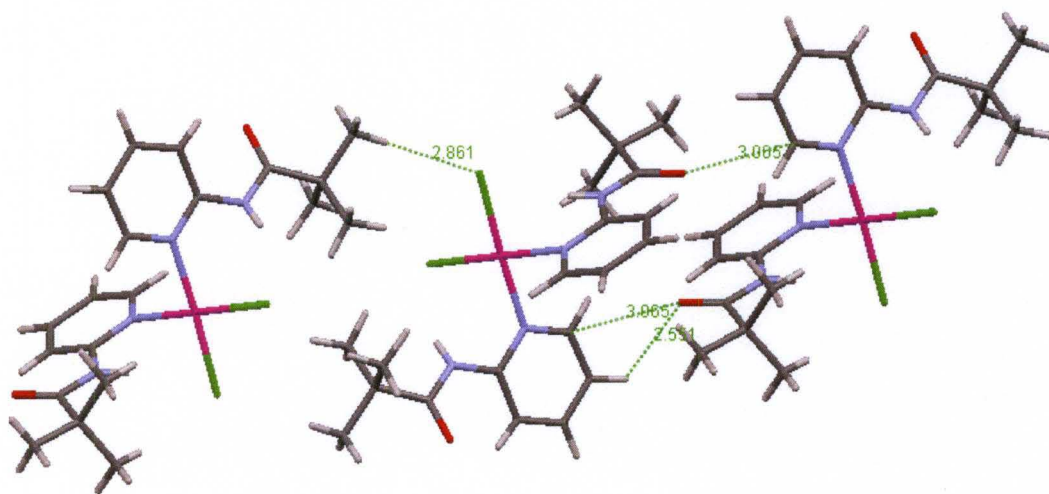


Figure 4.19: Crystal lattice packing diagram of compound **28**, view along the b-axis.

These interactions are similar to its 2-amino-1-methylbenzimidazole analogue.

The table below contains the parameters of hydrogen bonding found in the lattice.



Table 4.4: Hydrogen bonds for compound **28** [ $\text{\AA}$  and  $^\circ$ ].

D-H	d(D-H)	d(H..A)	$\angle$ DHA	d(D..A)	A
N2-H2N	0.708	2.599	145.17	3.206	C11
N4-H4N	0.827	2.756	131.42	3.361	C12

The H donor –acceptor separation is significantly less than that of its diiodo analogue, compound **25**. Thus, from a structural view point one would expect a relatively higher melting point (assuming equal number of total interactions).

### E: UV-vis of Pyridine Complexes

Figure 4.20 shows a typical UV spectrum of these pyridine platinum complexes in dichloromethane. The *cis* diiodo isomer, compound **25**, shows a third  $\lambda_{\text{max}}$  at 437 nm not seen in the other isolated isomers.

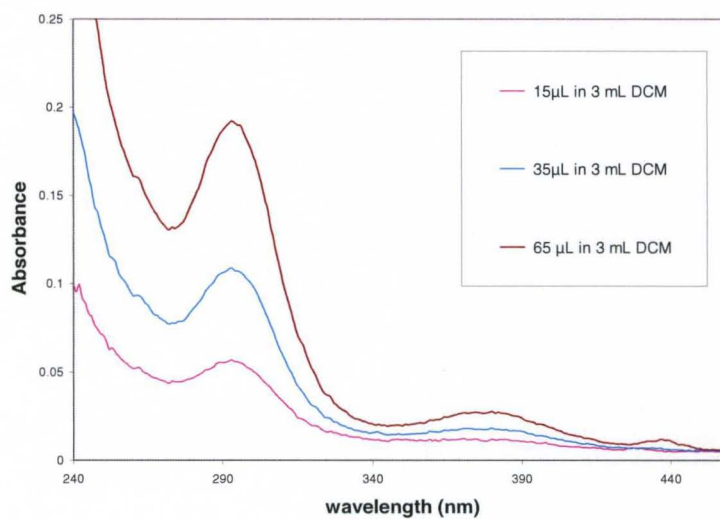


Figure 4.20: UV-vis spectrum of compound **25** in 3 mL dichloromethane at various concentrations (Stock conc. 4.5 mM, 1  $\mu\text{L}$  in 3 mL  $\equiv$  1.5  $\mu\text{M}$ )

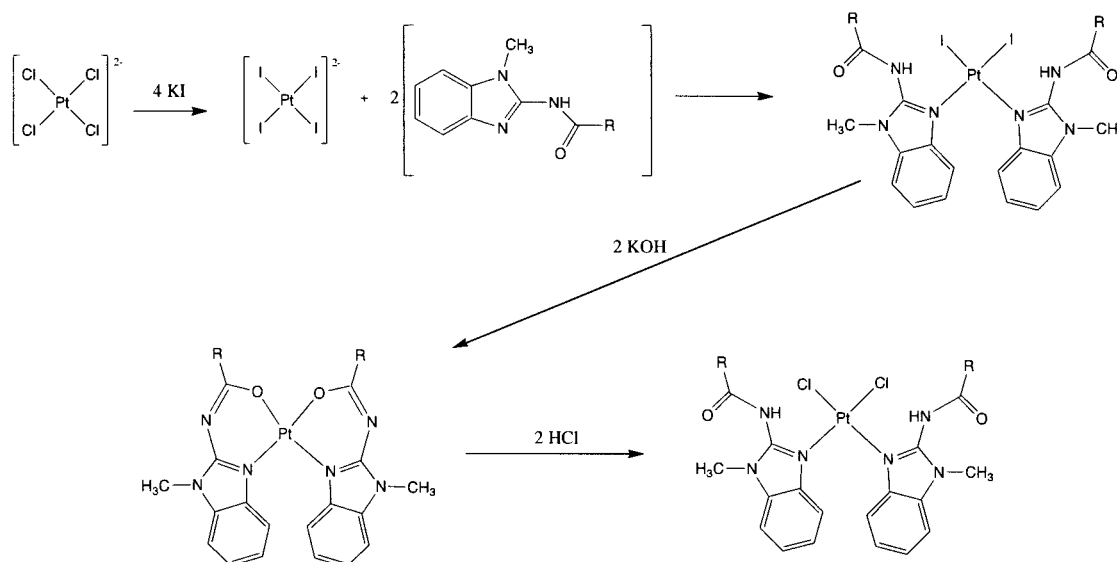
The molar absorptivity and  $\lambda_{\max}$  for these pyridine complexes have been compiled in the table below.

Table 4.5: UV-vis absorption data, (200 nm-1100 nm), for complexes 25-29 obtained using  $\text{CH}_2\text{Cl}_2$ .

Compd	$\lambda_{\max}$ (nm)	$\epsilon$ ( $\text{M}^{-1} \text{cm}^{-1}$ )	Concentration range (M)
<b>25</b>	293, 380, 437	$2.41 \times 10^6$ , $3.58 \times 10^5$ , $3.35 \times 10^5$	$6.23 \times 10^{-10}$ – $1.25 \times 10^{-8}$
<b>26</b>	236, 298	$1.49 \times 10^4$ , $5.86 \times 10^3$	$5.81 \times 10^{-6}$ – $1.74 \times 10^{-4}$
<b>27</b>	273, 355	$3.91 \times 10^1$ , $0.90 \times 10^1$	$8.46 \times 10^{-5}$ – $1.69 \times 10^{-3}$
<b>28</b>	242, 295	$5.30 \times 10^5$ , $3.38 \times 10^5$	$3.22 \times 10^{-6}$ – $6.44 \times 10^{-5}$
<b>29</b>	237, 295	$3.28 \times 10^3$ , $2.38 \times 10^3$	$1.72 \times 10^{-5}$ – $4.29 \times 10^{-4}$

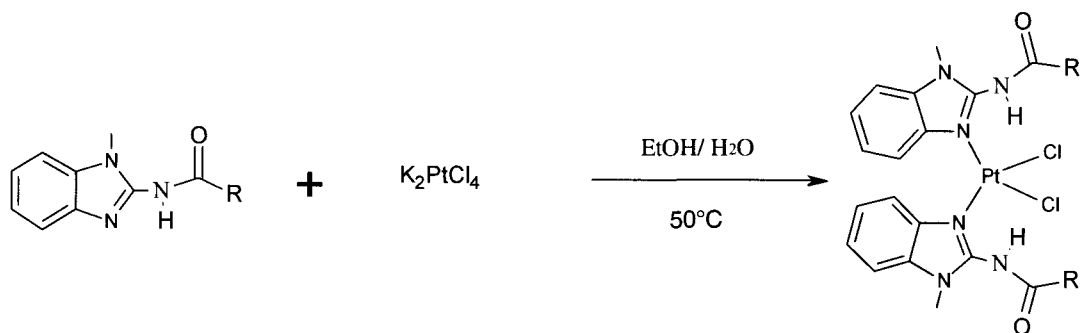
### (ii) Synthesis, characterization, and analysis of platinum- benzimidazole derivatives

Schemes 4.3 and 4.4 show two pathways of obtaining *cis* dichloro- analogues of platinum (II). Scheme 4.3 provides a pathway that converts tetrachloroplatinatate(II) to tetraiodoplatinatate(II). Addition of two equivalents of ligands affords a diiodo complex. The diiodo complex is then converted into an amido form with treatment of two equivalents of base. Treatment of the amido complex with HCl (g) yields the desired dichloro- isomer.



Scheme 4.3: Reaction protocol of benzimidazole-platinum complexes; R = alkyl or aryl

This pathway increases the overall yield of the reaction by taking advantage of ligand substitution chemistry involving platinum (II) compounds. Additionally, this synthetic route utilizes the greater *trans* effect of iodine compared to chlorine, hence the conversion of tetrachloroplatinate to tetraiodoplatinate. Furthermore, the retention of stereochemistry of the intermediate to generate the desired *cis*-isomer. However, controlling the stoichiometry of the gas in solution is difficult and excess HCl leads to the decomposition of the product. A more direct synthetic approach, Scheme 4.4, utilizes two equivalents of ligand and potassium tetrachloroplatinate dissolved in an organic solvent and water mixture (1:1v) at a temperature of 50-70°C.



Scheme 4.4: Generation of *cis*-isomers (R= alkyl, aryl)

This approach gives the desired *cis*- isomer in lower yields comparatively but is safer. However, in some cases, minute traces of the *trans*- isomer precipitates with the *cis* product when this synthetic route is used. This can be remedied by washing the precipitate with cold methanol or acetone followed by a water wash.

The organic solvents usually employed in this synthetic approach include ethanol, methanol, acetonitrile, and tetrahydrofuran. It is worth noting that the yield is

significantly affected when this reaction is carried out in tetrahydrofuran and water.

Therefore, the THF/water combination should be limited to ligand solubility considerations.

### **Characterization of Complexes**

The  $^1\text{H}$  NMR of these Pt(II) complexes are similar to that of their respective free ligands with the only exception being when they are bis-chelated to the metal (amido form). In this form, the aromatic protons of the benzimidazole are no longer aggregated. They appear as a doublet, triplet, triplet and doublet (Figure 4.28). Consequently, the respective  $^1\text{H}$  NMR spectra have been moved to the appendix. The chemical shifts of the peaks are listed in this section.

The mass spectrometric trace of compound **30** displayed in Figure 4.21 shows an ion peak at 150.74 m/z with an intensity of 100 %. This peak is due to a protonated 2-amino-1-methylbenzimidazole ion fragment,  $[\text{Hamb}]^+$ . Daughter ion peaks at 302.57 m/z and 340.46 m/z have relative intensities of 20 % and 10 %. These peaks correspond to the fragments  $[(\text{Hmbda})\text{H}]^+$  and  $[\text{HmbdaK}]^+$  respectively.

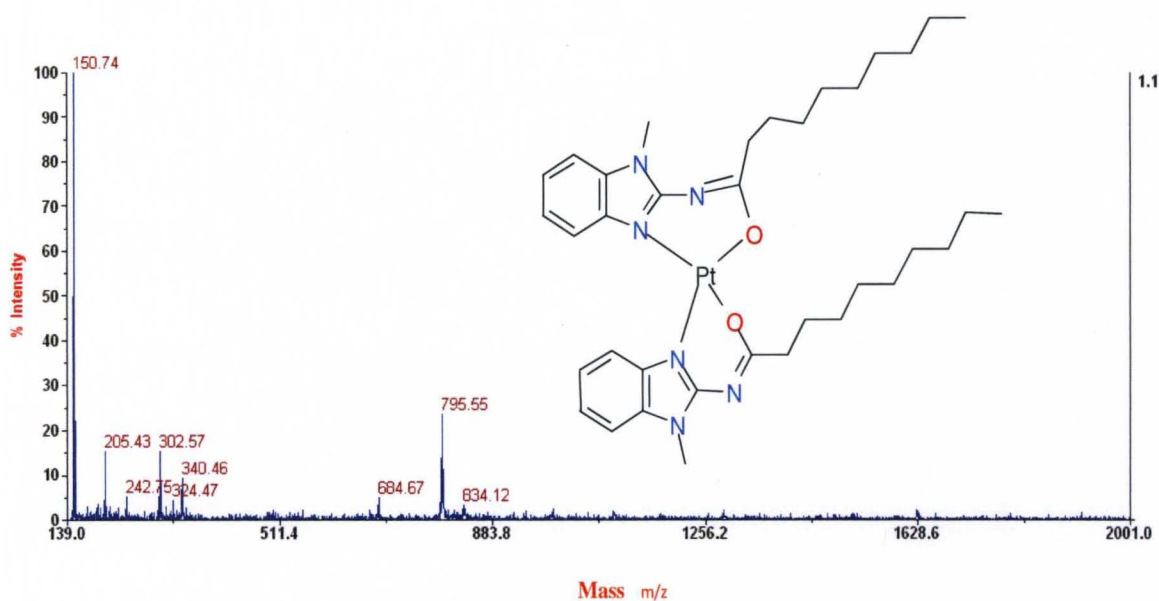


Figure 4.21: Mass spectrometric trace of compound **30**

The peak at 795.55 m/z corresponds to the molecular ion fragment  $[(\text{mbda})_2\text{Pt}]^+$  and agrees with the calculated theoretical mass of 797.40 g/mol. The  $^1\text{H}$  NMR spectrum of compound **30** shows benzimidazole proton peaks that appear as a doublet, triplet, triplet, and doublet in the aromatic region with chemical shifts of 7.15 ppm, 7.03 ppm, 6.67 ppm and 6.37 ppm. The methyl protons on the nitrogen of the benzimidazole, designated N1, appear as a singlet at 3.77 ppm. Peaks at 2.53 ppm, 1.82 ppm, 1.61 ppm, 1.44 ppm, and 0.88 ppm appear as a triplet, doublet of a doublet, singlet, multiplet, and triplet respectively. These peaks integrate in the ratio 4H:4H:8H:4H:6H. A broad peak at 1.29 ppm represents twelve protons of the pendant.

The mass spectrometric trace of compound **31** (Figure 4.22) shows a molecular ion peak,  $[(\text{Hmbchca})_2\text{PtI}_2\text{H}_2]^+$ , at 965 m/z with an intensity of 13 %. This peak is consistent with the calculated theoretical mass, 963.08 g/mol, for the compound.

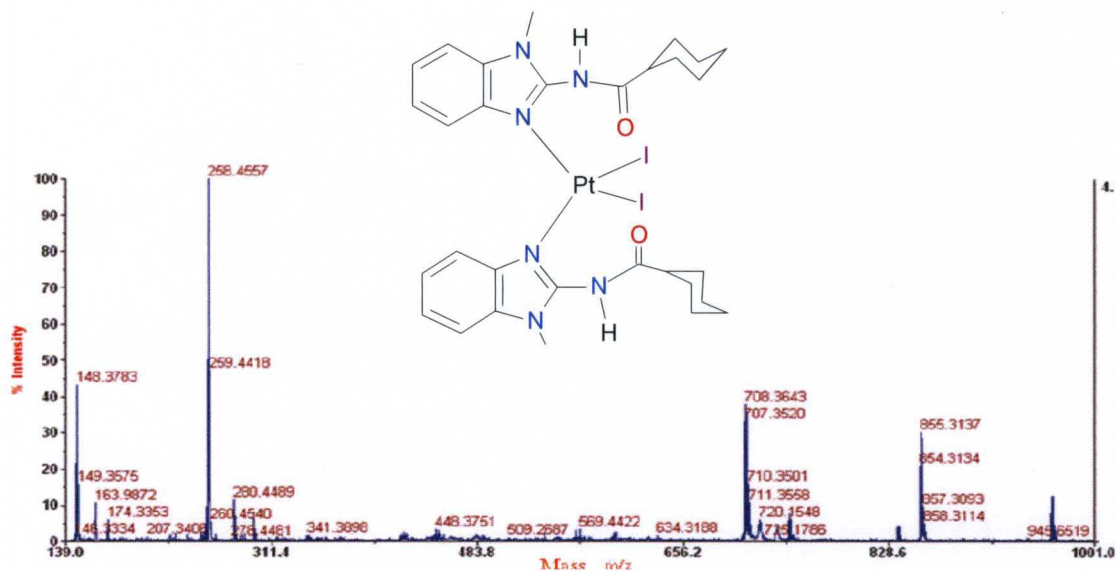


Figure 4.22: Mass spectrometric trace of compound **31**

Daughter ion peaks appear at 258.46 m/z, 708.36m/z and 855.31 m/z with intensities of 100%, 35% and 30%. These peaks correspond to the ion fragments  $[\text{Hmbchca}]^+$ ,  $[(\text{Hmbchca})_2\text{Pt}]^+$ , and  $[(\text{Hmbchca})_2\text{PtINa}]^+$  respectively. The  $^1\text{H}$  NMR spectrum displays a singlet at 9.73 ppm corresponding to the two amide peaks. The multiplet and singlet at 7.55 pm and 7.15 ppm represents the eight aromatic protons (6H:2H). The six methyl protons of the benzimidazole appear as a singlet at 3.67 ppm. Peaks corresponding to the twenty-two cyclohexyl protons appear at 2.80 ppm, 2.45 ppm, 2.29 ppm, 1.96 ppm, 1.50 ppm and 1.40 ppm. The  $^{13}\text{C}$  NMR spectrum displays peaks at 174.84 ppm, 144.82 ppm, 136.83 ppm, 132.76 ppm, 124.06 ppm, 123.74 ppm, 122.79 ppm, 117.00 ppm, 111.38 ppm, 110.02 ppm, 108.87 ppm, 48.41 ppm, 45.70 ppm, 32.27 ppm, 29.22 ppm, 28.28 ppm, and 25.973 ppm. The peak at 174.84 ppm corresponds to the carbonyl carbon.

Figure 4.23 displays the mass spectrometric trace of compound **32**. The molecular ion peak,  $[(\text{mbchca})_2\text{PtH}]^+$ , appears at 708.13 m/z with an intensity of 100 %. This peak is in agreement with the calculated theoretical mass 707.25 g/mol for compound **32**. The

peak at 258.35 m/z with an intensity of 46% is due to the ligand ion fragment [(Hmbchca)H]<sup>+</sup>.

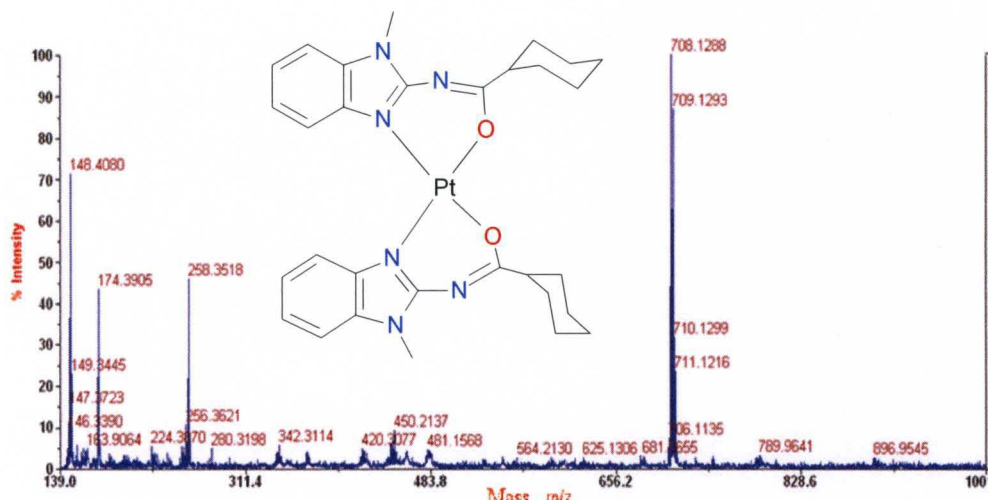


Figure 4.23: Mass spectrometric trace of compound **32**

The ion peaks at 148.40 m/z corresponds to the fragment [(amb)H]<sup>+</sup>. The <sup>1</sup>H NMR spectrum of compound **32** shows a proton splitting pattern in the aromatic region similar to compound **30**. The peaks appear as a doublet, triplet, triplet and doublet with chemical shifts of 7.14 ppm, 7.02 ppm, 6.66 ppm, and 6.38 ppm that correspond to the benzimidazole protons. The methyl protons on the nitrogen of the benzimidazole, designated N1, appear as a singlet at 3.65 ppm. Protons of the cyclohexyl pendant appear at 2.54 ppm, 2.11 ppm, 1.83 ppm, 1.70 ppm, 1.63 ppm, 1.57 ppm and 1.36 ppm as five triplets, a singlet and multiplet respectively. Its IR spectrum is similar to that of compound **36** with stretching frequencies at 3059 cm<sup>-1</sup>, 2925 cm<sup>-1</sup>, and 2852 cm<sup>-1</sup> corresponding to C<sub>sp2</sub>-H and C<sub>sp2</sub>-H stretches. A C = C stretch appears at 1615 cm<sup>-1</sup>.

The mass spectrometric trace of compound **33** (Figure 4.24) shows an ion peak at 258.48 m/z with an intensity of 100% and represents the ligand, [(Hmbchca)H]<sup>+</sup>.

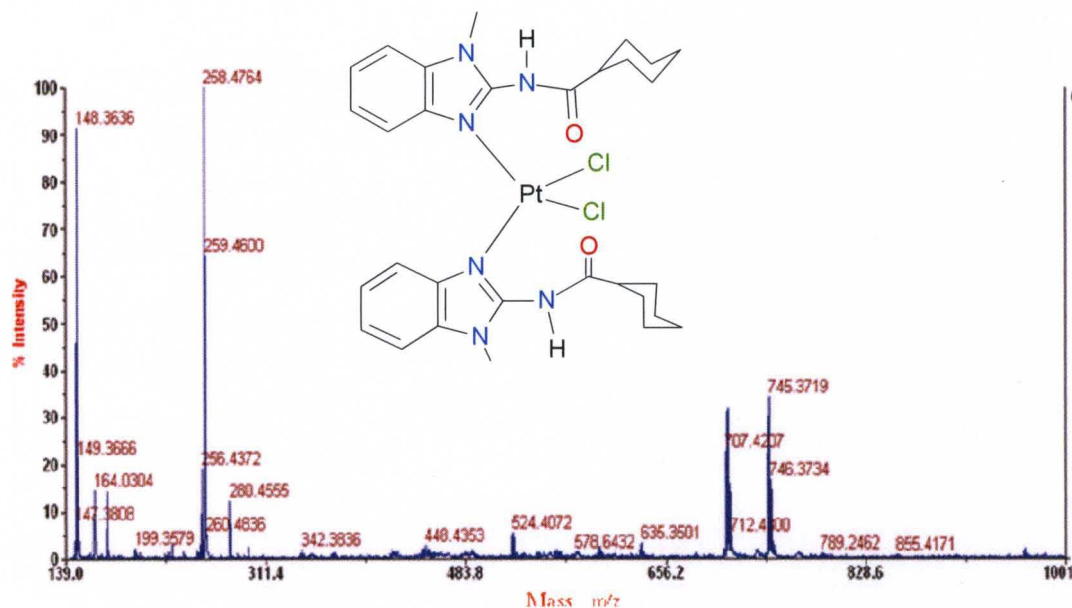


Figure 4.24: Mass spectrometric trace of compound **33**

The peaks at 280.46 m/z and 709.42 m/z with relative intensities of 12% and 30% represent the molecular fragments of  $[(\text{Hmbchca})\text{Na}]^+$ , a sodium ion peak, and  $[(\text{Pt}(\text{mbchca})_2)\text{H}]^+$  respectively. The molecular ion peak appears at 745.37 m/z with a peak intensity of 35% and represents the fragment  $[(\text{Hmbchca})_2\text{PtCl}]^+$ . This peak differs from the calculated theoretical molecular mass, 779.21 g/mol, by a chloride ion. The  $^1\text{H}$  NMR spectrum of compound **33** displays an amide peak at 10.14 ppm and a multiplet at 7.14 ppm corresponding to the benzimidazole protons. The six methyl protons appear as a singlet at 3.71 ppm. The twenty-two cyclohexyl proton peaks appear at 2.77 ppm, 2.41 ppm, 2.25 ppm, 1.96 ppm, 1.80 ppm, 1.50 and 1.37 ppm. The cyclohexyl protons splitting pattern is similar to the diiodo isomer compound **31** and the free ligand.



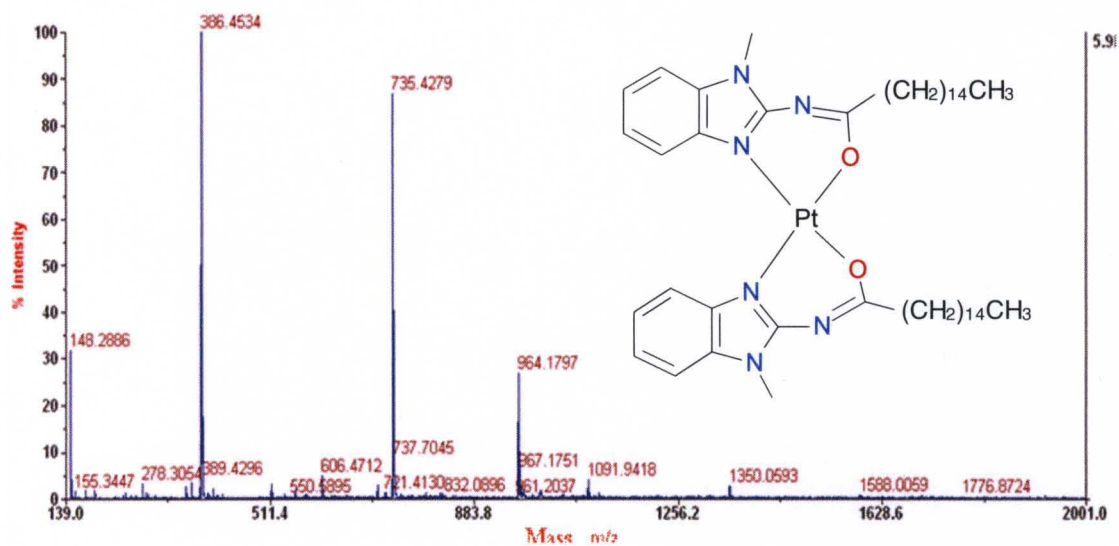


Figure 4.25: Mass spectrometric trace of compound **34**

The mass spectrometric trace of compound **34** (Figure 4.25) shows an ion peak at 386.45 m/z with an intensity of 100%. This peak is due to the ion fragment of the protonated ligand ion  $[(\text{Hmbhda})\text{H}]^+$ . The peak at 735.43 m/z with peak intensity of 88% corresponds the fragment  $[\text{Pt}(\text{mbhda})(\text{matrix-DBA})]^+$ . The molecular ion peak,  $[\text{Pt}(\text{mbhda})_2]^+$ , appears at 964.18 m/z and has a relative peak intensity of 30%. The theoretical and experimental masses of compound **34** are in agreement.

Compounds **35** – **37** have been characterized by  $^1\text{H}$  NMR in our laboratory [32]. The respective IR and mass spectrometric traces of compounds **36** and **37** are displayed in Figures 4.26- 4.30 for comparison to compounds in Chapter III. Figure 4.28 shows the aromatic region of the  $^1\text{H}$  NMR spectrum of compound **36**. This is a characteristic splitting pattern of the amido form and is also used as a diagnostic tool for *syn* isomeric intermediates for the 2-amino-1-methylbenzimidazole derivatives.

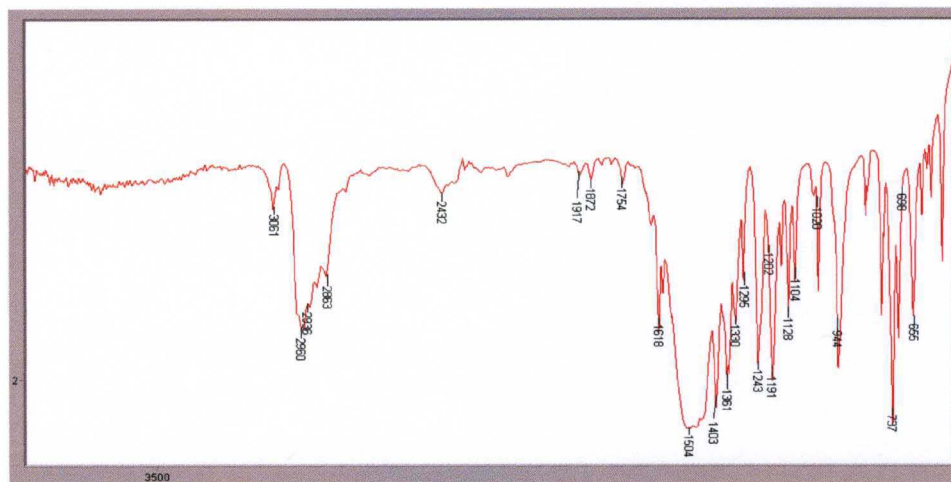


Figure 4.26: Infrared trace of compound **36**

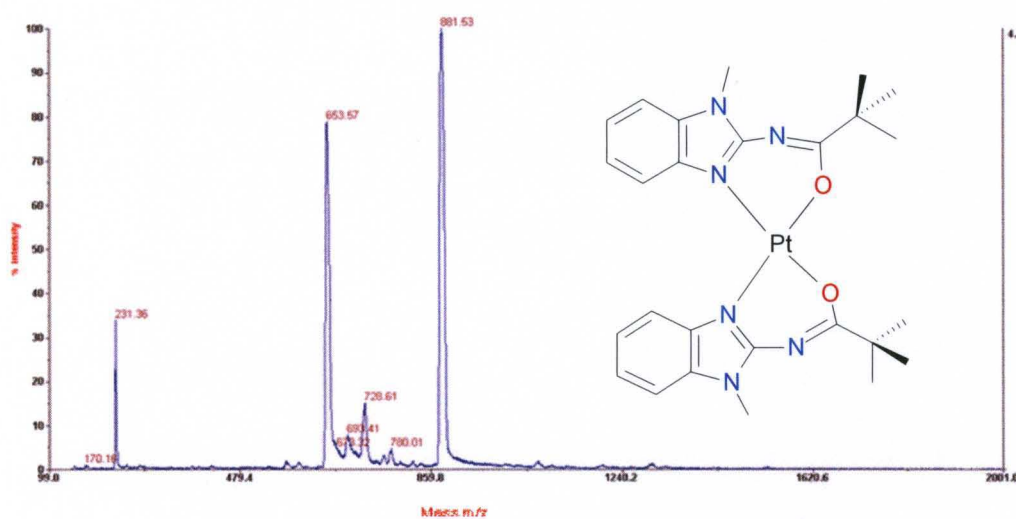


Figure 4.27: Mass spectrometric trace of compound **36**

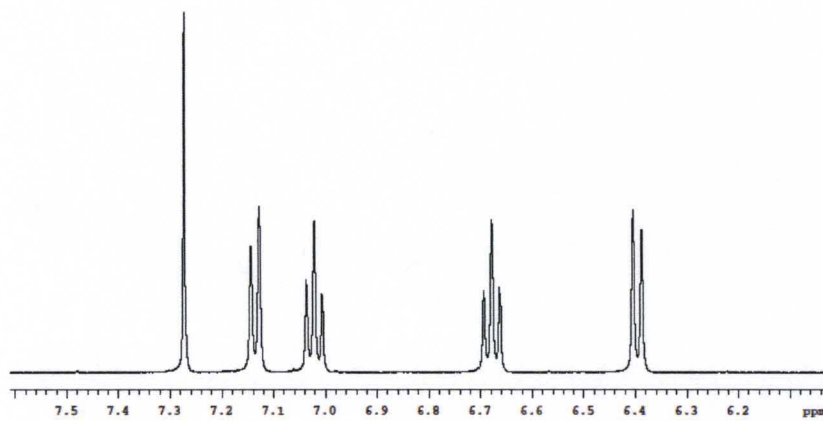


Figure 4.28: Aromatic region of the  $^1\text{H}$  NMR spectrum of compound **36**. The singlet is a solvent peak

$\text{CDCl}_3$

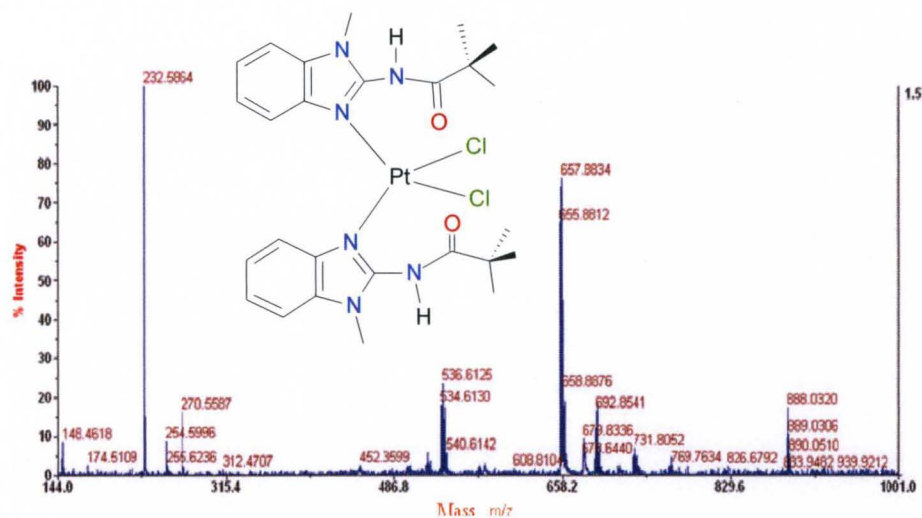


Figure 4.29: Mass spectrometric trace of compound **37**

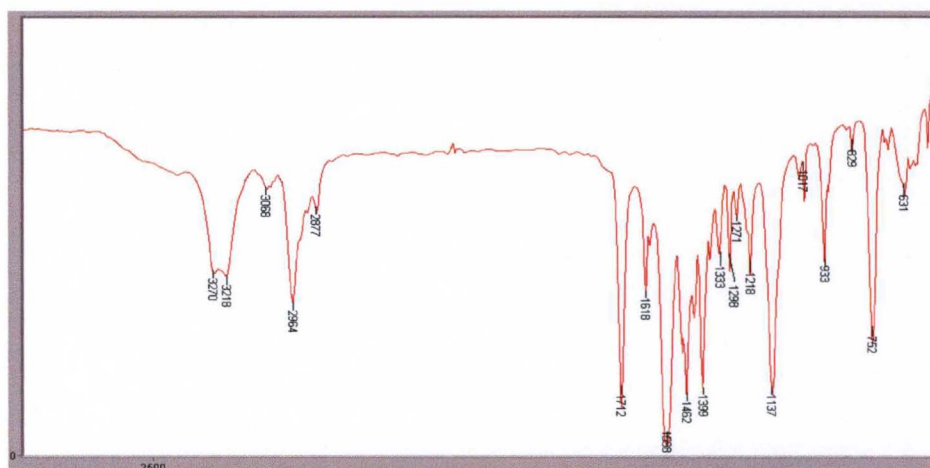


Figure 4.30: Infrared trace of compound **37**

The mass spectrometric trace of compound **38** (Figure 4.31) shows daughter ion peaks at 218.86  $m/z$ , 240.82  $m/z$ , 460.64  $m/z$ , 544.41  $m/z$ , 629.26  $m/z$ , 671.99  $m/z$ , 677.13  $m/z$ , 755.90  $m/z$ , and 888.49  $m/z$  with peak intensities of 100 %, 15.56 %, 10.04 %, 47.36 %, 47.36 %, 61.78 %, 67.02 %, 79.35 % and 26.92 %.

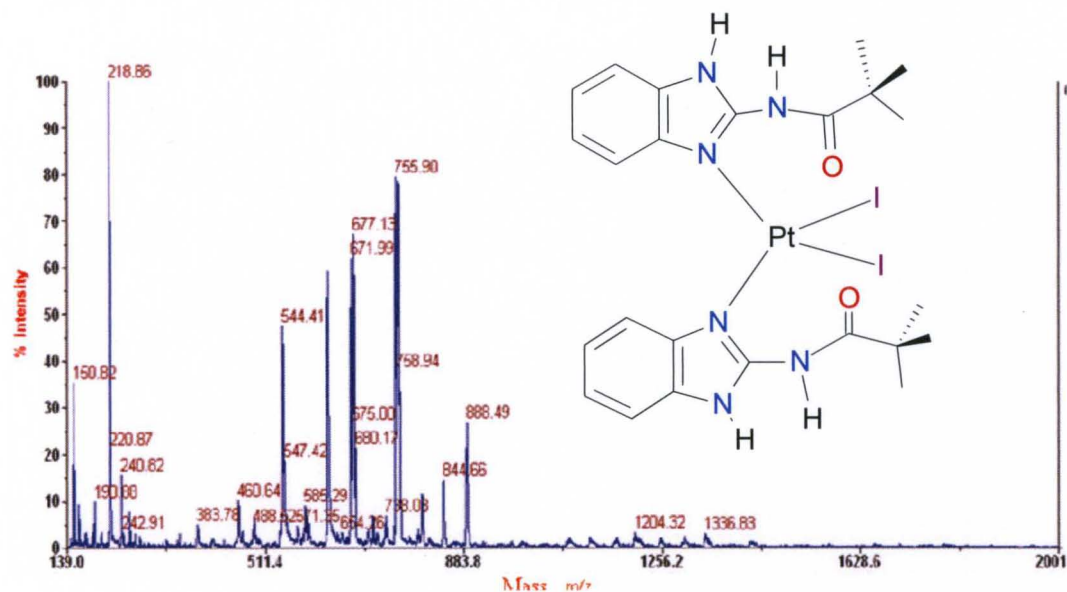


Figure 4.31: Mass spectrometric trace of compound **38**

These correspond to the ion fragments  $[\text{Hdmbp}]^+$ ,  $[\text{HdmbpNa}]^+$ ,  $[(\text{Hdmbp})_2\text{Na}]^+$ ,  $[\text{Pt}(\text{Hdmbp})(\text{benzimidazole})]^+$ ,  $[\text{Pt}(\text{Hdmbp})_2]^+$ ,  $[\text{Pt}(\text{Hdmbp})_2\text{K}]^+$ ,  $[\text{Pt}(\text{Hdmbp})_2\text{Na}_2]^+$ ,  $[\text{Pt}(\text{Hdmbp})_2\text{I}]^+$ ,  $[\text{Pt}(\text{Hdmbp})_2\text{I}_2]^+$ . The theoretical mass 883.02 g/mol is less than the experimental by five and might be due to isotopic effects.

The mass spectrometric trace of compound **39** (Figure 4.32) shows an ion peak at 219.04 m/z with an intensity of 100%. This peak is due to the ligand ion fragment  $[(\text{Hdmbp})\text{H}_2]^+$ . Daughter ion peaks at 241.06 m/z and 627.55 m/z have relative intensities of 18 % and 20 %.

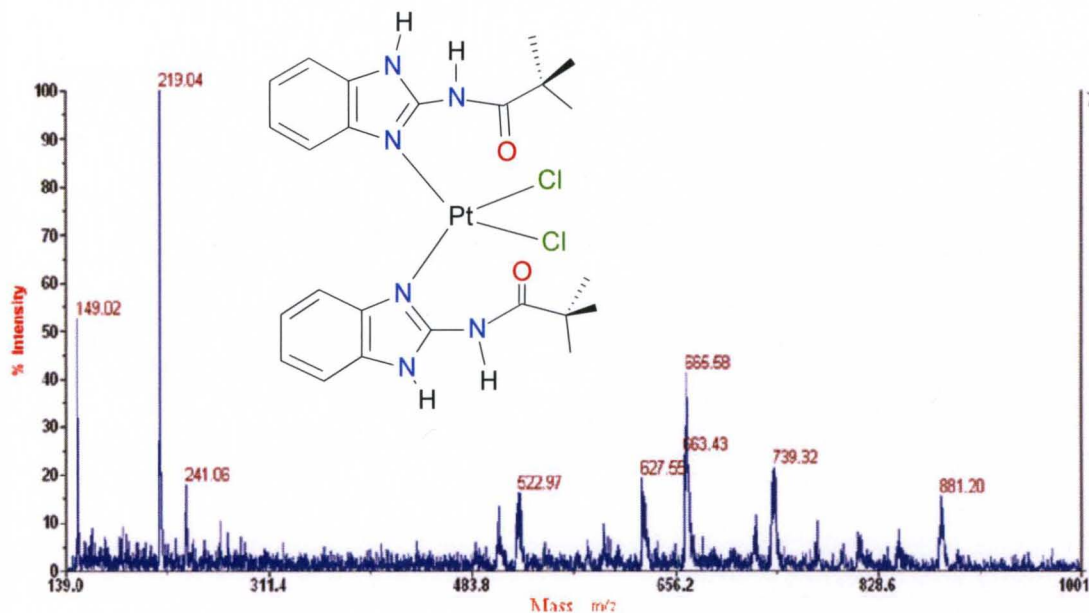


Figure 4.32: Mass spectrometric trace of compound **39**

These peaks correspond to the fragments  $[\text{HdmbpNa}]^+$  and  $[\text{Pt}(\text{Hdmbp})_2]^+$  respectively. The molecular peak,  $[\text{Pt}(\text{Hdmbp})_2\text{Cl}]^+$ , at 665.58 m/z has a peak intensity of 40% and differs from the theoretical mass, 699.15 g/mol, by the mass of a chloride ion. The peak at 739.32 m/z corresponds to the fragment  $[(\text{Pt}(\text{Hdmbp})_2\text{Cl}_2)\text{K}]^+$ . The  $^1\text{H}$  NMR shows a clean sample with an amide peak at 11.33 ppm. The peak at 10.436 ppm represents the proton of the N1 nitrogen of the benzimidazole. Aromatic protons appear as singlets with chemical shifts of 8.20 ppm and 7.39 ppm. The tert-butyl group appears as a singlet at 1.56 ppm. Both physical methods confirm the synthesis of the desired product.

The mass spectrometric trace of compound **40** (Figure 4.33) shows an ion peak,  $[(\text{Hbchca})_3\text{Pt}]^+$  at 924.19 m/z with an intensity of 37%. Daughter ion peaks appear at 244.88 m/z, 266.96 m/z, 282.73 m/z, 681.42 m/z and 808.12 m/z, with intensities of 100%, 24%, 8%, 20% and 44%.

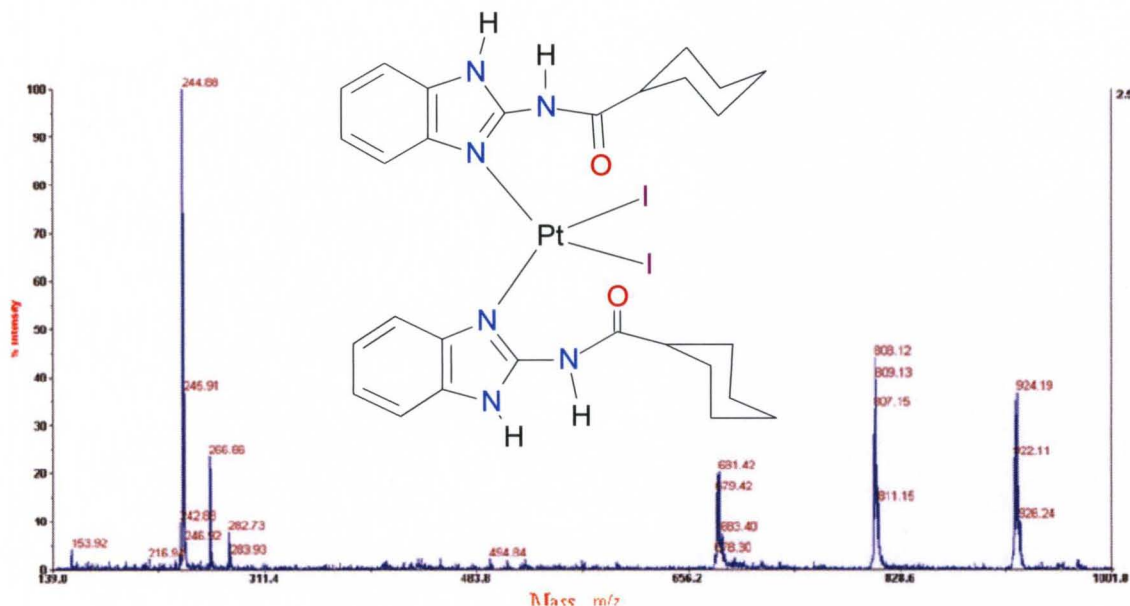


Figure 4.33: Mass spectrometric trace of compound **40**

These peaks correspond to the ion fragments  $[\text{Hbchca}]^+$ ,  $[\text{Hbchca Na}]^+$ ,  $[\text{HbchcaK}]^+$ ,  $[(\text{bchca})_2\text{Pt}]^+$ , and  $[(\text{Hbchca})_2\text{PtI}]^+$  respectively. The  $^{13}\text{C}$  NMR spectrum displays peaks at 123.15 ppm, 122.45 ppm, 118.86 ppm, 132.76 ppm, 124.06 ppm, 123.74 ppm, 122.79 ppm, 117.00 ppm, 111.38 ppm, 111.94 ppm, 44.77 ppm, 35.23 ppm, 26.53 ppm, 26.53 ppm, 25.44 ppm, and 25.19 ppm. The IR spectrum shows stretching frequencies at  $3312\text{ cm}^{-1}$ ,  $3058\text{ cm}^{-1}$ ,  $2929\text{ cm}^{-1}$ ,  $2853\text{ cm}^{-1}$  and  $1708\text{ cm}^{-1}$  corresponding to the N-H,  $\text{C}_{\text{sp}2}\text{-H}$ ,  $\text{C}_{\text{sp}3}\text{-H}$  and carbonyl stretches respectively.

The mass spectrometric trace of compound **41** (Figure 4.34) shows a ion peak at  $637.23\text{ m/z}$  with an intensity of 17.91%. This peak is due to the ion fragment  $[\text{Pt}(\text{Hmbp})_2\text{Cl}]^+$ . Daughter ion peaks at  $600.33\text{ m/z}$  and  $204.82\text{ m/z}$  have relative intensities of 30 % and 100 %.

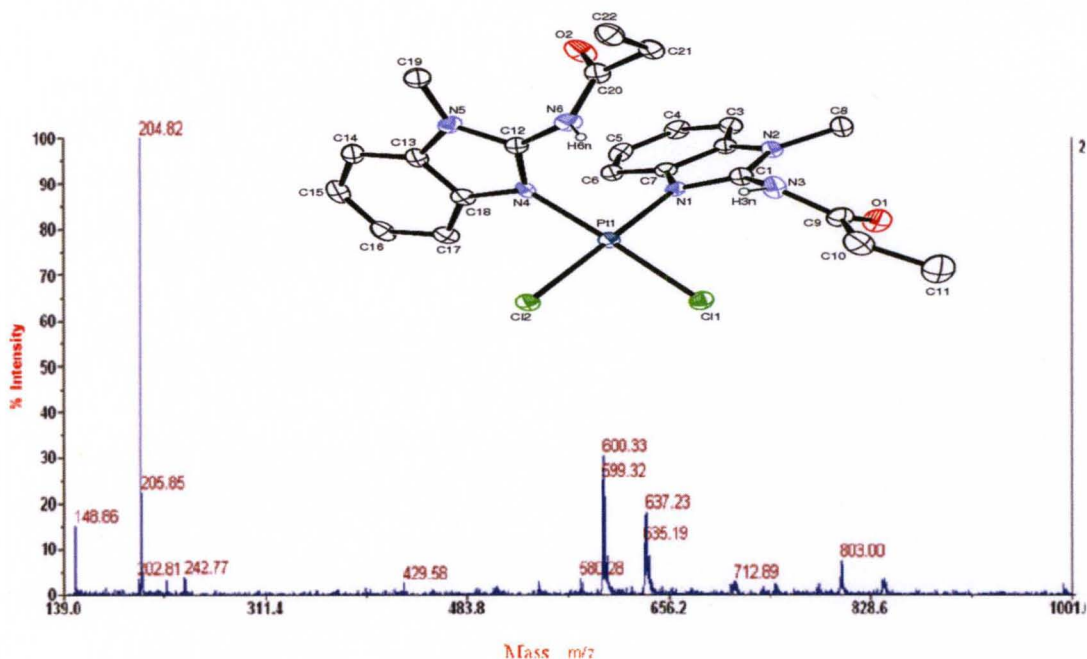


Figure 4.34: Mass spectrometric trace of compound **41**

These peaks correspond to the fragments  $[\text{Hmbp}]^+$  and  $[\text{Pt}(\text{Hmbp})_2]^+$  respectively. The  $^1\text{H}$  NMR spectrum shows an amide peak at 10.20 ppm, integrating to two protons. The peak at 3.74 ppm represents the six protons of the methyl groups attached to the N1 nitrogen of the benzimidazole. The eight aromatic protons appear as a multiplet centered at 7.17 ppm. Peaks at 1.21 ppm and 0.815 ppm correspond to the five protons of the propyl chain. The IR reveals stretches at  $3251\text{ cm}^{-1}$ ,  $3145\text{ cm}^{-1}$ ,  $2978\text{ cm}^{-1}$ ,  $2941\text{ cm}^{-1}$  and  $1699\text{ cm}^{-1}$  indicative of N-H,  $\text{C}_{\text{sp}2}\text{-H}$ ,  $\text{C}_{\text{sp}3}\text{-H}$  and carbonyl stretches respectively.

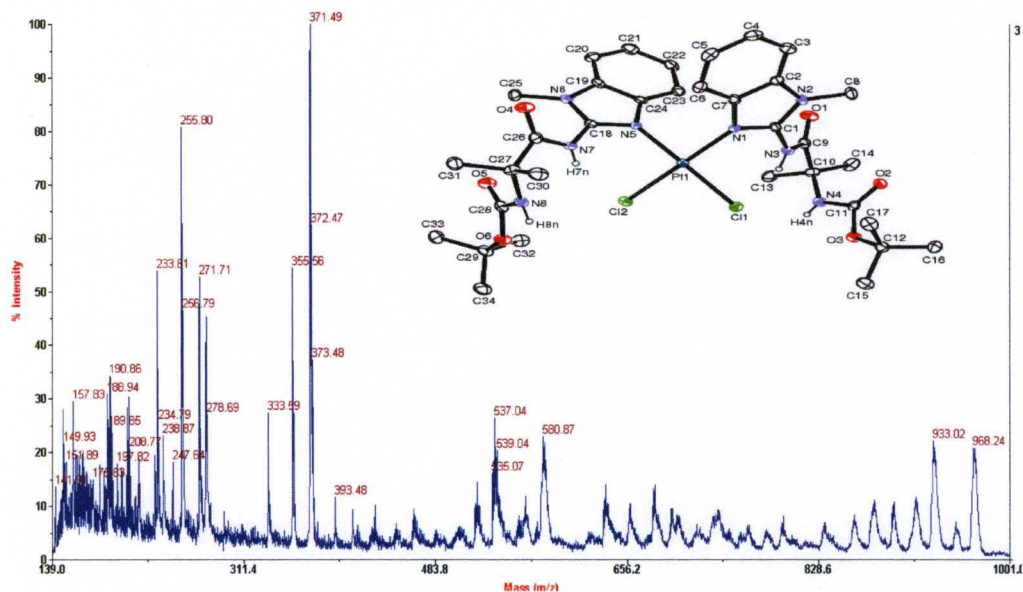


Figure 4.35: Mass spectrometric trace of compound **46**

The mass spectrometric trace of compound **46** (Figure 4.35), a second generation compound, shows a molecular ion peak,  $[\text{Pt}(\text{HL}^{\text{Boc}})_2\text{Cl}_2]^+$ , at 933.02 m/z with an intensity of 23%. Daughter ion peaks at 233.81 m/z, 255 m/z, 271.71 m/z, 333.59 m/z, 355.59 m/z, 371.49 m/z, 580.87 m/z, and 968.24 m/z have relative intensities of 53%, 81%, 52%, 28%, 53%, 100%, 28% and 22%. These peaks correspond to the fragments  $[(\text{HL}^{\text{Boc}} - \text{Boc})]^+$ ,  $[(\text{HL}^{\text{Boc}} - \text{Boc})\text{Na}]^+$ ,  $[(\text{HL}^{\text{Boc}} - \text{Boc})\text{K}]^+$ ,  $[(\text{HL}^{\text{Boc}})]^+$ ,  $[(\text{HL}^{\text{Boc}})\text{Na}]^+$ ,  $[(\text{HL}^{\text{Boc}})\text{K}]^+$ ,  $[\text{Pt}(\text{HL}^{\text{Boc}} - \text{Boc})(\text{amb})]^+$ ,  $[\text{Pt}(\text{HL}^{\text{Boc}})_2\text{Cl}_2\text{K}]^+$  respectively. The  $^1\text{H}$  NMR shows an amide peak at 10.59 ppm. A peak at 3.90 ppm represents the six protons of the N1 nitrogen of the benzimidazole. The aromatic protons appear as a multiplet with chemical shifts 7.17 ppm. Singlets at 2.00 ppm and 1.76 ppm correspond to the twelve protons of the four methyl groups of the pendant. The tert-butyl group of the Boc protecting group appears as a singlet at 1.45 ppm.



Overall, both the  $^1\text{H}$  NMR and mass spectrometric spectra confirm the synthesis of the respective desired products. The  $^1\text{H}$  NMR spectra of these complexes show clean products. Furthermore, complex spectra are similar to their respective free ligand differing only in the aromatic region. That is, the aromatic protons of the monodentates of the 2-amino-1-methylbenzimidazole derivatives show less aggregation than their respective free ligands whilst aromatic protons of the bis-chelates appears as doublets and triplets. Additionally, IR data confirm the presence or absence of amide protons in the respective complexes.

### F: X-ray Crystallographic Analysis of Complexes

X-ray structure analysis on six Pt(II), Pt(IV) complexes and a ligand are presented in this section. Tables 4.6 and 4.7 show selected crystallographic data including bond angles and bond lengths for these compounds.

Table 4.6: Crystallographic data for compounds **4**, **30**, **41**, **42a**, **41b**, **41c** and **46**

	<b>4</b>	<b>30</b>	<b>41</b>	<b>42a</b>	<b>42b</b>	<b>42c</b>	<b>46</b>
Crystal System	Monoclinic	Orthorhombic	Triclinic	Monoclinic	Monoclinic	Monoclinic	Monoclinic
Space Group	P2 <sub>1</sub> /n	P2 <sub>1</sub> 2 <sub>1</sub> 2 <sub>1</sub>	Pi	I2/a	I2/a	P2 <sub>1</sub> /c	P2 <sub>1</sub> /n
a	14.1720(3) Å	4.7998(5) Å	10.2102(5) Å	16.7763(13) Å	16.7763(13) Å	10.4180(9) Å	17.7393(5) Å
b	6.04320(8) Å	18.2520(17) Å	10.6491(6) Å	18.6042(13) Å	18.6042(13) Å	17.0912(14) Å	11.4632(3) Å
c	15.7484(3) Å	41.322(4) Å	12.0364(6) Å	18.2199(13) Å	18.2199(13) Å	8.0463(7) Å	19.3959(5) Å
$\alpha$	90°	90°	70.699(5)°	90°	90°	90°	90°
$\beta$	107.3724(19)°	90°	76.753(4)°	102.526(2)°	102.526(2)°	97.0640(10)°	99.794(3)°
$\gamma$	90°	90°	79.119(4)°	90°	90°	90°	90°
Volume	1287.24(4) Å <sup>3</sup>	3620.1(6) Å <sup>3</sup>	1193.16(11) Å <sup>3</sup>	5551.3(7) Å <sup>3</sup>	5551.3(7) Å <sup>3</sup>	1421.8(2) Å <sup>3</sup>	3886.66(17) Å <sup>3</sup>
Z	4	4	2	4	4	2	4
Density	1.328 Mg/m <sup>3</sup>	1.460 Mg/m <sup>3</sup>	1.872 Mg/m <sup>3</sup>	1.837 Mg/m <sup>3</sup>	1.837 Mg/m <sup>3</sup>	1.795 Mg/m <sup>3</sup>	1.591 Mg/m <sup>3</sup>
GOF	1.017	1.313	1.072	1.074	1.074	1.043	1.068
R1	0.0355	0.0691	0.0522	0.0279	0.0279	0.0147	0.0338
wR2	0.0812	0.1638	0.0984	0.0688	0.0688	0.0338	0.0716

Table 4.7: Bond lengths and angles of compounds **4**, **30**, **41**, **42a**, **42b**, **42c** and **46**

Bond Lengths (Å)							
	<b>4</b>	<b>30</b>	<b>41</b>	<b>42a</b>	<b>42b</b>	<b>42c</b>	<b>46</b>
Pt–N1		1.996(10)	2.029(5)	2.005(3)	2.016(3)	2.0144(16)	2.026(3)
Pt–N4		1.981(10)	2.023(5)	2.005(3)	2.016(3)	2.0143(16)	2.028(3)
Pt–O1		2.002(9)		2.006(2)			
Pt–O2		2.005(9)		2.006(2)			
Pt–Cl 1			2.2977(17)	2.3210(14)	2.3092(8)	2.3035(5)	2.2991(9)
Pt–Cl 2			2.2975(15)	2.3196(13)	2.3091(8)	2.3035(5)	2.3022(9)
C–O1	1.2186(12)	1.268(16)	1.219(8)	1.315(4)	1.210(4)	1.209(2)	1.207(4)
C–O2		1.289(14)					1.213(4)
C–O3							1.348(4)
Bond Angles (°)							
N1–Pt–N4		101.7(4)	91.37(19)	178.22(16)	89.84(16)	179.999(1)	90.28(11)
N1–Pt–O1		86.6(4)		88.40(11)			
N1–Pt–O2		165.8(4)		91.68(11)			
N1–Pt–Cl 1			90.66(15)	90.89(8)	176.50(8)	90.20(4)	90.69(8)
N1–Pt–Cl 2			176.79(15)	89.11(8)	90.15(8)	89.80(4)	177.39(9)
N4–Pt–O1		169.9(4)		91.69(11)			
N4–Pt–O2		90.1(4)		88.40(11)			
O1–Pt–O2		82.6(3)		174.82(15)			
O2–Pt–Cl 1				87.41(7)			
O2–Pt–Cl 2				92.59(7)			
N4–Pt–Cl 1			177.84(13)	90.89(8)	90.14(8)	89.80(4)	178.44(9)
N4–Pt–Cl 2			88.32(14)	89.11(8)	176.49(8)	90.20(4)	89.40(8)
Cl(1)–Pt–Cl 2			89.62(6)	180.0	90.09(4)	180.0	89.58(3)
C(11)–O(3)–C(12)							120.1(3)
C(28)–O(6)–C(29)							121.8(3)
O1–Cl–N1	121.91(9)						
O1–Cl–Cl10	123.19(9)						
N1–Cl–Cl10	114.81(8)						

Compound **4** has been included in this section because crystals were obtained from a acetonitrile/ water solution of  $K_2PtCl_2$  and methylene chloride. Compound **4** forms monoclinic crystals in the space group  $P2_1/n$ . The C–O bond length measures 1.2186(12) Å (Table 4.6) and is consistent with a carbonyl carbon–oxygen bond length.

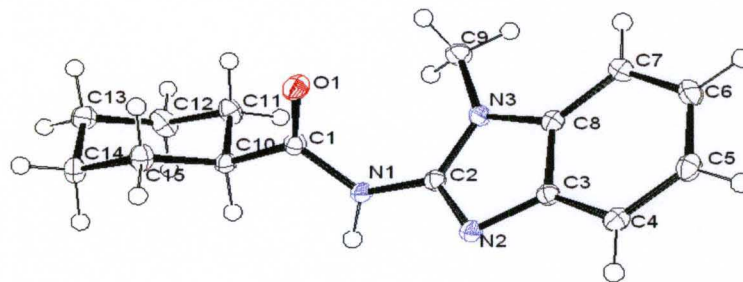


Figure 4.36: ORTEP diagram of compound **4**. Ellipsoids are shown at 50% probability.

The cyclohexyl group is in a chair configuration (Figure 4.36) with the hydrogens in the axial and equatorial positions. These hydrogens are engaged in either C-H ... $\pi$  interactions with the  $\pi$ - system of the benzimidazole or hydrogen bonding with the oxygen of the carbonyl (Figure 4.37).

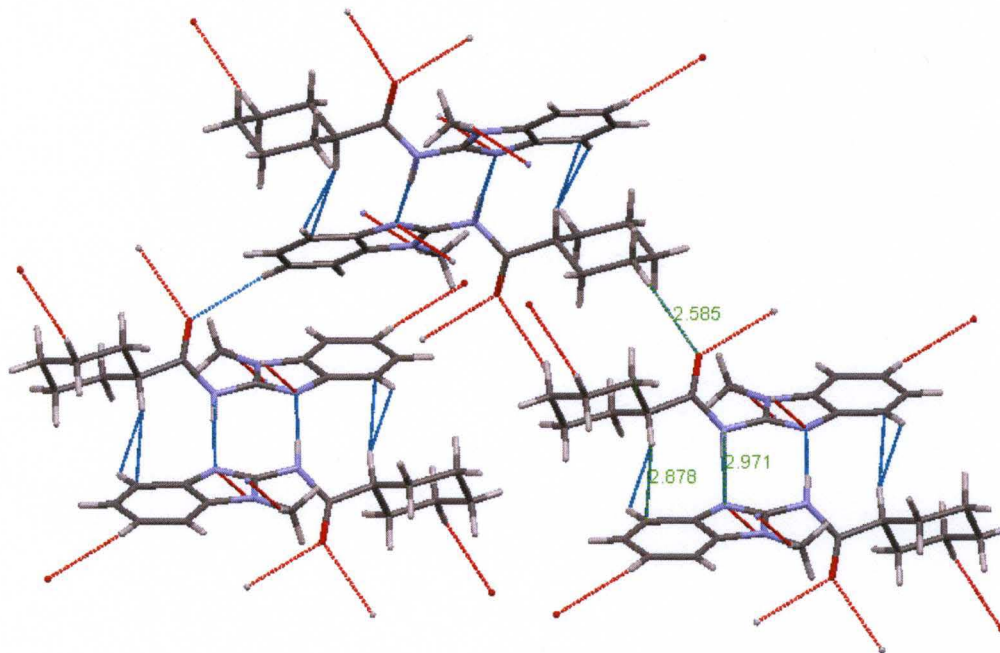


Figure 4.37: Some interactions and contacts in the crystal lattice of compound **4** along the a-axis .

C-H ... $\pi$  interactions are further facilitated by the twist of the cyclohexyl group with respect to the plane of the benzimidazole resulting in  $\llcorner$  C1-N1-C2 angle of  $120.95^\circ$  and a torsion angle of  $60.12^\circ$ . The amide proton is oriented such that, it interacts with the lone pair electron of the benzimidazole nitrogen (N3) of an adjacent molecule with an average distance of  $2.97 \text{ \AA}$ .

Compound **30** forms orthorhombic crystals in the space group  $P2_12_12_1$ . The coordination sphere around the Pt (II) ion, a  $d^8$  ion, can be described as distorted square planar (Figure 4.38). The ligand, N-(N'-1-methylbenzimidazol-2-yl)decanamide, is in its anionic form and chelates to the Pt (II) ion through the nitrogen of the benzimidazole and the oxygen of the carbonyl.

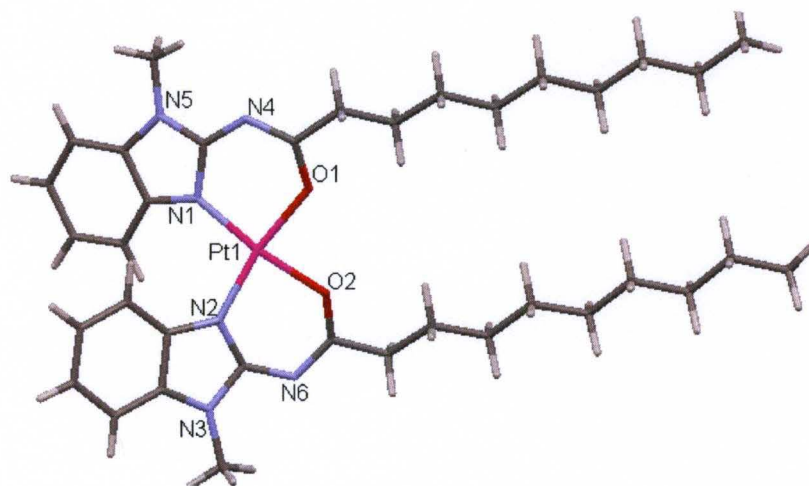


Figure 4.38: ORTEP diagram of compound **30**. Capped sticks are shown at 40% probability.

The chelated ligand assumes a *cis* configuration around the central atom with an average Pt-N bond length of  $1.988(6) \text{ \AA}$ . The average Pt-O bond length is  $2.004(4) \text{ \AA}$  whilst the C-O bond distance is  $1.2786(5) \text{ \AA}$ . Compound **30** has bond angles of  $101.7(4)^\circ$ ,  $86.6(4)^\circ$ ,  $165.8(4)^\circ$  and  $82.6(3)^\circ$  corresponding to N(1) – Pt – N(1'), N(1) – Pt –

O(1), N(1) – Pt – O(1') and O(1) – Pt – O(1') respectively (Table 4.6). The crystal lattice shows four molecules per asymmetric unit (Figure 4.39).

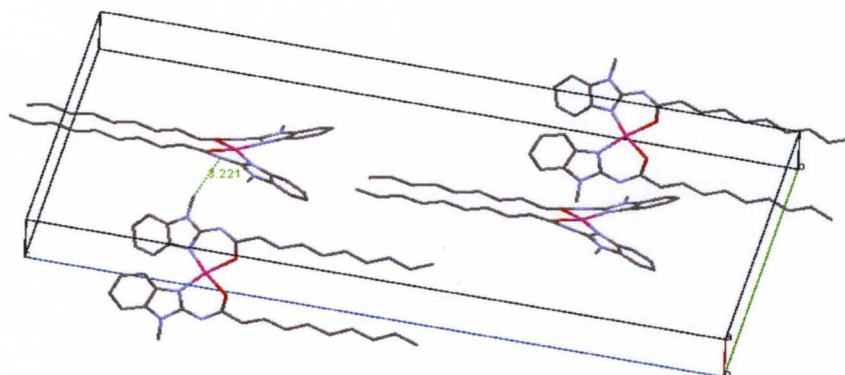


Figure 4.39: Unit cell of compound **30** with hydrogens omitted for clarity.

Unlike its  $\text{Cu}^{2+}$  analogue, compound **15**, the chelated benzimidazole ligands are *syn* and out of the plane of the central  $\text{Pt}^{2+}$  ion. The ligands form a combinational network of cooperative slipped / parallel displaced  $\pi$ - $\pi$  stacking and C-H...  $\pi$  interactions. C-H...  $\pi$  interactions are also visible between the aliphatic hydrogens ( $\text{C}_\alpha$ ) and adjacent oxygen atoms with a torsional angle,  $\ll \text{Pt1-O2-CH26A}$  of  $87.5^\circ$  and  $\ll \text{C26-H26A-O2}$  of  $113.1^\circ$  (Figure 4.40). This interaction differs from that of the  $\text{Cu}^{2+}$  analogue. That is, only one  $\text{C}_\alpha$ -hydrogen is engaged in a C-H...  $\pi$  interaction, whereas both hydrogens are engaged in the *trans*  $\text{Cu}^{2+}$  analogue (figure 4.40b).

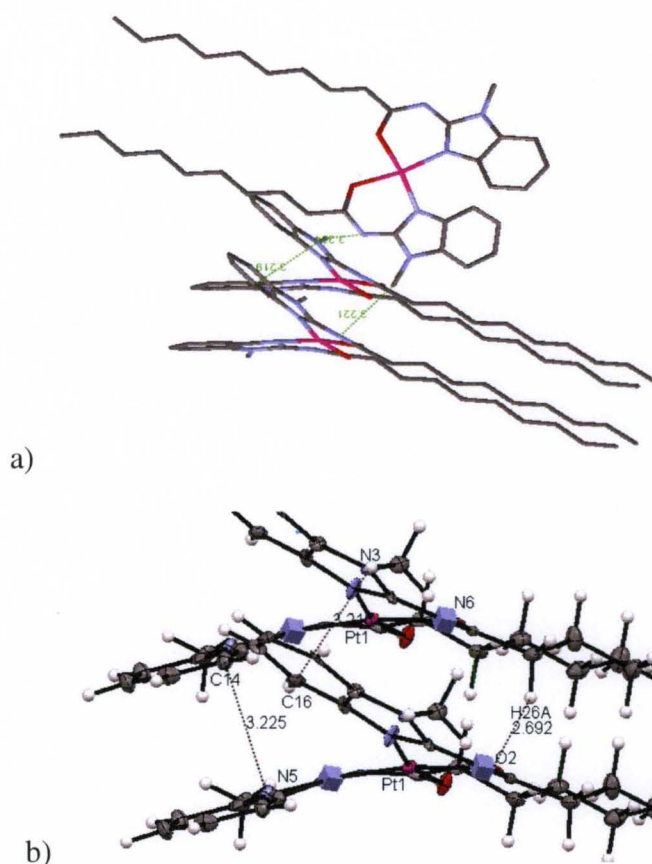


Figure 4.40: ORTEP diagram of compound **30** showing packing and hydrogen bonding interactions between stacks. Hydrogens have been omitted in (a) for clarity.

Compound **41** forms triclinic crystals in the space group  $P\bar{1}$ . The coordination sphere around the Pt (II) ion can be described as square planar (Figure 4. 41). The ligand, N-(N'-1-methylbenzimidazol-2-yl)propanamide, binds to the Pt (II) ion as a monodentate through the nitrogen (N3) of the benzimidazole and assumes a *cis* configuration around the central atom with an average Pt-N bond length of 2.026(5)Å. The average Pt-Cl and C-O bond distances are 2.2976 Å and 1.219(8) Å respectively. Compound **41** has bond angles of 91.37(19) Å, 90.66(15) Å and 176.79(15) Å corresponding to N(1) – Pt – N(1'), N(1) – Pt – Cl(1) and N(1) – Pt – Cl (1') respectively.

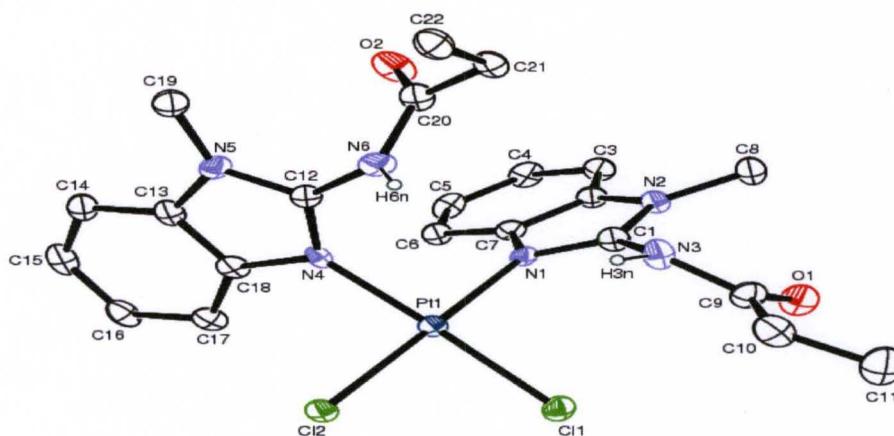


Figure 4.41: ORTEP diagram of compound **41**. Ellipsoids are shown at 50% probability. Hydrogen atoms have been omitted for clarity.

The crystal lattice of compound **41** is similar to that of dihalide compounds with short pendants of this system. The chlorides are engaged in C-H... $\pi$ (Cl) interactions with amide protons of adjacent molecules and are an average distance of 2.57 Å apart. There are also C-H... $\pi$  interactions involving methyl hydrogens and the benzimidazole ligands of adjacent molecules with an average distance of 2.93 Å separating them. There is no evidence of cooperative  $\pi$ -stacking in the lattice. However, T-shaped/point – face C-H... $\pi$  interactions amongst adjacent benzimidazoles are visible. Figure 4.42 displays some of

these interactions.

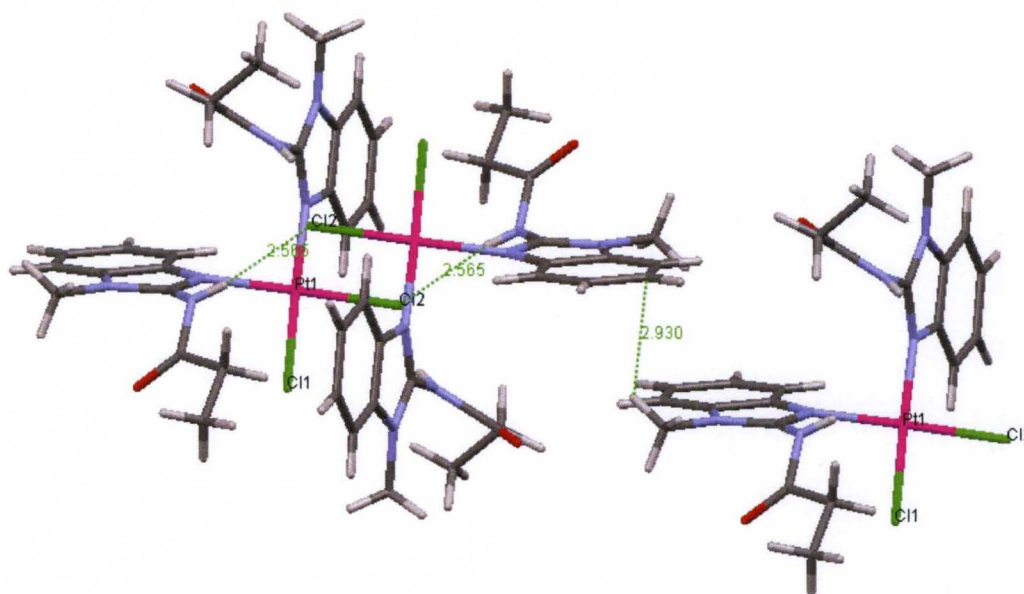


Figure 4.42: "Capped-sticks" ORTEP diagram of compound **41** showing packing and hydrogen bonding interactions in the crystal lattice.

Table 4.8 displays selected bond lengths and angles of hydrogen bonds found in the lattice of compound **41**.

Table 4.8: Hydrogen bonds for compound **41** [ $\text{\AA}$  and  $^\circ$ ].

D-H	d(D-H)	d(H..A)	$\angle$ DHA	d(D..A)	A
N3-H3N	0.762	2.565	156.55	3.278	Cl2 [ -x+1, -y+1, -z+1 ]
N6-H6N	0.663	2.612	160.80	3.245	Cl2 [ -x+1, -y+1, -z+1 ]

The angle between the H-donor (d) and acceptor (Cl2) for both N3-H3N and N6-H6N are  $156.6^\circ$  and  $160.8^\circ$  respectively. Furthermore, both hydrogens are  $2.6 \text{ \AA}$  from their respective acceptor atom (Cl2).

Figure 4.43 displays the packing arrangement seen in the lattice of compounds **42(a,b)**. The crystal lattice reveals an octahedral Pt(IV) bis-chelated complex, compound **42a**, with two chlorides occupying the axial position (Figure 4.44).



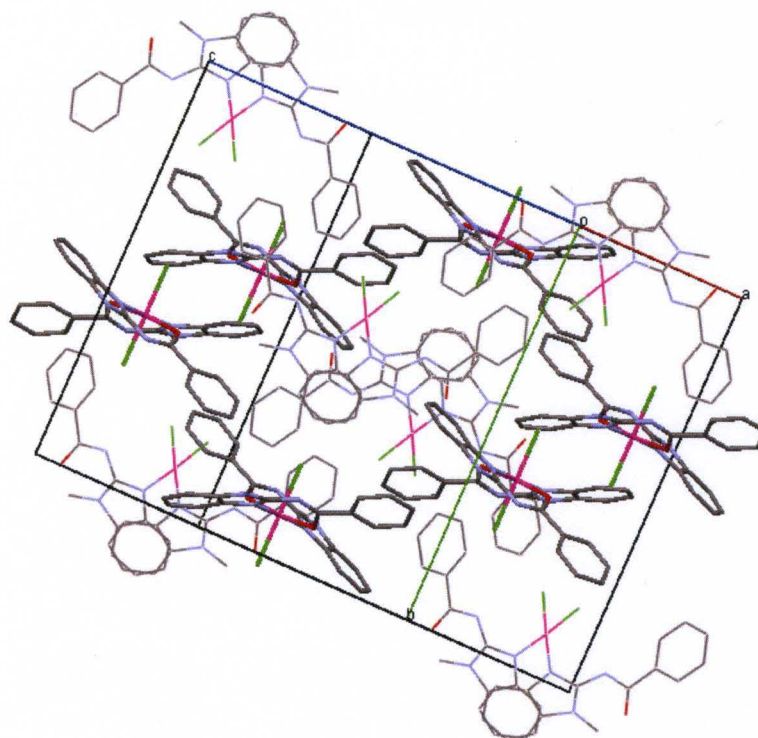


Figure 4.43: Packing of compounds **42a** and **42b**. “Capped-sticks” represent the Pt(IV) complex. The wireframe represents the Pt (II) complex. Hydrogens have been removed for clarity.

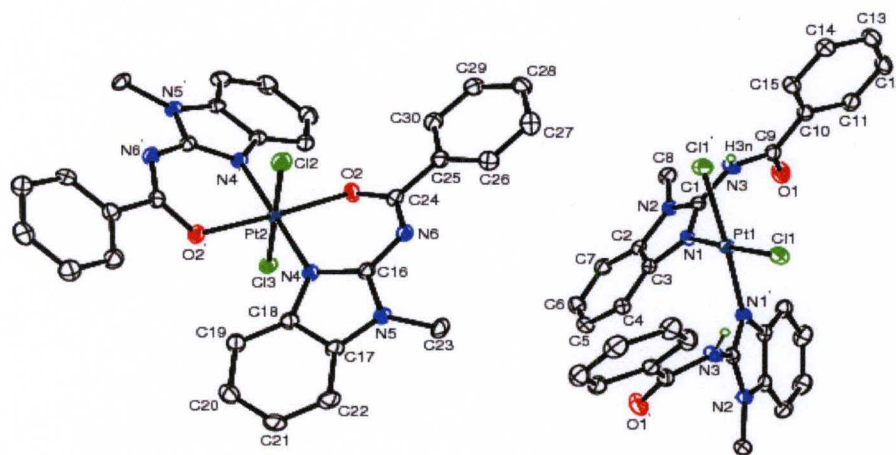


Figure 4.44: ORTEP diagram of compounds **42b** with a co-crystal of a Pt(IV) trans complex, **42a**( left).

Ellipsoids are shown at 40% probability. Hydrogen atoms have been omitted for clarity.

The twist in the bis-chelated benzimidazoles of compound **42a** is similar to compound **30**. Compound **42a** shows slipped  $\pi$ -stacking with adjacent Pt(IV) molecules with an

average distance of 3.38Å (Figure 4.45). The axial chlorides are engaged in C-H... $\pi$ (Cl) interactions with the hydrogens (H7, H8C) of adjacent benzimidazoles (2.95Å). Figures 4.45-4.47 display some interactions found in the lattice of compound **42**.

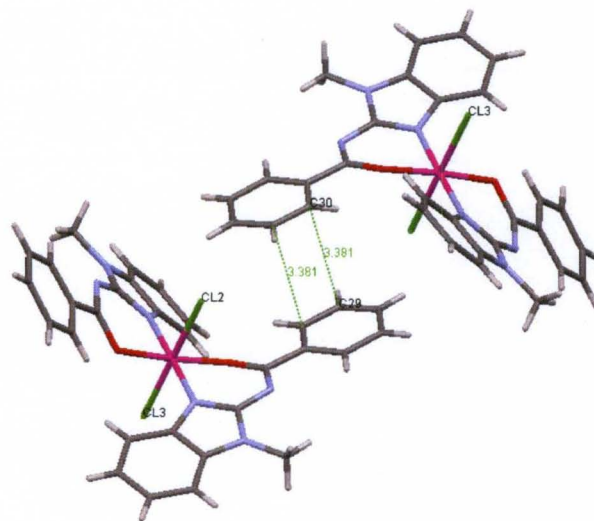


Figure 4.45: ORTEP diagram of compound **42a** showing axial chlorides and bis-chelated twisted out of the N-Pt-N plane and showing slipped  $\pi$ -stacking interactions in the crystal lattice.

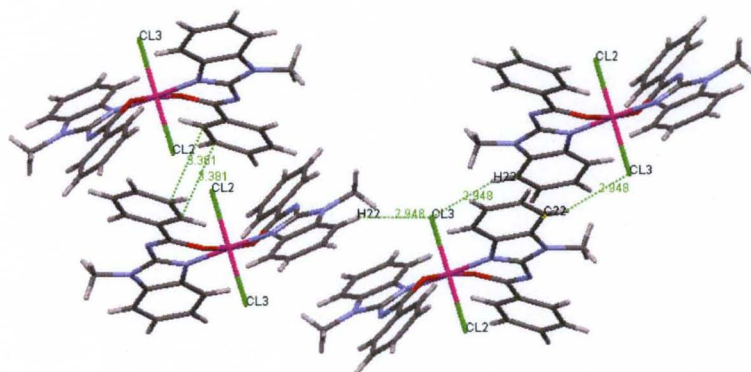


Figure 4.46: “Capped-sticks” ORTEP diagram of compound **42a** showing C-H... $\pi$  interactions in the crystal lattice.

The Pt(II) complex, compound **42b**, also shows ‘slipped’  $\pi$ ... $\pi$  interactions (3.39Å) amongst the phenyl groups of adjacent molecules. However, it has more overlap

compared to compound **42a**. Additionally, its chlorides are also engaged in C-H... $\pi$  (Cl) interactions with average distances of 2.81Å.

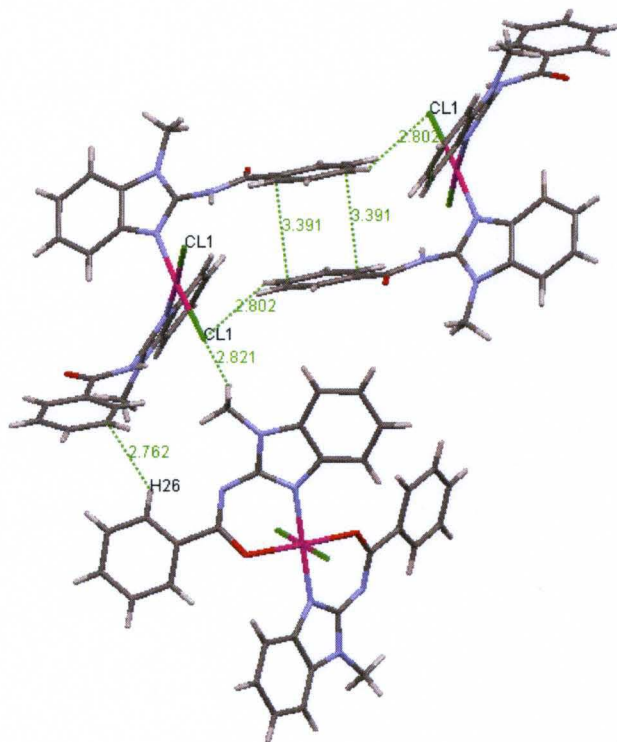


Figure 4.47: “Capped-sticks” ORTEP diagram of compounds **42a** and **42b** showing packing and some interactions in the crystal lattice.

The lattice also displays occasional point to face C-H...  $\pi$  interactions between benzimidazole protons and phenyl groups of both the Pt(II) and Pt(IV) moieties (Figure 4.47). The *trans* Pt(II) isomer of compound **42b**, compound **42c**, is displayed in Figure 4.48. It forms monoclinic crystals in the space group  $P2_1/c$ . Its molecular geometry is square planar. Examination of the coordination sphere shows the Pt (II) ion coordinated to two monodentate benzimidazole ligands and two chlorides in a *trans* configuration. The ligands, N-(N'-1-methylbenzimidaz-2-yl)benzamide, are coordinated through the nitrogen (N3) of the benzimidazole.

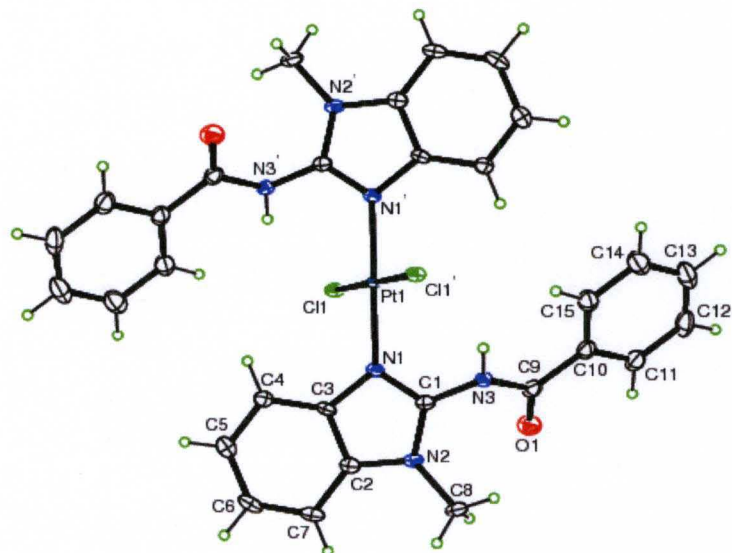


Figure 4.48: ORTEP diagram of compound **42c** showing packing and hydrogen bonding interactions between stacks. Hydrogens have been omitted for clarity.

Compound **42c** has bond angles of  $179.999^\circ$ ,  $90.20(4)^\circ$ ,  $89.80(4)^\circ$  and  $180.0^\circ$  corresponding to  $N(1) - Pt - N(1')$ ,  $N(1) - Pt - Cl(1)$ ,  $N(1) - Pt - Cl(1')$  and  $Cl(1) - Pt - Cl(1')$  respectively. The average  $Pt - N$  and  $Pt - Cl$  bond lengths are  $2.014^\circ$  and  $2.304^\circ$  respectively.

The crystal lattice shows a H-donor / acceptor ( $2.48^\circ$ ) relationship between the chlorides and the amide hydrogen (Figure 4.49). The phenyl groups are diagonal and out of the benzimidazole-Pt plane, an orientation previously seen in compound **4**, a cyclohexyl pendant. Another type of interaction visible in this lattice is a slipped  $\pi \dots \pi$  interactions (C1-C7), Figure 4.51.

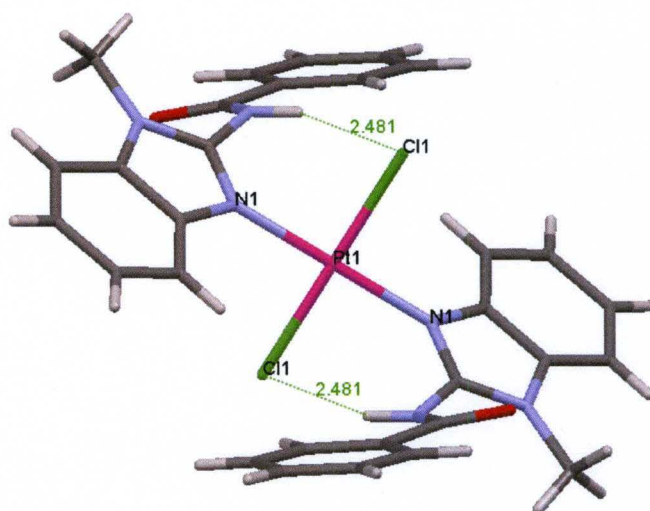


Figure 4.49: “Capped-sticks” ORTEP diagram of compound **42c** showing hydrogen bonding between chlorides and amide hydrogens in the crystal lattice.

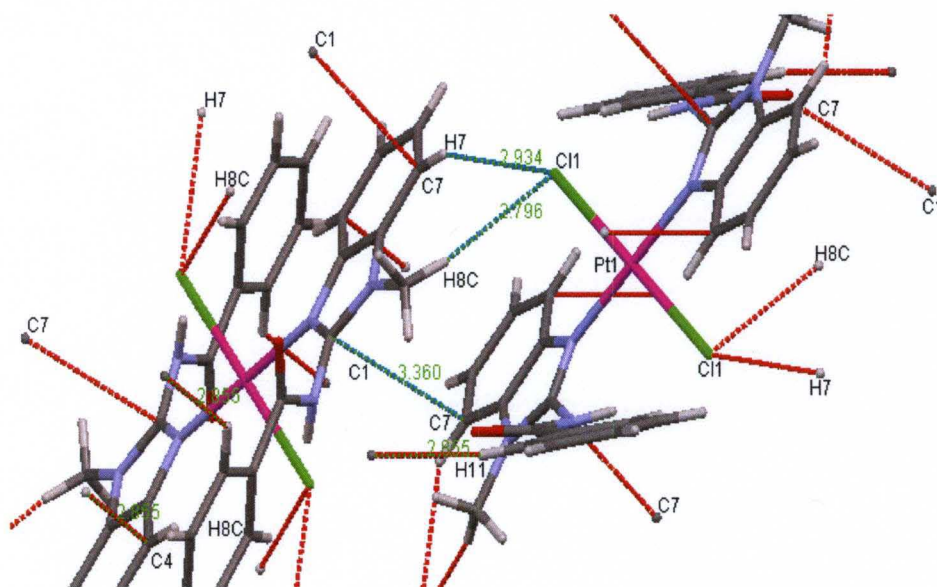


Figure 4.50: “Capped-sticks” ORTEP diagram of compounds **42c** showing packing and some interactions in the crystal lattice.

Compound **46** forms monoclinic crystals in the space group  $P2_1/n$ . The ligand, (N'-1-methylbenzimidazol-2-yl) – N-boc-2-amino-2,2-dimethylacetamide, binds to the Pt (II) ion through the nitrogen of the benzimidazole as a monodentate (Figure 4.51).

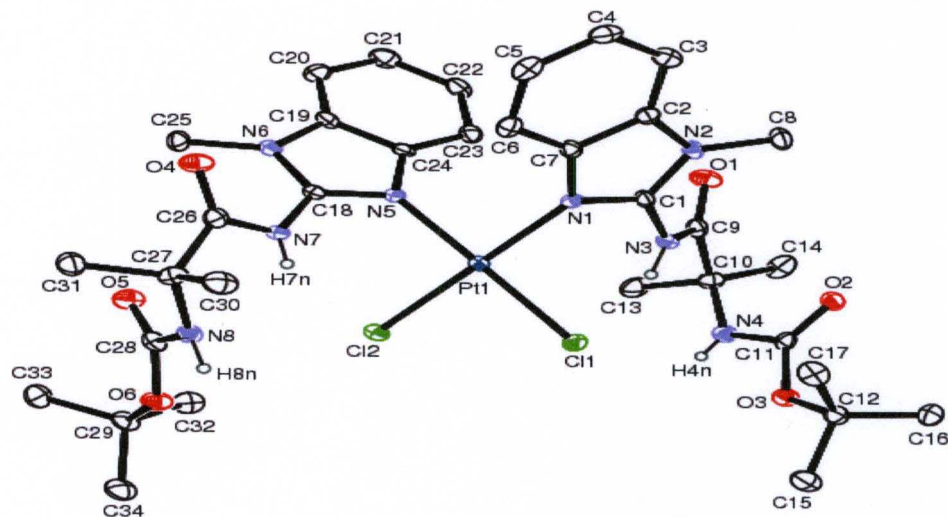


Figure 4.51: ORTEP diagram of compound **46**. Ellipsoids are shown at 50% probability. Hydrogen atoms have been omitted for clarity.

The ligand assumes a *cis* configuration around the central atom with an average Pt-N bond length of 2.027(3) Å. The average Pt-Cl and C-O bond lengths are 2.30 Å and 1.256 Å respectively. Compound **46** has bond angles of 90.28(11) Å, 90.69(8) Å and 177.39(9) Å corresponding to N(1) – Pt – N(1'), N(1) – Pt – Cl(1) and N(1) – Pt – Cl(1')

respectively. Its crystal lattice shows hydrogen bonding between the chlorides, amide protons and carbonyl oxygens. The parameters of these hydrogen bond interactions have been compiled in table 4.9.

Table 4.9: Hydrogen bonds for compound **46** [ $\text{\AA}$  and  $^\circ$ ].

D-H	d(D-H)	d(H..A)	$\angle$ DHA	d(D..A)	A
N3-H3N	0.793	2.392	144.38	3.071	Cl1
N4-H4N	0.701	2.440	163.01	3.117	O4 [ x, y-1, z ]
N7-H7N	0.694	2.300	116.03	2.678	N8
N7-H7N	0.694	2.535	140.04	3.099	Cl2
N8-H8N	0.879	2.602	169.49	3.469	Cl2 [ -x+2, -y+2, -z+2 ]

Additionally, the tert-butyl of both boc-groups are oriented in opposite directions. Figure 4.52 shows some of the interactions seen in the lattice.

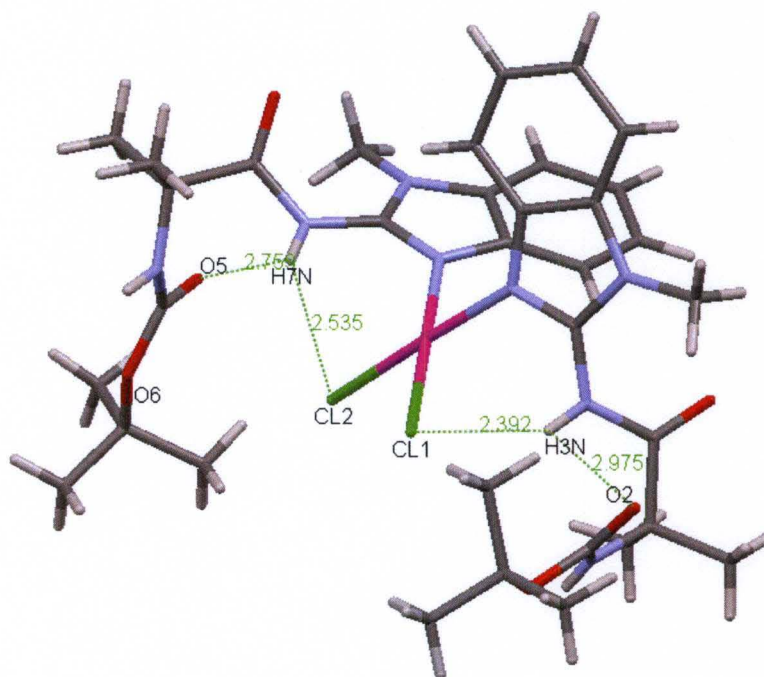


Figure 4.52: “Capped-sticks” ORTEP diagram of compound **46** showing hydrogen bonding interactions in the crystal lattice. T-butyl groups oriented in opposite direction.

The orientation of the benzimidazoles are similar to other dichlorides in this series. The dichlorides are also engaged in C-H... $\pi$ (Cl) interactions with benzimidazole protons.

There is no evidence of cooperative  $\pi$ -stacking in the crystal lattice. However, unlike previous compounds of this series, the platinum core appears to be more shielded by both the pendants and the benzimidazoles. This would likely prevent or slow down deactivating reactions with thiols such as glutathione (Figure 4.53).

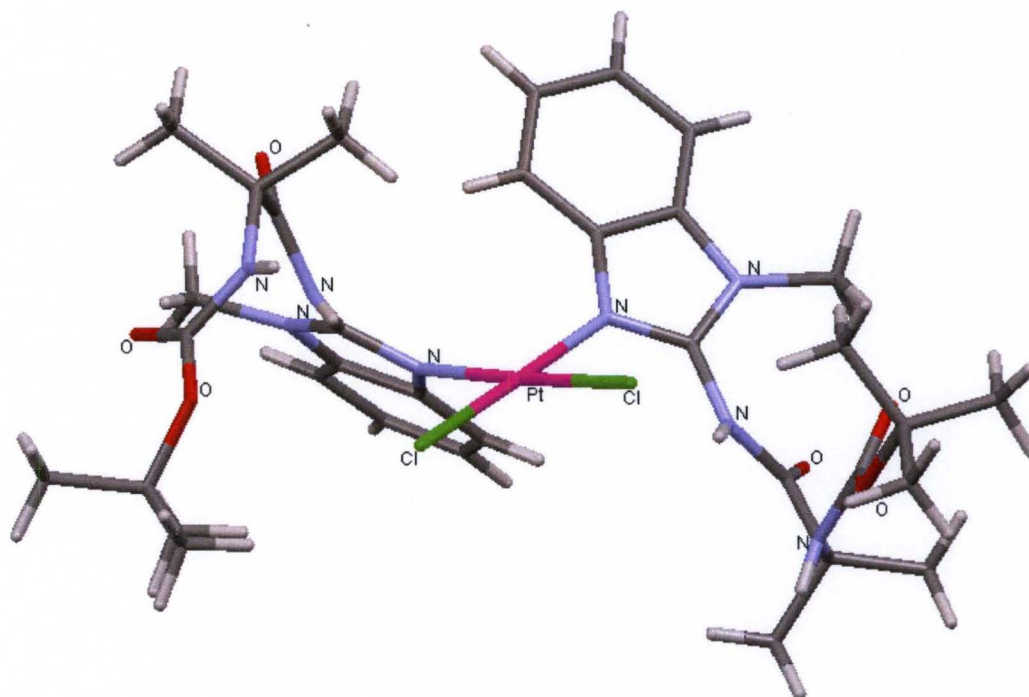


Figure 4.53: “Capped-sticks” ORTEP diagram of compound **46** showing a semi-encapsulation of the metal, preventing possible interactions with thiols such as glutathione.

Overall, the crystal structures are in agreement with the other physical methods. None of the lattices examined showed a full face to face  $\pi$ -stacking overlap. However, the interactions of the benzimidazole repeat motifs were usually slipped  $\pi$ -stacking with varying degrees of overlap. Furthermore, even though hydrogen bond interactions are the strongest of all non-covalent interactions, not all the lattices displayed it. Instead, lattices



avored interactions that brought about the most stability regardless of the hydrogen donor and acceptor capability of the respective complexes.

### G: UV-vis Studies of Complexes

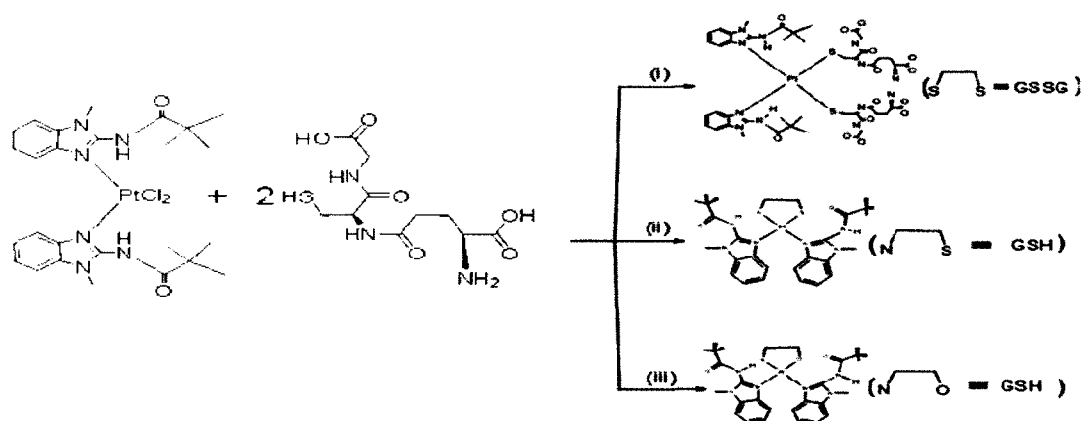
Table 4.9 shows  $\lambda_{\max}$  values of selected Pt(II) complexes performed in 3mL dichloromethane. The “Amb” refers to 2-amino-1-methylbenzimidazole whilst AB represents 2-amino-1H-benzimidazole.

Table 4.10:  $\lambda_{\max}$  values of selected Pt(II) complexes

Compound	Ligand	Complex	$\lambda_{\max}(\text{nm}), [\epsilon (\text{M}^{-1} \text{cm}^{-1})]$
<b>4</b>	Hmbchca	L	249 [17]; 300 [26]; 310 [34]
<b>30</b>	Amb-(CH <sub>2</sub> ) <sub>8</sub> CH <sub>3</sub>	PtL <sub>2</sub>	288 [28], 322[28]
<b>31</b>	Amb-C <sub>6</sub> H <sub>11</sub>	PtL <sub>2</sub> I <sub>2</sub>	248 [10], 299 [9], 310 [5]
<b>32</b>	Amb-C <sub>6</sub> H <sub>11</sub>	PtL <sub>2</sub>	288 [7], 324 [6]
<b>33</b>	Amb-C <sub>6</sub> H <sub>11</sub>	PtL <sub>2</sub> Cl <sub>2</sub>	279 [13]
<b>34</b>	Amb-(CH <sub>2</sub> ) <sub>14</sub> CH <sub>3</sub>	PtL <sub>2</sub>	280 [39], 364 [3]
<b>40</b>	AB-C <sub>6</sub> H <sub>11</sub>	PtL <sub>2</sub> I <sub>2</sub>	286 [11], 294
<b>41</b>	Amb-CH <sub>2</sub> CH <sub>3</sub>	PtL <sub>2</sub> Cl <sub>2</sub>	279 [10]

Compared to the diiodo- and amido forms of the 2-amino-1-methylbenzimidazole derivatives, the dichlorides have only one  $\lambda_{\max}$ (279 nm). The amido derivatives of this series have characteristic two  $\lambda_{\max}$ . The  $\lambda_{\max}$  of compound **31** is similar to that of its free ligand compound **4**.

**Solvent Effects on Compound 37:** Compound **37** showed comparable cytotoxicity (discussed later in the chapter) to cisplatin against prostate cancer cell lines (DU145). It showed better inhibitory activity in the concentration range 0.4 $\mu$ M- 8.0 $\mu$ M. Based on this information, UV studies were carried out to investigate the reactivity of compound **37** with glutathione, a known deactivating agent of platinum species in the cell. Scheme 4.5 shows possible interactions between compound **37** and glutathione (GSH).



Scheme 4.5: Possible interactions of glutathione with compound **37**. Carboxylic and amine hydrogens in the product have been omitted for clarity.

The first pathway (i), shows compound **37** ligated to the tripeptide, as a monodentate, through the sulfur [164]. The second possibility will be a chelation of one molecule of glutathione through a nitrogen and a sulfur (ii). Another possibility is a chelation to the monomer through a nitrogen and an oxygen.

The study was carried out in three different solvent systems. The first of which was a 7 mL water/ 3 mL methanol mixture. The second and third were 10 mL anhydrous dichloromethane (DCM) and 8 mL dimethylsulfoxide (DMSO) / 2 mL water. All three systems had a 1:2 ratio (compound **37**: GSH). The concentrations of compound **37** were  $8.39 \times 10^{-6} \mu\text{M}$ ,  $14.86 \times 10^{-4} \mu\text{M}$  and  $15.82 \times 10^{-4} \mu\text{M}$  respectively. Figure 4.54 shows a combined UV-vis spectra for all three solvent systems obtained after 14 days. The spectra for the individual reactants is displayed in Figure 4.55 for comparison.

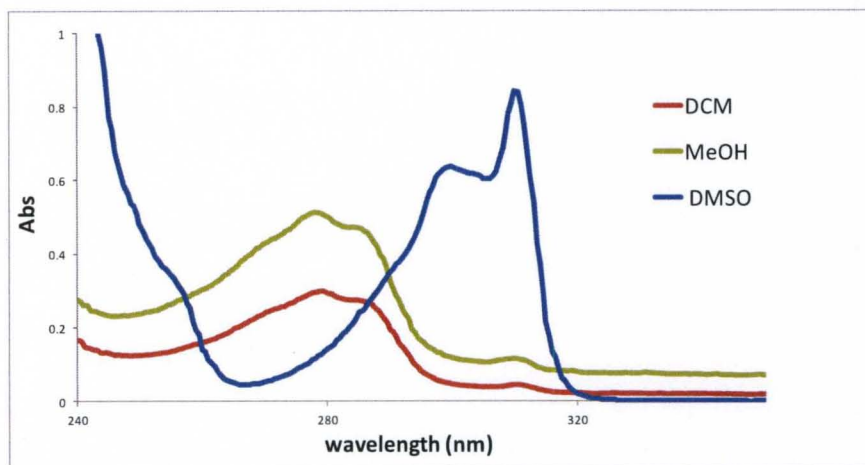


Figure 4.54: UV-vis spectrum of GSH and compound **37** in 100% DCM, 70% MeOH/ 30% water, and 80% DMSO/ 20% water after 14 days. A new  $\lambda_{\text{max}}$  appears at 310 nm with time.

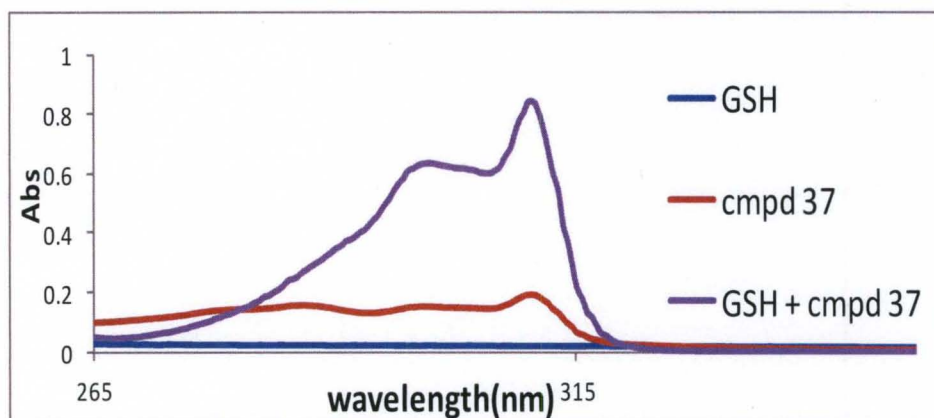


Figure 4.55: UV-vis spectrum of GSH, compound **37** and an aliquot of DMSO/water reaction solution system.

An absorption band with  $\lambda_{\text{max}}$  at 310 nm increases in intensity with time in all three solvent systems. However, the absorption is more intense in the DMSO solvent system. The various combinations of solvents were reached based on the solubility of the reactants. It should be noted that other tests have been designed to monitor the binding of platinum species to GSH including assays that have phosphate buffers and NADPH

coupled reactions [64, 165]. Additionally, this study is aimed at finding the effects of solvent on the reactivity of thiols and the platinated complexes of this series.

The absorption band with  $\lambda_{\text{max}}$  at 310 nm increases in intensity with time appreciably in the DMSO system compared to both the methanol/water and DCM systems. Unlike the two solvent systems, no precipitate was observed in the reaction vessel as time elapsed. The precipitate was confirmed as Pt-dmsO adducts by mass spectrometry. The absorption band with  $\lambda_{\text{max}}$  at 310 nm is due to free ligand. From the data, it can be concluded that decomposition of compound **37** is accelerated in the dmsO solvent system. No evidence of a Pt-GSH adduct formation was observed.

## H: Bioassay of Complexes

Selected compounds were tested to ascertain their cytotoxicity profile against prostate cancer cell lines, (DU145, PC3 and LNCaP), using the MTT assay method in Dr Bates Laboratory. This method measures the metabolism of MTT, (3-[4,5-dimethylthiazol-2-yl]-2,5-diphenyl tetrazolium bromide), at 570 nm. Figures 4.56 – 4.63 display the profiles of these compounds.

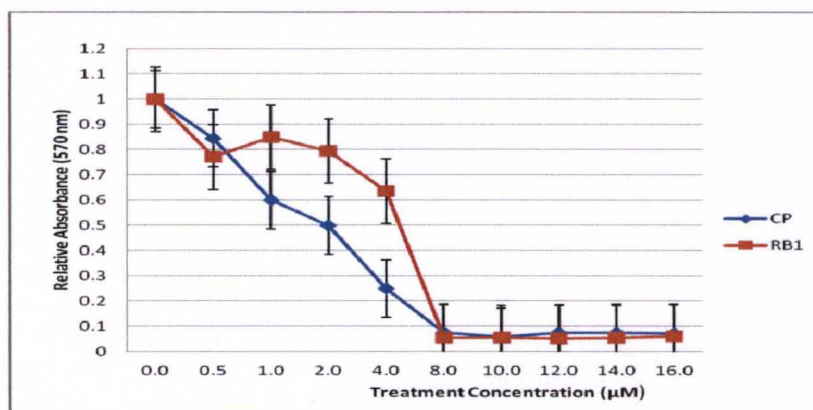


Figure 4.56: MTT Assay of Cell line: **DU145**; cytotoxicity of cisplatin (CP) and compound **37** (RB1)

Figure 4.56 shows the treatment of DU145 cancer cell lines with cisplatin and compound **37** designated CP and RB1 respectively. Compound **37** appears to have a higher dose response for the concentration ranges 0 – 0.5  $\mu\text{M}$  and 4.0-8.0  $\mu\text{M}$ . The responses are comparable for the ranges 8.0  $\mu\text{M}$  – 16.0  $\mu\text{M}$ . The pyridine analogue of compound **37**, compound **28**, shows a similar inhibition profile (Figure 4.57). However, compound **28** shows a slightly better dose response between 0 – 1.56  $\mu\text{M}$ . Compound **36**, a cis bis-chelate with a t-butyl pendant, has a similar profile to compound **28**. Both compounds show a better dose response compared to compound **42b**, a dichloride cisplatin analogue with phenyl pendants. Additionally, the  $\text{IC}_{50}$  values (discussed later in this chapter) confirm that overall, compounds **28** and **36** are better inhibitors than **42b**.

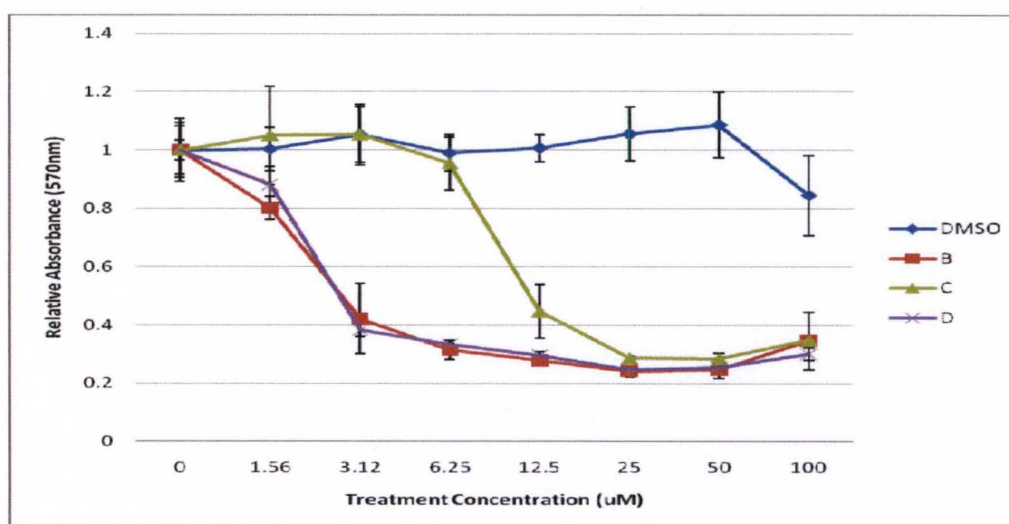


Figure 4.57: MTT Assay of Cell line: **DU145**. Cytotoxic profiles of compounds **28** (B), **42b** (C) and **36** (D)

However, all three compounds show the same cytotoxic profile against immortalized epithelial prostate cells, RWPE-1 (Figure 4.58). Against PC3 and LNCaP cell lines, both compounds **28** and **36** show identical cytotoxic activity with PC3 cells displaying acquired resistance to all three compounds after a treatment concentration of 6.25  $\mu\text{M}$ .

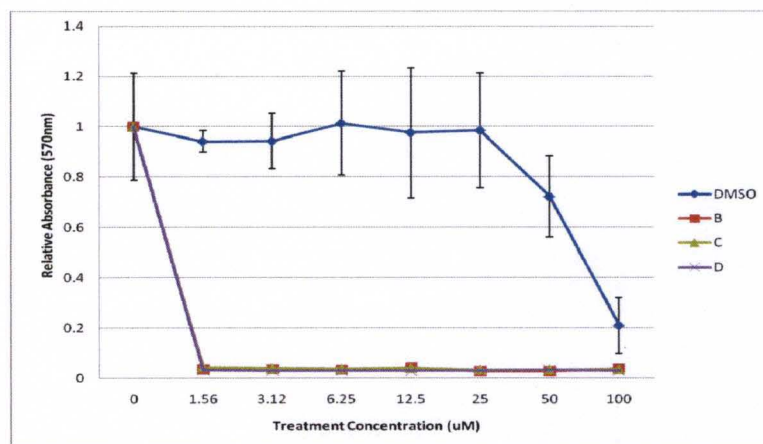


Figure 4.58: MTT Assay of Cell line: **RWPE-1**. Cytotoxic profiles of compds **28** (B), **42b** (C) and **36** (D)

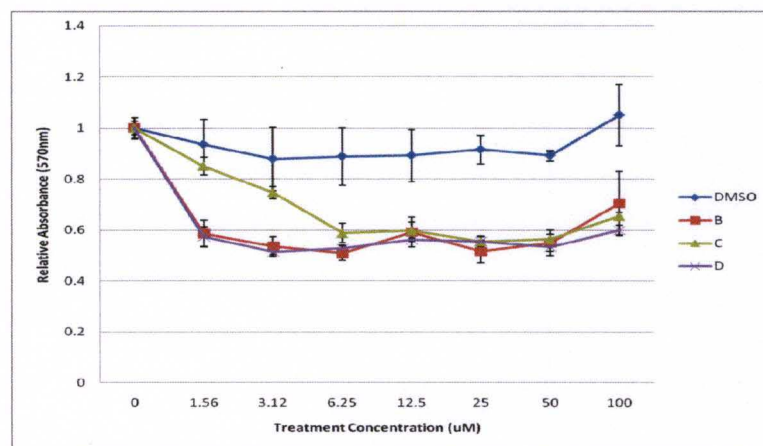


Figure 4.59: MTT Assay of Cell line: **PC3**. Cytotoxic profiles of compds **28** (B), **42b** (C) and **36** (D)

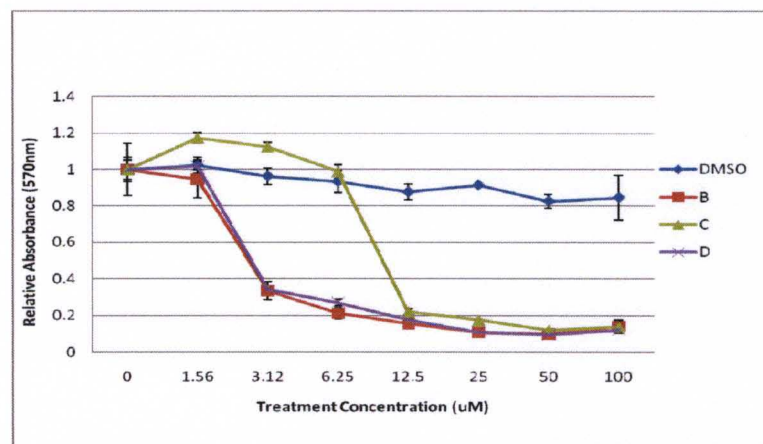


Figure 4.60: MTT Assay of the **LNCaP** Cell line: Cytotoxic profiles of compds **28** (B), **42b** (C) and **36** (D)

Figures 4.61- 4.63 displays cytotoxic profiles of compounds **27**, **36**, **42d** and **32** designated A,D,E, F. These bis-chelated complexes have t-butyl, phenyl and cyclohexyl pendants.

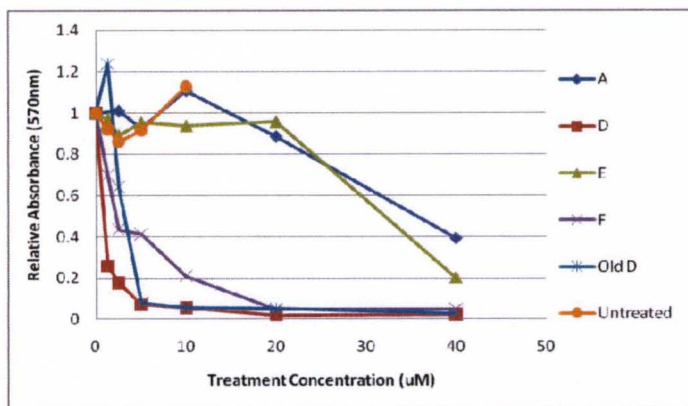


Figure 4.61: DU145 Cell line: Cytotoxic profiles of compds **27** (A), **36** (D), 42d (E) and **32** (F)

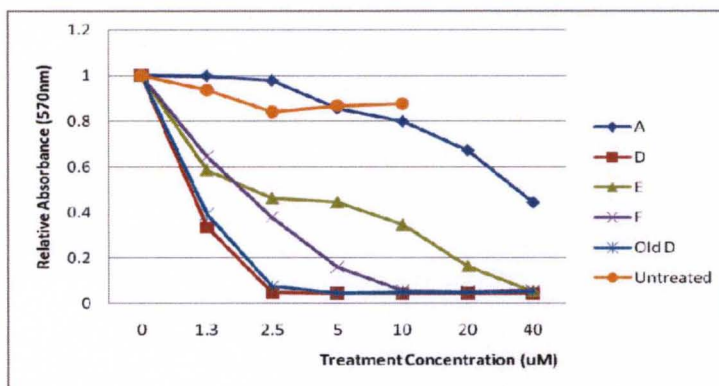


Figure 4.62: PC3 Cell line: Cytotoxic profiles of compds **27** (A), **36** (D), 42d (E) and **32** (F)

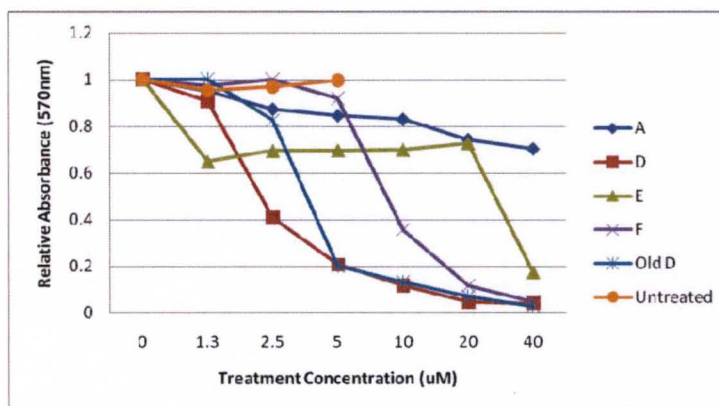


Figure 4.63: LNCaP Cell line: Cytotoxic profiles of compds **27** (A), **36** (D), 42d (E) and **32** (F)

Compound **27** is a *trans* pyridine analogue of the *cis* 2-amino-1-methylbenzimidazole, compound **36**. It shows the least cytotoxicity against all three cancer cell lines. For the

concentration range 1.3 $\mu$ M- 5.0  $\mu$ M, compounds **32** and **36** display higher dose responses against all three cell lines. Compound **42d**, however, requires slightly higher concentrations to attain comparable dose responses to both compounds **32** and **36**. The IC<sub>50</sub> values for all the selected compounds is displayed in the table below.

Table 4.11: IC<sub>50</sub> values ( $\mu$ M) of selected Pt(II) complexes

		IC <sub>50</sub> values ( $\mu$ M)			
Expt 1					
	Cisplatin	Compd 28	Compd 36	Compd 37	Compd 42b
DU 145	2.00	2.81	2.73	5.00	7.65
PC3	N/A			N/A	
LNCaP	N/A	2.57	2.73	N/A	7.23
RWPE-1	N/A	0.78	0.78	N/A	0.78
Expt 2					
	Compd 27	Compd 32	Compd 36	old-Compd 36	Compd 42d
DU 145	35.25	2.20	0.88	3.12	32.10
PC3	35.00	2.08	0.98	0.75	2.21
LNCaP	N/A	8.75	2.26	4.00	28.00

From the table, based on the IC<sub>50</sub> values, compounds **28**, **32** and **36** show comparable cytotoxicity to cisplatin. Old-compound **36**, which is just an old stock of compound **36** that was stored in distilled/ sterile DMSO, shows reduced cytotoxicity for both DU145 and LNCaP cell lines. This might be due to the decomposition in solution as seen earlier in the GSH experiment. However, against PC3 cell lines its cytotoxicity appears to be enhanced (IC<sub>50</sub> = 0.75  $\mu$ M). The enhanced activity could be attributed to the additional cytotoxic effects of the free ligand [166-167] and the metal.



## I: Conclusions

All physical methods are in agreement and confirm the successful synthesis of the desired compounds. The three ligand systems, 2-amino-1-methylbenzimidazole, 2-amino-1H benzimidazole, and the pyridine, show unique characteristics and some similarities. A comparison of the benzimidazole systems reveals subtle differences. For example, the diiodo analogues of the cyclohexyl pendants show differences in solubility. That is, the 1-methyl derivative dissolves in chloroform but does not dissolve in acetone. Its 1-H-benzimidazole analogue, however dissolves in acetone.

The pyridine system is affected by the composition and type of solvent during platinum complexation. Unlike the 2-amino-1-methylbenzimidazole system, a mixture of *cis* and *trans* isomers are obtained for the amido form. Ironically, separation of these isomers using column chromatography was unsuccessful. Although thin layer chromatography, using diethyl ether, showed selectivity for one isomer over the other, replication on a large scale was also not successful. Additional methods including solvent polarity variation and solvent mixture combinations were also not successful.

The packing arrangements in the pyridine dichloride and amido complexes are similar to that of the 2-amino-1-methyl benzimidazole analogues. A complete face-to-face overlap of the  $\pi$ -systems was not observed for the complexes discussed in this chapter. However, lattices displayed varying degrees of overlap and interactions ranging from strong hydrogen bonding to weak Van der waal.

Finally, the cytotoxicity of the complexes so far tested are comparable to cisplatin. The successful synthesis of the second generation type of complexes, compound **46**, provides promise for a targeted approach toward tumor cells. Furthermore,

preliminary bioassay results show a direct correlation between dose response and the type of heterocycle in the binding domain of type 1 complexes. Consequently, derivatives of successful compounds of this series could be used to circumvent acquired resistance.

## CHAPTER V

### CONCLUDING REMARKS

From a synthetic view point, the amidation of the 2-amino-1H-benzimidazole with acyl chlorides are not as straight forward as their 1-methylbenzimidazole counterparts. The N1 proton presents an additional site of amide bond formation and as a result, amide formation at the 2-amino position requires synthesis at higher temperatures. Ligands of both benzimidazole systems show evidence of tautomerization. As a result, their <sup>1</sup>H NMR spectra show broad or no amide peaks in solvents such as chloroform. However, amide protons are visible when solvents such as DMSO-<sub>d6</sub> are used. The collapse or aggregation of the aromatic protons is only seen in the 2-amino-1-methylbenzimidazole derivatives.

Attempts to obtain *cis* dichloro- or diiodo- analogues for some ligands of 1H-benzimidazole have failed. This might be due to solubility of ligands or the extra metal binding site provided by N1 which might be competing with N3. Additionally, the lack of solubility of these ligands also does not make it possible to use protocols developed for their 2-amino-1-methylbenzimidazole counterparts.

The diiodo- and dichloro- analogues of compound **11** could not be synthesized using the developed protocols. This might be due to a series of factors among which are the inductive electron-withdrawing effect of the trichloride pendant. This might reduce the availability of the lone pair of electrons of N3 of the benzimidazole to coordinate to

the platinum. Also, unlike its tert-butyl or methyl analogues which are electron donating, the chlorides provide lone pairs of their own and these might be competing with lone pairs of the N3 nitrogen of the benzimidazole. Nevertheless, the coordination of compound **11** to platinum needs another look because unlike its three analogues, its solubility in methanol and water is appreciably higher due to the additional hydrogen bonding ability through the chlorides. Successful synthesis of its cisplatin analogue will have the advantage of enhance water solubility. Additionally unlike its analogs, it would be possible to calculate its Log P value for comparison to known drugs in the market (both metal and non-metal based). Another potential advantage that can be drawn from a successful cisplatin analogue of compound **11** would be the ability to tune the reactivity of the metal, through variation of the degree of electron withdrawing /donating substituents, thereby making it slightly less reactive to deactivating moieties like glutathione.

The cis-isomer of the compound **27** could not be isolated via column chromatography even though thin layer paper chromatography showed separation of the isomers in ethyl ether, methanol, and chloroform, with ethyl ether giving the most separation. Based on our findings, all the isomeric conformers are affected by both the composition of the solvent system and temperature.

The *cis* dichloro- analogues of the pyridine and 2-amino-1-methylbenzimidazole systems have similar cytotoxic profiles. This suggests that changing the binding domain moieties does not significantly affect the cytotoxic properties of the compounds under discussion. Furthermore, this adds to the flexibility of the overall framework and could potentially be an answer to native drug resistance among populations, and acquired

resistance via cellular tolerance or effective combat or neutralization of these compounds/drugs. To this end, combinational therapeutics could greatly benefit from such effective compounds.

Although the Pt(II) dichloro complexes of compound **9** and 2-pivaloylamino pyridine have similar cytotoxic profiles, their reactivity with first row transition metal show great differences. Whereas, compound **9** forms bis-chelates with V(IV), Co(II), Ni(II), Cu(II) and Zn(II), no such complex formation have been reported or synthesized for the pyridine ligand. The inability to obtain similar bis-chelate analogs with the pyridine system could be partly due to the relatively limited number of atoms (compared to the 1-methylbenzimidazole system) that can participate in resonance or tautomerism and the stabilization of resultant charges of the intermediates. Additionally, the involvement of the metal binding nitrogen in such a process, directly destroys the aromaticity of only the pyridine system. While first row transition complexes were not tested for suitability as models for active sites of enzymes, some insight was gained in terms of the fundamental properties including reactivity of the metals, pyridine and 1-methylbenzimidazole systems. Our findings suggests that these amide functionalized benzimidazole moieties prefer to coordinate to first row transition metals as bis-chelates, binding through the nitrogen of the benzimidazole and the oxygen of the carbonyl. Based on the reaction conditions, these benzimidazole ligands tend to coordinate to first row transition metal, resulting in either tetrahedral or *trans* square planar geometries. Only Ni (II) and Zn (II) appear to have the ability to expand coordination number to five. The expansion of coordination spheres of both Ni (II) and Zn(II) 1-methylbenzimidazole complexes make them good candidates for catalytic studies. The distortions in solution

and the expansion of coordination of the Ni (II) complexes could also be potentially harnessed in enzyme modeling. It should be noted that additional properties of these complexes could find utility in other disciplines.

The crystal structure of compound **46** reveals a semi – protected metal core. This arrangement can disrupt or prevent the binding of glutathione or metallothionein, minimizing deactivation [108-110]. A similar ligand to compound **46**, compound **8** has been synthesized. The phthalimide can be removed via hydrolysis ( acid or based catalyzed). The removal of the phthalimide group can be accomplished using the Ing-Manske procedure [168]. Similarly, using Na<sub>2</sub>S in aqueous THF or acetone gives the desired primary amine [169]. Also, treatment with NaBH<sub>4</sub>-2-propanol followed by acetic acid [170] or 40% aqueous methylamine generates the primary amine [171]. It should be noted that these reactions are relatively slow and might hydrolyze the benzimidazole-glycyl peptidic linkage as well.

The successful synthesis of compound **46** suggests that this framework's recognition domain can be expanded to include binding to specific antibodies that are tailored toward specific targets on cancer cell membrane including transmembrane proteins. This would allow for localized drug delivery and minimize interactions with normal cells, thereby reducing potential side effects. The boc group of compound **46** can easily be removed by treatment with trifluoroacetic acid which will allow another peptidic coupling to nucleic acids for example. Subsequently, such a compound would have the advantage of two portions that can bind to DNA; the specific sequence of nucleic acids binding to a promoter region and the platinum to N7 of guanine during the S-phase of mitosis resulting in the interruption of transcription and translation. Also, the

peptidic linkages of compound **46** and similar compounds can serve as hydrogen bonding sites. These sites can interact with DNA through hydrogen bonding and facilitate the binding of the platinum to relatively guanine rich regions outside the telomeric regions.

## REFERENCES

1. Voet, D. and G.J. Voet, *Biochemistry*. 3 ed, ed. D. Harris and P. Fitzgerald. 2004, Hoboken, NJ: John Wiley & Sons.
2. Bruice, T.C., *Annu. Rev. Biochem.*, 1976. **45**: p. 331-373.
3. Breslow, R., *Acc. Chem. Res.*, 1995. **28**: p. 146-153.
4. Ma, J.K.-C., P.M.W. Drake, and P. Christou, *Nature reviews genetics*, 2003. **4**: p. 794-805.
5. Giddings, G., et al., *Nature Biotechnology*, 2000. **18**: p. 1151-1155.
6. Geilissen, G. and K. Melber, *Drug Res.*, 1996. **46**: p. 943-948.
7. Hollenberg, C.P. and G. Gellissen, *Current Opinion in Biotechnology*, 1997. **8**(5): p. 554-560.
8. Ma, J.K.-C., et al., *Vaccine*, 2005. **23**: p. 1814-1818.
9. Jiang, L., et al., *Science*, 2008. **319**: p. 1387-1391.
10. Fersht, A., *Structure and Mechanism in Protein Science*. 1999: Freeman.
11. Bender, M.L., R.J. Bergeron, and M. Komiyama, *The Bioorganic Chemistry of Enzymatic Catalysis*. 1984: Wiley.
12. Walsh, C., *Enzymatic Reactions Mechanisms* 1979: Freeman.
13. Sundberg, R.J. and B.R. Martin, *Chem. Rev.*, 1974. **74** (4): p. 471-514.
14. Comba, P., *Coord. Chem. Rev.* , 2000. **200-202**: p. 217-245.
15. Marks, D.B., *Biochemistry* 3ed. 1999: Williams and Wilkins
16. Bertini, I., et al., eds. *Biological inorganic chemistry: structure and reactivity*. 2007, University science books: Sausalito, CA.,USA.
17. Miessler, G.L. and D.A. Tarr, eds. *Inorganic Chemistry*. 3rd ed. 2004, Pearson Prentice Hall: Upper Saddle River, NJ.
18. Fridovich, I., *Adv. Inorg. Biochem.*, 1979. **1**: p. 67.
19. Strothcamp, K.G. and S.J. Lippard, *Biochemistry*, 1981. **20**: p. 7488.
20. Denisom, I.G., et al., *Chem. Rev.* , 2005. **30**: p. 2253-2277.
21. Zoidakis, J., et al., *J. Biol. Inorg. Chem.* , 2004. **9**: p. 289-296.
22. Tavares, P., et al., *Inorg. Biochem.* , 2006. **100**: p. 2087-2100.
23. Schenk, G., et al., *Biochemistry*, 2003. **42**: p. 7294-7302.
24. Rogers, M.S., et al., *Biochemistry* 2007. **46**: p. 4606-4618.
25. Valentine, J.S. and J.D. Freitas., *J. Chem. Educ.*, 1985. **62**: p. 728.
26. Karlin, S., Z.Y. Zhu, and K.D. Karlin, *PNAS*, 1997. **94**: p. 14225-14230.
27. Desiraju, G.R., *Angew. Chem., Int. Ed. Engl.*, 2011. **50**: p. 52-59.
28. Desiraju, G.R., *Acc. Chem. Res.*, 1996. **29**: p. 441-449.
29. Krische, M.J. and J.M. Lehn, *Molecular Self- Assembly*, 2000. **96**: p. 3-29.
30. Brammer, L., E.A. Bruton, and P. Sherwood, *Crystal Growth & Design*, 2001. **1**: p. 277-290.
31. Yuan, Q., et al., *J. Inorg. Biochem.*, 2009. **103**(8): p. 1156-1161.



32. Bauer, P., *Synthesis, Characterization and Analysis of Benzimidazole ligands and transition metal complexes.*, in *Chemistry*. 2009, University of Louisville: Louisville.
33. Magano, J. and J.R. Dunetz, *Chem. Rev.*, 2011. **111**: p. 2177–2250.
34. Roquette, P., et al., *Inorg. Chem.*, 2011. **50**: p. 1942-1955.
35. Buß, I., et al., *J. Inorg. Biochem.*, 2011. **105**(5): p. 709-717.
36. Yang, M., et al., *J. Inorg. Biochem.*, 2005. **2**: p. 376-382.
37. Ge, R. and H. Sun, *Acc. Chem. Res.*, 2007. **40**: p. 267-274.
38. Vāvere, A.L. and J.S. Lewis, *J. Chem. Soc. Dalton Transactions* 2007: p. 4893-4902.
39. Hambley, T.W., *J. Chem. Soc. Dalton Transactions* 2007: p. 4929-4937.
40. Fricker, S.P., *J. Chem. Soc. Dalton Transactions* 2007: p. 4903-4917.
41. Kostova, I., *Curr. Med. Chem.: Anti-Cancer Agents* 2005. **5**: p. 591-602.
42. Garbutcheon-Singh, B.K., et al., *Current Topics in Medicinal Chemistry*, 2011. **11**( 5): p. 521-542(22).
43. Das, S., M. Suman, and B. Jain, *J. Ind. Coun. Chem.*, 2010 **27**(2): p. 177-179.
44. Zhang, C.X. and S.J. Lippard, *Current Opinion in Chemical Biology* 2003. **7**: p. 481–489.
45. Heffeter, P., et al., *Drug Resistance Updates*, 2008. **11**: p. 1–16.
46. Crans, D.C., et al., *Inorg. Chem.*, 2000. **39**: p. 4409.
47. Barbosa, L.F., et al., *Dalton Trans.*, 2009. **8**: p. 1450-1459.
48. Galaris, D. and A. Evangelou, *Crit. Ver. Oncol. Hermatol.*, 2002. **42**: p. 93-103.
49. Kennedy, L.J., et al., *Chem. Res. Toxicol.*, 1997. **10**: p. 386-392.
50. Lloyd, D.R., P.L. Carmichael, and D.H. Phillips, *Chem. Res. Toxicol.*, 1998. **11**: p. 420-427.
51. Primik, M.F., et al., *Inorg. Chem.*, 2010. **49**: p. 11084-11095.
52. Tan, J., B. Wang, and L. Zhu, *J. Biol. Inorg. Chem.*, 2009. **14**: p. 727-739.
53. Hernández, W., et al., *Bioinorganic Chemistry and Applications*, 2005. **3**(3-4): p. 299-314.
54. Budzisz, E., et al., *Polyhedron*, 2009. **28**: p. 637-645.
55. Eryazici, I., C.N. Moorefield, and G.R. Newkome, *Chem. Rev.*, 2008. **108** (6): p. 1834–1895.
56. Reedijk, J., *Chem. Rev.*, 1999. **99**(9): p. 2499 - 2510.
57. Lippard, S.J. and E.R. Jamieson, *Chem. Rev.*, 1999. **99**(9): p. 2467-98.
58. Jung, Y., Y. Mikata, and S.J. Lippard, *J. Biol. Chem.*, 2001. **276**(47): p. 43589-43596.
59. Zhang, J., et al., *J. Chem. Soc. Dalton Trans.*, 2002: p. 591-597.
60. Mantri, Y., S.J. Lippard, and M.-H. Baik, *J. Am. Chem. Soc.*, 2007. **129**: p. 5023-5030.
61. Wang, D., et al., *PNAS* 2010. **107**(21): p. 9584-9.
62. Yongwon, J. and S.J. Lippard, *Chem. Rev.*, 2007. **107**(5): p. 1387-1407.
63. Segapelo, T.V., et al., *Inorg. Chim. Acta*, 2009. **362**: p. 3314-3324.
64. Mier-Vinué, J.d., et al., *J. Med. Chem.*. 2008. **51**: p. 424-431.
65. Dabrowiak, J.C., J. Goodisman, and A.-K. Souid, *Drug Metabolism and Disposition*, 2002. **30**(12): p. 1378-1384.
66. Stocker, B.L. and J.O. Hoberg, *Organometallics*, 2006. **25**: p. 4537-4541.

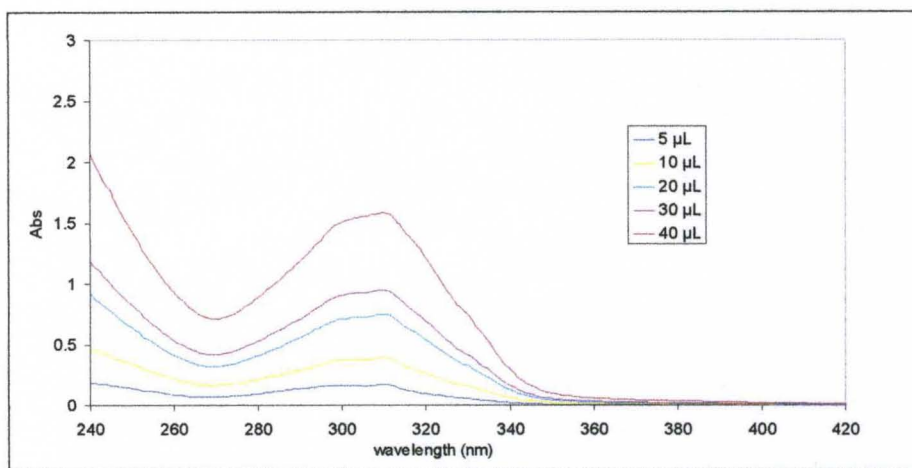
67. Bancroft, D.P., C.A. Lepre, and S.J. Lippard, *J. Am. Chem. Soc.*, 1990. **112**: p. 6860-6871.
68. Klein, A.V. and T.W. Hambley, *Chem. Rev.*, 2009. **109**: p. 4911-4920.
69. Fichtinger-Schepman, A.M.J., et al., *J. Biochem.*, 1985. **24**: p. 707.
70. Huang, H., et al., *Science*, 1995. **270**: p. 1842.
71. Takahara, P.M., et al., *Nature*, 1995. **377**: p. 649.
72. Teuben, J.M., et al., *J. Biochem.*, 1999. **38**: p. 12305.
73. Fuertes, A.M., C. Alonso, and J.M. Pérez, *Chem. Rev.*, 2003. **103**(3): p. 645-62.
74. Wong, E. and C.M. Giandomenico, *Chem. Rev.*, 1999. **99**(9): p. 2451-66.
75. Ma, E.S.F., et al., *J. Med. Chem.*, 2005. **48**(18): p. 5651-54.
76. Ljungman, M., *Chem. Rev.*, 2009. **109**(7): p. 2929-2950.
77. Hindi, K., et al., *Chem. Rev.*, 2009. **109**: p. 3859-3884.
78. Lippert, B., *Cisplatin: Chemistry and Biochemistry of a leading Anticancer Drug*. 1999, Weinheim: Wiley-VCH.
79. Kelland, L.R., *Nature Rev.*, 2007. **7**: p. 573-584.
80. Villanueva, J.M., et al., *Inorg. Chem.*, 1999. **38**: p. 6069-6080.
81. Calderone, V., et al., *Angew. Chem. Int. Ed.*, 2006. **45**: p. 1267-1269.
82. Peleg-Shulman, T., Y. Najajreh, and D. Gibson, *J. Inorg. Biochem.*, 2002. **91**: p. 306-311.
83. Ivanov, A.I., et al., *J. Biol. Chem.*, 1998. **273**: p. 14721-14730.
84. Esposito, P.B. and R. Najjar, *Coord. Chem. Rev.*, 2002. **232**: p. 137-149.
85. Hu, W., et al., *Chem. Comm.*, 2011. **47**: p. 6006-6008.
86. Mandal, R., R. Kalke, and X.F. Li, *Chem. Res. Toxicol.*, 2004. **17**: p. 1391-1397.
87. Sun, H., H. Li, and P.J. Salder, *Chem. Rev.*, 1999. **99**: p. 2817-2842.
88. Piccioli, F., et al., *J. Inorg. Biochem.*, 2004. **98**: p. 1135-1142.
89. Allardyce, C.S., et al., *Rapid Commun. Mass Spectrom.*, 2002. **16**: p. 933-935.
90. Cassini, A., et al., *Chem. Comm.*, 2007: p. 156-158.
91. Sze, C.M., et al., *J. Biol. Inorg. Chem.*, 2009. **14**: p. 163-165.
92. Hartinger, C.G., et al., *J. Inorg. Biochem.*, 2006. **100**: p. 891-904.
93. Rademaker-Lakhai, J.M., et al., *Clin. Cancer Res.*, 2004. **10**: p. 3717-3727.
94. Heetebrij, R.J., et al., *ChemBioChem*, 2003. **4**: p. 573-583.
95. Molenaar, C., et al., *J. Biol. Inorg. Chem.*, 2000. **5**: p. 655.
96. Kalayda, G.V., et al., *J. Biol. Inorg. Chem.*, 2004. **9**: p. 414.
97. Kalayda, G.V., et al., *J. Biol. Inorg. Chem.*, 2005. **10**: p. 305.
98. Jansen, B.A., et al., *J. Biol. Inorg. Chem.*, 2004. **9**: p. 414.
99. Galal, S.A., et al., *Eur. J. Med. Chem.*, 2009. **44**: p. 1500-1508.
100. Gümüş, F. and Ö. Algül, *J. Inorg. Biochem.*, 1997. **68**: p. 71-74.
101. Gümüş, F., et al., *Eur. J. Med. Chem.*, 2003. **38**: p. 473 - 480.
102. Gümüş, F., et al., *Pharm. Sci.*, 1996. **21**: p. 7-15.
103. Gümüş, F., et al., *Inorg. Biochem.*, 2003. **94**: p. 255 - 262.
104. Gökçe, M., et al., *Eur. J. Med. Chem.*, 2005. **40**: p. 135- 141.
105. Wisniewski, M.Z., et al., *Metal Based Drugs*, 2001. **8**(4): p. 189-194.
106. Ivanova, B.B. and L.I. Pindeva, *J. Mol. Struct.*, 2006. **797**: p. 144-153.
107. Gümüş, F., et al., *J. Med. Chem.*, 2009. **52**: p. 1345-1357.
108. Hall, M.D., et al., *Annu. Rev. Pharmacol. Toxicol.*, 2008. **48**: p. 495.

109. Hrubiko, M., A.T. McGown, and B.W. Fox, *Biochem. Pharmacol.*, 1993. **45**: p. 253.
110. Rabik, C.A. and M.E. Dolan, *Treatment Rev.*, 2007. **33**: p. 9.
111. Balendiran, G.K., R. Dabur, and D. Fraser, *Cell Biochem. Funct.*, 2004. **22**: p. 343-352.
112. Atwood, J.D., *Inorganic and organometallic reaction mechanisms*. 2 ed. 1997, New York, NY: VCH Publishers Inc.
113. Sliwa, w. and M. Deska, *Collect. Czech. Chem. Commun.*, 1999. **64**: p. 435-458.
114. Watt, G.W., L.K. Thompson, and A.J. Pappas, *Inorg. Chem.*, 1972. **11**(4): p. 747-749.
115. Marzilli, L.G., Y. Hayden, and M.D. Reily, *Inorg. Chem.*, 1986. **25**: p. 974-978.
116. Chval, Z., M. Sip, and J. Burda, *J. Comput Chem*, 2008. **29**(14): p. 2370-81.
117. Basolo, F. and R.G. Pearson, *Mechanisms of Inorganic reactions*, . 2 ed. 1968, New York, NY: John Wiley & Sons Inc.
118. Wilkins, R.J., *The study of kinetics and mechanisms of reactions of transition metal complexes*. 1974, Boston, NJ: Allyn and Bacon Inc.,.
119. Langford, C.H. and H.B. Gray, *Ligand Substitution Processes*. 1965, New York, NY: W. A. Benjamin Inc., .
120. Tobe, M.L., *Inorganic Reaction Mechanisms* 1972, London: Nelson Inc.
121. Wang, J.H., *J. Am. Chem. Soc.*, 1958, **80**, 3168. **80**: p. 3168.
122. Ochiai, E.I., *Bioinorganic Chemistry*. Vol. 1. 1977: Allyn and Bacon, Boston.
123. Meyer, T.E. and M.D.K. . *Adv. Protein Chem.*, 1982. **35**: p. 105.
124. Moore, G.R., C.G.S. Eley, and G. Williams, *Adv. Inorg. Bioinorg. Mech.*, 1984. **3**: p. 1.
125. Groves, J.T., *J. Chem. Educ.*, 1988. **11**: p. 928.
126. Rastogi, R. and S. Satyavan, *Synthesis*, , 1983: p. 861-882.
127. Gottlieb, H.E., V. Kotlyar, and A. Nudelman, *J. Org. Chem.*, 1997. **62**(21): p. 7512-7515.
128. Simonov, A.M. and N.D. Vitkevich, *Zhurnal Obshchei Khimii*, 1960. **30**: p. 590-592.
129. Takahashi, S. and H. Kano, *Tetrahedron Letters*, 1963. **25**: p. 1687-1691.
130. Khristich, B.I., A.M. Simonov, and G.M. Suvorova, *Khimiya Geterotsiklicheskih Soedinenii*, . 1973. **9**: p. 1293.
131. Sheinker, Y.N., et al., *Zhurnal Obshchei Khimii*, 1966. **2**: p. 917-924.
132. Mondelli, R. and L. Merlini, *Tetrahedron*, 1966. **22**: p. 3253-3273.
133. Sokol, V.I., et al., *Russian Journal of Inorganic Chemistry*, 1989. **34**: p. 1470-1475.
134. Gilli, G., et al., *J. Am. Chem. Soc.*, 1989. **111**: p. 1023-1028.
135. Bertolasi, V., et al., *J. Am. Chem. Soc.*, 1991 **113**: p. 4917-4925.
136. Nonoyama, M., S. Tomita, and K. Yamasaki, *Inorg. Chim. Acta*, 1975. **12**: p. 33-37.
137. Scheller-Krattiger, V., et al., *Inorg. Chim. Acta*, , 1982. **60**: p. 45-52.
138. Garnovskii, D.A., et al., *Koord. Khim.*, 1988. **14**(3): p. 299-306.
139. Knoch, R., H. Elias, and H. Paulusi, *Inorg. Chem.*, 1995. **34**: p. 4032-4040.
140. Nejo, A.A., et al., *J. of Coordination Chemistry*, 2010. **63**(24): p. 4367- 4379.
141. Schumann, M. and H. Elias, *Inorg. Chem.*, 1985. **24**: p. 3187-3192

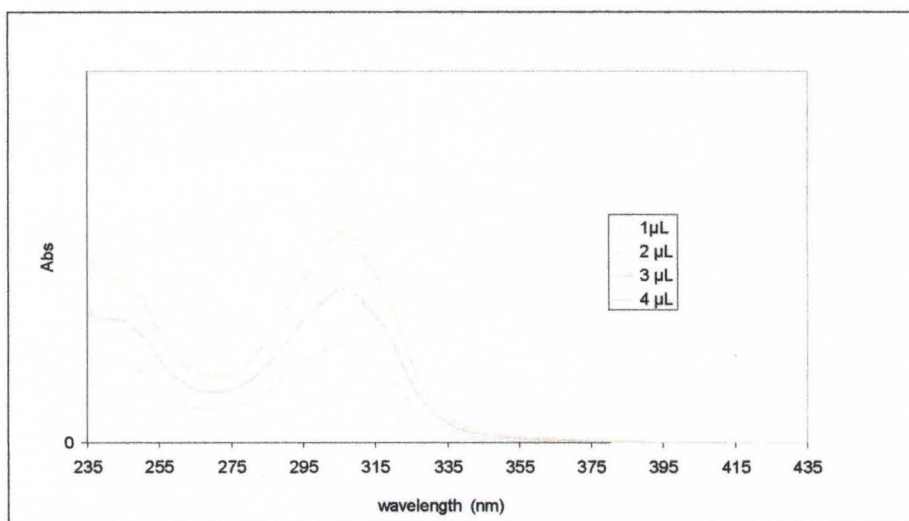
142. Schumann, M., et al., *Inorg. Chem.*, 1982. **21**: p. 606-612.
143. Sun, M.S., F. Grein, and D.G. Brewer, *Canadian Journal of Chemistry* 1972. **50**: p. 2626-2638.
144. Straws, M.J. and H. Schran, *J. Am. Chem. Soc.*, 1969. **91**: p. 3976-3978.
145. Janiak, C., *J. Chem. Soc., Dalton Trans.*, 2000: p. 3885–3896.
146. Antsyshkina, A.S., et al., *Russian Journal of Coordination Chemistry*, 2000. **26**(10): p. 730-740.
147. Addison, A.W. and T.N. Rao, *J. Chem. Soc. Dalton Trans.*, 1984: p. 1349-1356.
148. Garnovskii, e.a., *Journal of Academy of Sciences*, 1987. **296**(5): p. 1119-1121.
149. Antsyshkina, A.S., et al., *Koord. Khim.*, 1987. **13**(10): p. 1422.
150. Palm, M.E., et al., *PNAS*, 2011. **108**(17): p. 6951-6956.
151. Perez, J.M., C. Alonso, and M. Fuertes, *Chem. Rev.*, 2003. **103**(3): p. 645-660.
152. Jung, Y. and S.J. Lippard, *Chem. Rev.*, 2007. **107**(5): p. 1387-1407.
153. Lippard, S., R. Todd, and K. Lovejoy, *J. Am. Chem. Soc.*, 2007. **129**(20): p. 6370-6371.
154. Aller, S.G., et al., *Science*, 2009. **323**: p. 1718-1722.
155. Huang, Y., *Cancer Metastasis Rev.*, 2007. **26**: p. 183-201.
156. Akaboshi, M., et al., *Jpn. J. Cancer Res.*, 1992. **83**: p. 522.
157. Akaboshi, M., et al., *Jpn. J. Cancer Res.*, 1994. **85**: p. 106.
158. Jordan, P. and M. Carmo-Forseca, *Cell. Mol. Life Sci*, 2000. **57**: p. 1229.
159. Rivera, F., M.E. Vega-Villegas, and M.F. López-Brea, *Cancer Treatment Reviews*, 2007. **33**: p. 315-324.
160. Haake, P. and S.H. Mastin, *J. Am. Chem. Soc.*, 1971. **93**(25): p. 6823-8.
161. T.B. Tam, et al., *J. Chem. Soc. Dalton Trans.*, 1990: p. 1251-5.
162. Tessier, C. and F.D. Rochon, *Inorg. Chim. Acta*, 2001. **322**: p. 37-46.
163. Kato, M. and M. Ikemori, *Acta Cryst.*, 2003, . **C59**: p. m25- m26.
164. Kelland, L.R., *Drugs*, 2000. **59** (Suppl. 4): p. 1.
165. Coley, H.M., J. Sarju, and G. Wagner, *J. Med. Chem.*, 2008. **51**: p. 135-141.
166. El-Naema, S.I., et al., *Arch. Pharm. Pharm. Med. Chem.*, 2003. **1**: p. 7-17.
167. Ramla, M.M., et al., *Bioorganic & Medicinal Chem.*, 2007. **15**: p. 6489-6496.
168. Khan, M.N., *J. Org. Chem.*, 1995. **60**: p. 4536.
169. Kukolja, S. and S.R. Lammert, *J. Am. Chem. Soc.*, 1975, . **97**: p. 5582.
170. Osby, J.O., M.G. Martin, and B. Ganem, *Tetrahedron Lett.*, 1984. **25**: p. 2093.
171. Wolfe, S. and S.K. Hasan, *Can. J. Chem.*, 1970. **48**: p. 3572.

## APPENDIX

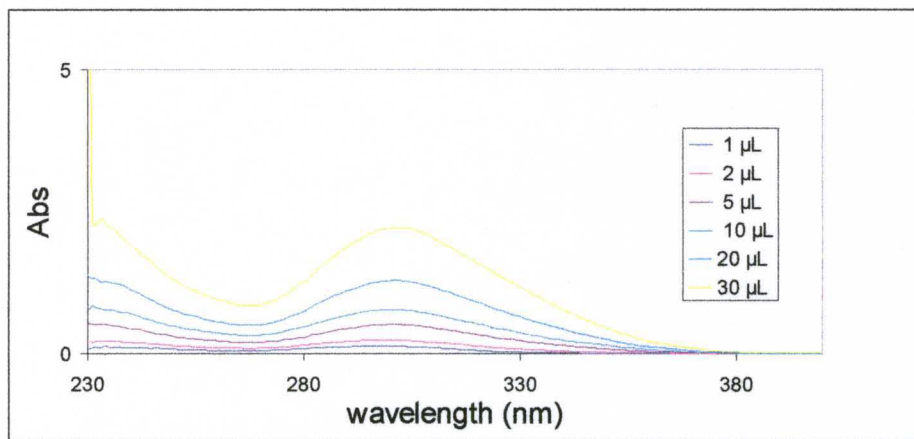
### UV-vis of Selected Compounds



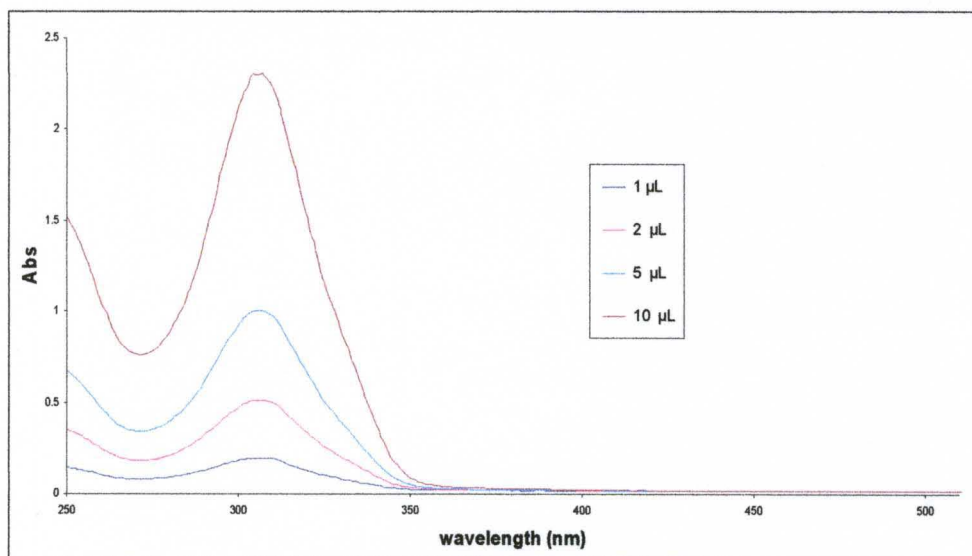
UV-vis absorption trace of compound 16 in 3 mL CH<sub>2</sub>Cl<sub>2</sub>.



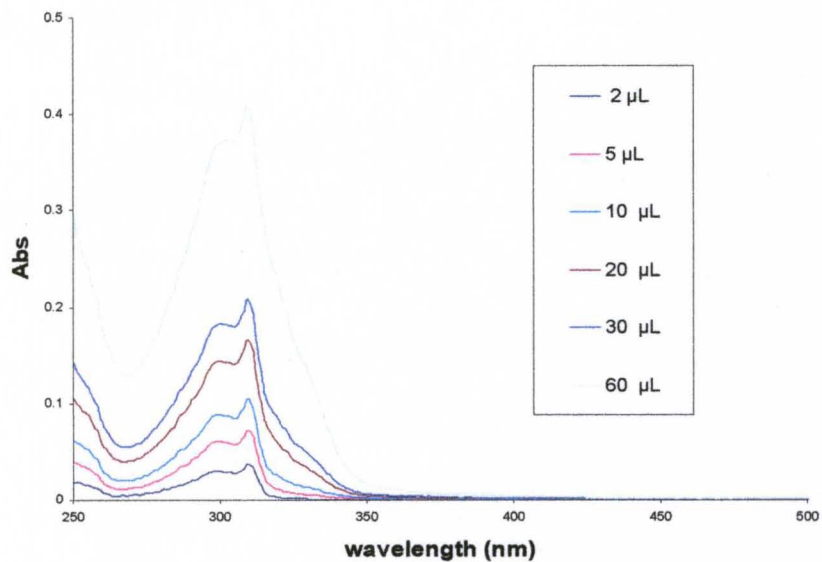
UV-vis absorption trace of compound 17 in 3 mL CH<sub>2</sub>Cl<sub>2</sub>.



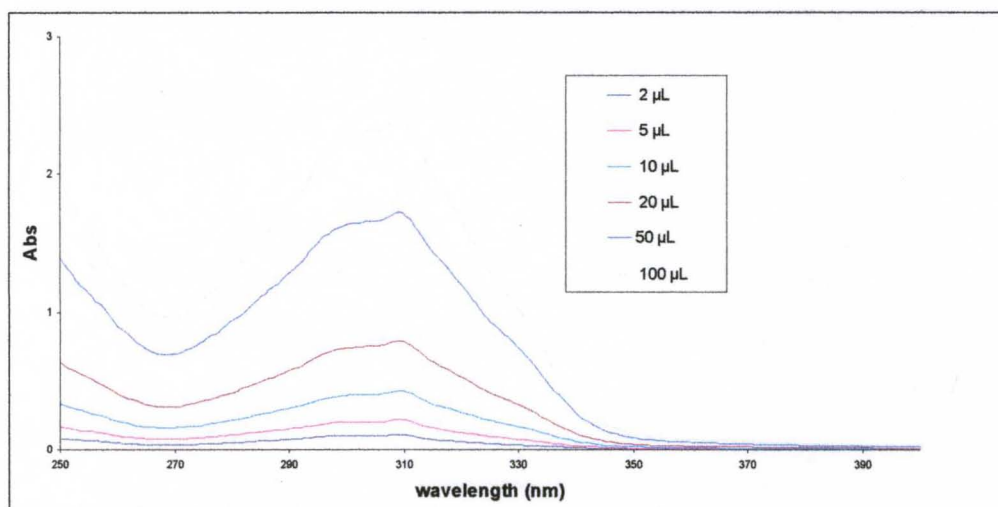
**UV-vis absorption trace of compound 18 in 3 mL CH<sub>2</sub>Cl<sub>2</sub>.**



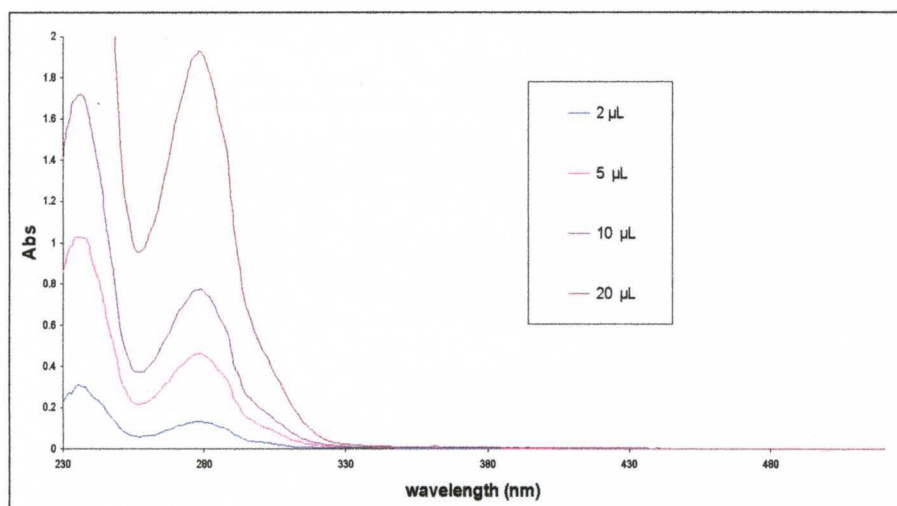
**UV-vis absorption trace of compound 19 in 3 mL CH<sub>2</sub>Cl<sub>2</sub>.**



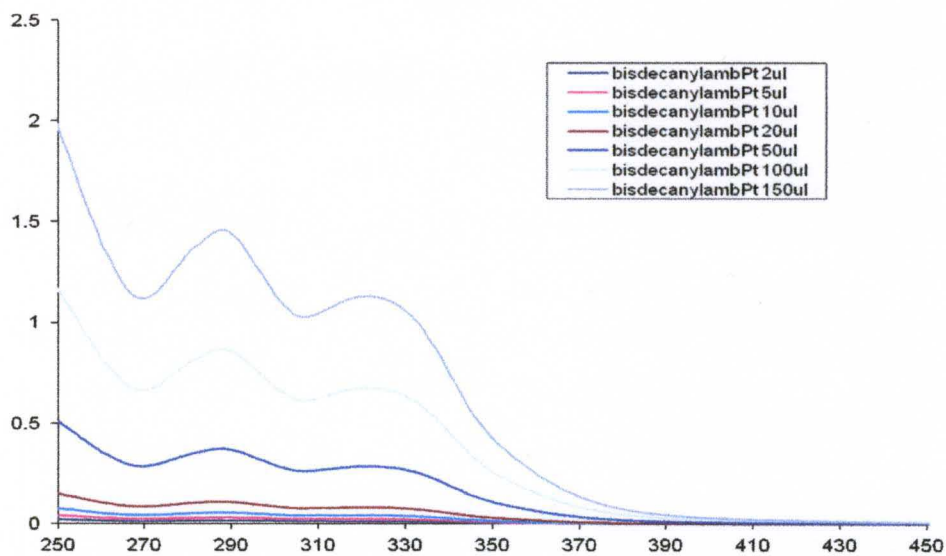
**UV-vis absorption trace of compound 20 in 3 mL CH<sub>2</sub>Cl<sub>2</sub>**



**UV-vis absorption trace of compound 21 in 3 mL CH<sub>2</sub>Cl<sub>2</sub>**

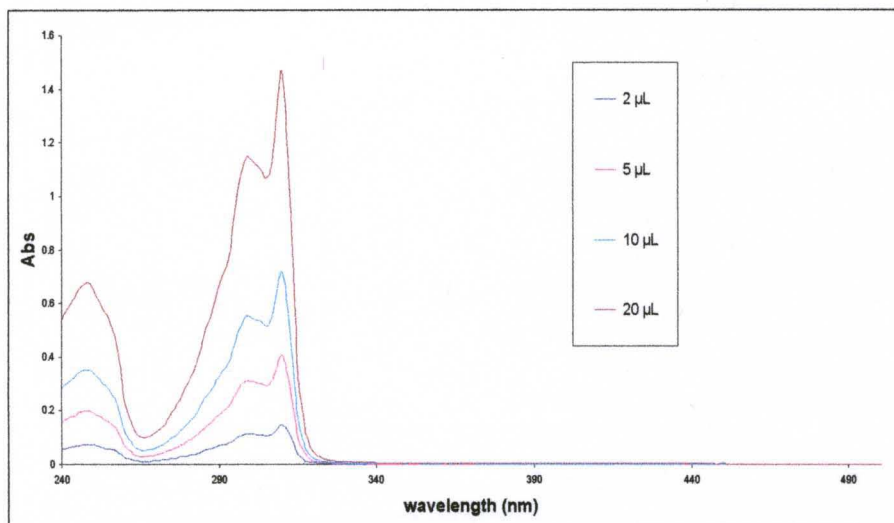


**UV-vis absorption trace of compound 24 in 3 mL CH<sub>2</sub>Cl<sub>2</sub>**

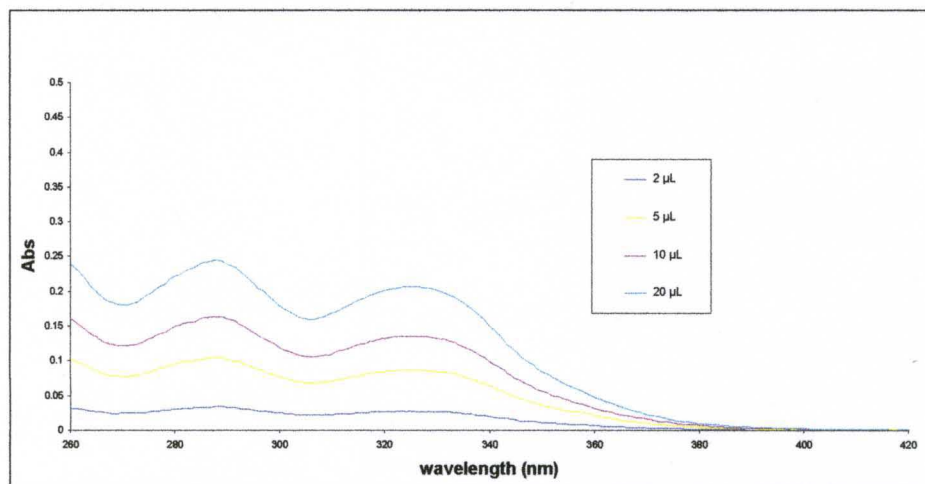


**UV-vis absorption trace of compound 30 in 3 mL CH<sub>2</sub>Cl<sub>2</sub>**

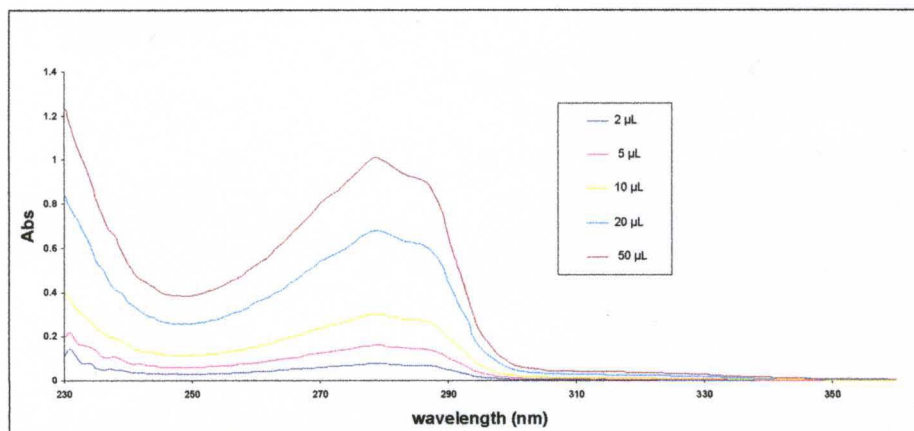




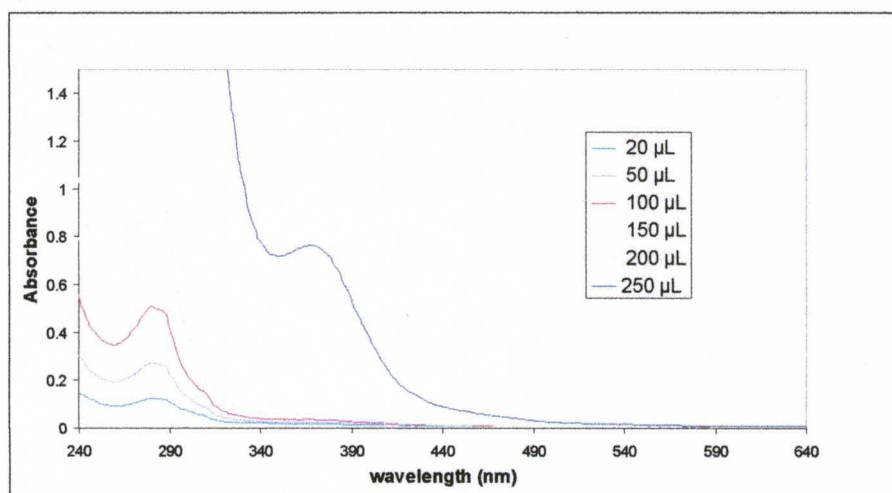
**UV-vis absorption trace of compound 31 in 3 mL CH<sub>2</sub>Cl<sub>2</sub>**



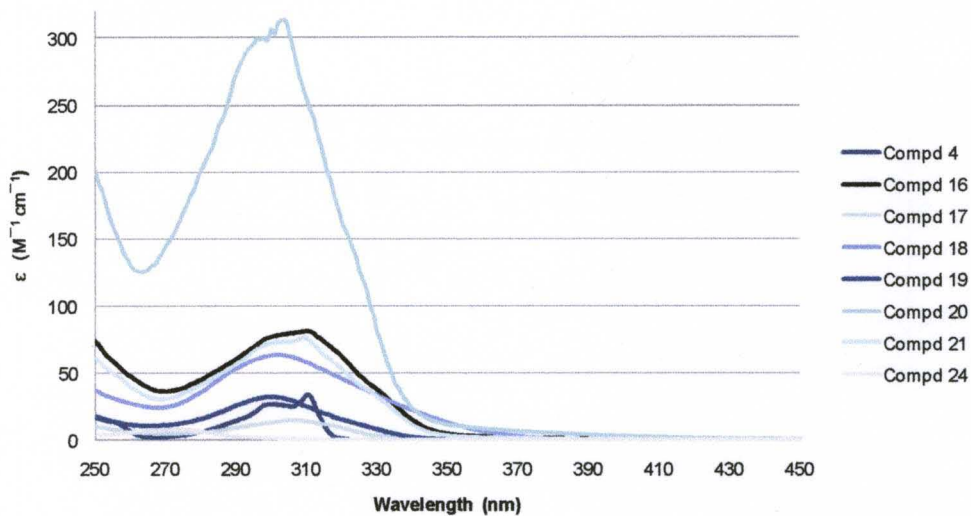
**UV-vis absorption trace of compound 32 in 3 mL CH<sub>2</sub>Cl<sub>2</sub>**



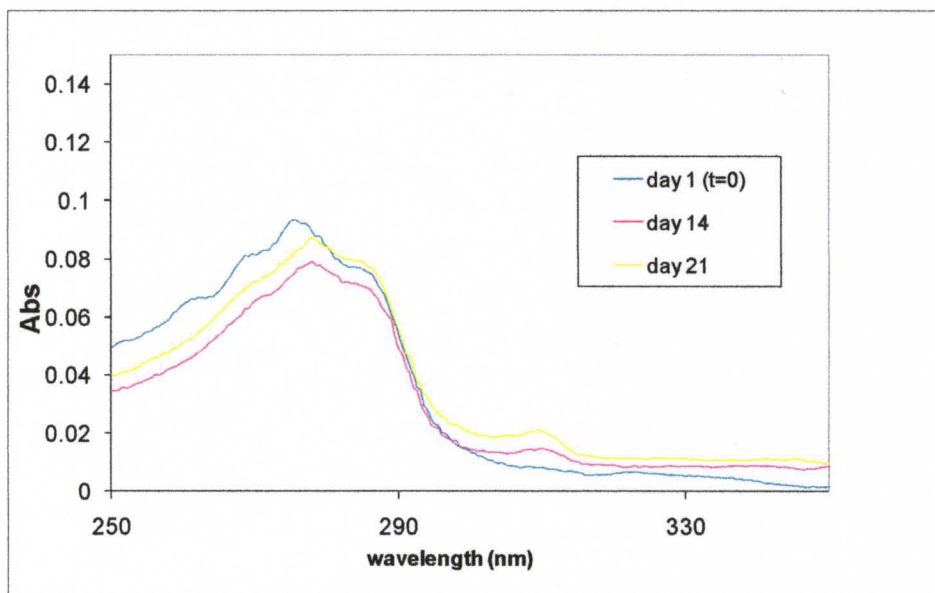
UV-vis absorption trace of compound 33 in 3 mL CH<sub>2</sub>Cl<sub>2</sub>



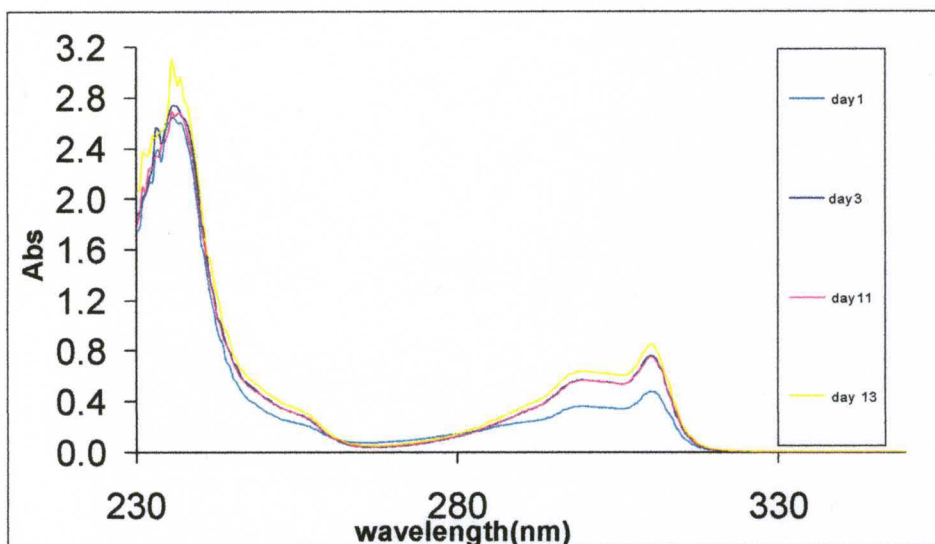
UV-vis absorption trace of compound 34 in 3 mL CH<sub>2</sub>Cl<sub>2</sub>



**UV-vis absorption trace of selected compounds in 3 mL CH<sub>2</sub>Cl<sub>2</sub>**

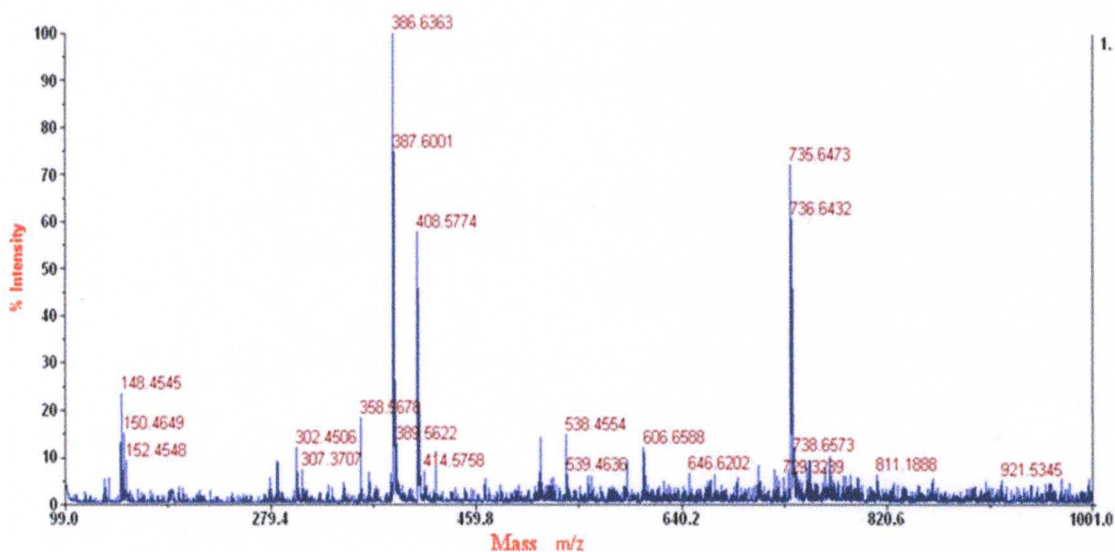


**UV-vis spectrum of GSH and compound 37 in anh. Dichloromethane showing the appearance of a new  $\lambda_{\text{max}}$  at 310 nm with time.**

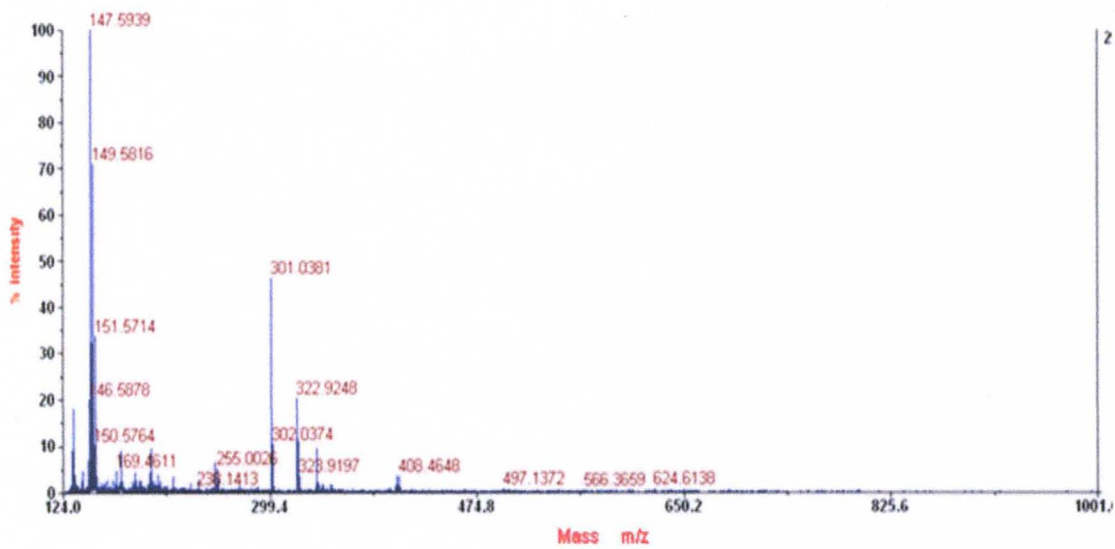


UV-vis spectrum of GSH and compound 37 reaction in 20% water/ 80%  
DMSO solution. A new  $\lambda_{\text{max}}$  appears at 310 nm with time.

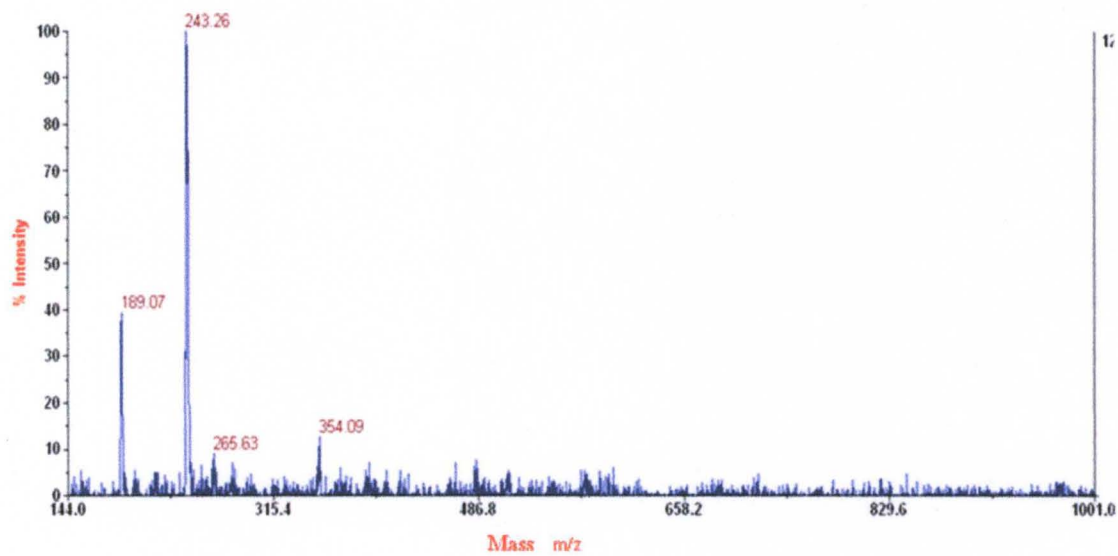
**Mass Spectrometric Traces :**



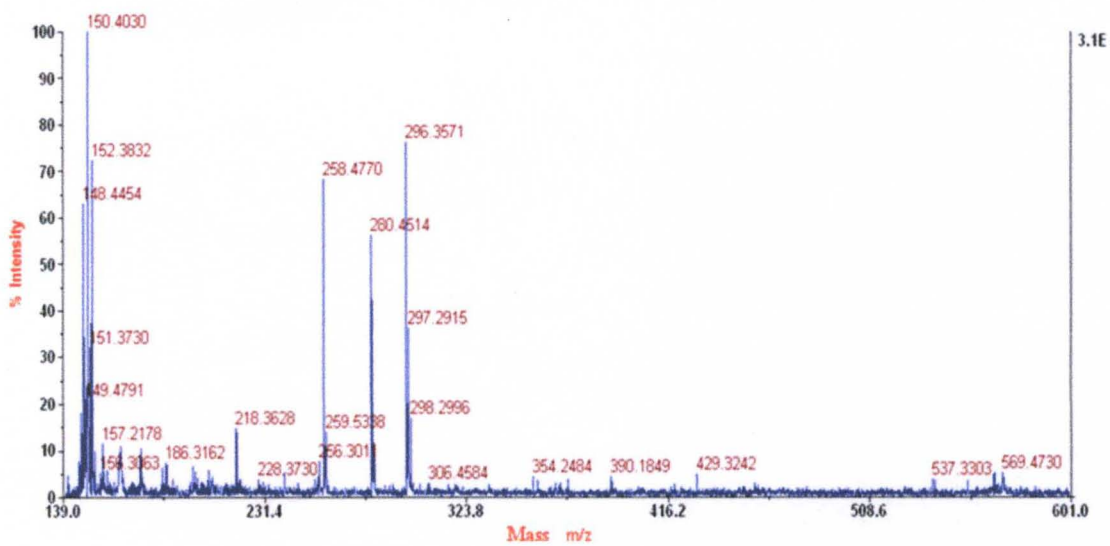
Mass spectrometric trace of **Compound 1**



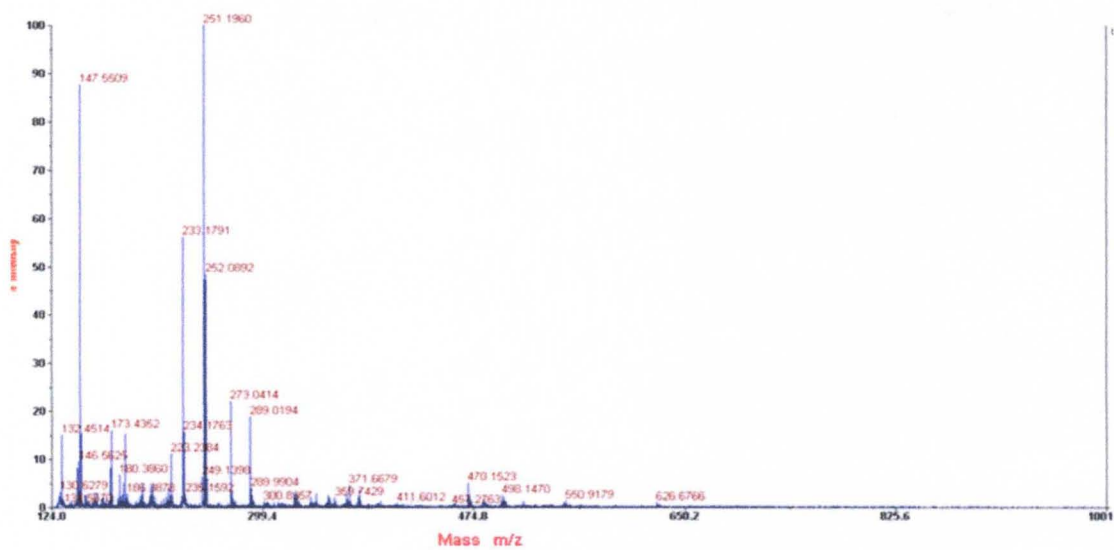
Mass spectrometric trace of **Compound 2**



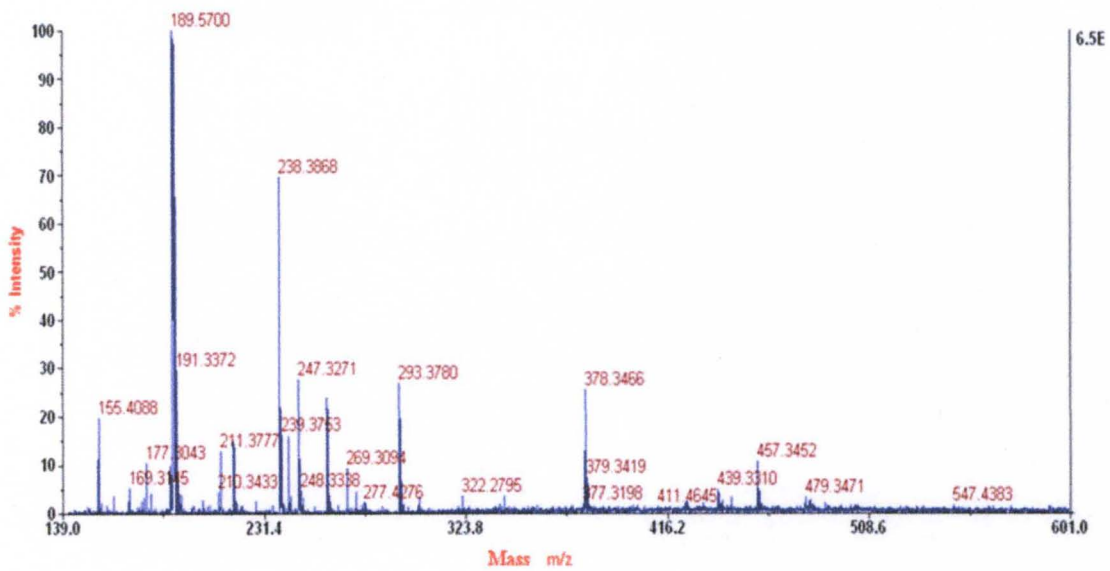
Mass spectrometric trace of **Compound 3**



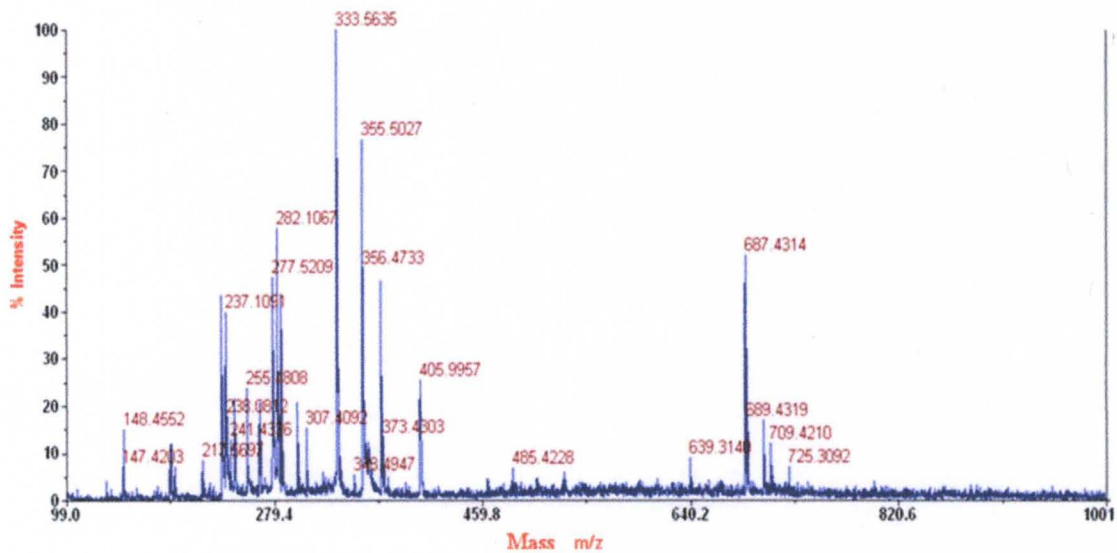
Mass spectrometric trace of **Compound 4**



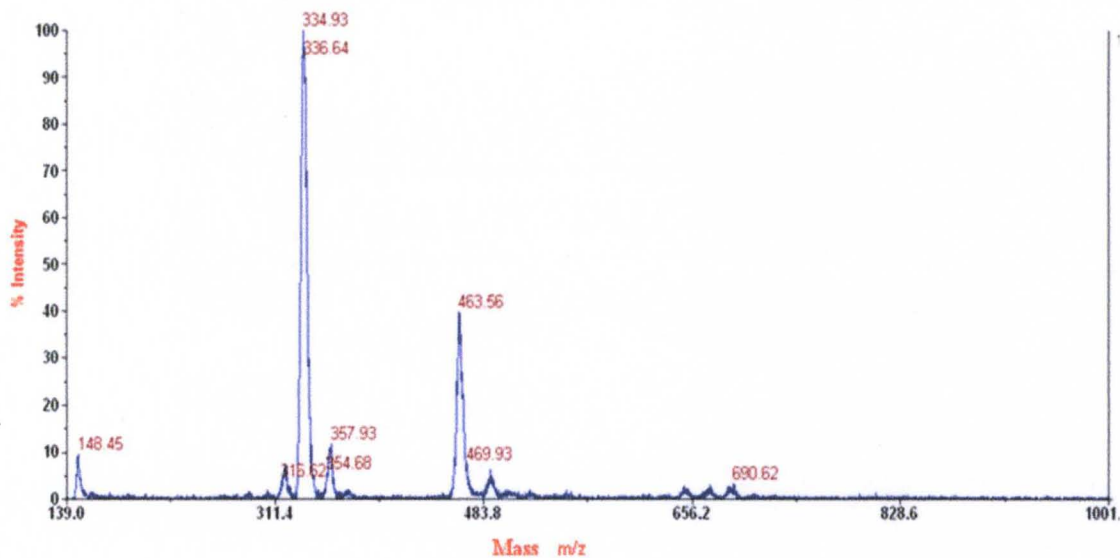
Mass spectrometric trace of **Compound 5**



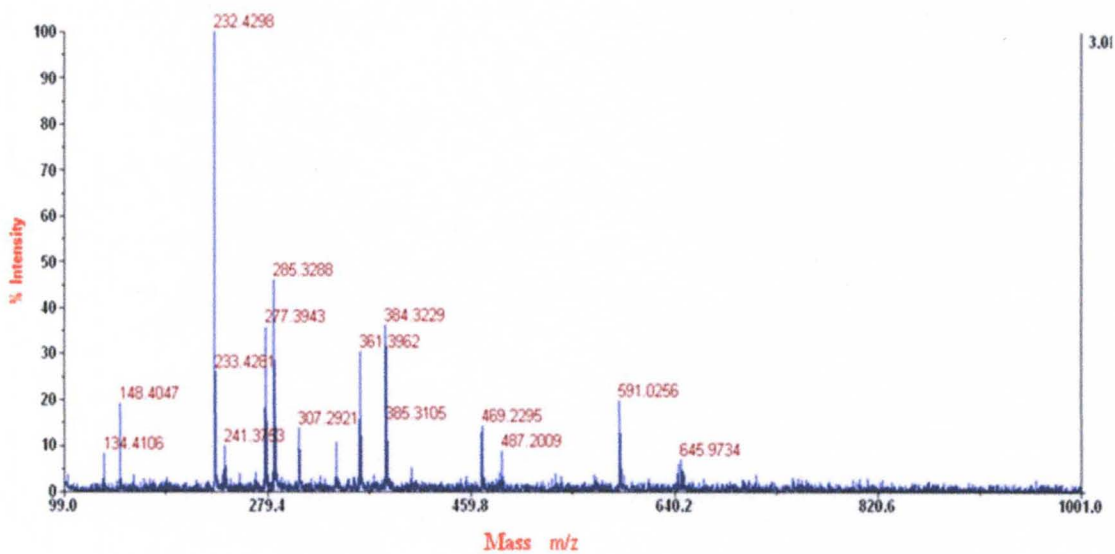
Mass spectrometric trace of **Compound 6**



Mass spectrometric trace of **compound 7**

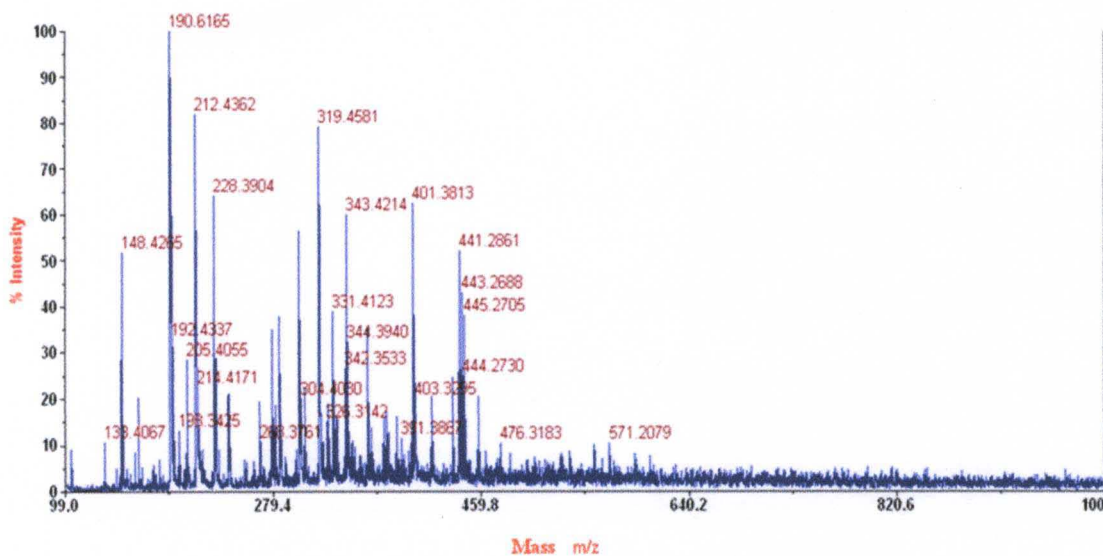


Mass spectrometric trace of **compound 8**

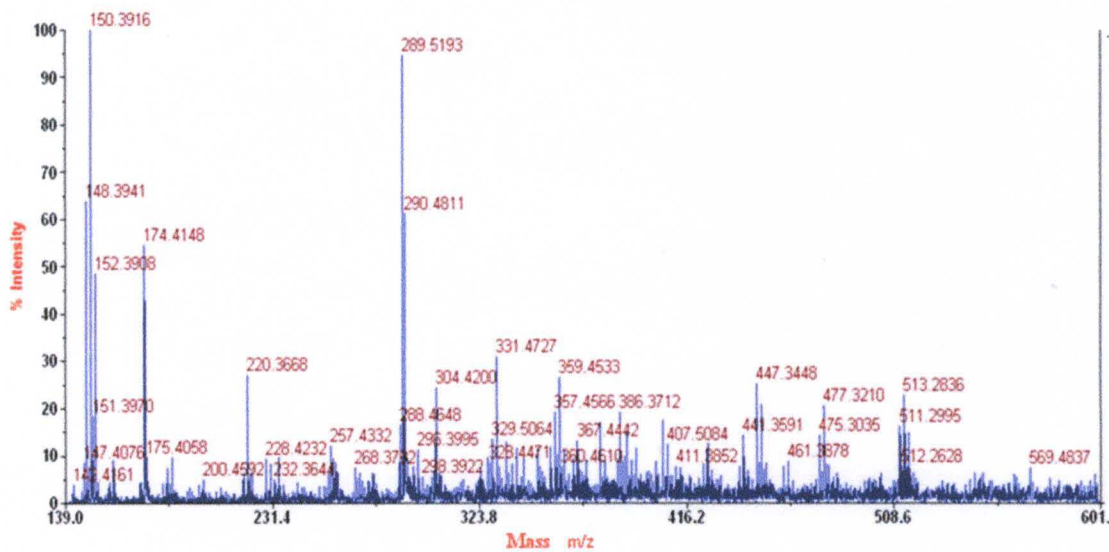


Mass spectrometric trace of **compound 9**

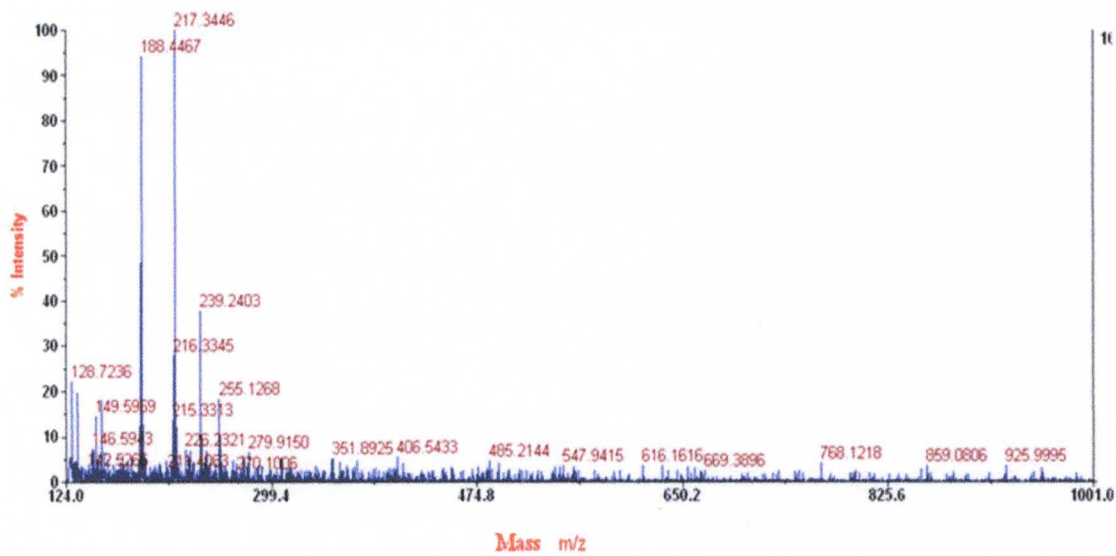




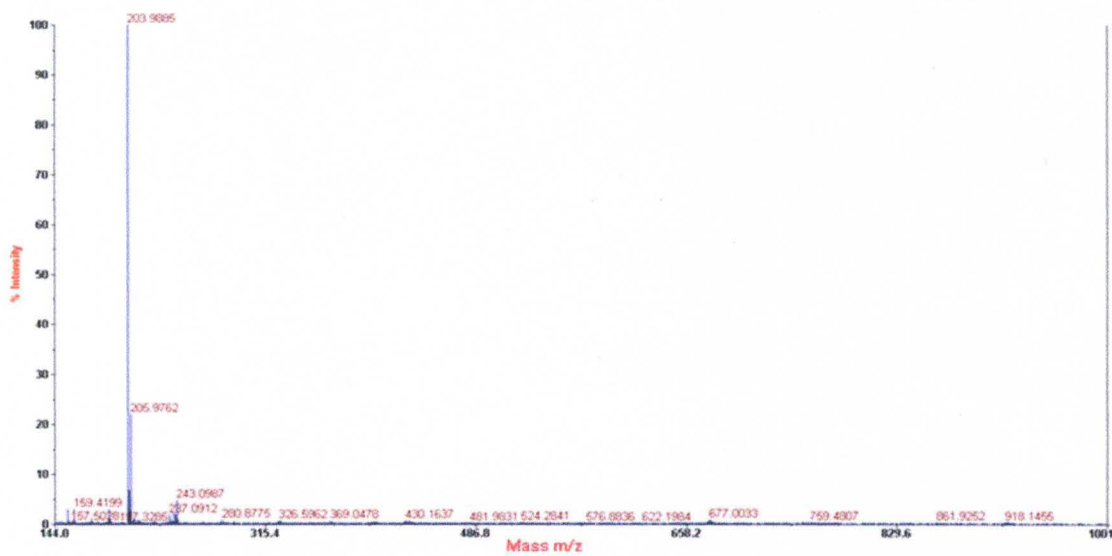
Mass spectrometric trace of **compound 10**



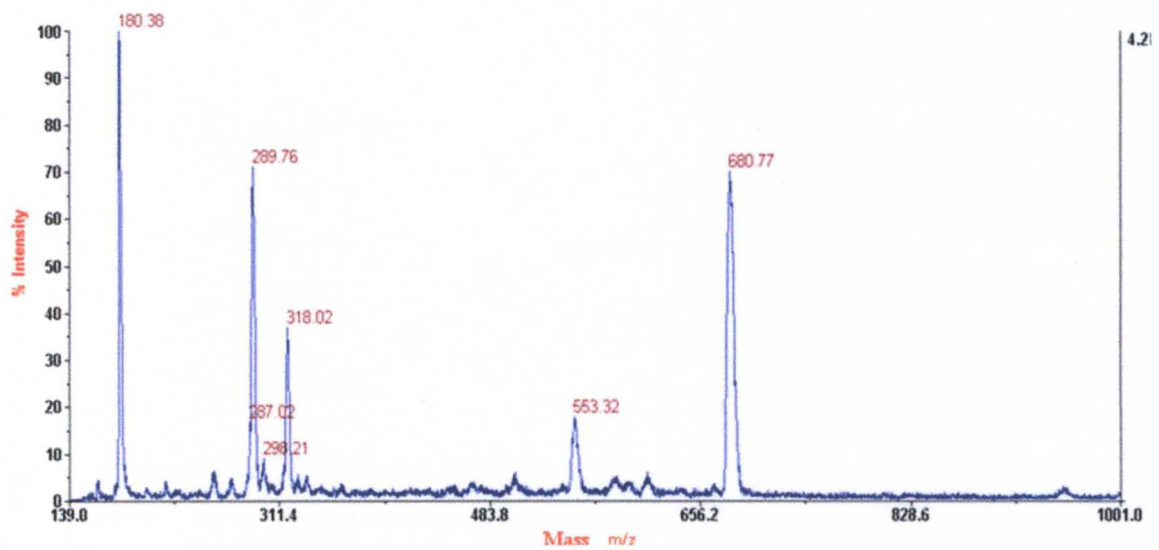
Mass spectrometric trace of **compound 11**



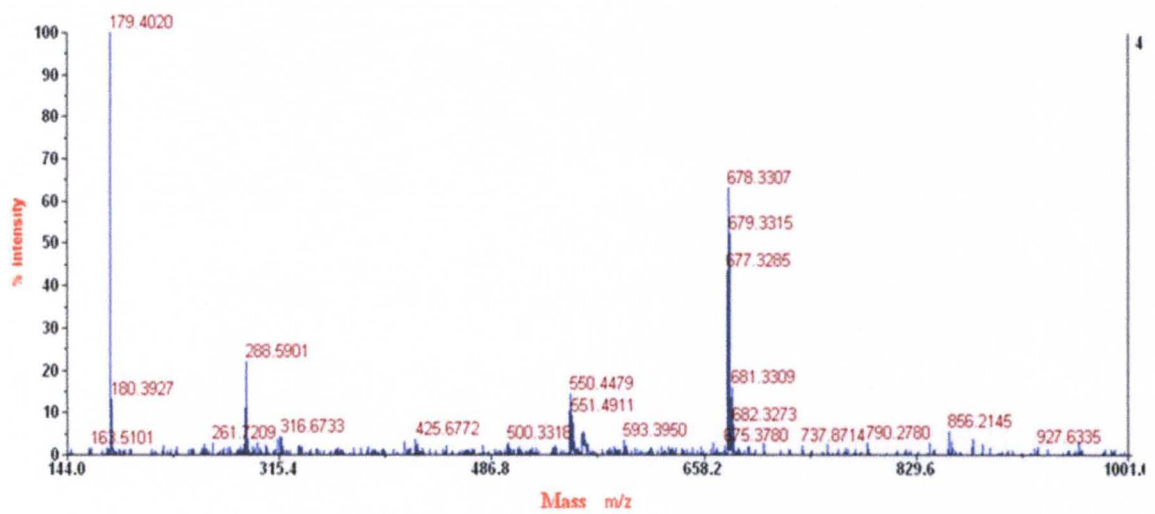
Mass spectrometric trace of **compound 12**



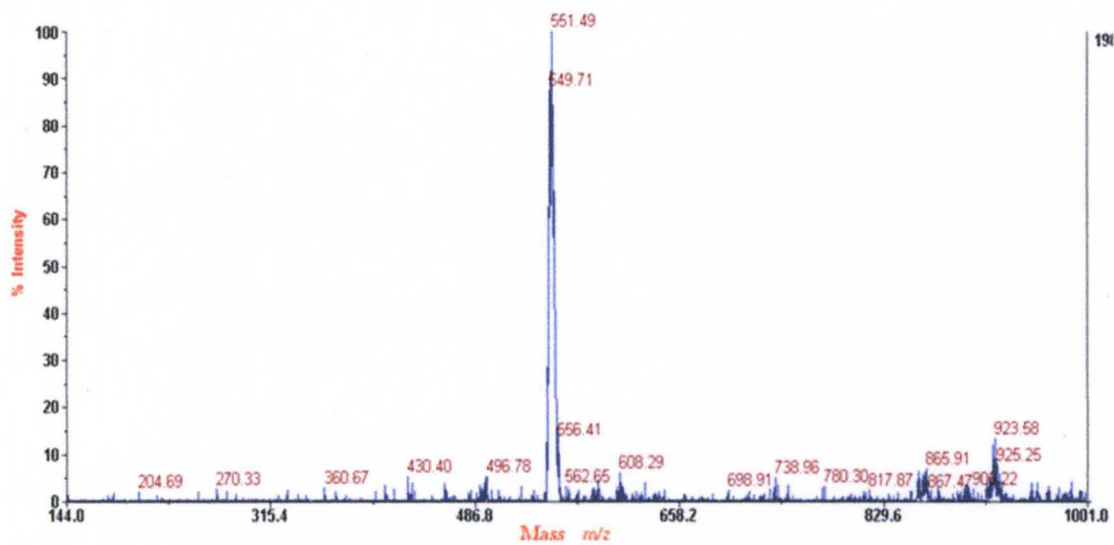
Mass spectrometric trace of **compound 13**



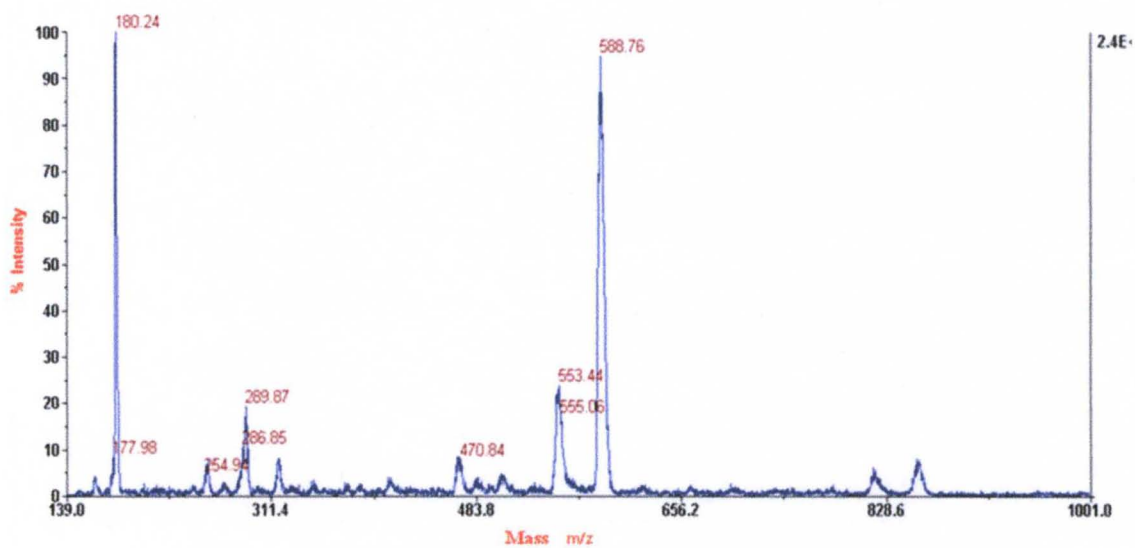
Mass spectrometric trace of **compound 25**



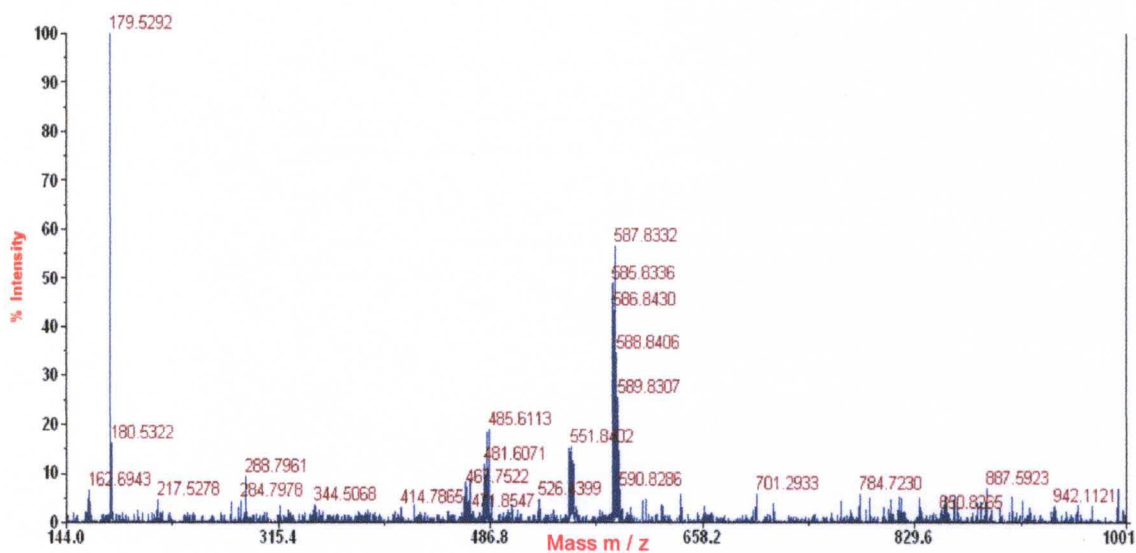
Mass spectrometric trace of **compound 26**



Mass spectrometric trace of **compound 27**

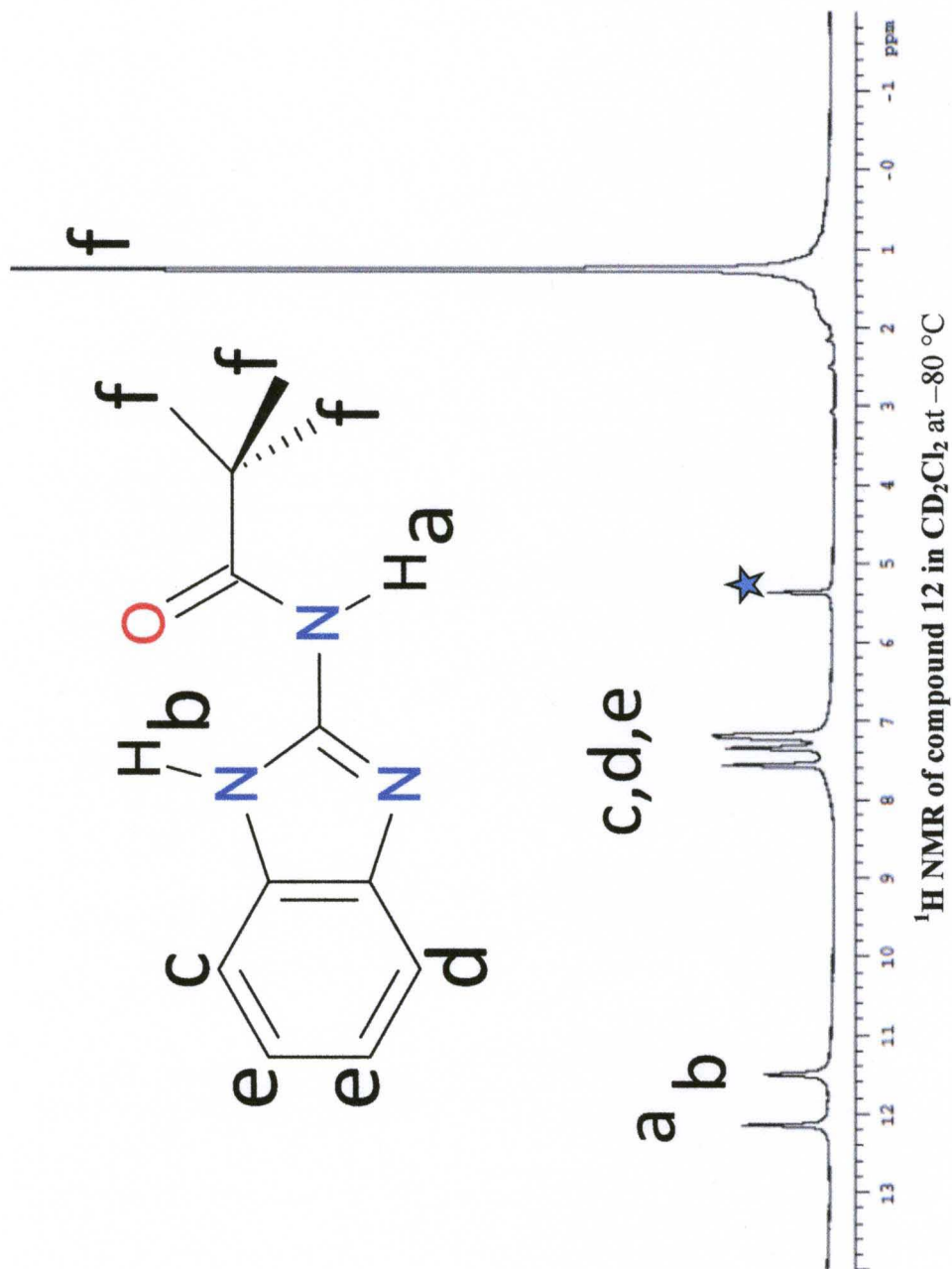


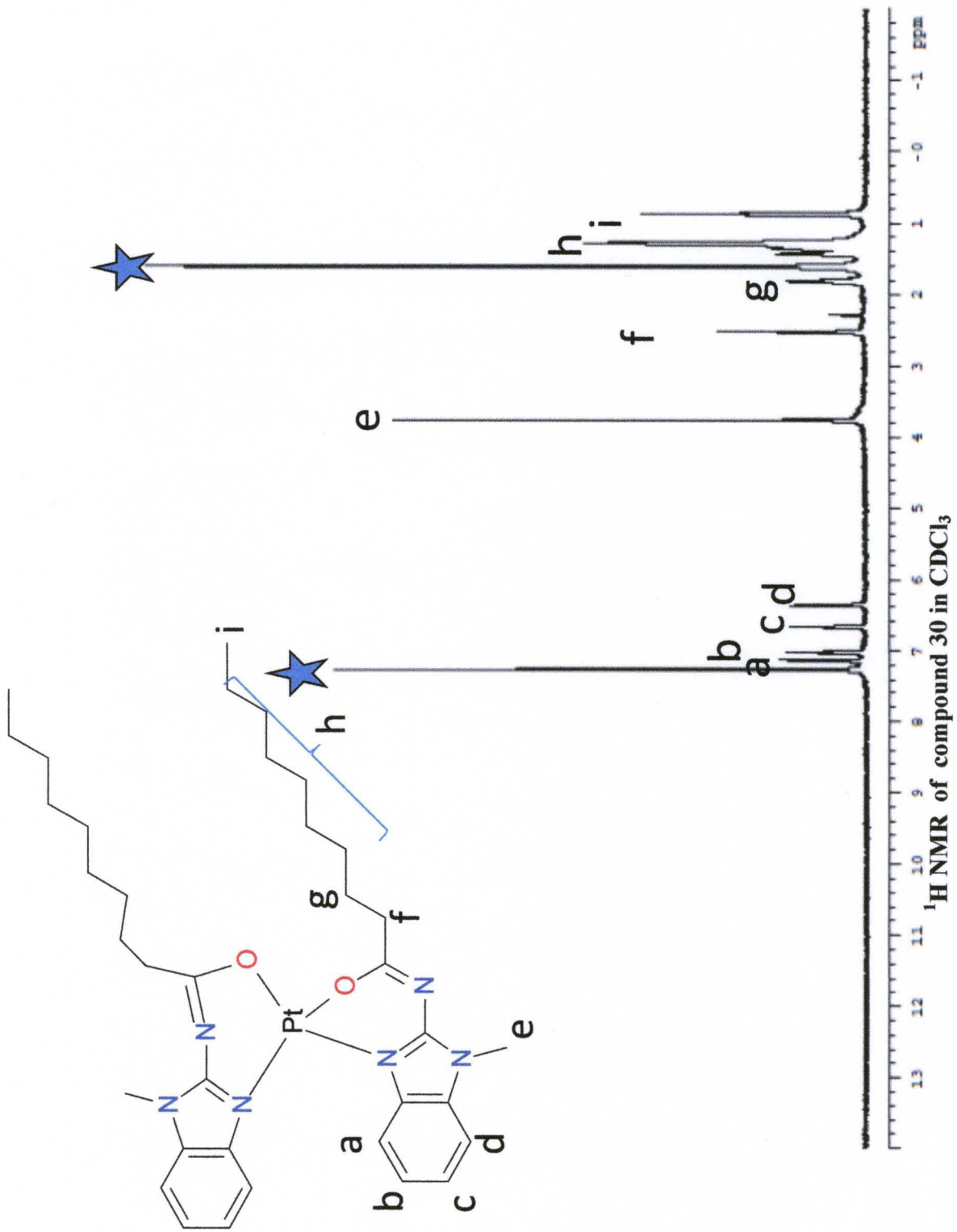
Mass spectrometric trace of **compound 28**

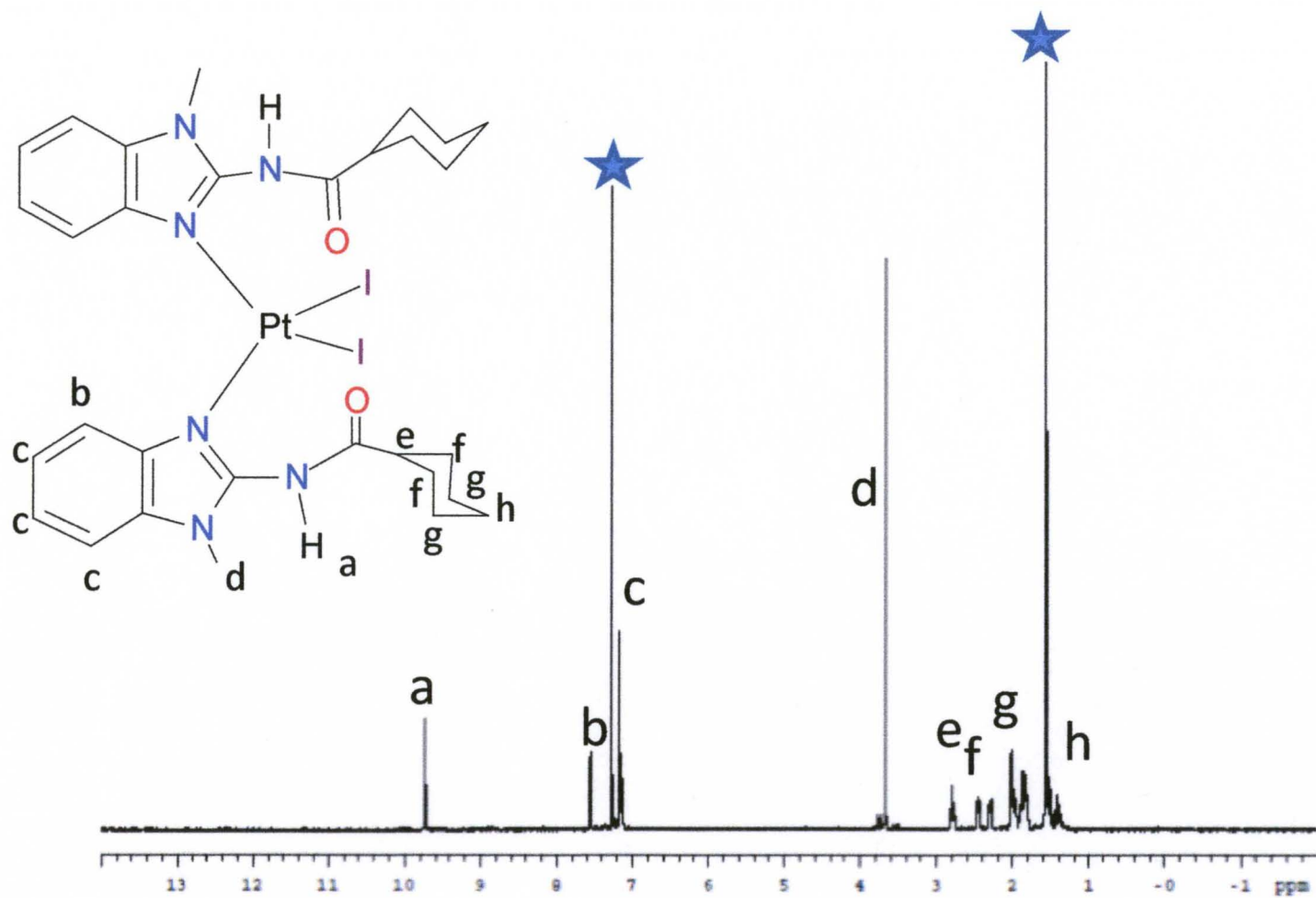


Mass spectrometric trace of **compound 29**

# $^1\text{H}$ NMR and $^{13}\text{C}$ NMR Spectra

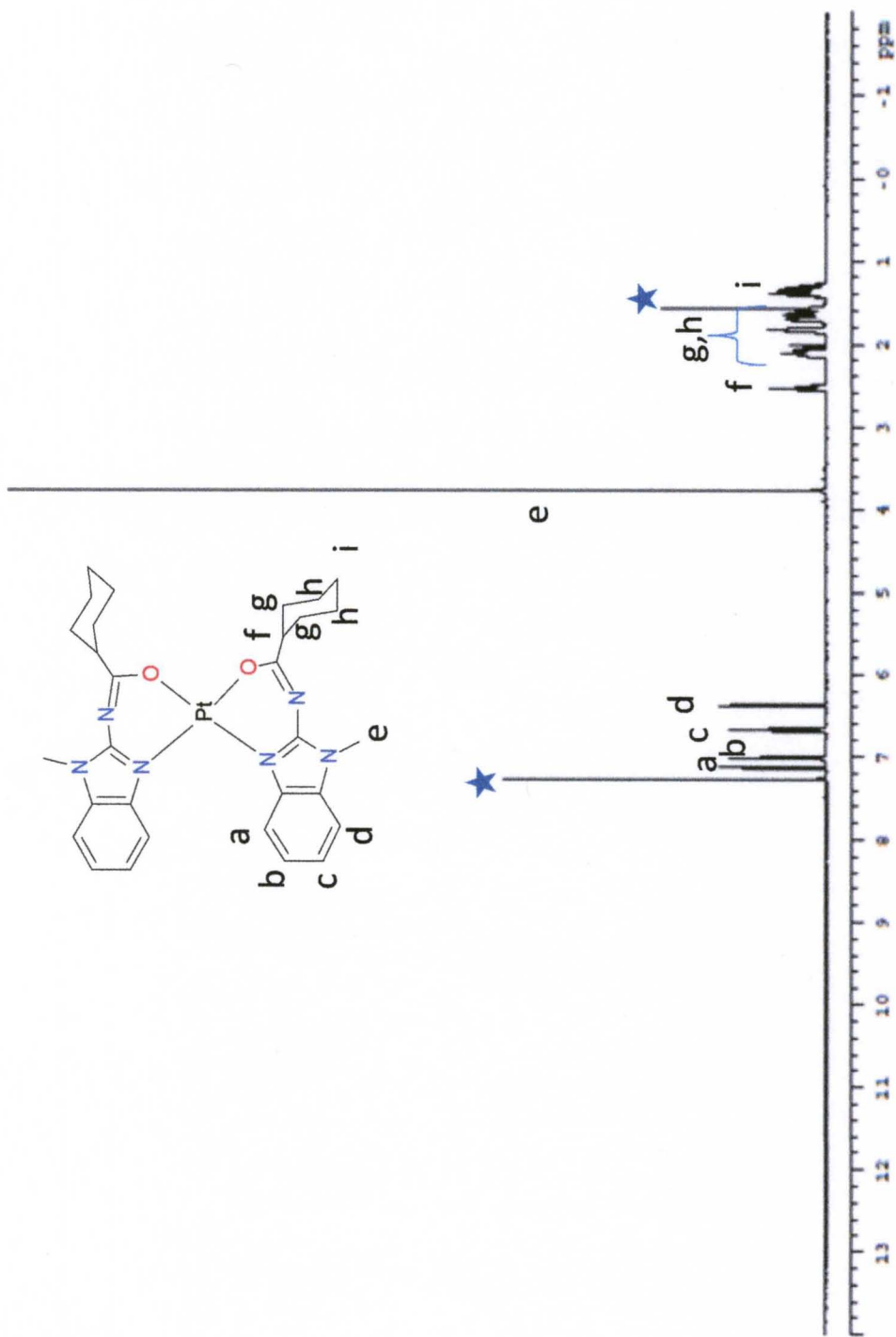




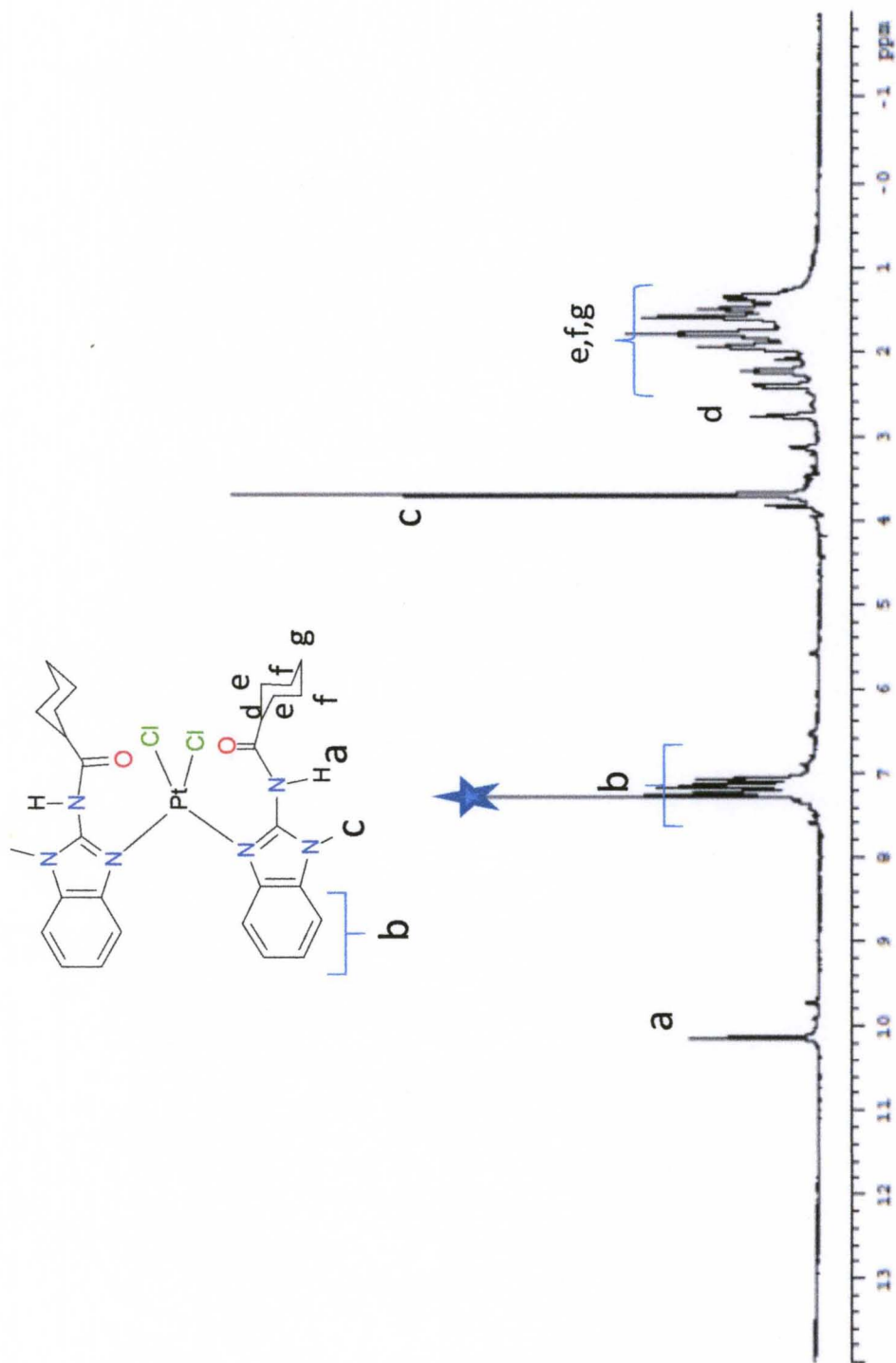


$^1\text{H}$  NMR of compound 31 in  $\text{CDCl}_3$

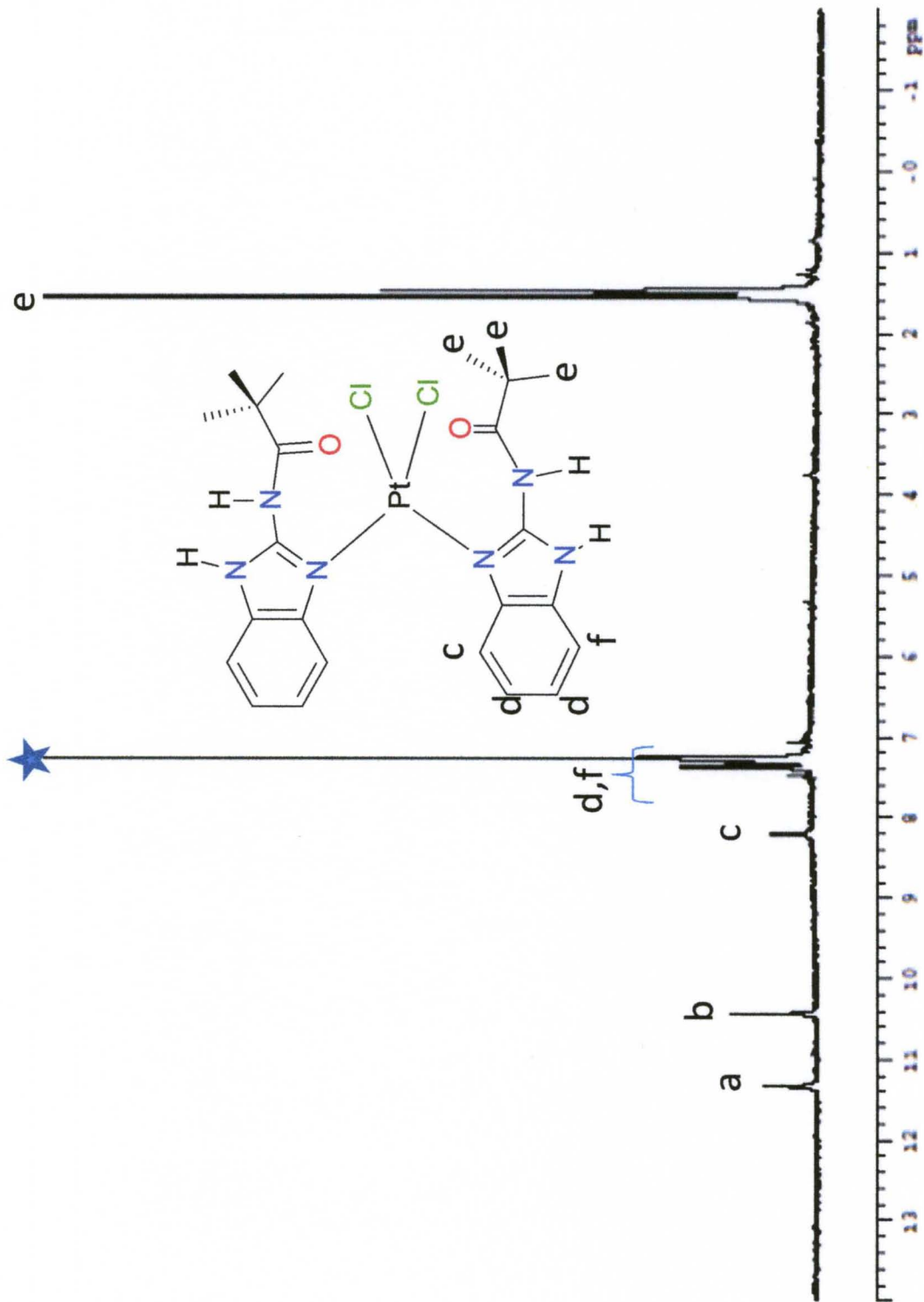




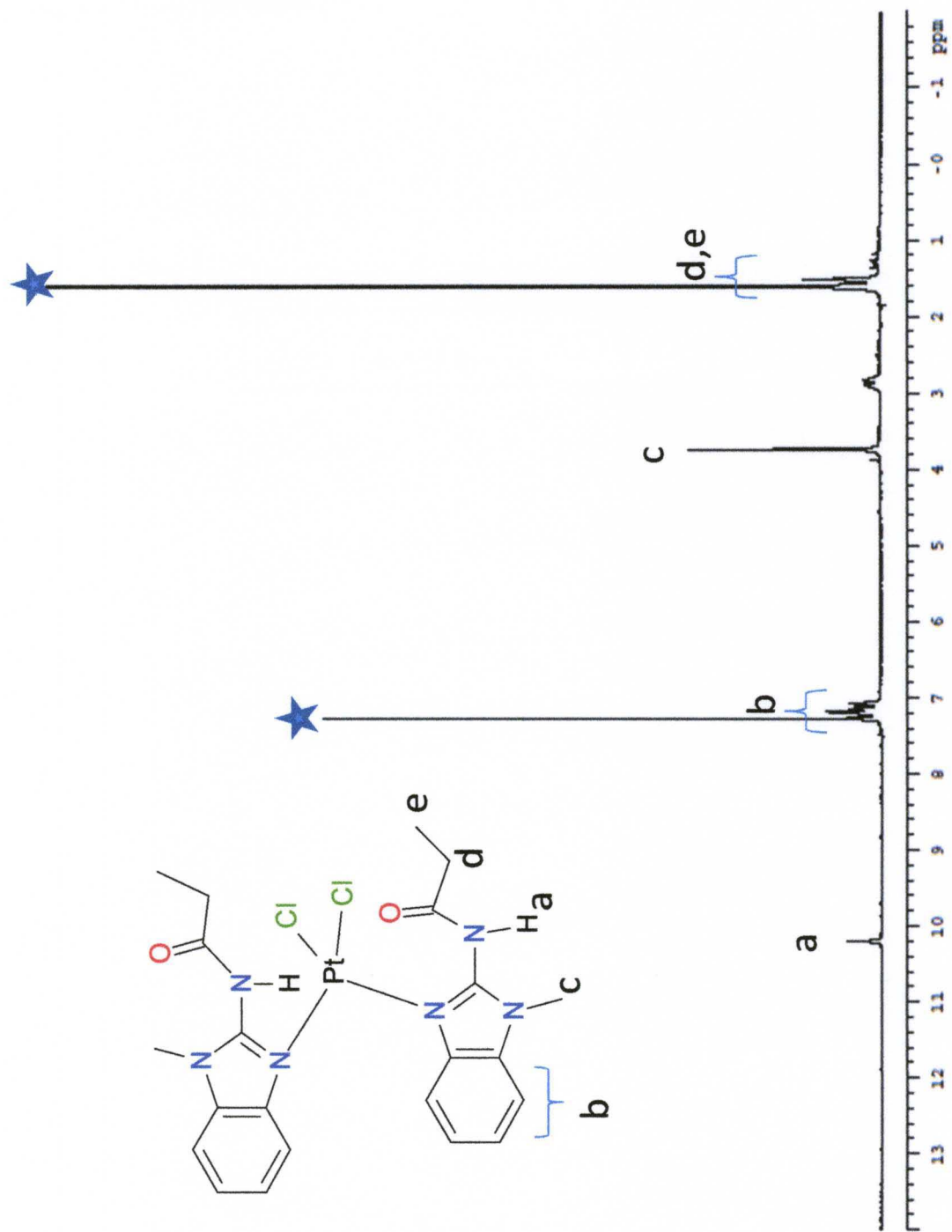
<sup>1</sup>H NMR of compound 32 in CDCl<sub>3</sub>



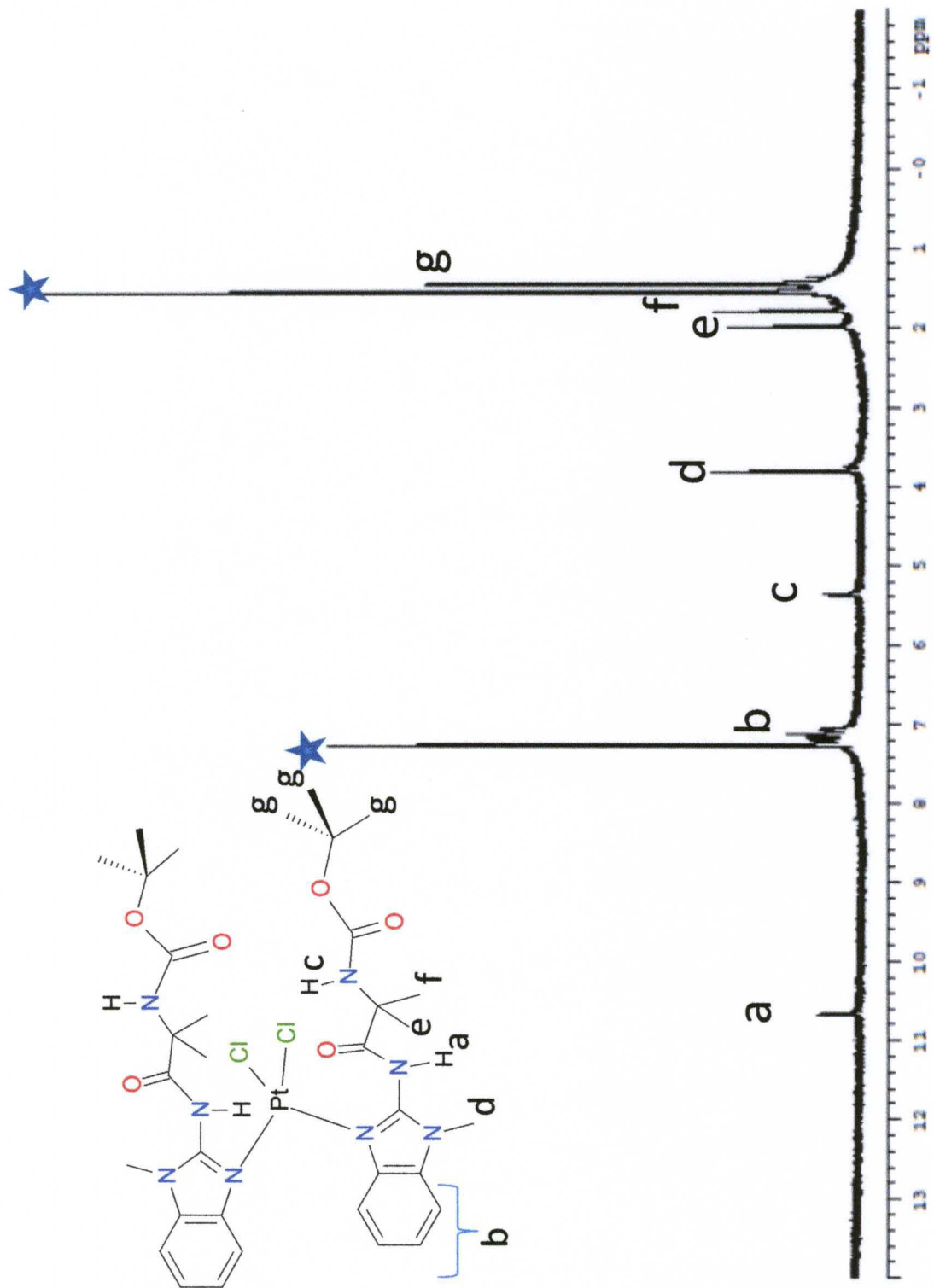
$^1\text{H}$  NMR of compound 33 in  $\text{CDCl}_3$



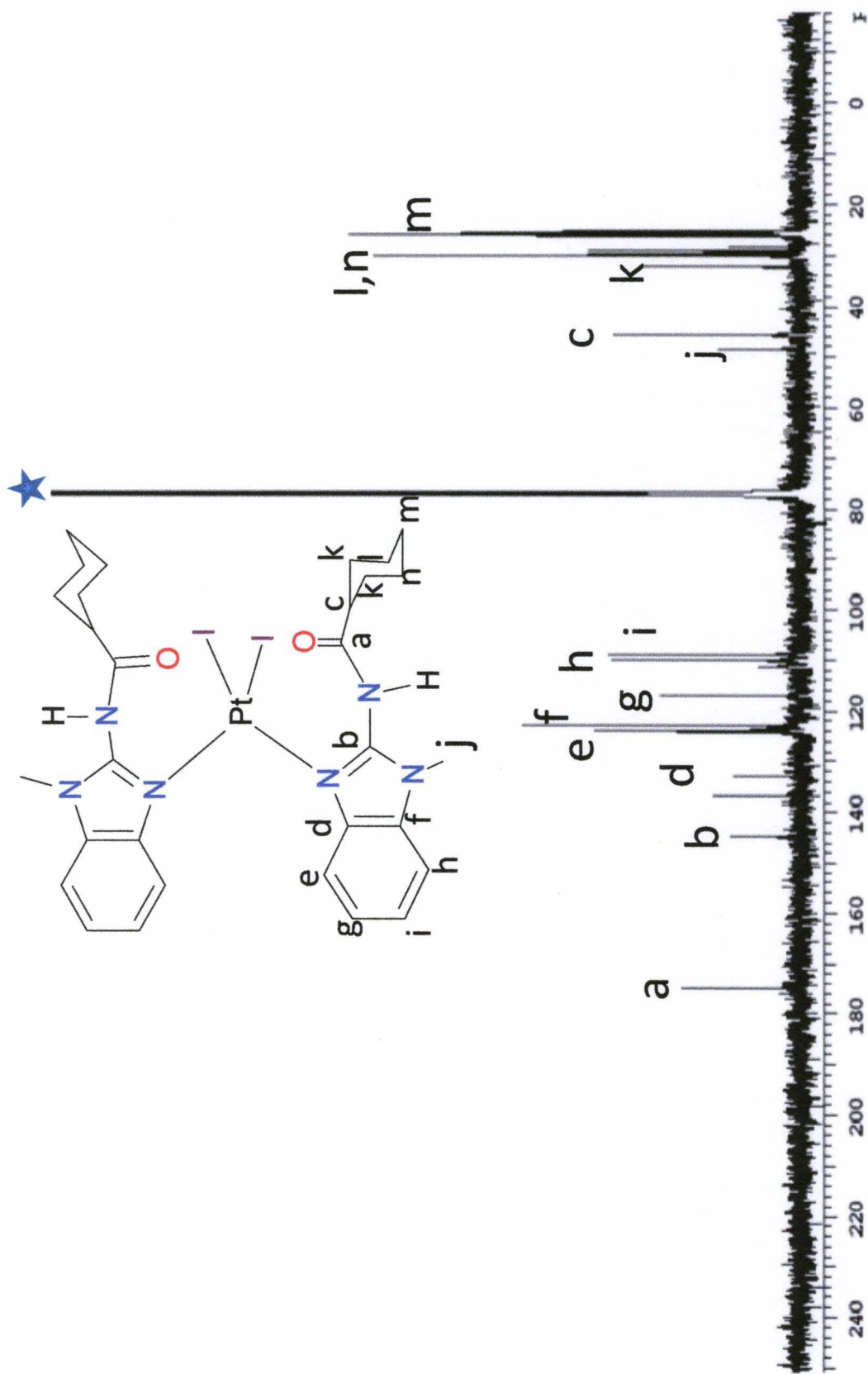
$^1\text{H}$  NMR of compound 39 in  $\text{CDCl}_3$



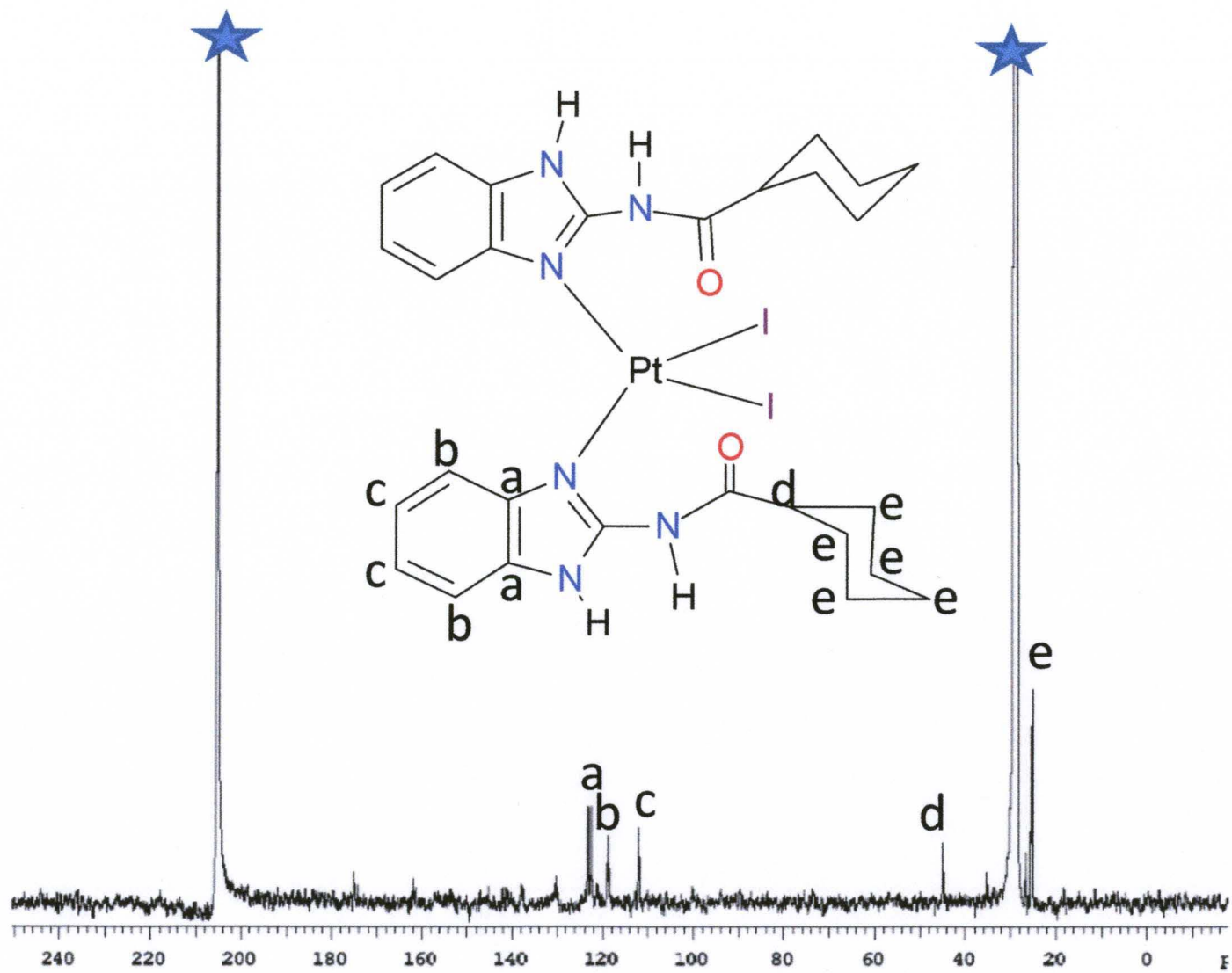
$^1\text{H}$  NMR of compound 41 in  $\text{CDCl}_3$



<sup>1</sup>H NMR of compound 46 in CDCl<sub>3</sub>

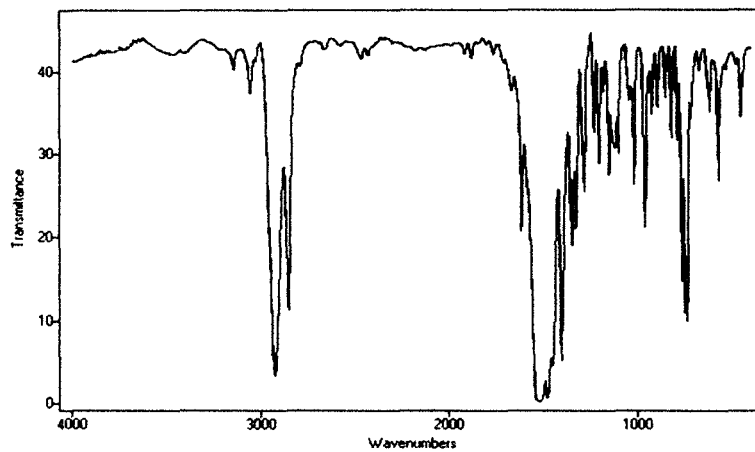


$^{13}\text{C}$  NMR of compound 31 in  $\text{CDCl}_3$

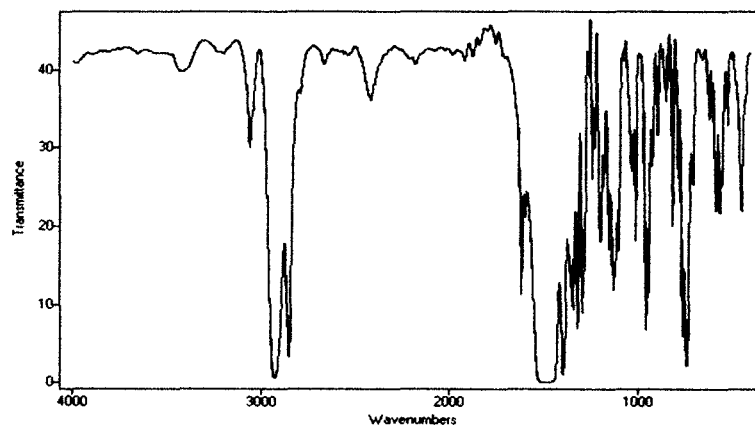


$^{13}\text{C}$  NMR spectrum of compound 40 in acetone

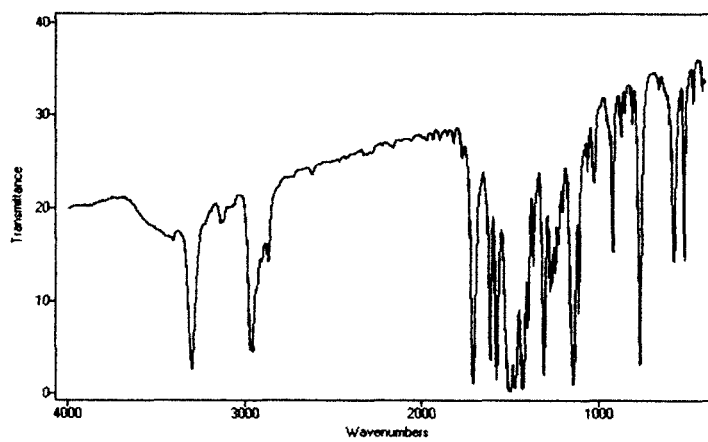
## IR Spectra



IR spectrum of compound 16

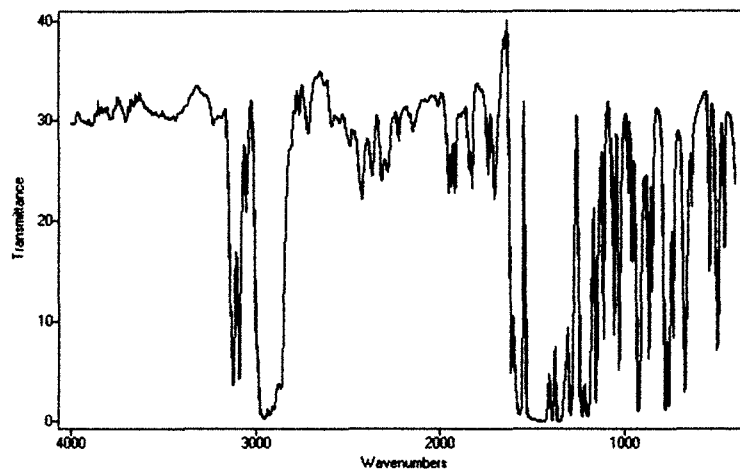


IR spectrum of compound 17

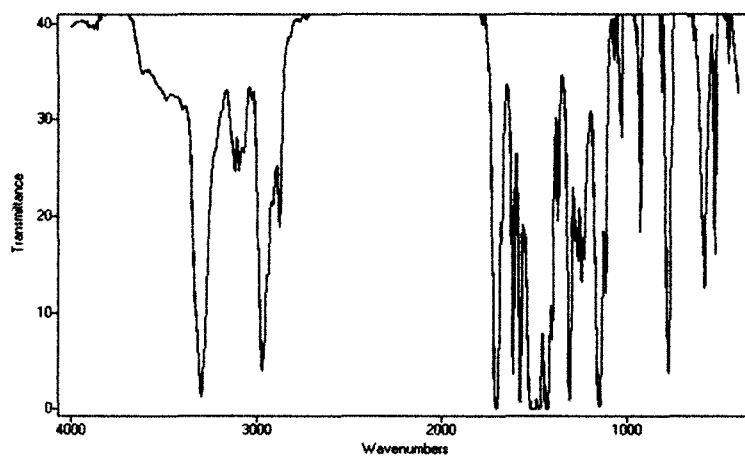


IR spectrum of compound 25

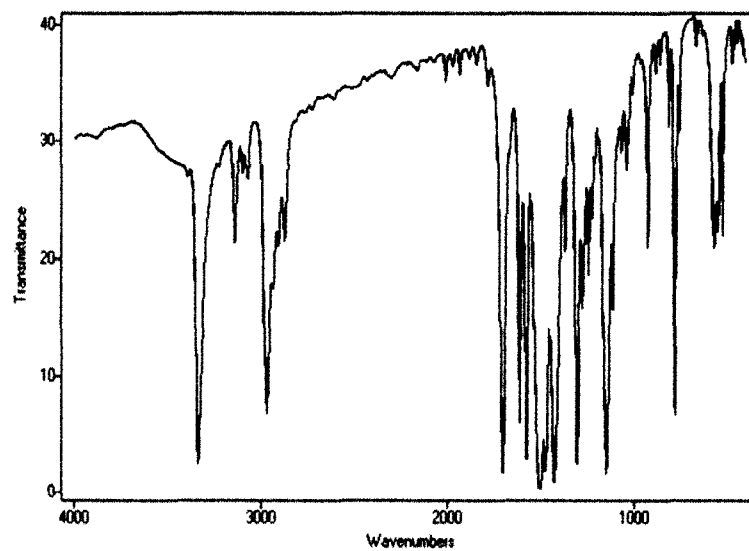




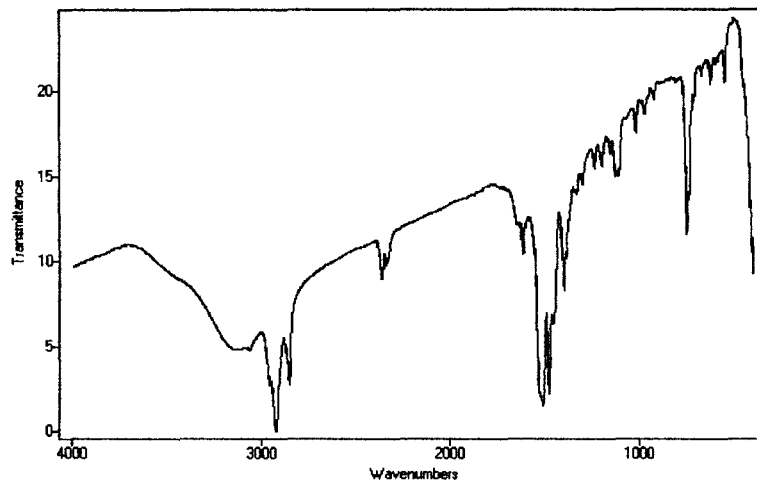
IR spectrum of **compound 26**



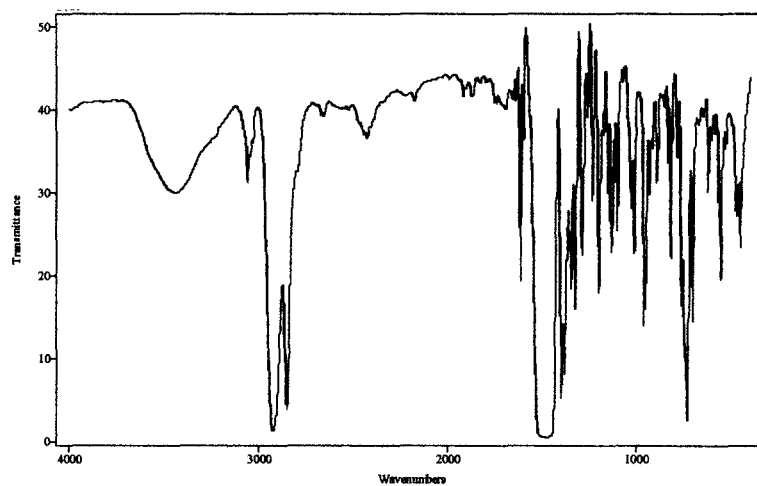
IR spectrum of **compound 27**



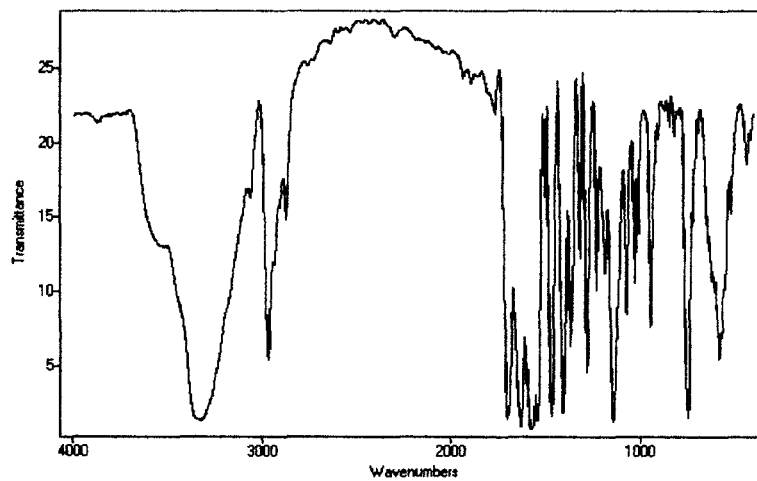
IR spectrum of **compound 28**



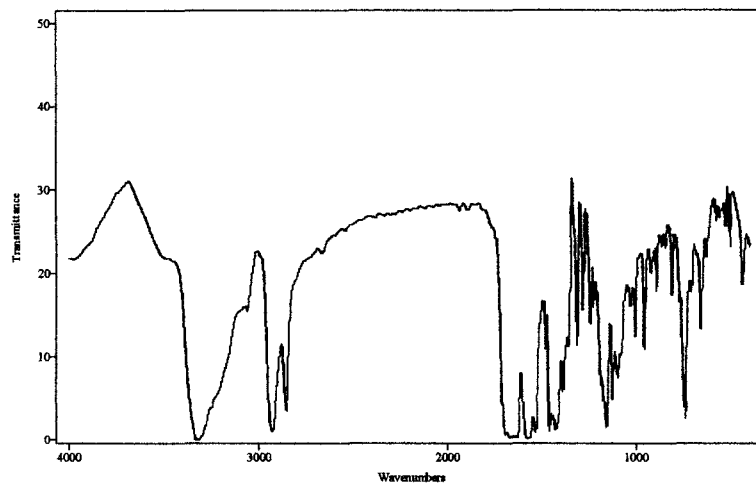
**IR of compound 29**



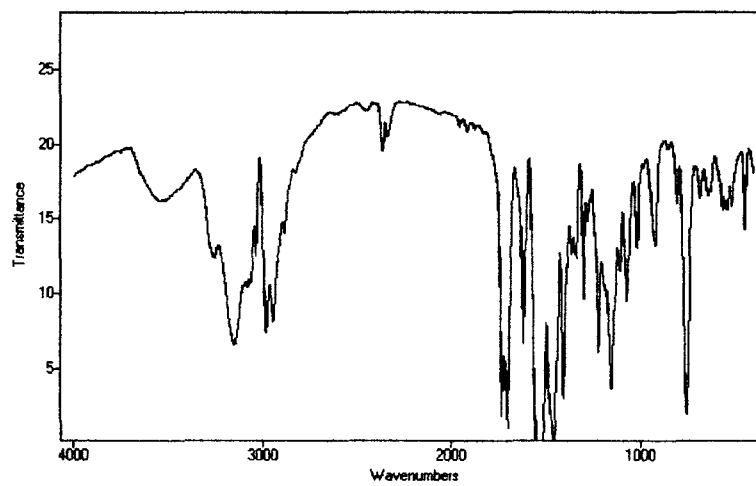
**IR of compound 31**



**IR of compound 37**



**IR of compound 39**



**IR of compound 40**

## Crystallographic Data

Table A1. Crystal data and structure refinement for Compound 4

Identification code	rmb320t	
Empirical formula	C <sub>15</sub> H <sub>19</sub> N <sub>3</sub> O	
Formula weight	257.33	
Temperature	100(2) K	
Wavelength	0.7107 Å	
Crystal system	Monoclinic	
Space group	P 1 2 <sub>1</sub> /n 1	
Unit cell dimensions	a = 14.1720(3) Å	α = 90°.
	b = 6.04320(8) Å	β = 107.3724(19)°.
	c = 15.7484(3) Å	γ = 90°.
Volume	1287.24(4) Å <sup>3</sup>	
Z	4	
Density (calculated)	1.328 Mg/m <sup>3</sup>	
Absorption coefficient	0.086 mm <sup>-1</sup>	
F(000)	552	
Crystal size	0.22 x 0.18 x 0.13 mm <sup>3</sup>	
Theta range for data collection	3.40 to 29.10°	
Index ranges	-19 ≤ h ≤ 19, -8 ≤ k ≤ 8, -21 ≤ l ≤ 21	
Reflections collected	27003	
Independent reflections	3264 [R(int) = 0.0267]	
Completeness to theta = 29.10°	94.4 %	
Completeness to theta = 26.32°	99.7 %	
Absorption correction	Semi-empirical from equivalents	
Max. and min. transmission	1.00000 and 0.95004	
Refinement method	Full-matrix least-squares on F <sup>2</sup>	
Data / restraints / parameters	3264 / 0 / 248	
Goodness-of-fit on F <sup>2</sup>	1.017	
Final R indices [I > 2σ(I)]	R <sub>1</sub> = 0.0355, wR <sub>2</sub> = 0.0812	
R indices (all data)	R <sub>1</sub> = 0.0452, wR <sub>2</sub> = 0.0840	
Largest diff. peak and hole	0.512 and -0.211 e.Å <sup>-3</sup>	

Table A2. Atomic coordinates ( $\times 10^4$ ) and equivalent isotropic displacement parameters ( $\text{\AA}^2 \times 10^3$ ) for rmb320lt.  $U(\text{eq})$  is defined as one third of the trace of the orthogonalized  $U^{ij}$  tensor.

	x	y	z	U(eq)
O(1)	9322(1)	7416(1)	2044(1)	22(1)
N(1)	9440(1)	6970(2)	645(1)	14(1)
N(2)	11156(1)	6468(1)	763(1)	15(1)
N(3)	10693(1)	9721(1)	1215(1)	14(1)
C(1)	8936(1)	6882(2)	1272(1)	15(1)
C(2)	10424(1)	7660(2)	877(1)	14(1)
C(3)	11982(1)	7843(2)	1065(1)	14(1)
C(4)	12979(1)	7454(2)	1142(1)	16(1)
C(5)	13649(1)	9136(2)	1488(1)	18(1)
C(6)	13353(1)	11165(2)	1759(1)	18(1)
C(7)	12371(1)	11571(2)	1700(1)	16(1)
C(8)	11704(1)	9872(2)	1351(1)	14(1)
C(9)	10064(1)	11443(2)	1400(1)	18(1)
C(10)	7864(1)	6208(2)	912(1)	15(1)
C(11)	7228(1)	8307(2)	835(1)	20(1)
C(12)	6125(1)	7758(2)	533(1)	24(1)
C(13)	5870(1)	6038(2)	1135(1)	22(1)
C(14)	6487(1)	3950(2)	1193(1)	20(1)
C(15)	7592(1)	4500(2)	1516(1)	19(1)

Table A3. Anisotropic displacement parameters ( $\text{\AA}^2 \times 10^3$ ) for rmb320lt. The anisotropic displacement factor exponent takes the form:  $-2\pi^2 [h^2 a^{*2} U^{11} + \dots + 2 h k a^* b^* U^{12}]$

	$U^{11}$	$U^{22}$	$U^{33}$	$U^{23}$	$U^{13}$	$U^{12}$
O(1)	17(1)	34(1)	15(1)	-3(1)	5(1)	-5(1)
N(1)	12(1)	17(1)	15(1)	-3(1)	5(1)	-1(1)
N(2)	13(1)	16(1)	15(1)	-1(1)	5(1)	0(1)
N(3)	12(1)	14(1)	15(1)	-1(1)	4(1)	0(1)
C(1)	14(1)	16(1)	16(1)	0(1)	5(1)	1(1)
C(2)	14(1)	15(1)	12(1)	0(1)	4(1)	0(1)
C(3)	14(1)	16(1)	12(1)	0(1)	4(1)	-1(1)
C(4)	15(1)	19(1)	16(1)	0(1)	5(1)	2(1)
C(5)	13(1)	24(1)	17(1)	1(1)	4(1)	0(1)
C(6)	16(1)	19(1)	17(1)	1(1)	2(1)	-4(1)
C(7)	17(1)	15(1)	16(1)	0(1)	3(1)	0(1)
C(8)	13(1)	16(1)	12(1)	2(1)	4(1)	1(1)
C(9)	16(1)	16(1)	22(1)	-2(1)	6(1)	2(1)
C(10)	13(1)	18(1)	15(1)	-2(1)	5(1)	-1(1)
C(11)	15(1)	17(1)	25(1)	2(1)	3(1)	-1(1)
C(12)	14(1)	20(1)	34(1)	1(1)	1(1)	2(1)
C(13)	13(1)	26(1)	28(1)	-6(1)	8(1)	-2(1)
C(14)	18(1)	20(1)	23(1)	2(1)	8(1)	-3(1)
C(15)	16(1)	19(1)	23(1)	4(1)	6(1)	1(1)

Table A4. Hydrogen coordinates ( $\times 10^4$ ) and isotropic displacement parameters ( $\text{\AA}^2 \times 10^3$ ) for rmb320lt.

	x	y	z	U(eq)
H(1N)	9230(10)	6130(20)	153(9)	25(3)
H(4)	13196(9)	6020(20)	976(8)	20(3)
H(5)	14343(10)	8910(20)	1545(8)	22(3)
H(6)	13850(9)	12280(20)	2002(9)	23(3)
H(7)	12156(9)	12950(20)	1885(8)	18(3)
H(9A)	9413(10)	11360(20)	958(9)	23(3)
H(9B)	9991(9)	11240(20)	1989(9)	22(3)
H(9C)	10376(9)	12870(20)	1364(8)	22(3)
H(10)	7738(9)	5590(20)	315(8)	16(3)
H(11A)	7386(10)	9360(20)	420(9)	28(3)
H(11B)	7414(9)	9030(20)	1433(9)	21(3)
H(12A)	5742(11)	9130(30)	529(10)	35(4)
H(12B)	5936(9)	7180(20)	-90(9)	23(3)
H(13A)	5176(10)	5660(20)	925(9)	28(3)
H(13B)	5994(10)	6650(20)	1747(9)	28(3)
H(14A)	6332(10)	2870(20)	1599(9)	26(3)
H(14B)	6335(9)	3230(20)	583(9)	22(3)
H(15A)	8002(11)	3120(20)	1534(9)	32(4)
H(15B)	7772(9)	5120(20)	2127(9)	24(3)

Table A5. Crystal data and structure refinement Compound 15

Identification code	rmb268p21c	
Empirical formula	C <sub>36</sub> H <sub>52</sub> Cu N <sub>6</sub> O <sub>2</sub>	
Formula weight	664.38	
Temperature	100(2) K	
Wavelength	0.71073 Å	
Crystal system	Monoclinic	
Space group	P2(1)/c	
Unit cell dimensions	a = 18.505(3) Å	α = 90°.
	b = 5.1189(7) Å	β = 93.823(2)°.
	c = 17.344(3) Å	γ = 90°.
Volume	1639.3(4) Å <sup>3</sup>	
Z	2	
Density (calculated)	1.346 Mg/m <sup>3</sup>	
Absorption coefficient	0.709 mm <sup>-1</sup>	
F(000)	710	
Crystal size	0.413x 0.109 x 0.026 mm <sup>3</sup>	
Crystal color, habit	green needle	
Theta range for data collection	2.21 to 25.07°	
Index ranges	-22 ≤ h ≤ 21, -6 ≤ k ≤ 6, -20 ≤ l ≤ 20	
Reflections collected	10932	
Independent reflections	2885 [R(int) = 0.0562]	
Completeness to theta = 25.07°	99.4 %	
Absorption correction	SADABS	
Max. and min. transmission	0.895 and 0.712	
Refinement method	Full-matrix least-squares on F <sup>2</sup>	
Data / restraints / parameters	2885 / 0 / 207	
Goodness-of-fit on F <sup>2</sup>	1.061	
Final R indices [I > 2σ(I)]	R1 = 0.0556, wR2 = 0.0952	
R indices (all data)	R1 = 0.0713, wR2 = 0.0999	
Largest diff. peak and hole	0.539 and -0.494 e.Å <sup>-3</sup>	

Table A6. Atomic coordinates ( $\times 10^4$ ) and equivalent isotropic displacement parameters ( $\text{\AA}^2 \times 10^3$ ) for rmb268P21c.  $U(\text{eq})$  is defined as one third of the trace of the orthogonalized  $U^{ij}$  tensor.

	x	y	z	U(eq)
Cu(1)	10000	5000	0	11(1)
O(1)	9195(1)	2956(5)	293(1)	16(1)
N(1)	10621(1)	3219(5)	824(2)	10(1)
N(2)	10859(1)	407(5)	1787(2)	12(1)
N(3)	9734(1)	-155(6)	1123(2)	15(1)
C(1)	10365(2)	1177(6)	1215(2)	11(1)
C(2)	11315(2)	3715(7)	1158(2)	11(1)
C(3)	11838(2)	5565(6)	998(2)	14(1)
C(4)	12487(2)	5564(7)	1449(2)	16(1)
C(5)	12621(2)	3766(7)	2047(2)	16(1)
C(6)	12111(2)	1927(7)	2216(2)	16(1)
C(7)	11463(2)	1942(7)	1764(2)	12(1)
C(8)	10750(2)	-1595(7)	2370(2)	16(1)
C(9)	9200(2)	820(6)	676(2)	11(1)
C(10)	8503(2)	-698(6)	616(2)	14(1)
C(11)	7880(2)	681(7)	981(2)	17(1)
C(12)	7172(2)	-811(7)	826(2)	17(1)
C(13)	6806(2)	-393(7)	20(2)	19(1)
C(14)	6128(2)	-1987(7)	-132(2)	19(1)
C(15)	5704(2)	-1354(7)	-894(2)	19(1)
C(16)	5037(2)	-3025(7)	-1057(2)	22(1)
C(17)	4580(2)	-2310(7)	-1784(2)	20(1)
C(18)	3925(2)	-4051(8)	-1934(2)	25(1)

Table A7. Anisotropic displacement parameters ( $\text{\AA}^2 \times 10^3$ ) for rmb268P21c. The anisotropic

displacement factor exponent takes the form:  $-2 \sum [ h^2 a^* 2 U^{11} + \dots + 2 h k a^* b^* U^{12} ]$

	$U^{11}$	$U^{22}$	$U^{33}$	$U^{23}$	$U^{13}$	$U^{12}$
Cu(1)	11(1)	11(1)	10(1)	5(1)	-1(1)	-1(1)
O(1)	13(1)	18(1)	17(1)	7(1)	0(1)	-2(1)
N(1)	9(1)	10(2)	10(1)	2(1)	-1(1)	0(1)
N(2)	15(1)	8(2)	13(1)	2(1)	1(1)	-1(1)
N(3)	13(1)	14(2)	17(1)	0(1)	1(1)	2(1)
C(1)	16(2)	10(2)	7(2)	-1(1)	1(1)	2(1)
C(2)	11(2)	12(2)	8(2)	-2(1)	2(1)	5(1)
C(3)	18(2)	13(2)	10(2)	1(1)	0(1)	-1(1)
C(4)	18(2)	13(2)	18(2)	1(1)	2(1)	-3(1)
C(5)	15(2)	21(2)	12(2)	-3(2)	-2(1)	0(2)



C(6)	22(2)	16(2)	8(2)	0(1)	-2(1)	3(2)
C(7)	14(2)	11(2)	12(2)	-2(1)	4(1)	1(1)
C(8)	19(2)	14(2)	15(2)	5(2)	1(2)	-4(2)
C(9)	15(2)	7(2)	10(2)	-2(1)	4(1)	1(1)
C(10)	17(2)	7(2)	16(2)	0(1)	0(1)	0(1)
C(11)	21(2)	16(2)	13(2)	-1(1)	1(1)	-2(1)
C(12)	17(2)	17(2)	19(2)	-1(2)	6(2)	-2(1)
C(13)	19(2)	17(2)	20(2)	0(2)	-1(1)	0(2)
C(14)	19(2)	17(2)	21(2)	1(2)	1(2)	0(2)
C(15)	19(2)	18(2)	21(2)	1(2)	-1(2)	1(2)
C(16)	24(2)	19(2)	22(2)	1(2)	-2(2)	0(2)
C(17)	22(2)	17(2)	22(2)	0(2)	1(2)	1(2)
C(18)	25(2)	24(2)	26(2)	-3(2)	-5(2)	1(2)

Table A8. Hydrogen coordinates ( $\times 10^4$ ) and isotropic displacement parameters ( $\text{\AA}^2 \times 10^3$ ) for rmb268P21c.

	x	y	z	U(eq)
H(3)	11753	6793	592	16
H(4)	12848	6815	1349	19
H(5)	13072	3811	2343	19
H(6)	12199	704	2623	19
H(8A)	10732	-767	2878	24
H(8B)	11151	-2845	2383	24
H(8C)	10293	-2512	2240	24
H(10A)	8584	-2414	870	16
H(10B)	8362	-1025	64	16
H(11A)	7826	2469	767	20
H(11B)	7991	830	1545	20
H(12A)	6831	-277	1213	21
H(12B)	7269	-2700	899	21
H(13A)	6684	1481	-45	22
H(13B)	7153	-849	-370	22
H(14A)	5809	-1700	297	23
H(14B)	6261	-3860	-130	23
H(15A)	5555	503	-888	23
H(15B)	6027	-1580	-1321	23
H(16A)	4731	-2896	-611	26
H(16B)	5191	-4870	-1098	26
H(17A)	4416	-478	-1741	24
H(17B)	4884	-2416	-2231	24
H(18A)	4084	-5857	-2003	38
H(18B)	3647	-3465	-2402	38
H(18C)	3621	-3958	-1494	38

Table A9. Crystal data and structure refinement for Compound 16.

Identification code	rmb316p21c	
Empirical formula	C <sub>15</sub> H <sub>18</sub> N <sub>3</sub> Ni <sub>0.50</sub> O <sub>1</sub>	
Formula weight	285.68	
Temperature	100(2) K	
Wavelength	0.71073 Å	
Crystal system	Monoclinic	
Space group	P2(1)/c	
Unit cell dimensions	a = 14.1057(8) Å	α = 90°.
	b = 15.1769(8) Å	β = 102.9570(10)°.
	c = 6.4460(4) Å	γ = 90°.
Volume	1344.83(13) Å <sup>3</sup>	
Z	4	
Density (calculated)	1.411 Mg/m <sup>3</sup>	
Absorption coefficient	0.761 mm <sup>-1</sup>	
F(000)	604	
Crystal size	0.45 x 0.16 x 0.07 mm <sup>3</sup>	
Theta range for data collection	2.68 to 27.54°	
Index ranges	-18 ≤ h ≤ 18, -19 ≤ k ≤ 19, -8 ≤ l ≤ 8	
Reflections collected	11331	
Independent reflections	3017 [R(int) = 0.0249]	
Completeness to theta = 27.54°	97.1 %	
Absorption correction	None	
Max. and min. transmission	0.9486 and 0.7257	
Refinement method	Full-matrix least-squares on F <sup>2</sup>	
Data / restraints / parameters	3017 / 0 / 179	
Goodness-of-fit on F <sup>2</sup>	1.086	
Final R indices [I > 2σ(I)]	R1 = 0.0450, wR2 = 0.1063	
R indices (all data)	R1 = 0.0487, wR2 = 0.1083	
Largest diff. peak and hole	0.399 and -0.276 e.Å <sup>-3</sup>	

Table A10. Atomic coordinates ( $\times 10^4$ ) and equivalent isotropic displacement parameters ( $\text{\AA}^2 \times 10^3$ ) for rmb316P21c.  $U(\text{eq})$  is defined as one third of the trace of the orthogonalized  $U^{ij}$  tensor.

	x	y	z	$U(\text{eq})$
Ni(1)	0	10000	0	13(1)
O(1)	1238(1)	9727(1)	1473(3)	19(1)
N(1)	-552(1)	9310(1)	1925(3)	14(1)
N(2)	-541(1)	8632(1)	5020(3)	16(1)
N(3)	979(1)	9055(1)	4545(3)	16(1)
C(1)	6(2)	9030(1)	3787(3)	14(1)
C(2)	-1509(2)	9043(2)	1940(4)	15(1)
C(3)	-2387(2)	9092(2)	433(4)	19(1)
C(4)	-3212(2)	8744(2)	965(4)	21(1)
C(5)	-3184(2)	8340(2)	2920(4)	20(1)
C(6)	-2316(2)	8262(2)	4418(4)	18(1)
C(7)	-1495(2)	8622(2)	3886(3)	15(1)
C(8)	-155(2)	8177(2)	7024(4)	19(1)
C(9)	1522(2)	9374(1)	3331(3)	15(1)
C(10)	2615(2)	9335(2)	4154(3)	15(1)
C(11)	2926(2)	8935(2)	6384(4)	23(1)
C(12)	4032(2)	8964(2)	7162(4)	28(1)
C(13)	4543(2)	8512(2)	5607(4)	31(1)
C(14)	4215(2)	8892(2)	3372(4)	30(1)
C(15)	3106(2)	8847(2)	2595(4)	23(1)

Table A11. Anisotropic displacement parameters ( $\text{\AA}^2 \times 10^3$ ) for rmb316P21c. The anisotropic displacement factor exponent takes the form:  $-2\pi^2 [h^2 a^{*2} U^{11} + \dots + 2 h k a^* b^* U^{12}]$

	$U^{11}$	$U^{22}$	$U^{33}$	$U^{23}$	$U^{13}$	$U^{12}$
Ni(1)	13(1)	14(1)	11(1)	3(1)	2(1)	0(1)
O(1)	14(1)	25(1)	17(1)	8(1)	2(1)	1(1)
N(1)	14(1)	12(1)	14(1)	2(1)	3(1)	0(1)
N(2)	18(1)	16(1)	13(1)	1(1)	4(1)	-2(1)
N(3)	17(1)	17(1)	13(1)	1(1)	2(1)	0(1)
C(1)	20(1)	12(1)	12(1)	-2(1)	6(1)	-1(1)
C(2)	18(1)	13(1)	16(1)	0(1)	5(1)	0(1)
C(3)	19(1)	16(1)	21(1)	4(1)	3(1)	0(1)
C(4)	15(1)	20(1)	27(1)	2(1)	4(1)	2(1)
C(5)	17(1)	18(1)	28(1)	0(1)	10(1)	0(1)
C(6)	21(1)	16(1)	20(1)	0(1)	10(1)	0(1)
C(7)	18(1)	14(1)	14(1)	-3(1)	4(1)	1(1)
C(8)	25(1)	19(1)	13(1)	3(1)	3(1)	-2(1)
C(9)	18(1)	13(1)	13(1)	0(1)	2(1)	0(1)
C(10)	16(1)	15(1)	13(1)	2(1)	1(1)	0(1)
C(11)	19(1)	34(1)	16(1)	7(1)	2(1)	3(1)
C(12)	20(1)	47(2)	14(1)	4(1)	-1(1)	6(1)
C(13)	22(1)	41(2)	27(1)	0(1)	-1(1)	13(1)
C(14)	20(1)	53(2)	19(1)	-5(1)	3(1)	11(1)
C(15)	20(1)	30(1)	16(1)	-4(1)	0(1)	6(1)

Table A12. Hydrogen coordinates ( $\times 10^4$ ) and isotropic displacement parameters ( $\text{\AA}^2 \times 10^3$ ) for rmb316P21c.

	x	y	z	U(eq)
H(3)	-2419	9350	-890	23
H(4)	-3805	8783	-18	25
H(5)	-3754	8120	3221	24
H(6)	-2283	7983	5716	22
H(8A)	-116	7557	6764	29
H(8B)	-576	8276	7982	29
H(8C)	483	8400	7647	29
H(10)	2855	9943	4246	18
H(11A)	2627	9261	7363	28
H(11B)	2705	8329	6355	28
H(12A)	4244	9573	7341	33
H(12B)	4216	8676	8537	33
H(13A)	4401	7886	5573	37
H(13B)	5240	8586	6092	37
H(14A)	4519	8565	2402	37
H(14B)	4426	9501	3372	37
H(15A)	2898	8237	2482	28
H(15B)	2915	9113	1195	28

Table A13. Crystal data and structure refinement for Compound 17 .

Identification code	rmb312lt	
Empirical formula	C60 H49 Co2 N12 O4	
Formula weight	1119.97	
Temperature	293(2) K	
Wavelength	0.71073 Å	
Crystal system	monoclinic	
Space group	P2 <sub>1</sub> /c	
Unit cell dimensions	a = 13.0866(4) Å	α = 90°.
	b = 23.0690(5) Å	β = 106.002(3)°.
	c = 19.5697(5) Å	γ = 90°.
Volume	5679.0(3) Å <sup>3</sup>	
Z	4	
Density (calculated)	1.310 Mg/m <sup>3</sup>	
Absorption coefficient	0.641 mm <sup>-1</sup>	
F(000)	2316	
Crystal size	? x ? x ? mm <sup>3</sup>	
Theta range for data collection	2.92 to 27.98°.	
Index ranges	-16 ≤ h ≤ 17, -29 ≤ k ≤ 30, -24 ≤ l ≤ 25	
Reflections collected	75925	
Independent reflections	12632 [R(int) = 0.0665]	
Completeness to theta = 27.98°	92.4 %	
Refinement method	Full-matrix least-squares on F <sup>2</sup>	
Data / restraints / parameters	12632 / 25 / 645	
Goodness-of-fit on F <sup>2</sup>	1.089	
Final R indices [I > 2σ(I)]	R1 = 0.0741, wR2 = 0.1706	
R indices (all data)	R1 = 0.1358, wR2 = 0.1816	
Largest diff. peak and hole	1.556 and -0.767 e.Å <sup>-3</sup>	

Table A14. Atomic coordinates ( $\times 10^4$ ) and equivalent isotropic displacement parameters ( $\text{\AA}^2 \times 10^3$ ) for rmb312lt.  $U(\text{eq})$  is defined as one third of the trace of the orthogonalized  $U^{ij}$  tensor.

	x	y	z	U(eq)
Co(1)	888(1)	3607(1)	1241(1)	34(1)
Co(2)	3612(1)	6210(1)	3444(1)	40(1)
O(1)	672(2)	3935(1)	2104(2)	35(1)
O(2)	-293(3)	3224(2)	563(2)	44(1)
O(3)	4701(3)	6724(1)	4022(2)	45(1)
O(4)	3943(3)	5855(1)	2633(2)	45(1)
N(1)	1237(3)	4366(2)	926(2)	32(1)
N(2)	1305(3)	5330(2)	940(2)	36(1)
N(3)	1113(3)	4903(2)	1985(2)	34(1)
N(4)	1725(3)	2892(2)	1418(2)	41(1)
N(5)	1958(4)	1933(2)	1387(3)	65(1)
N(6)	366(4)	2274(2)	650(3)	62(1)
N(7)	2529(3)	6815(2)	3315(2)	36(1)
N(8)	1966(3)	7731(2)	3266(2)	38(1)
N(9)	3776(3)	7603(2)	3806(2)	40(1)
N(10)	3496(3)	5452(2)	3874(2)	41(1)
N(11)	3984(3)	4532(2)	4090(3)	47(1)
N(12)	4011(3)	4880(2)	2970(3)	45(1)
C(1)	1378(3)	4562(2)	282(2)	34(1)
C(2)	1461(4)	4252(2)	-301(3)	44(1)
C(3)	1584(4)	4570(3)	-886(3)	51(1)
C(4)	1623(4)	5169(2)	-872(3)	46(1)
C(5)	1544(4)	5479(2)	-287(3)	43(1)
C(6)	1420(3)	5161(2)	286(2)	35(1)
C(7)	1202(3)	4844(2)	1312(3)	32(1)
C(8)	1292(5)	5924(2)	1185(3)	53(2)
C(9)	871(3)	4460(2)	2331(2)	30(1)
C(10)	775(4)	4583(2)	3066(2)	34(1)

C(11)	-362(4)	4777(2)	3018(2)	38(1)
C(12)	-478(5)	4916(2)	3759(3)	48(1)
C(13)	-179(5)	4400(2)	4254(3)	48(1)
C(14)	935(5)	4208(2)	4306(3)	53(2)
C(15)	1080(4)	4065(2)	3573(3)	44(1)
C(16)	2715(4)	2751(2)	1874(3)	49(1)
C(17)	3473(4)	3094(3)	2306(3)	63(2)
C(18)	4392(5)	2817(4)	2699(4)	88(2)
C(19)	4541(6)	2229(4)	2657(4)	94(3)
C(20)	3784(6)	1886(3)	2238(4)	87(2)
C(21)	2864(5)	2155(3)	1851(3)	61(2)
C(22)	1289(5)	2388(2)	1133(3)	50(1)
C(23)	1719(7)	1320(3)	1223(4)	94(3)
C(24)	-332(4)	2684(3)	391(3)	54(2)
C(25A)	-1305(7)	2619(4)	-279(5)	40(1)
C(26A)	-2064(7)	2184(4)	-84(5)	40(1)
C(27A)	-3038(7)	2090(4)	-756(5)	40(1)
C(28A)	-2732(8)	2399(4)	-1546(5)	40(1)
C(29A)	-1755(8)	1994(4)	-1412(5)	40(1)
C(30A)	-825(9)	2240(4)	-810(6)	40(1)
C(25B)	-1249(8)	2369(5)	-135(6)	49(1)
C(26B)	-2219(8)	2738(4)	-268(5)	49(1)
C(27B)	-3130(8)	2477(5)	-908(6)	49(1)
C(28B)	-2685(8)	1861(4)	-1318(6)	49(1)
C(29B)	-1914(9)	2248(5)	-1539(6)	49(1)
C(30B)	-968(10)	2409(5)	-880(6)	49(1)
C(32)	1432(4)	6828(2)	3004(2)	36(1)
C(33)	725(4)	6380(2)	2753(3)	46(1)
C(34)	-325(5)	6527(2)	2458(3)	57(2)
C(35)	-669(5)	7102(2)	2406(3)	56(2)
C(36)	31(4)	7548(2)	2658(3)	49(1)
C(37)	1076(4)	7401(2)	2963(2)	38(1)
C(38)	2829(4)	7372(2)	3477(2)	38(1)
C(39)	2005(4)	8360(2)	3360(3)	43(1)
C(40)	4620(4)	7280(2)	4074(3)	41(1)
C(41)	5592(6)	7604(3)	4487(4)	87(1)

C(42)	5298(6)	7990(3)	5057(4)	87(1)
C(43)	6264(6)	8325(4)	5502(4)	87(1)
C(44)	7147(6)	7973(3)	5802(4)	87(1)
C(45)	7461(6)	7582(3)	5266(4)	87(1)
C(46)	6505(5)	7235(3)	4854(4)	87(1)
C(47)	3418(4)	5306(2)	4548(3)	43(1)
C(48)	3090(4)	5628(2)	5043(3)	52(1)
C(49)	3132(4)	5365(3)	5684(3)	58(2)
C(50)	3492(5)	4799(3)	5825(4)	65(2)
C(51)	3791(4)	4468(3)	5335(3)	56(2)
C(52)	3746(4)	4725(2)	4691(3)	46(1)
C(53)	3834(4)	4976(2)	3605(3)	43(1)
C(54)	4351(4)	3954(2)	3985(3)	59(2)
C(55)	4035(4)	5309(2)	2533(3)	42(1)
C(56A)	4191(15)	5169(6)	1789(10)	70(2)
C(57A)	4196(11)	4528(5)	1643(7)	70(2)
C(58A)	4455(10)	4396(6)	966(6)	70(2)
C(59A)	5559(10)	4468(6)	1243(8)	70(2)
C(60A)	5647(10)	5278(6)	1114(7)	70(2)
C(61A)	5319(10)	5450(6)	1777(7)	70(2)
C(56B)	4245(19)	5095(8)	1850(11)	96(2)
C(57B)	5217(12)	4586(7)	1997(9)	96(2)
C(58B)	6193(12)	4709(7)	1746(8)	96(2)
C(59B)	5526(13)	4771(8)	886(8)	96(2)
C(60B)	4371(13)	5312(7)	617(8)	96(2)
C(61B)	4307(13)	5566(7)	1344(8)	96(2)

---



Table A15. Anisotropic displacement parameters ( $\text{\AA}^2 \times 10^3$ ) for rmb312lt. The anisotropic displacement factor exponent takes the form:  $-2 \square^2 [ h^2 a^2 U^{11} + \dots + 2 h k a^* b^* U^{12} ]$

	U <sup>11</sup>	U <sup>22</sup>	U <sup>33</sup>	U <sup>23</sup>	U <sup>13</sup>	U <sup>12</sup>
Co(1)	34(1)	35(1)	31(1)	0(1)	6(1)	-1(1)
Co(2)	46(1)	26(1)	47(1)	0(1)	12(1)	5(1)
O(1)	43(2)	30(2)	32(2)	-1(1)	11(2)	-4(2)
O(2)	38(2)	55(2)	35(2)	-8(2)	3(2)	-7(2)
O(3)	47(2)	33(2)	49(2)	0(2)	4(2)	2(2)
O(4)	54(2)	29(2)	56(2)	-2(2)	20(2)	2(2)
N(1)	28(2)	38(2)	29(2)	4(2)	7(2)	2(2)
N(2)	39(2)	36(2)	35(2)	4(2)	15(2)	-4(2)
N(3)	37(2)	34(2)	31(2)	2(2)	13(2)	-6(2)
N(4)	45(3)	41(2)	35(2)	-6(2)	7(2)	5(2)
N(5)	90(4)	45(3)	54(3)	-12(2)	10(3)	20(3)
N(6)	64(3)	58(3)	58(3)	-26(3)	5(3)	0(3)
N(7)	46(3)	23(2)	36(2)	-1(2)	8(2)	6(2)
N(8)	57(3)	26(2)	28(2)	-1(2)	11(2)	10(2)
N(9)	50(3)	30(2)	36(2)	-1(2)	7(2)	2(2)
N(10)	38(2)	31(2)	53(3)	5(2)	11(2)	1(2)
N(11)	37(2)	31(2)	72(3)	10(2)	13(2)	3(2)
N(12)	40(3)	32(2)	65(3)	-3(2)	14(2)	1(2)
C(1)	23(2)	50(3)	27(3)	2(2)	3(2)	1(2)
C(2)	42(3)	49(3)	40(3)	2(3)	11(2)	1(2)
C(3)	46(3)	75(4)	31(3)	-3(3)	8(2)	-4(3)
C(4)	38(3)	64(4)	34(3)	13(3)	5(2)	-2(3)
C(5)	35(3)	52(3)	41(3)	9(3)	9(2)	-3(2)
C(6)	25(2)	48(3)	31(3)	6(2)	7(2)	-1(2)
C(7)	24(2)	34(3)	38(3)	7(2)	7(2)	-2(2)
C(8)	72(4)	41(3)	55(4)	8(3)	31(3)	-10(3)
C(9)	25(2)	30(3)	35(3)	0(2)	7(2)	-4(2)
C(10)	37(3)	34(3)	29(3)	1(2)	8(2)	-7(2)
C(11)	48(3)	31(3)	36(3)	0(2)	15(2)	-1(2)
C(12)	64(4)	41(3)	45(3)	-9(2)	27(3)	-5(3)
C(13)	74(4)	42(3)	38(3)	-8(2)	30(3)	-16(3)

C(14)	73(4)	53(3)	29(3)	10(2)	8(3)	-12(3)
C(15)	45(3)	47(3)	37(3)	8(2)	9(2)	0(2)
C(16)	46(3)	56(3)	40(3)	-6(3)	3(3)	18(3)
C(17)	48(4)	67(4)	63(4)	-19(3)	-3(3)	14(3)
C(18)	57(4)	109(6)	77(5)	-25(4)	-15(4)	20(4)
C(19)	82(5)	109(6)	76(5)	-16(5)	-5(4)	62(5)
C(20)	117(6)	75(5)	56(4)	-10(4)	5(4)	58(5)
C(21)	72(4)	60(4)	45(3)	-13(3)	6(3)	33(3)
C(22)	62(4)	45(3)	41(3)	-12(3)	12(3)	9(3)
C(23)	155(8)	40(4)	82(5)	-20(3)	24(5)	21(4)
C(24)	47(3)	78(4)	37(3)	-26(3)	12(3)	-17(3)
C(32)	46(3)	30(3)	32(3)	-2(2)	11(2)	7(2)
C(33)	57(3)	29(3)	48(3)	-8(2)	8(3)	6(3)
C(34)	57(4)	43(3)	61(4)	-16(3)	2(3)	3(3)
C(35)	54(4)	53(4)	54(4)	-13(3)	2(3)	14(3)
C(36)	65(4)	43(3)	34(3)	-4(2)	6(3)	18(3)
C(37)	52(3)	33(3)	29(3)	-5(2)	10(2)	4(2)
C(38)	57(3)	32(3)	26(3)	1(2)	11(2)	5(3)
C(39)	64(4)	29(3)	35(3)	-4(2)	12(3)	9(2)
C(40)	53(3)	36(3)	35(3)	-2(2)	15(2)	-9(3)
C(41)	75(2)	99(2)	78(2)	-20(2)	6(2)	-27(2)
C(42)	75(2)	99(2)	78(2)	-20(2)	6(2)	-27(2)
C(43)	75(2)	99(2)	78(2)	-20(2)	6(2)	-27(2)
C(44)	75(2)	99(2)	78(2)	-20(2)	6(2)	-27(2)
C(45)	75(2)	99(2)	78(2)	-20(2)	6(2)	-27(2)
C(46)	75(2)	99(2)	78(2)	-20(2)	6(2)	-27(2)
C(47)	30(3)	40(3)	60(4)	5(3)	12(3)	-4(2)
C(48)	43(3)	50(3)	62(4)	11(3)	15(3)	1(3)
C(49)	46(3)	73(4)	57(4)	9(3)	18(3)	-7(3)
C(50)	47(4)	77(5)	65(4)	27(4)	5(3)	-18(3)
C(51)	42(3)	52(4)	69(4)	17(3)	5(3)	-6(3)
C(52)	31(3)	41(3)	64(4)	12(3)	8(3)	-3(2)
C(53)	34(3)	26(3)	67(4)	3(3)	9(3)	0(2)
C(54)	50(4)	31(3)	95(5)	12(3)	17(3)	6(3)
C(55)	34(3)	35(3)	59(4)	-2(3)	16(3)	0(2)

Table A16. Hydrogen coordinates ( $\times 10^4$ ) and isotropic displacement parameters ( $\text{\AA}^2 \times 10^3$ ) for rmb312lt.

	x	y	z	U(eq)
H(2)	1437	3849	-308	53
H(3)	1640	4374	-1289	61
H(4)	1705	5367	-1268	55
H(5)	1571	5882	-277	51
H(8A)	863	5948	1510	80
H(8B)	1002	6173	785	80
H(8C)	2005	6044	1421	80
H(10)	1254	4904	3265	41
H(11A)	-535	5118	2718	46
H(11B)	-856	4472	2802	46
H(12A)	-24	5242	3957	57
H(12B)	-1207	5026	3720	57
H(13A)	-235	4505	4723	58
H(13B)	-669	4084	4078	58
H(14A)	1100	3867	4608	63
H(14B)	1428	4512	4525	63
H(15A)	640	3734	3373	52
H(15B)	1816	3961	3623	52
H(17)	3380	3492	2335	75
H(18)	4924	3037	3001	105
H(19)	5175	2063	2922	113
H(20)	3880	1488	2212	104
H(23A)	2159	1176	941	141
H(23B)	985	1278	964	141
H(23C)	1857	1103	1658	141
H(33)	948	5995	2782	55
H(34)	-818	6234	2288	68
H(35)	-1383	7185	2197	67

H(36)	-193	7932	2623	59
H(39A)	2570	8459	3773	65
H(39B)	1340	8494	3421	65
H(39C)	2130	8540	2949	65
H(41)	5822	7859	4156	104
H(42A)	4747	8263	4823	104
H(42B)	5017	7748	5368	104
H(43)	6264	8725	5567	104
H(44A)	6991	7733	6168	104
H(44B)	7747	8219	6028	104
H(45A)	7727	7816	4941	104
H(45B)	8022	7321	5513	104
H(46A)	6710	6998	4505	104
H(46B)	6285	6977	5179	104
H(48)	2851	6007	4949	62
H(49)	2916	5571	6029	70
H(50)	3530	4640	6268	78
H(51)	4014	4086	5431	67
H(54A)	4818	3815	4422	89
H(54B)	4725	3966	3626	89
H(54C)	3751	3698	3835	89

---

Table A17. Crystal data and structure refinement for Compound 18.

Identification code	rmb311lt	
Empirical formula	C <sub>42</sub> H <sub>31</sub> N <sub>9</sub> O <sub>3</sub> Zn	
Formula weight	775.13	
Temperature	100(2) K	
Wavelength	0.7107 Å	
Crystal system	Triclinic	
Space group	P -1	
Unit cell dimensions	a = 9.7627(5) Å	α = 98.663(4)°.
	b = 10.0352(5) Å	β = 95.786(4)°.
	c = 19.3560(11) Å	γ = 100.010(4)°.
Volume	1830.38(16) Å <sup>3</sup>	
Z	2	
Density (calculated)	1.406 Mg/m <sup>3</sup>	
Absorption coefficient	0.725 mm <sup>-1</sup>	
F(000)	800	
Crystal color, habit	colorless prism	
Crystal size	0.32 x 0.25 x 0.16 mm <sup>3</sup>	
Theta range for data collection	2.92 to 27.99°	
Index ranges	-12 ≤ h ≤ 11, -12 ≤ k ≤ 13, -24 ≤ l ≤ 25	
Reflections collected	22843	
Independent reflections	7680 [R(int) = 0.0391]	
Completeness to theta = 27.99°	87.1 %	
Completeness to theta = 25.03°	99.8 %	
Absorption correction	Semi-empirical from equivalents	
Max. and min. transmission	1.00000 and 0.78143	
Refinement method	Full-matrix least-squares on F <sup>2</sup>	
Data / restraints / parameters	7680 / 0 / 511	
Goodness-of-fit on F <sup>2</sup>	1.027	
Final R indices [I > 2σ(I)]	R1 = 0.0353, wR2 = 0.0539	
R indices (all data)	R1 = 0.0647, wR2 = 0.0560	
Largest diff. peak and hole	0.501 and -0.448 e.Å <sup>-3</sup>	

Table A18. Atomic coordinates ( $\times 10^4$ ) and equivalent isotropic displacement parameters ( $\text{\AA}^2 \times 10^3$ ) for rmb311lt.  $U(\text{eq})$  is defined as one third of the trace of the orthogonalized  $U_{ij}$  tensor.

	x	y	z	U(eq)
Zn(1)	5185(1)	5969(1)	7357(1)	13(1)
O(1)	5836(1)	4368(1)	6712(1)	15(1)
O(2)	4297(1)	7313(1)	8005(1)	16(1)
O(3)	3798(2)	736(1)	8021(1)	27(1)
N(1)	7074(2)	7081(2)	7341(1)	12(1)
N(2)	9406(2)	7350(2)	7470(1)	15(1)
N(3)	8256(2)	5145(2)	6960(1)	14(1)
N(4)	3337(2)	5518(2)	6723(1)	12(1)
N(5)	983(2)	5082(2)	6526(1)	14(1)
N(6)	1939(2)	6323(2)	7635(1)	15(1)
N(7)	5411(2)	4849(2)	8182(1)	15(1)
N(8)	5301(2)	3072(2)	8758(1)	18(1)
N(9)	4313(2)	2660(2)	7539(1)	18(1)
C(1)	7657(2)	8438(2)	7666(1)	13(1)
C(2)	7012(2)	9531(2)	7890(1)	17(1)
C(3)	7866(2)	10760(2)	8204(1)	21(1)
C(4)	9328(2)	10914(2)	8296(1)	20(1)
C(5)	9977(2)	9834(2)	8076(1)	18(1)
C(6)	9117(2)	8611(2)	7755(1)	14(1)
C(7)	8172(2)	6463(2)	7240(1)	14(1)
C(8)	7106(2)	4200(2)	6735(1)	13(1)
C(9)	7310(2)	2759(2)	6491(1)	15(1)
C(10)	8542(2)	2324(2)	6698(1)	17(1)
C(11)	8652(2)	953(2)	6510(1)	22(1)
C(12)	7535(2)	24(2)	6126(1)	27(1)
C(13)	6308(2)	445(2)	5911(1)	28(1)
C(14)	6190(2)	1808(2)	6089(1)	21(1)
C(15)	2882(2)	4806(2)	6029(1)	12(1)
C(16)	3657(2)	4410(2)	5491(1)	16(1)
C(17)	2904(2)	3750(2)	4845(1)	18(1)
C(18)	1442(2)	3459(2)	4738(1)	19(1)
C(19)	675(2)	3837(2)	5270(1)	16(1)
C(20)	1429(2)	4525(2)	5910(1)	12(1)
C(21)	2141(2)	5674(2)	6995(1)	14(1)
C(22)	3010(2)	7086(2)	8086(1)	14(1)
C(23)	2597(2)	7788(2)	8750(1)	15(1)
C(24)	1311(2)	7337(2)	8974(1)	21(1)
C(25)	945(2)	8038(2)	9581(1)	28(1)
C(26)	1844(2)	9188(2)	9961(1)	30(1)
C(27)	3135(2)	9626(2)	9747(1)	27(1)
C(28)	3509(2)	8924(2)	9147(1)	19(1)
C(29)	6070(2)	5320(2)	8885(1)	15(1)
C(30)	6696(2)	6629(2)	9226(1)	20(1)
C(31)	7260(2)	6772(2)	9927(1)	23(1)
C(32)	7200(2)	5647(2)	10274(1)	25(1)
C(33)	6568(2)	4336(2)	9939(1)	24(1)
C(34)	6006(2)	4208(2)	9241(1)	18(1)
C(35)	4990(2)	3515(2)	8145(1)	16(1)

C(36)	3740(2)	1293(2)	7500(1)	19(1)
C(37)	3050(2)	559(2)	6796(1)	17(1)
C(38)	2994(2)	-846(2)	6638(1)	24(1)
C(39)	2388(2)	-1566(2)	5981(1)	30(1)
C(40)	1829(2)	-882(2)	5484(1)	28(1)
C(41)	1853(2)	507(2)	5642(1)	26(1)
C(42)	2471(2)	1237(2)	6298(1)	22(1)

Table A19. Anisotropic displacement parameters ( $\text{\AA}^2 \times 10^3$ ) for rmb311lt. The anisotropic displacement factor exponent takes the form:  $-2\pi^2 [h^2 a^{*2} U^{11} + \dots + 2hk a^* b^* U^{12}]$

	$U^{11}$	$U^{22}$	$U^{33}$	$U^{23}$	$U^{13}$	$U^{12}$
Zn(1)	10(1)	16(1)	15(1)	2(1)	4(1)	4(1)
O(1)	9(1)	18(1)	17(1)	-2(1)	3(1)	3(1)
O(2)	8(1)	19(1)	19(1)	-1(1)	4(1)	4(1)
O(3)	32(1)	21(1)	27(1)	8(1)	5(1)	2(1)
N(1)	10(1)	14(1)	13(1)	2(1)	3(1)	4(1)
N(2)	8(1)	17(1)	20(1)	-1(1)	2(1)	5(1)
N(3)	11(1)	16(1)	14(1)	0(1)	3(1)	3(1)
N(4)	8(1)	17(1)	13(1)	3(1)	5(1)	4(1)
N(5)	5(1)	22(1)	16(1)	1(1)	2(1)	4(1)
N(6)	10(1)	22(1)	14(1)	0(1)	4(1)	4(1)
N(7)	15(1)	15(1)	16(1)	2(1)	4(1)	6(1)
N(8)	21(1)	16(1)	20(1)	5(1)	6(1)	6(1)
N(9)	22(1)	17(1)	16(1)	8(1)	6(1)	2(1)
C(1)	13(1)	14(1)	12(1)	2(1)	4(1)	2(1)
C(2)	12(1)	21(1)	19(1)	5(1)	7(1)	5(1)
C(3)	24(1)	19(1)	23(1)	1(1)	9(1)	9(1)
C(4)	20(1)	15(1)	20(1)	-1(1)	4(1)	-3(1)
C(5)	12(1)	21(1)	20(1)	2(1)	2(1)	0(1)
C(6)	13(1)	16(1)	14(1)	3(1)	5(1)	4(1)
C(7)	12(1)	20(1)	12(1)	4(1)	5(1)	4(1)
C(8)	15(1)	20(1)	6(1)	3(1)	4(1)	6(1)
C(9)	13(1)	16(1)	15(1)	3(1)	7(1)	2(1)
C(10)	17(1)	20(1)	16(1)	4(1)	6(1)	3(1)
C(11)	23(1)	25(1)	22(1)	8(1)	12(1)	12(1)
C(12)	36(2)	18(1)	28(1)	-2(1)	14(1)	6(1)
C(13)	24(1)	23(1)	32(2)	-7(1)	9(1)	0(1)
C(14)	17(1)	23(1)	23(1)	-1(1)	7(1)	5(1)
C(15)	11(1)	13(1)	14(1)	4(1)	1(1)	2(1)
C(16)	12(1)	18(1)	19(1)	6(1)	5(1)	1(1)
C(17)	21(1)	16(1)	18(1)	4(1)	7(1)	4(1)
C(18)	22(1)	15(1)	17(1)	1(1)	-3(1)	3(1)
C(19)	13(1)	13(1)	23(1)	4(1)	1(1)	2(1)
C(20)	14(1)	9(1)	16(1)	4(1)	5(1)	3(1)
C(21)	10(1)	15(1)	17(1)	4(1)	2(1)	4(1)
C(22)	17(1)	15(1)	15(1)	7(1)	5(1)	8(1)

C(23)	12(1)	21(1)	12(1)	5(1)	3(1)	6(1)
C(24)	19(1)	32(1)	16(1)	7(1)	4(1)	9(1)
C(25)	19(1)	50(2)	19(1)	8(1)	11(1)	12(1)
C(26)	33(2)	50(2)	13(1)	2(1)	9(1)	19(1)
C(27)	28(1)	33(2)	17(1)	-2(1)	1(1)	10(1)
C(28)	17(1)	27(1)	16(1)	6(1)	6(1)	8(1)
C(29)	11(1)	20(1)	17(1)	5(1)	6(1)	7(1)
C(30)	18(1)	24(1)	19(1)	6(1)	5(1)	6(1)
C(31)	18(1)	28(1)	20(1)	-2(1)	4(1)	5(1)
C(32)	22(1)	40(2)	17(1)	5(1)	4(1)	11(1)
C(33)	25(1)	31(2)	22(1)	12(1)	7(1)	14(1)
C(34)	14(1)	21(1)	19(1)	3(1)	5(1)	6(1)
C(35)	14(1)	20(1)	16(1)	4(1)	6(1)	8(1)
C(36)	15(1)	17(1)	28(1)	6(1)	9(1)	4(1)
C(37)	14(1)	15(1)	22(1)	5(1)	4(1)	1(1)
C(38)	25(1)	20(1)	26(1)	9(1)	-1(1)	3(1)
C(39)	38(2)	15(1)	35(2)	7(1)	2(1)	-1(1)
C(40)	32(1)	24(1)	24(1)	4(1)	-2(1)	-5(1)
C(41)	25(1)	23(1)	30(2)	11(1)	0(1)	2(1)
C(42)	23(1)	15(1)	29(1)	5(1)	5(1)	3(1)

Table A20. Hydrogen coordinates ( $\times 10^4$ ) and isotropic displacement parameters ( $\text{\AA}^2 \times 10^3$ )  
for rmb311lt

	x	y	z	U(eq)
H(2N)	10260(20)	7095(18)	7534(9)	18
H(5N)	90(20)	5029(19)	6621(10)	20(6)
H(8N)	5050(20)	2250(20)	8798(11)	30(7)
H(9N)	4438(18)	3007(18)	7186(9)	10(50)
H(2)	6041	9434	7831	20
H(3)	7460	11505	8358	26
H(64)	9874	11759	8509	23
H(5)	10948	9928	8141	22
H(10)	9296	2950	6962	21
H(11)	9480	668	6645	26
H(12)	7604	-893	6009	32
H(13)	5559	-189	5647	33
H(14)	5367	2089	5940	25
H(16)	4632	4579	5562	19
H(17)	3392	3497	4473	22
H(18)	977	3001	4302	23
H(19)	-301	3643	5204	20
H(24)	699	6567	8718	26
H(25)	90	7732	9732	34
H(26)	1585	9668	10361	37
H(27)	3747	10393	10006	32
H(28)	4381	9214	9008	23
H(30)	6738	7381	8995	24
H(31)	7688	7639	10171	27



H(32)	7596	5782	10743	30
H(33)	6524	3583	10170	29
H(38)	3364	-1304	6974	28
H(39)	2356	-2506	5873	36
H(40)	1434	-1365	5040	34
H(41)	1456	955	5309	31
H(42)	2499	2177	6403	27

---

Table A21. Crystal data and structure refinement for Compound 19

Identification code	rmb260pbca	
Empirical formula	C <sub>26</sub> H <sub>32</sub> N <sub>6</sub> O <sub>3</sub> V	
Formula weight	527.52	
Temperature	100(2) K	
Wavelength	0.71073 Å	
Crystal system	Orthorhombic	
Space group	Pbca	
Unit cell dimensions	a = 12.9214(13) Å	α = 90°.
	b = 17.1388(17) Å	β = 90°.
	c = 23.445(2) Å	γ = 90°.
Volume	5192.1(9) Å <sup>3</sup>	
Z	8	
Density (calculated)	1.350 Mg/m <sup>3</sup>	
Absorption coefficient	0.421 mm <sup>-1</sup>	
F(000)	2216	
Crystal size	0.46 x 0.18 x 0.08 mm <sup>3</sup>	
Crystal color, habit	blue plate	
Theta range for data collection	2.16 to 28.07°	
Index ranges	-17 ≤ h ≤ 16, -22 ≤ k ≤ 21, -30 ≤ l ≤ 29	
Reflections collected	43202	
Independent reflections	6183 [R(int) = 0.0328]	
Completeness to theta = 28.07°	97.9 %	
Absorption correction	SADABS	
Max. and min. transmission	0.912 and 0.785	
Refinement method	Full-matrix least-squares on F <sup>2</sup>	
Data / restraints / parameters	6183 / 0 / 333	
Goodness-of-fit on F <sup>2</sup>	1.061	
Final R indices [I > 2σ(I)]	R1 = 0.0537, wR2 = 0.1088	
R indices (all data)	R1 = 0.0715, wR2 = 0.1257	
Largest diff. peak and hole	0.461 and -0.554 e.Å <sup>-3</sup>	

Table A22. Atomic coordinates ( $\times 10^4$ ) and equivalent isotropic displacement parameters ( $\text{\AA}^2 \times 10^3$ ) for rmb260Pbca.  $U(\text{eq})$  is defined as one third of the trace of the orthogonalized  $U_{ij}$  tensor.

	x	y	z	$U(\text{eq})$
V(1)	2827(1)	1036(1)	4103(1)	18(1)
O(1)	3578(1)	1143(1)	4830(1)	22(1)
O(2)	2737(1)	306(1)	3464(1)	24(1)
O(3)	2061(1)	1749(1)	4014(1)	28(1)
N(1)	4201(2)	1417(1)	3748(1)	20(1)
N(2)	5850(2)	1800(1)	3696(1)	26(1)
N(3)	5253(2)	1544(1)	4615(1)	21(1)
N(4)	1945(2)	219(1)	4520(1)	21(1)
N(5)	1237(2)	-936(1)	4715(1)	25(1)
N(6)	1826(2)	-783(1)	3778(1)	24(1)
C(1)	5063(2)	1574(1)	4046(1)	20(1)
C(2)	4449(2)	1551(1)	3176(1)	21(1)
C(3)	3852(2)	1498(2)	2685(1)	26(1)
C(4)	4326(2)	1676(2)	2169(1)	30(1)
C(5)	5359(2)	1906(2)	2137(1)	31(1)
C(6)	5957(2)	1973(2)	2627(1)	31(1)
C(7)	5483(2)	1792(2)	3142(1)	24(1)
C(8)	6903(2)	1964(2)	3874(1)	38(1)
C(9)	4514(2)	1331(1)	4964(1)	20(1)
C(10)	4787(2)	1273(2)	5597(1)	23(1)
C(11)	4651(3)	424(2)	5778(1)	45(1)
C(12)	5892(2)	1544(2)	5706(1)	47(1)
C(13)	4044(2)	1776(2)	5944(1)	31(1)
C(14)	1701(2)	-487(1)	4311(1)	22(1)
C(15)	1570(2)	236(2)	5076(1)	22(1)
C(16)	1531(2)	838(2)	5470(1)	27(1)
C(17)	1067(2)	686(2)	5993(1)	31(1)
C(18)	646(2)	-45(2)	6120(1)	30(1)
C(19)	662(2)	-646(2)	5725(1)	30(1)
C(20)	1132(2)	-493(2)	5204(1)	24(1)
C(21)	938(2)	-1746(2)	4641(1)	33(1)
C(22)	2299(2)	-369(1)	3392(1)	22(1)
C(23)	2382(2)	-707(2)	2791(1)	28(1)
C(24)	1899(3)	-1521(2)	2761(1)	36(1)
C(25)	1801(3)	-160(2)	2381(1)	40(1)
C(26)	3528(2)	-746(2)	2628(1)	34(1)

Table A23. Anisotropic displacement parameters ( $\text{\AA}^2 \times 10^3$ ) for rmb260Pbca. The anisotropic

displacement factor exponent takes the form:  $-2 \sum [h^2 a^2 U^{11} + \dots + 2 h k a^* b^* U^{12}]$

	U <sup>11</sup>	U <sup>22</sup>	U <sup>33</sup>	U <sup>23</sup>	U <sup>13</sup>	U <sup>12</sup>
V(1)	17(1)	19(1)	19(1)	-1(1)	-1(1)	-1(1)
O(1)	18(1)	29(1)	19(1)	-2(1)	-3(1)	-3(1)
O(2)	28(1)	23(1)	21(1)	-6(1)	1(1)	-6(1)
O(3)	26(1)	29(1)	30(1)	1(1)	-2(1)	3(1)
N(1)	19(1)	21(1)	19(1)	1(1)	1(1)	-3(1)
N(2)	20(1)	30(1)	27(1)	1(1)	1(1)	-5(1)
N(3)	20(1)	22(1)	22(1)	-1(1)	-2(1)	-2(1)
N(4)	20(1)	23(1)	20(1)	-2(1)	1(1)	-4(1)
N(5)	26(1)	24(1)	25(1)	3(1)	1(1)	-4(1)
N(6)	27(1)	23(1)	22(1)	-2(1)	-2(1)	-3(1)
C(1)	20(1)	17(1)	23(1)	-1(1)	-1(1)	-1(1)
C(2)	25(1)	18(1)	21(1)	-1(1)	2(1)	2(1)
C(3)	31(1)	26(1)	21(1)	2(1)	-2(1)	-2(1)
C(4)	42(2)	27(1)	21(1)	1(1)	-2(1)	4(1)
C(5)	38(2)	30(1)	25(1)	5(1)	9(1)	4(1)
C(6)	29(1)	32(1)	32(1)	5(1)	8(1)	1(1)
C(7)	26(1)	21(1)	25(1)	1(1)	2(1)	0(1)
C(8)	22(1)	55(2)	38(2)	5(1)	-1(1)	-10(1)
C(9)	22(1)	17(1)	21(1)	-3(1)	-3(1)	2(1)
C(10)	26(1)	24(1)	19(1)	-3(1)	-6(1)	1(1)
C(11)	82(3)	26(1)	25(1)	0(1)	-10(2)	7(2)
C(12)	28(2)	84(3)	27(2)	-4(2)	-8(1)	-5(2)
C(13)	38(2)	34(1)	23(1)	-6(1)	-3(1)	9(1)
C(14)	22(1)	20(1)	23(1)	0(1)	-1(1)	-3(1)
C(15)	17(1)	28(1)	21(1)	-1(1)	0(1)	-1(1)
C(16)	24(1)	34(1)	24(1)	-1(1)	1(1)	-4(1)
C(17)	28(1)	40(2)	24(1)	-3(1)	1(1)	2(1)
C(18)	27(1)	42(2)	22(1)	5(1)	3(1)	1(1)
C(19)	27(1)	34(1)	28(1)	10(1)	0(1)	-1(1)
C(20)	22(1)	27(1)	23(1)	3(1)	-2(1)	-1(1)
C(21)	41(2)	21(1)	36(2)	4(1)	-1(1)	-6(1)
C(22)	21(1)	22(1)	23(1)	-4(1)	-4(1)	-1(1)
C(23)	35(1)	26(1)	23(1)	-6(1)	-2(1)	0(1)
C(24)	48(2)	31(1)	30(1)	-9(1)	1(1)	-7(1)
C(25)	54(2)	37(2)	30(2)	-4(1)	-15(1)	1(1)
C(26)	42(2)	36(2)	25(1)	-5(1)	7(1)	0(1)

Table A24. Hydrogen coordinates ( $\times 10^4$ ) and isotropic displacement parameters ( $\text{\AA}^2 \times 10^3$ )  
for rmb260Pbca.

	x	y	z	U(eq)
H(3)	3146	1346	2701	31
H(4)	3934	1640	1828	36
H(5)	5658	2018	1776	38
H(6)	6659	2136	2610	37
H(8A)	6912	2081	4283	57
H(8B)	7167	2414	3661	57
H(8C)	7340	1508	3798	57
H(11A)	4799	373	6186	67
H(11B)	5130	94	5561	67
H(11C)	3938	259	5703	67
H(12A)	5965	2089	5584	70
H(12B)	6373	1217	5489	70
H(12C)	6047	1502	6114	70
H(13A)	4205	1723	6351	47
H(13B)	3332	1605	5874	47
H(13C)	4119	2323	5830	47
H(16)	1811	1337	5386	32
H(17)	1034	1089	6270	37
H(18)	344	-131	6484	37
H(19)	364	-1140	5806	35
H(21A)	899	-1868	4233	49
H(21B)	260	-1833	4817	49
H(21C)	1452	-2085	4823	49
H(24A)	2252	-1868	3030	54
H(24B)	1972	-1727	2373	54
H(24C)	1163	-1489	2860	54
H(25A)	1071	-132	2492	60
H(25B)	1855	-362	1991	60
H(25C)	2108	362	2398	60
H(26A)	3832	-223	2651	51
H(26B)	3594	-943	2237	51
H(26C)	3892	-1097	2890	51

Table A25. Crystal data and structure refinement for compound 23.

Identification code	rmb317p21c	
Empirical formula	C <sub>20</sub> H <sub>20</sub> N <sub>6</sub> O <sub>2</sub> Zn	
Formula weight	441.79	
Temperature	373(2) K	
Wavelength	0.71073 Å	
Crystal system	Monoclinic	
Space group	P2 <sub>1</sub> /c	
Unit cell dimensions	a = 8.2544(14) Å	α = 90°.
	b = 22.984(4) Å	β = 100.364(3)°.
	c = 10.3376(18) Å	γ = 90°.
Volume	1929.2(6) Å <sup>3</sup>	
Z	4	
Density (calculated)	1.521 Mg/m <sup>3</sup>	
Absorption coefficient	1.303 mm <sup>-1</sup>	
F(000)	912	
Crystal size	0.22 x 0.16 x 0.14 mm <sup>3</sup>	
Theta range for data collection	1.77 to 27.54°	
Index ranges	-10 ≤ h ≤ 10, -29 ≤ k ≤ 29, -13 ≤ l ≤ 13	
Reflections collected	16202	
Independent reflections	4323 [R(int) = 0.0657]	
Completeness to theta = 27.54°	97.1 %	
Absorption correction	SADABS	
Max. and min. transmission	0.8386 and 0.7625	
Refinement method	Full-matrix least-squares on F <sup>2</sup>	
Data / restraints / parameters	4323 / 0 / 286	
Goodness-of-fit on F <sup>2</sup>	1.087	
Final R indices [I > 2σ(I)]	R1 = 0.0753, wR2 = 0.1508	
R indices (all data)	R1 = 0.0839, wR2 = 0.1549	
Largest diff. peak and hole	0.643 and -0.773 e.Å <sup>-3</sup>	

Table A26. Atomic coordinates (x 104) and equivalent isotropic displacement parameters ( $\text{\AA}^2 \times 10^3$ ) for rmb317P21c. U(eq) is defined as one third of the trace of the orthogonalized  $U_{ij}$  tensor.

	x	y	z	U(eq)
Zn(1)	2902(1)	3789(1)	-816(1)	16(1)
O(1)	1220(4)	3369(2)	-2056(3)	24(1)
O(2)	4079(4)	4223(1)	-1992(3)	20(1)
N(1)	3689(5)	3075(2)	94(4)	16(1)
N(2)	3852(5)	2120(2)	399(4)	17(1)
N(3)	2054(5)	2413(2)	-1500(4)	18(1)
N(4)	2466(5)	4490(2)	114(4)	16(1)
N(5)	2162(5)	5447(2)	320(4)	16(1)
N(6)	3336(5)	5169(2)	-1475(4)	18(1)
C(1)	3139(6)	2556(2)	-391(5)	16(1)
C(2)	4901(6)	2363(2)	1455(5)	16(1)
C(3)	5875(6)	2114(2)	2537(5)	20(1)
C(4)	6761(6)	2492(2)	3439(5)	21(1)
C(5)	6664(6)	3098(2)	3255(5)	22(1)
C(6)	5681(6)	3344(2)	2168(4)	18(1)
C(7)	4788(6)	2966(2)	1260(4)	16(1)
C(8)	3572(7)	1499(2)	178(5)	23(1)
C(9)	1218(6)	2818(2)	-2232(5)	18(1)
C(10)	63(6)	2600(2)	-3440(5)	21(1)
C(11)	2694(5)	5017(2)	-404(5)	15(1)
C(12)	1586(6)	5195(2)	1364(4)	16(1)
C(13)	927(6)	5434(2)	2393(5)	20(1)
C(14)	469(7)	5047(2)	3275(5)	25(1)
C(15)	688(7)	4448(2)	3174(5)	26(1)
C(16)	1356(6)	4211(2)	2147(5)	21(1)
C(17)	1787(6)	4594(2)	1231(4)	16(1)
C(18)	2165(6)	6067(2)	28(5)	20(1)
C(19)	3937(6)	4770(2)	-2179(4)	16(1)
C(20)	4498(6)	4995(2)	-3403(5)	21(1)

Table A27. Anisotropic displacement parameters ( $\text{\AA}^2 \times 10^3$ ) for rmb317P21c. The anisotropic displacement factor exponent takes the form:  $-2 \square^2 [ h^2 a^* 2U_{11} + \dots + 2 h k a^* b^* U_{12} ]$

	$U^{11}$	$U^{22}$	$U^{33}$	$U^{23}$	$U^{13}$	$U^{12}$
Zn(1)	23(1)	10(1)	15(1)	0(1)	3(1)	1(1)
O(1)	28(2)	15(2)	25(2)	-3(1)	-2(2)	3(1)
O(2)	29(2)	14(2)	20(2)	0(1)	10(1)	3(1)
N(1)	22(2)	12(2)	14(2)	0(2)	5(2)	2(2)
N(2)	21(2)	14(2)	14(2)	0(2)	2(2)	-1(2)
N(3)	24(2)	13(2)	16(2)	-2(2)	4(2)	-3(2)
N(4)	22(2)	12(2)	14(2)	-3(2)	2(2)	0(2)
N(5)	23(2)	13(2)	13(2)	-1(2)	3(2)	1(2)
N(6)	23(2)	14(2)	17(2)	1(2)	6(2)	1(2)
C(1)	17(2)	15(2)	17(2)	0(2)	9(2)	0(2)
C(2)	18(2)	14(2)	17(2)	-1(2)	7(2)	0(2)
C(3)	24(3)	16(2)	19(2)	3(2)	3(2)	0(2)
C(4)	25(3)	25(2)	14(2)	5(2)	4(2)	0(2)
C(5)	26(3)	23(2)	16(2)	-5(2)	1(2)	-5(2)
C(6)	24(2)	17(2)	14(2)	1(2)	7(2)	-3(2)
C(7)	21(2)	17(2)	12(2)	2(2)	8(2)	1(2)
C(8)	35(3)	13(2)	19(2)	-1(2)	3(2)	-2(2)
C(9)	19(2)	21(2)	16(2)	-1(2)	5(2)	-1(2)
C(10)	26(3)	19(2)	18(2)	-2(2)	3(2)	-1(2)
C(11)	12(2)	15(2)	17(2)	-3(2)	1(2)	1(2)
C(12)	17(2)	16(2)	15(2)	0(2)	0(2)	2(2)
C(13)	24(3)	21(2)	14(2)	-5(2)	0(2)	6(2)
C(14)	27(3)	34(3)	16(2)	-2(2)	8(2)	7(2)
C(15)	31(3)	31(3)	18(2)	6(2)	6(2)	4(2)
C(16)	23(3)	24(2)	17(2)	2(2)	2(2)	2(2)
C(17)	19(2)	15(2)	12(2)	-1(2)	-1(2)	0(2)
C(18)	29(3)	11(2)	21(2)	0(2)	6(2)	1(2)
C(19)	17(2)	16(2)	13(2)	-3(2)	-1(2)	0(2)
C(20)	29(3)	15(2)	19(2)	-3(2)	7(2)	0(2)



Table A28. Hydrogen coordinates ( $\times 10^4$ ) and isotropic displacement parameters ( $\text{\AA}^2 \times 10^3$ )  
for rmb317P21c.

	x	y	z	U(eq)
H(3)	5934	1713	2654	13(12)
H(4)	7435	2342	4183	23(15)
H(5)	7277	3339	3881	27(15)
H(6)	5620	3745	2051	22(14)
H(8A)	2868	1357	753	80(30)
H(8B)	4607	1297	356	60(20)
H(8C)	3058	1435	-719	44(19)
H(10A)	-1054	2683	-3357	29(16)
H(10B)	199	2188	-3523	80(30)
H(10C)	311	2792	-4206	60(20)
H(13)	803	5833	2479	16(13)
H(14)	-4	5190	3962	25(15)
H(15)	382	4203	3804	50(20)
H(16)	1507	3812	2079	33(16)
H(18A)	3246	6223	332	23(14)
H(18B)	1386	6262	464	27(15)
H(18C)	1866	6125	-904	25(15)
H(20A)	5518	4812	-3490	14(13)
H(20B)	4653	5409	-3335	32(16)
H(20C)	3678	4908	-4161	18(14)

Table A29. Crystal data and structure refinement for Compound 24

Identification code	rmb329lt	
Empirical formula	C <sub>14</sub> H <sub>20</sub> Cu N <sub>2</sub> O <sub>5</sub>	
Formula weight	359.86	
Temperature	100(2) K	
Wavelength	0.71073 Å	
Crystal system	monoclinic	
Space group	P2(1)/c	
Unit cell dimensions	a = 13.8508(8) Å	α = 90°
	b = 11.0612(5) Å	β = 104.508(6)°
	c = 11.0301(6) Å	γ = 90°
Volume	1635.98(15) Å <sup>3</sup>	
Z	4	
Density (calculated)	1.461 Mg/m <sup>3</sup>	
Absorption coefficient	1.358 mm <sup>-1</sup>	
F(000)	748	
Crystal color, habit	blue-green cut block	
Crystal size	0.41 x 0.38 x 0.38 mm <sup>3</sup>	
Theta range for data collection	3.55 to 28.88°	
Index ranges	-18 ≤ h ≤ 10, -9 ≤ k ≤ 14, -12 ≤ l ≤ 14	
Reflections collected	6513	
Independent reflections	3607 [R(int) = 0.0276]	
Completeness to theta = 28.88°	83.9 %	
Completeness to theta = 26.32°	96.7%	
Refinement method	Full-matrix least-squares on F <sup>2</sup>	
Data / restraints / parameters	3607 / 0 / 208	
Goodness-of-fit on F <sup>2</sup>	1.058	
Final R indices [I > 2σ(I)]	R1 = 0.0335, wR2 = 0.0951	
R indices (all data)	R1 = 0.0469, wR2 = 0.0972	
Largest diff. peak and hole	0.666 and -0.532 e.Å <sup>-3</sup>	

Table A30. Atomic coordinates ( $\times 10^4$ ) and equivalent isotropic displacement parameters ( $\text{\AA}^2 \times 10^3$ ) for rmb329lt.  $U(\text{eq})$  is defined as one third of the trace of the orthogonalized  $U^{\text{ij}}$  tensor.

	x	y	z	U(eq)
Cu(1)	5713(1)	-136(1)	1022(1)	11(1)
O(1)	5250(2)	-1831(2)	833(2)	16(1)
O(3)	4658(1)	238(2)	1868(2)	18(1)
O(2)	5996(2)	1602(2)	895(2)	18(1)
O(4)	6575(1)	-439(2)	-123(2)	16(1)
O(5)	9608(2)	1144(2)	3468(2)	23(1)
N(1)	6839(2)	-565(2)	2761(2)	13(1)
N(2)	8138(2)	462(2)	2260(2)	18(1)
C(1)	5480(2)	2219(2)	-2(2)	14(1)
C(5)	6465(2)	-1254(2)	3544(2)	15(1)
C(2)	5760(2)	3530(3)	-73(3)	23(1)
C(6)	7017(2)	-1628(2)	4701(2)	16(1)
C(3)	6242(2)	-435(2)	-1299(2)	13(1)
C(7)	8008(2)	-1299(3)	5062(3)	18(1)
C(4)	6955(2)	-691(3)	-2093(3)	23(1)
C(8)	8415(2)	-600(3)	4276(3)	17(1)
C(9)	7804(2)	-245(2)	3133(2)	14(1)
C(10)	8992(2)	1128(2)	2468(3)	15(1)
C(11)	9152(2)	1895(3)	1371(3)	18(1)
C(12)	9147(3)	3213(3)	1782(4)	42(1)
C(14)	10178(2)	1568(4)	1185(3)	32(1)
C(13)	8377(3)	1697(4)	133(3)	35(1)

Table A31. Anisotropic displacement parameters ( $\text{\AA}^2 \times 10^3$ ) for rmb329lt. The anisotropic displacement factor exponent takes the form:  $-2h^2 a^* U^{11} + \dots + 2hk a^* b^* U^{12}$

	$U^{11}$	$U^{22}$	$U^{33}$	$U^{23}$	$U^{13}$	$U^{12}$
Cu(1)	10(1)	12(1)	11(1)	0(1)	3(1)	1(1)
O(1)	16(1)	13(1)	20(1)	1(1)	2(1)	0(1)
O(3)	15(1)	24(1)	15(1)	-1(1)	4(1)	7(1)
O(2)	17(1)	12(1)	23(1)	0(1)	-1(1)	0(1)
O(4)	12(1)	20(1)	15(1)	1(1)	4(1)	2(1)
O(5)	19(1)	28(1)	19(1)	6(1)	0(1)	-8(1)
N(1)	12(1)	15(1)	13(1)	1(1)	4(1)	0(1)
N(2)	12(1)	27(1)	13(1)	7(1)	0(1)	-5(1)
C(1)	13(1)	14(1)	18(1)	-2(1)	7(1)	-1(1)
C(5)	15(1)	16(1)	16(1)	-1(1)	5(1)	-4(1)

C(2)	23(2)	15(1)	29(2)	2(1)	2(1)	-3(1)
C(6)	21(2)	13(1)	13(1)	2(1)	7(1)	-3(1)
C(3)	15(1)	9(1)	17(1)	0(1)	7(1)	0(1)
C(7)	20(2)	19(1)	13(1)	4(1)	0(1)	-2(1)
C(4)	20(2)	32(2)	19(2)	-2(1)	10(1)	4(1)
C(8)	13(1)	21(1)	16(1)	1(1)	1(1)	-4(1)
C(9)	13(1)	14(1)	14(1)	0(1)	4(1)	-1(1)
C(10)	14(1)	16(1)	17(1)	1(1)	5(1)	0(1)
C(11)	15(1)	21(1)	18(1)	4(1)	6(1)	-3(1)
C(12)	71(3)	21(2)	43(2)	10(2)	29(2)	2(2)
C(14)	22(2)	50(2)	27(2)	8(2)	12(1)	-1(2)
C(13)	24(2)	58(2)	23(2)	19(2)	2(1)	-12(2)

Table A32. Hydrogen coordinates ( $\times 10^4$ ) and isotropic displacement parameters ( $\text{\AA}^2 \times 10^{-3}$ ) for rmb329lt.

	x	y	z	U(eq)
H(5)	5801	-1490	3289	18
H(2A)	5430	3850	-880	35
H(2B)	6469	3595	47	35
H(2C)	5560	3979	568	35
H(6)	6729	-2088	5224	19
H(7)	8403	-1548	5833	21
H(4A)	7115	50	-2452	34
H(4B)	6652	-1243	-2750	34
H(4C)	7554	-1043	-1583	34
H(8)	9083	-373	4508	20
H(12A)	9281	3729	1143	63
H(12B)	9651	3331	2547	63
H(12C)	8505	3409	1913	63
H(14A)	10198	721	1004	48
H(14B)	10682	1752	1934	48
H(14C)	10300	2028	499	48
H(13A)	8550	2170	-511	53
H(13B)	7732	1940	221	53
H(13C)	8360	857	-89	53
H(20)	7780(30)	480(30)	1600(30)	20(9)

Table A33. Crystal data and structure refinement for compound 25

Identification code	rmb317repro55	
Empirical formula	C <sub>20</sub> H <sub>26</sub> I <sub>2</sub> N <sub>4</sub> O <sub>2</sub> Pt	
Formula weight	803.34	
Temperature	373(2) K	
Wavelength	0.71073 Å	
Crystal system	Triclinic	
Space group	P-1	
Unit cell dimensions	a = 9.502(2) Å	α = 102.244(4)°.
	b = 10.692(3) Å	β = 98.049(4)°.
	c = 14.141(4) Å	γ = 113.604(3)°.
Volume	1245.3(5) Å <sup>3</sup>	
Z	2	
Density (calculated)	2.142 Mg/m <sup>3</sup>	
Absorption coefficient	8.135 mm <sup>-1</sup>	
F(000)	748	
Crystal size	0.24 x 0.16 x 0.15 mm <sup>3</sup>	
Theta range for data collection	1.52 to 27.66°	
Index ranges	-12 ≤ h ≤ 12, -13 ≤ k ≤ 13, -18 ≤ l ≤ 18	
Reflections collected	10877	
Independent reflections	5546 [R(int) = 0.0194]	
Completeness to theta = 27.66°	95.2 %	
Absorption correction	SADABS	
Max. and min. transmission	0.3750 and 0.2456	
Refinement method	Full-matrix least-squares on F <sup>2</sup>	
Data / restraints / parameters	5546 / 0 / 276	
Goodness-of-fit on F <sup>2</sup>	1.050	
Final R indices [I > 2σ(I)]	R1 = 0.0281, wR2 = 0.0719	
R indices (all data)	R1 = 0.0305, wR2 = 0.0734	
Largest diff. peak and hole	2.259 and -1.344 e.Å <sup>-3</sup>	

Table A34. Atomic coordinates ( $\times 10^4$ ) and equivalent isotropic displacement parameters ( $\text{\AA}^2 \times 10^3$ ) for rmb317repro55.  $U(\text{eq})$  is defined as one third of the trace of the orthogonalized  $U_{ij}$  tensor.

	x	y	z	$U(\text{eq})$
Pt(1)	5137(1)	7998(1)	7501(1)	17(1)
I(1)	7848(1)	8829(1)	7050(1)	23(1)
I(2)	5372(1)	10555(1)	8032(1)	28(1)
O(1)	6874(4)	4997(4)	9531(3)	30(1)
O(2)	-726(4)	6132(4)	5337(3)	28(1)
N(1)	4936(4)	5955(4)	7089(3)	19(1)
N(2)	6486(4)	6455(4)	8668(3)	18(1)
N(3)	2947(5)	7172(4)	7827(3)	20(1)
N(4)	1786(5)	7385(4)	6368(3)	23(1)
C(1)	4112(5)	5104(5)	6160(3)	23(1)
C(2)	3992(6)	3752(5)	5810(4)	25(1)
C(3)	4714(5)	3246(5)	6464(4)	24(1)
C(4)	5555(5)	4106(5)	7419(4)	21(1)
C(5)	5656(5)	5472(5)	7728(3)	18(1)
C(6)	7066(5)	6182(5)	9512(4)	22(1)
C(7)	8028(5)	7496(5)	10423(3)	22(1)
C(8)	7969(6)	8869(5)	10306(4)	27(1)
C(9)	7392(7)	7158(6)	11324(4)	31(1)
C(10)	9757(6)	7704(6)	10587(4)	30(1)
C(11)	2872(6)	6788(5)	8685(4)	24(1)
C(12)	1470(6)	6111(6)	8917(4)	31(1)
C(13)	76(6)	5827(5)	8266(4)	27(1)
C(14)	116(6)	6228(5)	7405(4)	24(1)
C(15)	1587(5)	6902(5)	7193(3)	21(1)
C(16)	631(5)	7032(5)	5503(4)	21(1)
C(17)	1264(6)	7928(5)	4809(4)	24(1)
C(18)	2703(7)	7784(8)	4542(4)	42(1)
C(19)	1701(7)	9480(6)	5345(4)	37(1)
C(20)	-38(6)	7411(6)	3846(4)	28(1)

Table A35. Anisotropic displacement parameters ( $\text{\AA}^2 \times 10^3$ ) for rmb317repro55. The anisotropic displacement factor exponent takes the form:  $-2\pi^2 [h^2 a^{*2} U^{11} + \dots + 2 h k a^* b^* U^{12}]$

	U <sup>11</sup>	U <sup>22</sup>	U <sup>33</sup>	U <sup>23</sup>	U <sup>13</sup>	U <sup>12</sup>
Pt(1)	17(1)	14(1)	19(1)	6(1)	1(1)	6(1)
I(1)	21(1)	19(1)	21(1)	4(1)	5(1)	3(1)
I(2)	29(1)	17(1)	37(1)	7(1)	3(1)	11(1)
O(1)	34(2)	19(2)	31(2)	9(2)	-3(2)	8(2)
O(2)	22(2)	28(2)	28(2)	10(2)	2(1)	6(2)
N(1)	15(2)	19(2)	18(2)	4(2)	3(1)	4(2)
N(2)	18(2)	19(2)	15(2)	3(1)	0(1)	8(2)
N(3)	21(2)	17(2)	25(2)	8(2)	6(2)	10(2)
N(4)	21(2)	25(2)	23(2)	10(2)	2(2)	9(2)
C(1)	20(2)	24(2)	22(2)	9(2)	2(2)	7(2)
C(2)	22(2)	18(2)	25(2)	2(2)	4(2)	3(2)
C(3)	18(2)	17(2)	32(3)	3(2)	4(2)	6(2)
C(4)	16(2)	18(2)	29(2)	10(2)	5(2)	7(2)
C(5)	16(2)	17(2)	19(2)	1(2)	2(2)	6(2)
C(6)	18(2)	23(2)	24(2)	10(2)	4(2)	7(2)
C(7)	20(2)	20(2)	22(2)	7(2)	3(2)	6(2)
C(8)	33(3)	19(2)	22(2)	1(2)	-1(2)	11(2)
C(9)	38(3)	34(3)	25(3)	11(2)	13(2)	16(2)
C(10)	19(2)	27(3)	34(3)	-2(2)	-1(2)	7(2)
C(11)	25(2)	28(3)	24(2)	10(2)	4(2)	15(2)
C(12)	34(3)	35(3)	32(3)	19(2)	13(2)	18(2)
C(13)	25(2)	30(3)	30(3)	13(2)	10(2)	14(2)
C(14)	20(2)	28(2)	24(2)	9(2)	2(2)	12(2)
C(15)	20(2)	19(2)	23(2)	6(2)	1(2)	9(2)
C(16)	20(2)	18(2)	25(2)	6(2)	4(2)	10(2)
C(17)	22(2)	25(2)	23(2)	10(2)	2(2)	8(2)
C(18)	28(3)	68(4)	37(3)	26(3)	13(2)	22(3)
C(19)	50(3)	28(3)	30(3)	16(2)	-1(2)	12(3)
C(20)	25(2)	32(3)	24(2)	10(2)	-1(2)	10(2)

Table A36. Hydrogen coordinates ( $\times 10^4$ ) and isotropic displacement parameters ( $\text{\AA}^2 \times 10^{-3}$ )  
for rmb317repro55.

	x	y	z	U(eq)
H(1)	3606	5439	5738	14(12)
H(2)	3445	3192	5157	39(17)
H(3)	4626	2327	6253	12(11)
H(4)	6050	3778	7853	22(13)
H(8A)	8332	9067	9730	40
H(8B)	8641	9651	10891	40
H(8C)	6899	8750	10225	40
H(9A)	6318	7034	11220	47
H(9B)	8038	7933	11918	47
H(9C)	7422	6297	11399	47
H(10A)	9785	6827	10619	45
H(10B)	10389	8440	11203	45
H(10C)	10172	7977	10043	45
H(11)	3811	6997	9129	37(16)
H(12)	1450	5844	9502	40(17)
H(13)	-892	5363	8411	26(14)
H(14)	-816	6056	6970	11(11)
H(18A)	2992	8238	4035	62
H(18B)	2449	6790	4298	62
H(18C)	3576	8232	5127	62
H(19A)	791	9543	5529	56
H(19B)	2043	10055	4908	56
H(19C)	2544	9818	5935	56
H(20A)	-933	7532	4006	42
H(20B)	-358	6419	3527	42
H(20C)	362	7957	3404	42



Table A37. Crystal data and structure refinement for compound 26

Identification code	rmb322ltb	
Empirical formula	C <sub>20</sub> H <sub>28</sub> I <sub>2</sub> N <sub>4</sub> O <sub>2</sub> Pt	
Formula weight	805.35	
Temperature	100(2) K	
Wavelength	0.71073 Å	
Crystal system	orthorhombic	
Space group	Pbca	
Unit cell dimensions	a = 12.78166(14) Å	α = 90°.
	b = 9.19192(9) Å	β = 90°.
	c = 20.5324(2) Å	γ = 90°.
Volume	2412.30(4) Å <sup>3</sup>	
Z	4	
Density (calculated)	2.218 Mg/m <sup>3</sup>	
Absorption coefficient	8.399 mm <sup>-1</sup>	
F(000)	1504	
Crystal color, shape	thin yellow plate	
Crystal size	0.37 x 0.34 x 0.02 mm <sup>3</sup>	
Theta range for data collection	3.38 to 29.02°	
Index ranges	-17 ≤ h ≤ 16, -12 ≤ k ≤ 11, -26 ≤ l ≤ 26	
Reflections collected	31818	
Independent reflections	3043 [R(int) = 0.0463]	
Completeness to theta = 29.02°	94.4 % (final refinements)	
Completeness to theta = 26.32°	99.6%	
Absorption correction	SCALE3 ABSPACK	
Max. and min. transmission	0.998 and 0.187	
Refinement method	Full-matrix least-squares on F <sup>2</sup>	
Data / restraints / parameters	3043 / 1 / 189	
Goodness-of-fit on F <sup>2</sup>	1.022	
Final R indices [I > 2σ(I)]	R1 = 0.0222, wR2 = 0.0628	
R indices (all data)	R1 = 0.0274, wR2 = 0.0647	
Largest diff. peak and hole	1.955 and -1.461 e.Å <sup>-3</sup>	

Table A38. Atomic coordinates ( $\times 10^4$ ) and equivalent isotropic displacement parameters ( $\text{\AA}^2 \times 10^3$ ) for rmb322ltb.  $U(\text{eq})$  is defined as one third of the trace of the orthogonalized  $U_{ij}$  tensor.

	x	y	z	U(eq)
Pt(1)	5000	0	5000	12(1)
I(1)	5628(1)	2081(1)	5761(1)	19(1)
O(1)	5899(2)	3027(2)	2858(1)	25(1)
N(1)	6343(2)	234(2)	4476(1)	14(1)
N(2)	5444(2)	1640(3)	3731(1)	18(1)
C(1)	7234(2)	-396(3)	4699(2)	17(1)
C(2)	8176(3)	-230(3)	4393(2)	20(1)
C(3)	8217(2)	618(3)	3837(2)	19(1)
C(4)	7331(2)	1263(3)	3601(2)	17(1)
C(5)	6389(2)	1056(3)	3928(1)	14(1)
C(6)	5226(2)	2568(3)	3224(2)	16(1)
C(7)	4063(2)	2969(3)	3172(1)	18(1)
C(8)	3742(3)	3773(4)	3794(2)	23(1)
C(9)	3917(3)	3961(4)	2582(2)	28(1)
C(10)	3399(3)	1600(4)	3095(2)	23(1)

Table A39. Anisotropic displacement parameters ( $\text{\AA}^2 \times 10^3$ ) for rmb322ltb. The anisotropic displacement factor exponent takes the form:  $-2\pi^2 [h^2 a^{*2} U^{11} + \dots + 2 h k a^* b^* U^{12}]$

	$U^{11}$	$U^{22}$	$U^{33}$	$U^{23}$	$U^{13}$	$U^{12}$
Pt(1)	10(1)	13(1)	12(1)	2(1)	1(1)	1(1)
I(1)	19(1)	18(1)	20(1)	-4(1)	3(1)	-3(1)
O(1)	22(1)	31(1)	21(1)	11(1)	4(1)	-2(1)
N(1)	14(1)	14(1)	13(1)	1(1)	2(1)	0(1)
N(2)	11(1)	25(1)	18(1)	9(1)	5(1)	0(1)
C(1)	15(1)	19(1)	18(2)	4(1)	1(1)	1(1)
C(2)	12(1)	24(1)	23(2)	-2(1)	0(1)	5(1)
C(3)	13(1)	21(1)	24(2)	-2(1)	4(1)	-6(1)
C(4)	17(1)	19(1)	15(1)	1(1)	3(1)	-2(1)
C(5)	15(1)	14(1)	12(1)	0(1)	0(1)	-1(1)
C(6)	18(1)	14(1)	17(2)	0(1)	2(1)	-2(1)
C(7)	18(1)	19(1)	17(2)	4(1)	-2(1)	2(1)
C(8)	22(2)	22(2)	26(2)	-2(1)	1(1)	5(1)
C(9)	25(2)	30(2)	29(2)	12(2)	0(1)	6(2)
C(10)	20(2)	21(2)	29(2)	1(1)	-8(1)	0(1)

Table A40. Hydrogen coordinates ( $\times 10^4$ ) and isotropic displacement parameters ( $\text{\AA}^2 \times 10^{-3}$ ) for rmb322ltb.

	x	y	z	U(eq)
H(2N)	5010(20)	1510(40)	3957(15)	15(9)
H(1)	7190(30)	-980(40)	5036(15)	18(9)
H(2)	8690(30)	-530(40)	4558(19)	32(10)
H(3)	8850(20)	750(30)	3645(15)	13(8)
H(4)	7360(30)	1760(40)	3265(17)	20(9)
H(8A)	3840(40)	3170(50)	4180(20)	43(13)
H(8B)	4200(30)	4590(50)	3851(19)	28(9)
H(8C)	3040(30)	4000(40)	3777(17)	24(9)
H(9A)	4190(30)	3500(40)	2227(19)	29(10)
H(9B)	3210(40)	4040(50)	2510(20)	57(15)
H(9C)	4260(20)	4760(40)	2659(16)	7(8)
H(10A)	3430(30)	1030(50)	3440(20)	45(12)
H(10B)	3550(30)	1040(40)	2731(18)	28(9)
H(10C)	2740(30)	1870(40)	2991(17)	26(10)

Table A41. Crystal data and structure refinement for compound 27.

Identification code	rmb319ltn	
Empirical formula	C <sub>10</sub> H <sub>13</sub> N <sub>2</sub> O Pt <sub>0.50</sub>	
Formula weight	274.77	
Temperature	100(2) K	
Wavelength	0.71073 Å	
Crystal system	Monoclinic	
Space group	P 1 2 <sub>1</sub> /c 1	
Unit cell dimensions	a = 6.0476(2) Å	α = 90°.
	b = 13.5698(5) Å	β = 95.157(3)°.
	c = 11.8620(4) Å	γ = 90°.
Volume	969.52(6) Å <sup>3</sup>	
Z	4	
Density (calculated)	1.882 Mg/m <sup>3</sup>	
Absorption coefficient	7.259 mm <sup>-1</sup>	
F(000)	536	
Crystal size	0.38 x 0.36 x 0.34 mm <sup>3</sup>	
Theta range for data collection	3.38 to 28.99°	
Index ranges	-7 ≤ h ≤ 8, -18 ≤ k ≤ 18, -16 ≤ l ≤ 15	
Reflections collected	32994	
Independent reflections	2484 [R(int) = 0.0574]	
Completeness to theta = 28.99°	96.2 %	
Absorption correction	Semi-empirical from equivalents	
Max. and min. transmission	1.00000 and 0.53725	
Refinement method	Full-matrix least-squares on F <sup>2</sup>	
Data / restraints / parameters	2484 / 0 / 176	
Goodness-of-fit on F <sup>2</sup>	1.038	
Final R indices [I > 2σ(I)]	R1 = 0.0193, wR2 = 0.0477	
R indices (all data)	R1 = 0.0289, wR2 = 0.0499	
Largest diff. peak and hole	2.251 and -0.925 e.Å <sup>-3</sup>	

Table A42. Atomic coordinates ( $\times 10^4$ ) and equivalent isotropic displacement parameters ( $\text{\AA}^2 \times 10^3$ ) for rmb319LTn.  $U(\text{eq})$  is defined as one third of the trace of the orthogonalized  $U_{ij}$  tensor.

	x	y	z	$U(\text{eq})$
Pt(1)	5000	5000	5000	10(1)
O(1)	4760(3)	3557(2)	4736(2)	21(1)
N(1)	2376(4)	4963(1)	5946(2)	13(1)
N(2)	1934(4)	3173(2)	5895(2)	18(1)
C(1)	1384(5)	4106(2)	6227(2)	14(1)
C(2)	-427(5)	4138(2)	6904(3)	17(1)
C(3)	-1210(5)	5014(2)	7290(3)	16(1)
C(4)	-180(5)	5885(2)	6994(3)	17(1)
C(5)	1557(5)	5825(2)	6333(3)	16(1)
C(6)	3442(4)	2974(2)	5218(2)	15(1)
C(7)	3816(4)	1877(2)	4973(3)	16(1)
C(8)	4825(6)	1739(2)	3841(3)	25(1)
C(9)	5424(5)	1498(2)	5952(3)	24(1)
C(10)	1634(5)	1314(2)	4934(3)	22(1)

Table A43. Anisotropic displacement parameters ( $\text{\AA}^2 \times 10^3$ ) for rmb319LTn. The anisotropic displacement factor exponent takes the form:  $-2 \sum [h^2 a^2 U^{11} + \dots + 2 h k a^* b^* U^{12}]$

	$U^{11}$	$U^{22}$	$U^{33}$	$U^{23}$	$U^{13}$	$U^{12}$
Pt(1)	11(1)	7(1)	13(1)	-1(1)	2(1)	0(1)
O(1)	25(1)	7(1)	32(1)	-2(1)	12(1)	0(1)
N(1)	13(1)	10(1)	15(1)	-1(1)	2(1)	2(1)
N(2)	26(1)	9(1)	20(1)	0(1)	3(1)	3(1)
C(1)	17(1)	13(1)	12(1)	1(1)	0(1)	1(1)
C(2)	18(1)	14(1)	20(2)	1(1)	6(1)	-1(1)
C(3)	15(1)	19(2)	15(1)	-1(1)	4(1)	0(1)
C(4)	19(1)	13(1)	19(2)	-4(1)	5(1)	2(1)
C(5)	17(1)	12(2)	22(2)	-1(1)	6(1)	-2(1)
C(6)	18(1)	11(1)	15(1)	0(1)	-2(1)	-2(1)
C(7)	19(2)	10(1)	20(2)	-2(1)	5(1)	1(1)
C(8)	35(2)	14(2)	27(2)	-4(1)	12(2)	1(1)
C(9)	26(2)	12(2)	32(2)	5(1)	-2(1)	1(1)
C(10)	28(2)	13(2)	25(2)	-4(1)	7(1)	-1(1)

Table A44. Hydrogen coordinates ( $\times 10^4$ ) and isotropic displacement parameters ( $\text{\AA}^2 \times 10^3$ ) for rmb319LTn.

	x	y	z	U(eq)
H(2)	-1170(60)	3510(30)	7000(30)	40(11)
H(3)	-2430(80)	5034(16)	7720(40)	23(11)
H(4)	-590(60)	6540(30)	7270(30)	32(10)
H(5)	2270(60)	6220(30)	6130(30)	33(12)
H(8A)	3870(50)	2070(20)	3190(30)	32(9)
H(8B)	6460(40)	2008(19)	3890(20)	14(7)
H(8C)	4990(50)	1070(30)	3630(30)	34(10)
H(9A)	6800(50)	1810(20)	6000(30)	15(7)
H(9B)	5860(50)	860(30)	5790(30)	40(10)
H(9C)	4780(50)	1510(20)	6720(30)	25(9)
H(10A)	1890(50)	650(30)	4760(30)	33(9)
H(10B)	920(50)	1390(20)	5590(30)	19(8)
H(10C)	570(50)	1520(20)	4300(30)	26(9)

Table A45. Crystal data and structure refinement for compound 28

Identification code	rmb321tmpp1bar	
Empirical formula	C <sub>20</sub> H <sub>28</sub> Cl <sub>2</sub> N <sub>4</sub> O <sub>2</sub> Pt	
Formula weight	622.45	
Temperature	293(2) K	
Wavelength	0.71073 Å	
Crystal system	triclinic	
Space group	P-1	
Unit cell dimensions	a = 8.5986(3) Å	α = 77.623(2)°.
	b = 11.1609(4) Å	β = 85.944(2)°.
	c = 13.2153(4) Å	γ = 72.662(3)°.
Volume	1182.45(7) Å <sup>3</sup>	
Z	2	
Density (calculated)	1.748 Mg/m <sup>3</sup>	
Absorption coefficient	6.182 mm <sup>-1</sup>	
F(000)	608	
Crystal color, habit	yellow block	
Crystal size	0.34 x 0.23 x 0.20 mm <sup>3</sup>	
Theta range for data collection	3.31 to 29.05°	
Index ranges	-10 ≤ h ≤ 11, -15 ≤ k ≤ 15, -16 ≤ l ≤ 16	
Reflections collected	15524	
Independent reflections	5644 [R(int) = 0.019]	
Completeness to theta = 29.05°	89.4 %	
Completeness to theta = 26.32°	99.8%	
Absorption correction	multi-scan	
Max. and min. transmission	1.000 and 0.791	
Refinement method	Full-matrix least-squares on F <sup>2</sup>	
Data / restraints / parameters	5644 / 0 / 374	
Goodness-of-fit on F <sup>2</sup>	1.086	
Final R indices [I > 2σ(I)]	R1 = 0.0160, wR2 = 0.0390	
R indices (all data)	R1 = 0.0180, wR2 = 0.0393	
Largest diff. peak and hole	1.744 and -0.522 e.Å <sup>-3</sup>	

Table A46. Atomic coordinates ( $\times 10^4$ ) and equivalent isotropic displacement parameters ( $\text{\AA}^2 \times 10^3$ ) for rmb321tmpP1bar.  $U(\text{eq})$  is defined as one third of the trace of the orthogonalized  $U_{ij}$  tensor.

	x	y	z	$U(\text{eq})$
C(1)	9397(3)	5424(2)	7682(2)	18(1)
C(2)	10212(3)	4179(2)	8119(2)	20(1)
C(3)	9798(3)	3686(2)	9126(2)	18(1)
C(4)	8607(3)	4439(2)	9657(2)	15(1)
C(5)	7827(3)	5703(2)	9175(2)	13(1)
C(6)	5762(3)	6318(2)	10542(2)	16(1)
C(7)	4620(3)	7534(2)	10849(2)	16(1)
C(8)	5620(3)	8380(2)	11063(2)	20(1)
C(9)	3713(3)	7143(3)	11842(2)	23(1)
C(10)	3406(3)	8270(3)	9975(2)	22(1)
C(11)	4790(3)	6722(2)	7132(2)	18(1)
C(12)	3867(3)	6198(2)	6661(2)	21(1)
C(13)	3995(3)	6313(2)	5592(2)	20(1)
C(14)	5044(3)	6937(2)	5040(2)	18(1)
C(15)	5961(3)	7446(2)	5560(2)	14(1)
C(16)	7777(3)	7975(2)	4121(2)	17(1)
C(17)	8771(3)	8896(2)	3670(2)	18(1)
C(18)	10563(3)	8150(3)	3957(3)	33(1)
C(19)	8277(3)	10132(3)	4089(2)	22(1)
C(20)	8574(4)	9228(3)	2492(2)	29(1)
Cl(1)	5980(1)	10076(1)	6606(1)	18(1)
Cl(2)	8599(1)	8706(1)	8485(1)	20(1)
N(1)	5837(2)	7336(2)	6604(1)	13(1)
N(2)	7018(2)	8114(2)	5058(2)	16(1)
N(3)	8221(2)	6179(2)	8195(1)	13(1)
N(4)	6660(2)	6564(2)	9648(1)	15(1)
O(1)	5900(2)	5240(2)	11019(1)	25(1)
O(2)	7725(2)	7109(2)	3705(1)	28(1)
Pt(1)	7152(1)	8015(1)	7456(1)	12(1)



Table A47. Anisotropic displacement parameters ( $\text{\AA}^2 \times 10^3$ ) for rmb321tmpP1bar. The anisotropic displacement factor exponent takes the form:  $-2\pi^2 [h^2 a^{*2} U^{11} + \dots + 2 h k a^* b^* U^{12}]$

	$U^{11}$	$U^{22}$	$U^{33}$	$U^{23}$	$U^{13}$	$U^{12}$
C(1)	21(1)	20(1)	14(1)	-3(1)	2(1)	-8(1)
C(2)	18(1)	19(1)	20(1)	-8(1)	0(1)	0(1)
C(3)	21(1)	13(1)	18(1)	-3(1)	-5(1)	-4(1)
C(4)	22(1)	15(1)	10(1)	-1(1)	-2(1)	-7(1)
C(5)	16(1)	15(1)	11(1)	-4(1)	0(1)	-7(1)
C(6)	20(1)	19(1)	10(1)	-4(1)	2(1)	-9(1)
C(7)	18(1)	17(1)	14(1)	-4(1)	2(1)	-5(1)
C(8)	23(1)	21(1)	19(1)	-7(1)	4(1)	-7(1)
C(9)	25(1)	28(1)	17(1)	-6(1)	5(1)	-8(1)
C(10)	20(1)	22(1)	20(1)	-3(1)	-1(1)	-4(1)
C(11)	21(1)	19(1)	13(1)	1(1)	0(1)	-6(1)
C(12)	22(1)	20(1)	21(1)	1(1)	-2(1)	-9(1)
C(13)	20(1)	18(1)	22(1)	-3(1)	-6(1)	-5(1)
C(14)	20(1)	17(1)	15(1)	-4(1)	-3(1)	1(1)
C(15)	15(1)	12(1)	12(1)	-1(1)	-1(1)	1(1)
C(16)	16(1)	20(1)	13(1)	-2(1)	0(1)	-1(1)
C(17)	17(1)	26(1)	13(1)	-6(1)	1(1)	-8(1)
C(18)	17(1)	46(2)	38(2)	-20(2)	3(1)	-4(1)
C(19)	23(1)	26(1)	22(1)	-7(1)	4(1)	-11(1)
C(20)	41(2)	38(2)	16(1)	-3(1)	3(1)	-28(2)
Cl(1)	24(1)	12(1)	14(1)	0(1)	0(1)	-2(1)
Cl(2)	28(1)	21(1)	15(1)	0(1)	-4(1)	-13(1)
N(1)	14(1)	12(1)	11(1)	0(1)	-2(1)	-2(1)
N(2)	20(1)	15(1)	12(1)	-4(1)	1(1)	-5(1)
N(3)	16(1)	13(1)	11(1)	-2(1)	-1(1)	-5(1)
N(4)	22(1)	10(1)	12(1)	1(1)	3(1)	-4(1)
O(1)	35(1)	16(1)	20(1)	0(1)	10(1)	-8(1)
O(2)	40(1)	23(1)	24(1)	-12(1)	14(1)	-13(1)
Pt(1)	15(1)	12(1)	8(1)	0(1)	1(1)	-4(1)

Table A48. Hydrogen coordinates ( $\times 10^4$ ) and isotropic displacement parameters ( $\text{\AA}^2 \times 10^3$ ) for rmb321tmpP1bar.

	x	y	z	U(eq)
H(1)	9640(30)	5850(20)	6940(20)	21(7)
H(2)	11030(30)	3710(20)	7710(20)	21(7)
H(3)	10300(30)	2830(20)	9480(18)	12(6)
H(4)	8270(30)	4150(20)	10350(20)	17(6)
H(8A)	6390(30)	7900(20)	11644(19)	14(6)
H(8B)	4850(30)	9150(30)	11260(20)	24(7)
H(8C)	6140(40)	8560(30)	10570(20)	27(8)
H(9A)	3040(30)	7900(30)	12070(20)	27(7)
H(9B)	3130(30)	6630(30)	11710(20)	29(8)
H(9C)	4430(30)	6740(30)	12360(20)	24(7)
H(10A)	3850(30)	8560(20)	9330(20)	21(7)
H(10B)	2670(40)	8920(30)	10190(20)	30(8)
H(10C)	2750(30)	7730(30)	9800(20)	27(7)
H(11)	4740(30)	6640(30)	7890(20)	28(7)
H(12)	3210(30)	5680(30)	7100(20)	26(7)
H(13)	3370(30)	5960(30)	5250(20)	28(8)
H(14)	5220(30)	7030(20)	4350(20)	21(7)
H(18A)	10710(40)	7880(30)	4790(30)	45(9)
H(18B)	11260(40)	8690(30)	3700(20)	34(8)
H(18C)	10870(30)	7400(30)	3620(20)	29(8)
H(19A)	7180(30)	10530(30)	3970(20)	21(7)
H(19B)	8410(30)	10010(30)	4830(20)	23(7)
H(19C)	8920(40)	10710(30)	3740(20)	32(8)
H(20A)	9300(40)	9720(30)	2240(20)	33(8)
H(20B)	7490(40)	9660(30)	2340(20)	41(9)
H(20C)	9010(30)	8460(30)	2220(20)	29(8)
H(2N)	7070(30)	8650(30)	5240(20)	16(8)
H(4N)	6490(30)	7310(30)	9330(19)	14(6)

Table A49. Crystal data and structure refinement for compound 30

Identification code	rmb272p212121	
Empirical formula	C <sub>36</sub> H <sub>52</sub> N <sub>6</sub> O <sub>2</sub> Pt	
Formula weight	795.93	
Temperature	100(2) K	
Wavelength	0.71073 Å	
Crystal system	Orthorhombic	
Space group	P2 <sub>1</sub> 2 <sub>1</sub> 2 <sub>1</sub>	
Unit cell dimensions	a = 4.7998(5) Å	α = 90°.
	b = 18.2520(17) Å	β = 90°.
	c = 41.322(4) Å	γ = 90°.
Volume	3620.1(6) Å <sup>3</sup>	
Z	4	
Density (calculated)	1.460 Mg/m <sup>3</sup>	
Absorption coefficient	3.915 mm <sup>-1</sup>	
F(000)	1616	
Crystal size	0.26 x 0.15 x 0.04 mm <sup>3</sup>	
Crystal color, habit	pale-yellow plate	
Theta range for data collection	1.22 to 28.12°	
Index ranges	-6 ≤ h ≤ 6, -23 ≤ k ≤ 24, -54 ≤ l ≤ 53	
Reflections collected	31733	
Independent reflections	8405 [R(int) = 0.0446]	
Completeness to theta = 28.12°	97.0 %	
Absorption correction	SADABS	
Max. and min. transmission	0.923 and 0.726	
Refinement method	Full-matrix least-squares on F <sup>2</sup>	
Data / restraints / parameters	8405 / 0 / 302	
Goodness-of-fit on F <sup>2</sup>	1.313	
Final R indices [I > 2σ(I)]	R1 = 0.0691, wR2 = 0.1638	
R indices (all data)	R1 = 0.0745, wR2 = 0.1659	
Absolute structure parameter	0.025(19)	
Largest diff. peak and hole	7.429 and -9.333 e.Å <sup>-3</sup>	

Table A50. Atomic coordinates ( $\times 10^4$ ) and equivalent isotropic displacement parameters ( $\text{\AA}^2 \times 10^3$ ) for rmb272p212121.  $U(\text{eq})$  is defined as one third of the trace of the orthogonalized  $U_{ij}$  tensor.

	x	y	z	$U(\text{eq})$
Pt(1)	7424(1)	5248(1)	7555(1)	11(1)
O(1)	9013(16)	4660(5)	7920(2)	15(1)
O(2)	5729(17)	5824(5)	7918(2)	15(1)
N(1)	8860(20)	4465(6)	7262(2)	14(1)
N(2)	11430(20)	3495(6)	7120(3)	14(1)
N(3)	12200(20)	3938(5)	7647(2)	14(1)
N(4)	6040(20)	5982(5)	7240(2)	12(1)
N(5)	3660(20)	6989(5)	7095(2)	12(1)
N(6)	2640(30)	6568(4)	7617(2)	12(1)
C(1)	8080(20)	4254(6)	6952(3)	15(1)
C(2)	5960(30)	4486(7)	6748(3)	15(1)
C(3)	5590(30)	4128(7)	6453(3)	15(1)
C(4)	7250(30)	3551(5)	6362(2)	15(1)
C(5)	9360(30)	3286(7)	6571(3)	15(1)
C(6)	9690(30)	3639(7)	6867(3)	15(1)
C(7)	10900(20)	4011(7)	7360(3)	15(1)
C(8)	11200(30)	4272(7)	7904(3)	15(2)
C(9)	12660(40)	4147(6)	8218(3)	21(2)
C(10)	10850(30)	4194(9)	8520(3)	24(3)
C(11)	12450(40)	4157(7)	8836(3)	27(3)
C(12)	10580(30)	4245(10)	9133(3)	31(3)
C(13)	12120(40)	4214(10)	9453(3)	35(4)
C(14)	10290(40)	4324(11)	9750(3)	36(4)
C(15)	11830(30)	4267(11)	10070(4)	42(4)
C(16)	9950(40)	4392(12)	10362(4)	47(5)
C(17)	11540(40)	4322(15)	10686(4)	64(7)
C(18)	7000(20)	6222(6)	6938(3)	17(1)
C(19)	9130(30)	5949(7)	6745(3)	17(1)
C(20)	9520(30)	6272(7)	6448(3)	17(1)
C(21)	7910(30)	6882(6)	6348(3)	17(1)
C(22)	5800(30)	7164(7)	6540(3)	17(1)
C(23)	5440(30)	6834(7)	6839(3)	17(1)
C(24)	4070(30)	6509(7)	7336(3)	17(1)
C(25)	3590(20)	6244(6)	7883(3)	14(2)
C(26)	2010(20)	6358(6)	8193(3)	14(2)
C(27)	3750(30)	6328(7)	8495(3)	20(3)
C(28)	2060(30)	6377(7)	8805(3)	18(3)
C(29)	3810(30)	6332(8)	9109(3)	23(3)
C(30)	2150(40)	6415(7)	9422(3)	24(3)
C(31)	3930(30)	6364(9)	9728(3)	27(3)
C(32)	2240(40)	6470(8)	10037(3)	29(3)
C(33)	3970(40)	6418(9)	10344(4)	33(4)
C(34)	2230(50)	6531(9)	10652(3)	42(4)
C(35)	13360(20)	2885(6)	7144(3)	15(3)
C(36)	1760(20)	7618(7)	7114(3)	20(3)

Table A51. Anisotropic displacement parameters ( $\text{\AA}^2 \times 10^3$ ) for rmb272p212121. The anisotropic displacement factor exponent takes the form:  $-2h^2 [h^2 a^{*2} U^{11} + \dots + 2hk a^* b^* U^{12}]$

	U <sup>11</sup>	U <sup>22</sup>	U <sup>33</sup>	U <sup>23</sup>	U <sup>13</sup>	U <sup>12</sup>
Pt(1)	8(1)	11(1)	13(1)	-1(1)	-1(1)	1(1)
O(1)	12(3)	17(3)	17(3)	-1(3)	1(2)	3(2)
O(2)	12(3)	17(3)	17(3)	-1(3)	1(2)	3(2)
N(1)	12(3)	13(3)	16(3)	-1(2)	-6(2)	6(2)
N(2)	12(3)	13(3)	16(3)	-1(2)	-6(2)	6(2)
N(3)	12(3)	13(3)	16(3)	-1(2)	-6(2)	6(2)
N(4)	13(3)	10(2)	14(3)	-3(2)	-4(2)	-4(2)
N(5)	13(3)	10(2)	14(3)	-3(2)	-4(2)	-4(2)
N(6)	13(3)	10(2)	14(3)	-3(2)	-4(2)	-4(2)
C(1)	17(2)	13(2)	14(2)	3(2)	1(2)	-2(2)
C(2)	17(2)	13(2)	14(2)	3(2)	1(2)	-2(2)
C(3)	17(2)	13(2)	14(2)	3(2)	1(2)	-2(2)
C(4)	17(2)	13(2)	14(2)	3(2)	1(2)	-2(2)
C(5)	17(2)	13(2)	14(2)	3(2)	1(2)	-2(2)
C(6)	17(2)	13(2)	14(2)	3(2)	1(2)	-2(2)
C(7)	17(2)	13(2)	14(2)	3(2)	1(2)	-2(2)
C(8)	18(6)	16(6)	9(6)	1(5)	-2(4)	-13(5)
C(9)	20(6)	22(6)	21(6)	-1(4)	2(7)	-10(8)
C(10)	23(7)	32(8)	17(7)	2(6)	3(5)	7(6)
C(11)	24(6)	41(7)	18(6)	-3(5)	-2(9)	-2(10)
C(12)	28(8)	47(10)	19(7)	3(7)	-1(6)	3(7)
C(13)	27(9)	55(9)	23(7)	0(6)	-2(7)	18(8)
C(14)	44(10)	48(10)	15(7)	2(7)	-2(6)	4(8)
C(15)	29(10)	71(12)	25(8)	-2(8)	-4(6)	20(8)
C(16)	60(12)	64(13)	17(8)	6(8)	-3(8)	2(10)
C(17)	59(13)	120(20)	18(8)	12(11)	-3(7)	25(13)
C(18)	16(2)	17(2)	18(2)	1(2)	2(2)	-1(2)
C(19)	16(2)	17(2)	18(2)	1(2)	2(2)	-1(2)
C(20)	16(2)	17(2)	18(2)	1(2)	2(2)	-1(2)
C(21)	16(2)	17(2)	18(2)	1(2)	2(2)	-1(2)
C(22)	16(2)	17(2)	18(2)	1(2)	2(2)	-1(2)
C(23)	16(2)	17(2)	18(2)	1(2)	2(2)	-1(2)
C(24)	16(2)	17(2)	18(2)	1(2)	2(2)	-1(2)
C(25)	11(4)	7(4)	23(4)	-5(3)	-2(3)	4(3)
C(26)	11(4)	7(4)	23(4)	-5(3)	-2(3)	4(3)
C(27)	22(6)	18(7)	21(7)	2(5)	-1(5)	-7(5)
C(28)	18(8)	12(5)	26(6)	-2(4)	0(5)	0(5)
C(29)	24(7)	18(7)	28(8)	-4(6)	-2(6)	1(5)
C(30)	22(8)	29(6)	21(6)	-2(5)	4(6)	12(7)
C(31)	31(8)	30(8)	21(8)	1(6)	-1(6)	4(6)
C(32)	24(8)	40(7)	22(6)	-1(5)	4(7)	12(8)
C(33)	42(9)	33(9)	22(8)	2(6)	-1(7)	-1(7)
C(34)	44(10)	57(10)	23(7)	0(6)	-5(9)	5(11)
C(35)	17(6)	8(5)	20(6)	-3(5)	-1(4)	8(4)
C(36)	11(6)	26(7)	23(7)	1(5)	-6(4)	3(4)

Table A52. Hydrogen coordinates ( $\times 10^4$ ) and isotropic displacement parameters ( $\text{\AA}^2 \times 10^3$ )  
for mmb272p212121.

	x	y	z	U(eq)
H(2)	4790	4883	6808	17
H(3)	4151	4287	6312	17
H(4)	6974	3327	6157	17
H(5)	10499	2883	6511	17
H(9A)	14177	4511	8238	25
H(9B)	13532	3656	8212	25
H(10A)	9796	4660	8513	29
H(10B)	9483	3789	8515	29
H(11A)	13880	4547	8838	33
H(11B)	13419	3679	8849	33
H(12A)	9603	4721	9118	38
H(12B)	9156	3854	9130	38
H(13A)	13585	4596	9453	42
H(13B)	13055	3733	9471	42
H(14A)	9406	4812	9736	43
H(14B)	8787	3953	9747	43
H(15A)	13353	4632	10074	50
H(15B)	12682	3774	10087	50
H(16A)	8412	4031	10358	57
H(16B)	9117	4887	10348	57
H(17A)	12110	3811	10718	96
H(17B)	10326	4474	10865	96
H(17C)	13197	4636	10681	96
H(19)	10276	5555	6816	20
H(20)	10894	6081	6306	20
H(21)	8288	7103	6145	20
H(22)	4667	7561	6470	20
H(26A)	536	5980	8208	16
H(26B)	1072	6841	8183	16
H(27A)	5107	6737	8491	24
H(27B)	4818	5864	8496	24
H(28A)	1025	6846	8806	22
H(28B)	680	5975	8807	22
H(29A)	5250	6719	9101	28
H(29B)	4778	5853	9112	28
H(30A)	1189	6896	9420	29
H(30B)	700	6029	9430	29
H(31A)	4845	5878	9734	33
H(31B)	5407	6742	9718	33
H(32A)	1324	6956	10029	35
H(32B)	752	6093	10045	35
H(33A)	5464	6792	10337	39
H(33B)	4874	5930	10354	39
H(34A)	1349	7015	10645	62
H(34B)	3435	6497	10842	62
H(34C)	783	6152	10664	62
H(35A)	12345	2440	7203	23
H(35B)	14765	2993	7310	23

H(35C)	14285	2813	6935	23
H(36A)	432	7542	7291	30
H(36B)	746	7667	6910	30
H(36C)	2838	8065	7155	30

---

Table A53. Crystal data and structure refinement for compound 41

Identification code	rmb331p1bar	
Empirical formula	C <sub>22</sub> H <sub>26</sub> Cl <sub>2</sub> N <sub>6</sub> O <sub>2</sub> Pt	
Formula weight	672.48	
Temperature	100(2) K	
Wavelength	0.71073 Å	
Crystal system	Triclinic	
Space group	P-1	
Unit cell dimensions	a = 10.2102(5) Å	α = 70.699(5)°
	b = 10.6491(6) Å	β = 76.753(4)°
	c = 12.0364(6) Å	γ = 79.119(4)°
Volume	1193.16(11) Å <sup>3</sup>	
Z	2	
Density (calculated)	1.872 Mg/m <sup>3</sup>	
Absorption coefficient	6.136 mm <sup>-1</sup>	
F(000)	656	
Crystal color, habit	yellow block	
Crystal size	0.10 x 0.08 x 0.05 mm <sup>3</sup>	
Theta range for data collection	3.45 to 28.97°	
Index ranges	-13 ≤ h ≤ 13, -14 ≤ k ≤ 14, -16 ≤ l ≤ 15	
Reflections collected	25551	
Independent reflections	5829 [R(int) = 0.1178]	
Completeness to theta = 28.97°	92.2 %	
Completeness to theta = 26.32°	99.4 %	
Absorption correction	Semi-empirical from equivalents	
Max. and min. transmission	1.00 and 0.493	
Refinement method	Full-matrix least-squares on F <sup>2</sup>	
Data / restraints / parameters	5829 / 0 / 310	
Goodness-of-fit on F <sup>2</sup>	1.072	
Final R indices [I > 2σ(I)]	R1 = 0.0522, wR2 = 0.0984	
R indices (all data)	R1 = 0.0883, wR2 = 0.1076	
Largest diff. peak and hole	2.280 and -2.033 e.Å <sup>-3</sup>	



Table A54. Atomic coordinates ( $\times 10^4$ ) and equivalent isotropic displacement parameters ( $\text{\AA}^2 \times 10^3$ ) for rmb331P1bar.  $U(\text{eq})$  is defined as one third of the trace of the orthogonalized  $U_{ij}$  tensor.

	x	y	z	U(eq)
Pt(1)	4955(1)	4969(1)	3184(1)	22(1)
Cl(1)	4685(2)	2733(2)	3980(2)	31(1)
Cl(2)	2907(2)	5486(2)	4313(1)	27(1)
O(1)	8268(5)	860(5)	3483(5)	43(1)
O(2)	8687(5)	7767(6)	1617(4)	43(1)
N(1)	6708(5)	4529(5)	2110(5)	22(1)
N(2)	8639(5)	3423(6)	1504(5)	26(1)
N(3)	7887(6)	2971(7)	3631(5)	33(1)
N(4)	5116(5)	6954(5)	2506(4)	21(1)
N(5)	5735(5)	8940(5)	2228(5)	27(1)
N(6)	7107(6)	6996(7)	3236(6)	30(1)
C(1)	7726(6)	3603(7)	2457(6)	27(1)
C(2)	8169(6)	4247(7)	476(6)	28(1)
C(3)	8682(7)	4426(7)	-718(6)	31(2)
C(4)	7925(7)	5350(7)	-1536(6)	34(2)
C(5)	6709(7)	6045(7)	-1139(7)	34(2)
C(6)	6210(6)	5876(7)	52(6)	27(1)
C(7)	6951(6)	4954(6)	877(6)	23(1)
C(8)	9925(7)	2538(7)	1498(7)	35(2)
C(9)	7971(7)	1575(7)	4135(7)	33(2)
C(10)	7678(8)	1081(8)	5470(7)	42(2)
C(11)	7984(9)	-396(9)	5968(8)	55(2)
C(12)	6017(6)	7597(6)	2675(5)	23(1)
C(13)	4580(6)	9174(7)	1734(6)	29(2)
C(14)	3889(7)	10364(7)	1106(6)	33(2)
C(15)	2761(7)	10242(8)	733(6)	38(2)
C(16)	2337(7)	9001(8)	932(6)	34(2)
C(17)	3052(6)	7820(7)	1526(6)	30(2)
C(18)	4194(6)	7945(7)	1911(6)	27(1)
C(19)	6426(7)	9933(7)	2373(7)	35(2)
C(20)	8419(7)	7148(7)	2658(6)	32(2)
C(21)	9464(6)	6520(7)	3461(6)	30(2)
C(22)	9327(7)	7218(8)	4403(7)	37(2)

Table A55. Anisotropic displacement parameters ( $\text{\AA}^2 \times 10^3$ ) for rmb331P1bar. The anisotropic

displacement factor exponent takes the form:  $-2\pi^2 [h^2 a^2 U^{11} + \dots + 2 h k a^* b^* U^{12}]$

	$U^{11}$	$U^{22}$	$U^{33}$	$U^{23}$	$U^{13}$	$U^{12}$
Pt(1)	24(1)	24(1)	14(1)	0(1)	-2(1)	-2(1)
Cl(1)	36(1)	27(1)	23(1)	-1(1)	-3(1)	-3(1)
Cl(2)	26(1)	29(1)	16(1)	0(1)	2(1)	-2(1)
O(1)	52(3)	40(3)	33(3)	-11(3)	-3(2)	-3(2)
O(2)	33(3)	60(4)	16(3)	8(3)	3(2)	-1(2)
N(1)	26(3)	18(3)	15(3)	1(2)	3(2)	-4(2)
N(2)	25(3)	29(3)	16(3)	-2(3)	1(2)	-1(2)
N(3)	37(3)	36(4)	21(3)	-6(3)	-5(3)	6(3)
N(4)	17(2)	27(3)	14(3)	-4(2)	-3(2)	3(2)
N(5)	33(3)	23(3)	21(3)	-2(3)	1(2)	-6(2)
N(6)	33(3)	32(4)	17(4)	3(3)	0(3)	-9(3)
C(1)	30(3)	30(4)	20(4)	-7(3)	-3(3)	-2(3)
C(2)	28(3)	28(4)	20(4)	-2(3)	4(3)	-4(3)
C(3)	33(3)	34(4)	25(4)	-10(3)	0(3)	-4(3)
C(4)	49(4)	36(4)	11(4)	-2(3)	2(3)	-8(3)
C(5)	51(4)	28(4)	28(4)	-6(3)	-18(3)	-6(3)
C(6)	30(3)	28(4)	16(4)	0(3)	0(3)	-3(3)
C(7)	28(3)	25(3)	14(3)	-4(3)	4(2)	-7(3)
C(8)	34(4)	35(4)	23(4)	-1(3)	3(3)	5(3)
C(9)	38(4)	33(4)	23(4)	-4(3)	-2(3)	-6(3)
C(10)	38(4)	53(5)	32(5)	-11(4)	-8(3)	0(4)
C(11)	68(6)	50(5)	34(5)	-7(4)	4(4)	2(4)
C(12)	27(3)	25(3)	9(3)	-1(3)	3(2)	-3(3)
C(13)	29(3)	31(4)	15(3)	0(3)	3(3)	3(3)
C(14)	37(4)	28(4)	25(4)	-3(3)	2(3)	2(3)
C(15)	40(4)	42(5)	14(4)	2(3)	2(3)	13(3)
C(16)	26(3)	47(5)	23(4)	-4(3)	-7(3)	6(3)
C(17)	27(3)	39(4)	19(4)	-2(3)	-3(3)	-4(3)
C(18)	27(3)	32(4)	11(3)	4(3)	3(2)	-3(3)
C(19)	37(4)	32(4)	30(4)	-5(4)	0(3)	-4(3)
C(20)	33(4)	34(4)	22(4)	-5(3)	1(3)	-1(3)
C(21)	26(3)	35(4)	21(4)	-4(3)	1(3)	-1(3)
C(22)	32(4)	43(4)	34(5)	-9(4)	-11(3)	0(3)

Table A56. Hydrogen coordinates ( $\times 10^4$ ) and isotropic displacement parameters ( $\text{\AA}^2 \times 10^3$ ) for mmb331P1bar.

	x	y	z	U(eq)
H(3N)	7500(70)	3410(70)	4020(70)	30(20)
H(6N)	6960(70)	6590(70)	3790(60)	10(20)
H(3)	9498	3955	-971	37
H(4)	8238	5501	-2352	41
H(5)	6218	6644	-1701	41
H(6)	5403	6361	302	33
H(8A)	10208	2327	2253	53
H(8B)	10602	2980	868	53
H(8C)	9806	1726	1370	53
H(10A)	8209	1513	5779	50
H(10B)	6728	1344	5746	50
H(11A)	7409	-832	5722	83
H(11B)	7825	-642	6826	83
H(11C)	8916	-670	5679	83
H(14)	4177	11193	950	40
H(15)	2258	11014	332	46
H(16)	1564	8967	663	41
H(17)	2782	6988	1660	36
H(19A)	6962	9512	2987	53
H(19B)	5768	10622	2595	53
H(19C)	7004	10323	1632	53
H(21A)	10365	6571	2977	36
H(21B)	9356	5581	3852	36
H(22A)	9350	8162	4022	55
H(22B)	10062	6862	4837	55
H(22C)	8482	7071	4947	55

Table A57. Crystal data and structure refinement for compounds 42a and b

Identification code	rmb291i21a	
Empirical formula	C <sub>60</sub> H <sub>50</sub> Cl <sub>4</sub> N <sub>12</sub> O <sub>4</sub> Pt <sub>2</sub>	
Formula weight	1535.10	
Temperature	373(2) K	
Wavelength	0.71073 Å	
Crystal system	Monoclinic	
Space group	I2/a	
Unit cell dimensions	a = 16.7763(13) Å	α = 90°.
	b = 18.6042(13) Å	β = 102.526(2)°.
	c = 18.2199(13) Å	γ = 90°.
Volume	5551.3(7) Å <sup>3</sup>	
Z	4	
Density (calculated)	1.837 Mg/m <sup>3</sup>	
Absorption coefficient	5.289 mm <sup>-1</sup>	
F(000)	3000	
Crystal size	0.38 x 0.23 x 0.21 mm <sup>3</sup>	
Crystal color, habit	orange prism	
Theta range for data collection	2.19 to 28.08°.	
Index ranges	-22 ≤ h ≤ 21, -24 ≤ k ≤ 24, -23 ≤ l ≤ 23	
Reflections collected	24271	
Independent reflections	6487 [R(int) = 0.0209]	
Completeness to theta = 28.08°	96.0 %	
Absorption correction	SADABS	
Max. and min. transmission	0.719 and 0.984	
Refinement method	Full-matrix least-squares on F <sup>2</sup>	
Data / restraints / parameters	6487 / 0 / 378	
Goodness-of-fit on F <sup>2</sup>	1.074	
Final R indices [I > 2σ(I)]	R1 = 0.0279, wR2 = 0.0688	
R indices (all data)	R1 = 0.0346, wR2 = 0.0716	
Largest diff. peak and hole	2.979 and -0.813 e.Å <sup>-3</sup>	

Table A58. Atomic coordinates ( $\times 10^4$ ) and equivalent isotropic displacement parameters ( $\text{\AA}^2 \times 10^3$ ) for rmb2911t.  $U(\text{eq})$  is defined as one third of the trace of the orthogonalized  $U_{ij}$  tensor.

	x	y	z	$U(\text{eq})$
Pt(1)	2500	3991(1)	5000	20(1)
Cl(1)	1545(1)	3114(1)	5070(1)	25(1)
O(1)	3261(2)	4956(1)	2724(1)	35(1)
N(1)	3307(2)	4758(2)	4871(2)	21(1)
N(2)	4150(2)	5386(2)	4324(2)	21(1)
N(3)	3624(2)	4266(2)	3761(2)	23(1)
C(1)	3675(2)	4801(2)	4292(2)	21(1)
C(2)	4081(2)	5764(2)	4965(2)	22(1)
C(3)	3560(2)	5367(2)	5312(2)	22(1)
C(4)	3389(2)	5584(2)	5994(2)	27(1)
C(5)	3765(2)	6211(2)	6306(2)	33(1)
C(6)	4277(2)	6611(2)	5948(2)	34(1)
C(7)	4449(2)	6396(2)	5274(2)	28(1)
C(8)	4698(2)	5560(2)	3826(2)	26(1)
C(9)	3400(2)	4363(2)	2993(2)	25(1)
C(10)	3344(2)	3685(2)	2545(2)	24(1)
C(11)	3014(2)	3737(2)	1777(2)	30(1)
C(12)	2936(2)	3120(2)	1335(2)	34(1)
C(13)	3175(2)	2461(2)	1659(2)	36(1)
C(14)	3501(2)	2403(2)	2418(2)	32(1)
C(15)	3595(2)	3018(2)	2861(2)	30(1)
Pt(2)	7500	3988(1)	10000	20(1)
Cl(2)	7500	2740(1)	10000	30(1)
Cl(3)	7500	5234(1)	10000	26(1)
O(2)	7029(2)	3939(1)	8891(1)	28(1)
N(4)	6357(2)	4004(2)	10166(2)	22(1)
N(5)	5017(2)	3863(2)	9862(2)	23(1)
N(6)	5727(2)	3493(2)	8945(2)	24(1)
C(16)	5728(2)	3776(2)	9629(2)	22(1)
C(17)	5194(2)	4186(2)	10565(2)	24(1)
C(18)	6044(2)	4274(2)	10759(2)	24(1)
C(19)	6419(2)	4595(2)	11437(2)	27(1)
C(20)	5909(2)	4820(2)	11898(2)	33(1)
C(21)	5058(2)	4735(2)	11698(2)	34(1)
C(22)	4685(2)	4415(2)	11025(2)	30(1)
C(23)	4207(2)	3664(2)	9438(2)	30(1)
C(24)	6346(2)	3587(2)	8630(2)	23(1)
C(25)	6281(2)	3272(2)	7860(2)	24(1)
C(26)	5590(2)	2889(2)	7533(2)	26(1)
C(27)	5526(2)	2549(2)	6834(2)	34(1)
C(28)	6163(2)	2617(2)	6462(2)	30(1)
C(29)	6844(2)	3027(2)	6783(2)	31(1)
C(30)	6912(2)	3342(2)	7481(2)	29(1)

Table A59. Anisotropic displacement parameters ( $\text{\AA}^2 \times 10^3$ ) for rmb2911t. The anisotropic displacement factor exponent takes the form:  $-2\pi^2 [h^2 a^{*2} U^{11} + \dots + 2 h k a^* b^* U^{12}]$

	U <sup>11</sup>	U <sup>22</sup>	U <sup>33</sup>	U <sup>23</sup>	U <sup>13</sup>	U <sup>12</sup>
Pt(1)	21(1)	23(1)	16(1)	0	4(1)	0
Cl(1)	28(1)	24(1)	24(1)	-3(1)	8(1)	-3(1)
O(1)	43(2)	31(1)	25(1)	5(1)	-4(1)	1(1)
N(1)	23(1)	24(1)	15(1)	-1(1)	3(1)	1(1)
N(2)	19(1)	24(1)	18(1)	2(1)	2(1)	2(1)
N(3)	29(2)	23(2)	19(2)	0(1)	7(1)	-1(1)
C(1)	20(2)	25(2)	16(2)	2(1)	2(1)	5(1)
C(2)	17(2)	27(2)	20(2)	0(1)	0(1)	5(1)
C(3)	19(2)	26(2)	19(2)	-3(1)	0(1)	3(1)
C(4)	23(2)	34(2)	22(2)	-4(1)	2(1)	3(1)
C(5)	27(2)	40(2)	29(2)	-14(2)	3(2)	2(2)
C(6)	30(2)	31(2)	37(2)	-12(2)	0(2)	-2(2)
C(7)	20(2)	30(2)	32(2)	-1(2)	3(2)	-2(1)
C(8)	23(2)	32(2)	23(2)	7(1)	5(1)	1(1)
C(9)	21(2)	33(2)	19(2)	0(1)	2(1)	1(1)
C(10)	21(2)	34(2)	19(2)	-2(1)	5(1)	-4(1)
C(11)	22(2)	45(2)	22(2)	0(2)	5(1)	-1(2)
C(12)	30(2)	56(3)	17(2)	-8(2)	4(1)	-5(2)
C(13)	32(2)	46(2)	30(2)	-14(2)	9(2)	-5(2)
C(14)	29(2)	35(2)	31(2)	-6(2)	6(2)	1(2)
C(15)	28(2)	39(2)	21(2)	-5(2)	3(1)	2(2)
Pt(2)	12(1)	34(1)	14(1)	0	2(1)	0
Cl(2)	23(1)	36(1)	31(1)	0	5(1)	0
Cl(3)	17(1)	35(1)	25(1)	0	5(1)	0
O(2)	21(1)	46(2)	16(1)	-4(1)	2(1)	-6(1)
N(4)	15(1)	34(2)	18(1)	-1(1)	4(1)	-2(1)
N(5)	15(1)	32(2)	22(2)	0(1)	5(1)	-1(1)
N(6)	17(1)	34(2)	20(2)	-1(1)	3(1)	1(1)
C(16)	16(2)	29(2)	21(2)	2(1)	3(1)	-1(1)
C(17)	18(2)	32(2)	22(2)	4(1)	7(1)	-2(1)
C(18)	19(2)	32(2)	21(2)	1(1)	6(1)	-2(1)
C(19)	23(2)	36(2)	23(2)	1(2)	4(1)	-2(2)
C(20)	36(2)	41(2)	21(2)	-1(2)	7(2)	-1(2)
C(21)	32(2)	49(2)	25(2)	1(2)	15(2)	8(2)
C(22)	22(2)	40(2)	32(2)	5(2)	12(2)	1(2)
C(23)	14(2)	43(2)	32(2)	-1(2)	3(1)	-6(2)
C(24)	19(2)	26(2)	22(2)	4(1)	1(1)	2(1)
C(25)	24(2)	27(2)	21(2)	3(1)	3(1)	4(1)
C(26)	28(2)	30(2)	23(2)	4(1)	8(1)	-3(1)
C(27)	35(2)	36(2)	30(2)	3(2)	0(2)	-6(2)
C(28)	38(2)	31(2)	22(2)	-2(1)	4(2)	6(2)
C(29)	27(2)	37(2)	30(2)	-1(2)	7(2)	5(2)
C(30)	23(2)	35(2)	29(2)	0(2)	3(2)	1(2)

Table A60. Hydrogen coordinates (x 10<sup>4</sup>) and isotropic displacement parameters (Å<sup>2</sup> x 10<sup>3</sup>) for rmb2911t

	x	y	z	U(eq)
H(3N)	3590(30)	3910(20)	3920(30)	29(13)
H(4)	3042	5322	6228	32
H(5)	3675	6369	6765	39
H(6)	4507	7034	6171	41
H(7)	4793	6661	5039	33
H(8A)	4916	5124	3665	39
H(8B)	5138	5855	4089	39
H(8C)	4402	5816	3394	39
H(11)	2849	4181	1561	36
H(12)	2721	3151	821	41
H(13)	3114	2051	1360	43
H(14)	3656	1957	2632	38
H(15)	3827	2984	3371	35
H(19)	6982	4654	11574	33
H(20)	6139	5036	12355	39
H(21)	4739	4896	12023	41
H(22)	4121	4356	10889	36
H(23A)	4245	3498	8948	45
H(23B)	3854	4075	9389	45
H(23C)	3990	3288	9698	45
H(26)	5161	2855	7780	32
H(27)	5063	2283	6623	41
H(28)	6134	2390	6002	36
H(29)	7259	3090	6523	37
H(30)	7379	3601	7696	35

Table A61. Crystal data and structure refinement for compound 42c

Identification code	rmb292ltp21c	
Empirical formula	C30 H26 Cl2 N6 O2 Pt	
Formula weight	768.56	
Temperature	373(2) K	
Wavelength	0.71073 Å	
Crystal system	Monoclinic	
Space group	P2 <sub>1</sub> /c	
Unit cell dimensions	a = 10.4180(9) Å	α = 90°.
	b = 17.0912(14) Å	β = 97.0640(10)°.
	c = 8.0463(7) Å	γ = 90°.
Volume	1421.8(2) Å <sup>3</sup>	
Z	2	
Density (calculated)	1.795 Mg/m <sup>3</sup>	
Absorption coefficient	5.162 mm <sup>-1</sup>	
F(000)	752	
Crystal size	0.20 x 0.20 x 0.10 mm <sup>3</sup>	
Crystal color, habit	yellow prism	
Theta range for data collection	1.97 to 28.03°	
Index ranges	-13 ≤ h ≤ 13, -22 ≤ k ≤ 21, -10 ≤ l ≤ 10	
Reflections collected	12376	
Independent reflections	3324 [R(int) = 0.0176]	
Completeness to theta = 28.03°	96.5 %	
Absorption correction	SADABS	
Max. and min. transmission	0.712 and 0.984	
Refinement method	Full-matrix least-squares on F <sup>2</sup>	
Data / restraints / parameters	3324 / 0 / 239	
Goodness-of-fit on F <sup>2</sup>	1.043	
Final R indices [I > 2σ(I)]	R1 = 0.0147, wR2 = 0.0338	
R indices (all data)	R1 = 0.0186, wR2 = 0.0355	
Largest diff. peak and hole	0.844 and -0.424 e.Å <sup>-3</sup>	



Table A62. Atomic coordinates ( $\times 10^4$ ) and equivalent isotropic displacement parameters ( $\text{\AA}^2 \times 10^3$ ) for rmb292ltP21c.  $U(\text{eq})$  is defined as one third of the trace of the orthogonalized  $U_{ij}$  tensor.

	x	y	z	$U(\text{eq})$
Pt(1)	10000	0	0	9(1)
Cl(1)	9849(1)	120(1)	-2869(1)	14(1)
O(1)	6301(1)	1773(1)	176(2)	25(1)
N(1)	9880(1)	1171(1)	223(2)	12(1)
N(2)	9074(2)	2340(1)	762(2)	14(1)
N(3)	8019(2)	1184(1)	1672(2)	15(1)
C(1)	8953(2)	1555(1)	873(2)	14(1)
C(2)	10177(2)	2477(1)	-6(2)	14(1)
C(3)	10688(2)	1744(1)	-324(2)	13(1)
C(4)	11829(2)	1678(1)	-1057(2)	16(1)
C(5)	12423(2)	2366(1)	-1444(2)	21(1)
C(6)	11893(2)	3099(1)	-1139(3)	21(1)
C(7)	10764(2)	3170(1)	-421(2)	18(1)
C(8)	8252(2)	2939(1)	1374(3)	18(1)
C(9)	6702(2)	1265(1)	1150(2)	17(1)
C(10)	5852(2)	681(1)	1866(2)	19(1)
C(11)	4523(2)	775(1)	1429(3)	24(1)
C(12)	3671(2)	220(2)	1927(3)	30(1)
C(13)	4132(2)	-420(1)	2835(3)	32(1)
C(14)	5453(2)	-519(1)	3296(3)	28(1)
C(15)	6315(2)	33(1)	2823(3)	22(1)

Table A63. Anisotropic displacement parameters ( $\text{\AA}^2 \times 10^3$ ) for rmb292lt. The anisotropic displacement factor exponent takes the form:  $-2\pi^2 [h^2 a^{*2} U^{11} + \dots + 2 h k a^* b^* U^{12}]$

	$U^{11}$	$U^{22}$	$U^{33}$	$U^{23}$	$U^{13}$	$U^{12}$
Pt(1)	10(1)	6(1)	12(1)	0(1)	1(1)	0(1)
Cl(1)	20(1)	10(1)	13(1)	1(1)	2(1)	1(1)
O(1)	19(1)	20(1)	33(1)	2(1)	-5(1)	1(1)
N(1)	13(1)	9(1)	14(1)	1(1)	0(1)	-1(1)
N(2)	17(1)	9(1)	16(1)	-2(1)	0(1)	1(1)
N(3)	13(1)	11(1)	22(1)	1(1)	3(1)	2(1)
C(1)	15(1)	11(1)	14(1)	0(1)	-1(1)	1(1)
C(2)	16(1)	13(1)	13(1)	0(1)	-3(1)	-1(1)
C(3)	16(1)	9(1)	14(1)	2(1)	-2(1)	-2(1)
C(4)	17(1)	13(1)	18(1)	-1(1)	2(1)	-1(1)
C(5)	20(1)	23(1)	19(1)	1(1)	3(1)	-6(1)
C(6)	28(1)	14(1)	20(1)	3(1)	0(1)	-10(1)
C(7)	26(1)	9(1)	18(1)	2(1)	-3(1)	-1(1)
C(8)	20(1)	10(1)	24(1)	-3(1)	0(1)	4(1)
C(9)	15(1)	16(1)	21(1)	-5(1)	1(1)	1(1)
C(10)	17(1)	19(1)	23(1)	-8(1)	6(1)	-1(1)

C(11)	18(1)	25(1)	29(1)	-9(1)	4(1)	0(1)
C(12)	16(1)	39(1)	36(1)	-16(1)	8(1)	-7(1)
C(13)	32(1)	35(1)	30(1)	-12(1)	16(1)	-18(1)
C(14)	32(1)	27(1)	27(1)	-2(1)	10(1)	-8(1)
C(15)	20(1)	24(1)	23(1)	-4(1)	5(1)	-4(1)

Table A64. Hydrogen coordinates ( $\times 10^4$ ) and isotropic displacement parameters ( $\text{\AA}^2 \times 10^3$ ) for rmb292lt

	x	y	z	U(eq)
H(3N)	8280(20)	769(13)	2170(30)	20(6)
H(4)	12170(20)	1185(12)	-1290(20)	11(5)
H(5)	13180(20)	2343(13)	-1920(30)	23(6)
H(6)	12310(20)	3549(13)	-1410(30)	24(6)
H(7)	10430(20)	3647(15)	-200(30)	27(6)
H(8A)	7610(20)	3080(13)	480(30)	23(6)
H(8B)	7830(20)	2736(13)	2320(30)	23(6)
H(8C)	8750(20)	3391(13)	1690(30)	20(6)
H(11)	4240(20)	1237(13)	780(30)	23(6)
H(12)	2810(30)	269(16)	1630(30)	39(7)
H(13)	3560(20)	-791(14)	3150(30)	29(6)
H(14)	5750(20)	-972(14)	3940(30)	31(6)
H(15)	7190(30)	-52(11)	3160(30)	25(7)

Table A65. Crystal data and structure refinement for compound 46

Identification code	rmb332ltb	
Empirical formula	C <sub>34</sub> H <sub>48</sub> Cl <sub>2</sub> N <sub>8</sub> O <sub>6</sub> Pt	
Formula weight	930.79	
Temperature	100.1 K	
Wavelength	0.7107 Å	
Crystal system	Monoclinic	
Space group	P2 <sub>1</sub> /n	
Unit cell dimensions	a = 17.7393(5) Å	α = 90°.
	b = 11.4632(3) Å	β = 99.794(3)°.
	c = 19.3959(5) Å	γ = 90°.
Volume	3886.66(17) Å <sup>3</sup>	
Z	4	
Density (calculated)	1.591 Mg/m <sup>3</sup>	
Absorption coefficient	3.801 mm <sup>-1</sup>	
F(000)	1872	
Crystal size	0.31 x 0.20 x 0.08 mm <sup>3</sup>	
Theta range for data collection	3.25 to 29.00°	
Index ranges	-23 ≤ h ≤ 23, -15 ≤ k ≤ 14, -25 ≤ l ≤ 26	
Reflections collected	36021	
Independent reflections	9266 [R(int) = 0.0407]	
Completeness to theta = 29.0°	89.5 %	
Completeness to theta = 26.3°	99.7 %	
Absorption correction	Semi-empirical from equivalents	
Max. and min. transmission	0.743 and 0.425	
Refinement method	Full-matrix least-squares on F <sup>2</sup>	
Data / restraints / parameters	9266 / 0 / 486	
Goodness-of-fit on F <sup>2</sup>	1.068	
Final R indices [I > 2σ(I)]	R1 = 0.0338, wR2 = 0.0716	
R indices (all data)	R1 = 0.0486, wR2 = 0.0793	
Largest diff. peak and hole	2.156 and -1.513 e.Å <sup>-3</sup>	

Table A66. Atomic coordinates ( $\times 10^4$ ) and equivalent isotropic displacement parameters ( $\text{\AA}^2 \times 10^3$ ) for rmb332ltb.  $U(\text{eq})$  is defined as one third of the trace of the orthogonalized  $U^{ij}$  tensor.

	x	y	z	U(eq)
Pt(1)	9660(1)	9009(1)	7865(1)	15(1)
Cl(1)	10464(1)	7522(1)	8320(1)	26(1)
Cl(2)	9056(1)	8897(1)	8824(1)	20(1)
O(1)	9347(2)	6557(2)	5682(1)	28(1)
O(2)	11006(2)	4957(2)	6717(1)	21(1)
O(3)	11066(1)	4417(2)	7861(1)	21(1)
O(4)	9203(2)	13485(2)	8327(1)	26(1)
O(5)	8101(2)	11715(2)	9523(1)	26(1)
O(6)	8673(2)	10590(2)	10438(1)	23(1)
N(1)	10154(2)	9059(2)	6997(2)	15(1)
N(2)	10509(2)	8435(2)	6016(1)	17(1)
N(3)	10015(2)	7030(3)	6747(2)	18(1)
N(4)	9946(2)	4823(3)	7214(2)	20(1)
N(5)	8926(2)	10293(2)	7469(1)	16(1)
N(6)	8149(2)	11825(3)	7453(1)	20(1)
N(7)	9101(2)	11530(3)	8472(2)	18(1)
N(8)	9395(2)	11678(3)	9870(2)	19(1)
C(1)	10213(2)	8140(3)	6591(2)	16(1)
C(2)	10633(2)	9635(3)	6042(2)	18(1)
C(3)	10898(2)	10383(3)	5575(2)	22(1)
C(4)	10971(2)	11545(3)	5769(2)	25(1)
C(5)	10782(2)	11932(3)	6400(2)	25(1)
C(6)	10504(2)	11191(3)	6856(2)	20(1)
C(7)	10421(2)	10018(3)	6668(2)	17(1)
C(8)	10767(2)	7632(3)	5516(2)	25(1)
C(9)	9586(2)	6285(3)	6280(2)	19(1)
C(10)	9395(2)	5118(3)	6592(2)	21(1)
C(11)	10707(2)	4743(3)	7220(2)	18(1)
C(12)	11904(2)	4521(3)	8048(2)	21(1)
C(13)	8618(2)	5276(4)	6813(2)	31(1)
C(14)	9353(3)	4176(3)	6024(2)	32(1)
C(15)	12037(2)	4268(4)	8828(2)	28(1)
C(16)	12285(2)	3595(4)	7665(2)	28(1)
C(17)	12162(2)	5755(3)	7919(2)	28(1)
C(18)	8743(2)	11228(3)	7813(2)	17(1)
C(19)	7944(2)	11251(3)	6813(2)	19(1)
C(20)	7387(2)	11505(3)	6245(2)	25(1)
C(21)	7324(2)	10729(4)	5690(2)	29(1)
C(22)	7789(2)	9743(4)	5705(2)	25(1)
C(23)	8351(2)	9504(3)	6274(2)	21(1)
C(24)	8426(2)	10287(3)	6832(2)	16(1)
C(25)	7683(2)	12706(3)	7730(2)	23(1)
C(26)	9263(2)	12636(3)	8714(2)	20(1)
C(28)	8664(2)	11362(3)	9915(2)	21(1)
C(27)	9562(2)	12739(3)	9501(2)	21(1)
C(29)	7964(2)	10082(3)	10605(2)	23(1)
C(30)	10426(2)	12858(4)	9586(2)	28(1)
C(31)	9221(3)	13821(3)	9794(2)	28(1)

C(32)	7668(2)	9185(3)	10057(2)	29(1)
C(33)	7373(3)	11026(4)	10670(2)	33(1)
C(34)	8237(2)	9532(4)	11315(2)	31(1)

Table A67. Anisotropic displacement parameters ( $\text{\AA}^2 \times 10^3$ ) for rmb332ltb. The anisotropic displacement factor exponent takes the form:  $-2\pi^2 [h^2 a^{*2} U^{11} + \dots + 2 h k a^* b^* U^{12}]$

	U <sup>11</sup>	U <sup>22</sup>	U <sup>33</sup>	U <sup>23</sup>	U <sup>13</sup>	U <sup>12</sup>
Pt(1)	17(1)	17(1)	12(1)	0(1)	3(1)	2(1)
Cl(1)	34(1)	26(1)	15(1)	0(1)	0(1)	13(1)
Cl(2)	23(1)	23(1)	15(1)	3(1)	6(1)	0(1)
O(1)	30(2)	35(2)	16(1)	2(1)	0(1)	-4(1)
O(2)	21(1)	26(1)	18(1)	-1(1)	4(1)	3(1)
O(3)	14(1)	30(1)	17(1)	2(1)	0(1)	-1(1)
O(4)	28(2)	26(1)	25(2)	8(1)	5(1)	-4(1)
O(5)	18(1)	33(2)	26(1)	6(1)	3(1)	0(1)
O(6)	21(2)	28(1)	22(1)	6(1)	6(1)	-4(1)
N(1)	14(2)	17(2)	13(2)	2(1)	0(1)	3(1)
N(2)	19(2)	19(2)	15(2)	-4(1)	3(1)	0(1)
N(3)	24(2)	17(2)	14(2)	2(1)	5(1)	2(1)
N(4)	20(2)	21(2)	21(2)	3(1)	5(1)	-1(1)
N(5)	18(2)	18(2)	14(2)	3(1)	5(1)	4(1)
N(6)	21(2)	24(2)	15(2)	3(1)	6(1)	5(1)
N(7)	22(2)	20(2)	13(2)	5(1)	5(1)	4(1)
N(8)	17(2)	23(2)	17(2)	0(1)	4(1)	1(1)
C(1)	17(2)	20(2)	13(2)	-3(1)	3(1)	3(1)
C(2)	14(2)	21(2)	16(2)	1(1)	-1(2)	2(1)
C(3)	18(2)	28(2)	20(2)	1(2)	3(2)	-5(2)
C(4)	22(2)	24(2)	28(2)	10(2)	2(2)	-1(2)
C(5)	18(2)	19(2)	35(2)	-1(2)	-2(2)	-1(2)
C(6)	18(2)	20(2)	22(2)	-4(2)	-2(2)	2(2)
C(7)	14(2)	20(2)	16(2)	0(1)	3(1)	1(1)
C(8)	28(2)	25(2)	23(2)	-6(2)	10(2)	2(2)
C(9)	14(2)	23(2)	19(2)	-4(2)	2(2)	1(1)
C(10)	18(2)	23(2)	21(2)	2(2)	0(2)	-1(2)
C(11)	19(2)	13(2)	19(2)	-4(1)	1(2)	2(1)
C(12)	16(2)	26(2)	20(2)	0(2)	3(2)	0(2)
C(13)	19(2)	37(2)	38(2)	11(2)	4(2)	6(2)
C(14)	29(2)	24(2)	38(3)	-5(2)	-6(2)	1(2)
C(15)	18(2)	44(2)	21(2)	1(2)	2(2)	-1(2)
C(16)	23(2)	33(2)	28(2)	1(2)	5(2)	8(2)
C(17)	24(2)	31(2)	29(2)	-6(2)	5(2)	-8(2)
C(18)	19(2)	19(2)	13(2)	4(1)	7(2)	3(1)
C(19)	19(2)	26(2)	14(2)	-1(2)	6(2)	-1(2)
C(20)	23(2)	28(2)	24(2)	6(2)	3(2)	6(2)
C(21)	21(2)	44(2)	19(2)	2(2)	-1(2)	0(2)
C(22)	24(2)	35(2)	16(2)	-4(2)	5(2)	0(2)
C(23)	19(2)	26(2)	20(2)	1(2)	6(2)	2(2)
C(24)	16(2)	23(2)	11(2)	4(1)	4(1)	1(1)
C(25)	20(2)	24(2)	27(2)	0(2)	10(2)	4(2)

C(26)	15(2)	22(2)	23(2)	1(2)	7(2)	1(2)
C(28)	21(2)	25(2)	19(2)	-2(2)	8(2)	-2(2)
C(27)	22(2)	18(2)	22(2)	3(2)	1(2)	-1(2)
C(29)	17(2)	33(2)	21(2)	3(2)	10(2)	-2(2)
C(30)	21(2)	37(2)	28(2)	5(2)	7(2)	-2(2)
C(31)	32(2)	25(2)	27(2)	-3(2)	9(2)	-1(2)
C(32)	22(2)	33(2)	32(2)	3(2)	4(2)	-3(2)
C(33)	30(2)	39(2)	35(2)	5(2)	21(2)	7(2)
C(34)	28(2)	40(2)	27(2)	6(2)	14(2)	-1(2)

Table A68. Hydrogen coordinates ( $\times 10^4$ ) and isotropic displacement parameters ( $\text{\AA}^2 \times 10^3$ ) for rmb332ltb.

	x	y	z	U(eq)
H(3N)	10050(20)	6860(30)	7150(20)	22
H(4N)	9770(30)	4650(40)	7490(20)	24
H(7N)	9180(30)	11090(30)	8720(20)	18(13)
H(8N)	9770(20)	11430(40)	10200(20)	27(12)
H(3)	11020	10118	5155	26
H(4)	11150	12078	5473	30
H(5)	10846	12717	6516	30
H(6)	10376	11463	7273	25
H(8A)	10864	6878	5728	38
H(8B)	11229	7927	5383	38
H(8C)	10379	7566	5108	38
H(13A)	8439	4537	6953	47
H(13B)	8260	5579	6427	47
H(13C)	8664	5812	7199	47
H(14A)	9845	4097	5884	48
H(14B)	8980	4396	5627	48
H(14C)	9209	3446	6206	48
H(15A)	11752	4812	9058	42
H(15B)	12572	4343	9014	42
H(15C)	11872	3489	8906	42
H(16A)	12098	2839	7766	42
H(16B)	12829	3624	7817	42
H(16C)	12170	3736	7171	42
H(17A)	12072	5911	7426	42
H(17B)	12698	5832	8100	42
H(17C)	11880	6300	8151	42
H(20)	7074	12157	6234	30
H(21)	6959	10870	5295	34
H(22)	7719	9237	5325	30
H(23)	8665	8852	6283	26
H(25A)	7674	12547	8214	34
H(25B)	7171	12683	7472	34
H(25C)	7898	13465	7685	34
H(30A)	10636	12955	10072	43

H(30B)	10551	13525	9328	43
H(30C)	10636	12169	9411	43
H(31A)	8677	13727	9754	42
H(31B)	9328	14497	9535	42
H(31C)	9443	13918	10278	42
H(32A)	7508	9566	9615	44
H(32B)	7242	8781	10191	44
H(32C)	8067	8637	10014	44
H(33A)	7615	11657	10950	49
H(33B)	6973	10704	10889	49
H(33C)	7159	11311	10213	49
H(34A)	8634	8979	11279	46
H(34B)	7817	9142	11470	46
H(34C)	8432	10128	11645	46

Table A69. Hydrogen bonds for Compound 18 [ $\text{\AA}$  and  $^\circ$ ].

D-H	d(D-H)	d(H..A)	<DHA	d(D..A)	A
N2-H2N	0.911	1.940	172.96	2.846	N6 [ x+1, y, z ]
N5-H5N	0.900	1.987	171.01	2.880	N3 [ x-1, y, z ]
N8-H8N	0.840	2.085	124.99	2.657	O3
N9-H9N	0.823	2.133	145.75	2.852	O1

Table A70. Hydrogen bonds for Compound 24 [ $\text{\AA}$  and  $^\circ$ ].

D-H	d(D-H)	d(H..A)	<DHA	d(D..A)	A
N2-H20	0.768	2.420	152.24	3.121	O4

Table A71. Hydrogen bonds for compound 26 [ $\text{\AA}$  and  $^\circ$ ].

D-H	d(D-H)	d(H..A)	<DHA	d(D..A)
N2-H2N	0.729			

(H donor with no acceptor)

Table A72. Hydrogen bonds for compound 28 [Å and °].

D-H	d(D-H)	d(H..A)	<DHA	d(D..A)	A
N2-H2N	0.708	2.599	145.17	3.206	C11
N4-H4N	0.827	2.756	131.42	3.361	C12

Table A73. Hydrogen bonds for compound 41 [Å and °].

D-H	d(D-H)	d(H..A)	<DHA	d(D..A)	A
N3-H3N	0.762	2.565	156.55	3.278	C12 [ -x+1, -y+1, -z+1 ]
N6-H6N	0.663	2.612	160.80	3.245	C12 [ -x+1, -y+1, -z+1 ]

Table A74. Hydrogen bonds for compound 46 [Å and °].

D-H	d(D-H)	d(H..A)	<DHA	d(D..A)	A
N3-H3N	0.793	2.392	144.38	3.071	C11
N4-H4N	0.701	2.440	163.01	3.117	O4 [ x, y-1, z ]
N7-H7N	0.694	2.300	116.03	2.678	N8
N7-H7N	0.694	2.535	140.04	3.099	C12
N8-H8N	0.879	2.602	169.49	3.469	C12 [ -x+2, -y+2, -z+2 ]



## CURRICULUM VITAE

**Name :** Samuel S. K. Asem

**ADDRESS:** Department of Chemistry  
University of Louisville  
2320 Brook Street, Room 138  
Louisville, Ky 40292

**EDUCATION:** **PhD, Chemistry, Expected Graduation- December 2011**  
University of Louisville, Louisville, Kentucky  
Dissertation: Rational design, synthesis and characterization of amide functionalized pyridine and benzimidazole transition metal complexes.  
Research Advisor: Prof. Robert M. Buchanan

**Abstract:**

**Synthesis of novel amide functionalized organic moieties for complexation to first row transition metals as potential catalytic models of enzymes**

- Complexation of novel functionalized amide moieties to platinum as potential anticancer chemotherapeutics.

**BA, Chemistry, May 2000**

Berea College, Berea, Kentucky  
College Soccer Team, Cosmopolitan Club, African Students Association

**PROFESSIONAL EXPERIENCE:**

**Nov 2000- Jul 2004 Associate Scientist, Invitrogen Life Technologies CPI, Frederick, MD**

- Performed quality analysis of Oligonucleotides of the entire production platform to assure quality of finished products.
- Synthesized and processed DNA, RNA with special modifiers including amino linkers, biotin and hexachlorofluorescein as part of small project team.
- Utilized diverse physical methods to process and purified Oligonucleotides. Instrumentation included: HPLC, PAGE and Column Chromatography.

**Apr 2002 – Jun 2002 Special Volunteer, National Cancer Institute Genomic Diversity Lab, Fort Detrick, Fredrick, MD**

- Designed Primers as input into the development and application of genomic resources in the domestic cat, to contribute to our understanding of human hereditary disease analogues and neoplasia.

- Amplified and purified primers utilizing PCR and Gel Electrophoresis.

**Summer 1998:            Researcher, Chemistry Department, Berea College, Berea, KY**

- Synthesis, Characterization and Reactivity of Urea derivatives  
Coordinated to Cobalt (III) Possible Relevance to Urease.

**TEACHING EXPERIENCE:**

**Aug 2006-Dec 2009    Graduate Teaching Assistant, University of Louisville, Dept. of Chemistry, Louisville, KY**

- Tutored, mentored, graded and proctored exams for multiple chemistry classes and labs-Organic Chemistry, General Chemistry and Inorganic Chemistry.

**Aug 1997- May 2000    General & Organic Chem. Lab Instructor/Teaching Assistant, Berea College, Berea, KY**

- Taught safe lab procedures to undergraduate Chemistry Students.
- Led experiments on NMR.
- Mentored students and graded all homework assignments.

**VOLUNTEER EXPERIENCE:**

**Sep 2003-Mar 2004    Volunteer, Emergency Department, Frederick Hospital, Frederick, MD**

- Shadowed Doctors on duty and assisted in patient care.
- Assisted in streamlining patient intake procedures to minimize wait times.

**Fall 1999-Spring 2000    Vice President, Berea College African Students Association, Berea College, Berea, KY**

- Provided leadership to influential, active student organization.
- Owned and led organization of Annual Cultural Awareness Week-multi-faceted event with many stakeholders.

**Summer 1997:            Mentor & Student Counselor, Science Focus Boot camp, Berea, KY**

- Responsible for eighteen students-counseled/mentored rising high school students.
- Led planning and implementation of educational science & social activities for this selective boot camp for high potential seniors.

**PRESENTATIONS AT SCIENTIFIC MEETINGS:**

Samuel Asem, Robert M. Buchanan, Mark Mashuta, Paula Bates; *Synthesis and properties of several new Pt(II) complexes containing pyridine and benzimidazole functionalized amide ligands*, 38<sup>th</sup> Annual National NOBCChE Conference, Houston, TX, April 20<sup>th</sup>, 2011.

Samuel Asem, Robert M Buchanan, Mark Mashuta; *Synthesis and Characterization of selected transition metal complexes using amide functionalized benzimidazole ligands as potential enzyme models*, 4<sup>th</sup> Annual

University of Kentucky Graduate Student Interdisciplinary Conference,  
Lexington, KY, April 9<sup>th</sup>, 2010.

Samuel Asem, Robert M Buchanan, Mark Mashuta, Paula Bates; *New Pt(II) complexes as novel chemotherapeutics*, 37<sup>th</sup> annual Conference of the Institute of Molecular Development and Drug Design(IMD<sup>3</sup>), Louisville, KY, March 9<sup>th</sup>, 2010.

Samuel Asem, Robert M. Buchanan, Mark Mashuta, Paula Bates; *Synthesis and properties of several new Pt(II) complexes containing pyridine and benzimidazole functionalized amide ligands*, University of Louisville Graduate Research Symposium, Louisville, KY, March 5<sup>th</sup>, 2010.

**PUBLICATIONS / MANUSCRIPTS IN REVIEW OR PREPARATION:**

Samuel Asem, Mark Mashuta, Robert M. Buchanan; *Title: Tetra- $\mu$ -acetato- $K^{\delta}$  O:O'-bis[(N-pyridine-2-yl-2,2-dimethylpropanamide-KN<sup>l</sup>)copper(II)] (I)*, Submitted 20<sup>th</sup> June, 2011.(*Acta Cryst. E* id: hq2006).

Samuel Asem, Mark Mashuta, Robert M. Buchanan; *Synthesis and Characterization of isomeric conformers of dichloro, diamido and diiodo Pt(II) pyridinyl moieties*, 1<sup>st</sup> Quarter 2012.

**AWARDS:** *All American Scholar- competitive national award; University of Louisville Fellow-full tuition and stipend award; University of Louisville dissertation award; NOBCCChE Advancing Science award- competitive national award; Nyerere Award-competitive award for integrity & leadership; Berea College Service Award-selective recognition for service to the school*

**MEMBERSHIPS:** National Organization for the Professional Advancement of Black Chemists and Chemical Engineers (NOBCCChE), American Chemical Society (ACS).

**SAMPLE COURSES:**

Advanced Biochemistry I & II, Coordination Chemistry, Advanced Analytical Chemistry, Advanced Organic Chemistry I & II, Advanced Inorganic Chemistry.

**OTHER:** Sports enthusiast, keen Ping Pong & Chess Player, enjoy travel, avid Wall Street markets follower.